TECHNICAL UNIVERSITY OF CATALONIA

DEPARTMENT OF GEOTECHNICAL ENGINEERING AND GEOSCIENCES

SCHOOL OF CIVIL ENGINEERING

THERMO-HYDRO-MECHANICAL COUPLED ANALYSIS IN LOW PERMEABILITY MEDIA

PhD Thesis

by:

Marcelo Sánchez Castilla

Supervised by:

Antonio Gens Solé
Sebastià Olivella Pastallé

Barcelona, June 2004

A Lichi, Catalina y Julia

ABSTRACT

Thermo-Hydro-Mechanical (*THM*) analysis of engineering problems involving low permeability materials is a complex problem in which several factors make significant contributions. This Thesis is aimed mainly to the study of coupled *THM* process in engineered clay barriers and seals designed for the isolation of radioactive waste. Therefore, special attention has been placed on expansive clay behaviour. In the last few years, several laboratory investigations have shown the strong influence of pore structure on *THM* behaviour of swelling materials. Therefore, a main objective of this Thesis is the proposal of a *THM* framework which allows the inclusion of the effects of the material fabric on the analyses of real problems in geological media.

A general double structure *THM* formulation developed for porous media in which two distinctive types of voids are present has been proposed. This formulation expresses in a mathematical way the various *THM* phenomena deemed relevant in each structural level, and their main interactions. Concepts of double porosity theory have been used to extend a fully coupled *THM* single porosity formulation to the case of double structure media. The approach is able to handle non-saturated, non-isothermal multiphase flows coupled with the deformations of each medium. A central part of the approach is the mechanical constitutive law, a key point in the modelling of the expansive clay behaviour. The existence of two structural levels (a macrostructural one and the microstructural one) has been explicitly included in the model. The macrostructure accounts for the large scale structure of the material, while the microstructure is associated with the active clay particles responsible for the swelling behaviour. The mechanical law is completed by establishing the interaction between the two structural levels. The model has been formulated using concepts of elasto-plasticity for strain hardening materials and generalized plasticity theory. The formulation has been implemented in the finite element program CODE_BRIGHT and has been used to solve a variety of problems.

The proposed double structure *THM* formulation is general and it is not limited to analyze problems in which expansive materials are involved. For instance, the problem of consolidation in fissured clays has been presented in this Thesis, as well as, the simulation of a water-flooding process in a petroleum exploitation.

Work has also been performed toward the experimental validation of the suggested approach. This work has been mainly supported by experimental data generated in the framework of the FEBEX (Full-scale Engineered Barriers Experiment) project. The data of laboratory tests have been used to identify the main parameters of the constitutive laws related to the thermal and hydraulic problems and, also, to validate the mechanical constitutive model. In addition, a large scale heating test has allowed the application of the approach to an actual case in which experimental information of the main *THM* variables are available. The evolution of the heating test has been analyzed in detail, focusing the study on the unexpected slowing down hydration observed. The effect of the clay-fabric evolution and its influence on the permeability field has been included in the analysis to help to explain the barrier behaviour. The heating test has also been analyzed considering the presence of other flow phenomena such as the existence of a threshold gradient and the influence of thermo-osmotic effects.

RESUMEN

El análisis de problemas Termo-Hidro-Mecánicos (*THM*) en medios de baja permeabilidad es un problema complejo en el cual confluyen diversos factores. Esta Tesis está orientada principalmente al estudio de procesos *THM* acoplados en barreras de ingeniería destinadas al almacenamiento de residuos radiactivos. Especial atención se ha dedicado al estudio de arcillas expansivas. Diversos ensayos de laboratorio han mostrado la fuerte influencia que tiene la estructura de poros en el comportamiento *THM* de arcillas expansivas. Una motivación de este trabajo es la inclusión de la fábrica del material en el análisis de problemas de ingeniería en medios geológicos.

Una formulación *THM* de doble estructura, desarrollada para medios porosos que presentan dos tipos característicos de vacíos se propone en esta Tesis. La formulación expresa en forma matemática los diversos fenómenos *THM* considerados relevantes en cada nivel estructural y las principales interacciones entre ellos. Conceptos de doble porosidad han sido utilizados para su desarrollo. La formulación permite considerar flujo no-saturado en condiciones no isotermas, acoplados con las deformaciones de cada medio. Un aspecto importante del marco propuesto es el modelo constitutivo mecánico. Dos niveles estructurales han sido explícitamente incluidos en el modelo. La macroestructura considera el esqueleto granular conformado por los agregados de arcilla, mientras que la microestructura está asociada con las partículas de arcilla, responsables del comportamiento expansivo de estos materiales. El modelo mecánico se completa estableciendo la interacción entre los dos niveles estructurales. El modelo se ha formulado considerando conceptos de elasto-plasticidad para materiales con endurecimiento por deformación y también conceptos de la teoría de la plasticidad generalizada. La formulación se ha implementado en el programa de elementos finitos CODE_BRIGHT y se la ha utilizado para resolver diferentes problemas de ingeniería.

La formulación *THM* de doble estructura propuesta es general y no se limita al análisis de problemas relacionados con materiales expansivos. Por ejemplo, la aplicación al problema de consolidación en arcillas fisuradas se presenta en esta Tesis. Se modela también la extracción de petróleo, asistida mediante inyección de agua a presión, en un medio heterogéneo.

La validación experimental de la formulación es una parte importante del trabajo realizado. Esta tarea se ha apoyado principalmente en los datos experimentales generados en el marco del proyecto FEBEX (Full-scale Engineered Barriers Experiment). Los resultados de los ensayos de laboratorio se han utilizado para identificar gran parte de los parámetros de las leyes constitutivas asociadas al problema térmico e hidráulico, como así también para validar el modelo constitutivo mecánico. Además, un ensayo de hidratación y calentamiento a escala real, ha permitido la aplicación de la formulación a un caso real en el que se tienen disponible información experimental de las principales variables *THM*. La evolución del ensayo de calentamiento ha sido analizada en detalle, centrando la atención en el estudio de una disminución, no esperada, de la tasa de hidratación de la barrera. La influencia de la fábrica de las arcillas expansivas (y su evolución) en el campo de permeabilidad se ha incluido en los análisis como elemento de ayuda en la explicación del comportamiento no esperado de la barrera. El ensayo también ha sido analizado considerando la presencia de otros fenómenos observados en estos materiales, tales como la existencia de un gradiente umbral en la ley de flujo o la influencia de efectos termo-osmóticos.

AGRADECIMIENTOS

Quiero expresar mi agradecimiento, en primer lugar, a los profesores Antonio Gens y Sebastiá Olivella por la dirección de esta Tesis. Trabajar junto a ellos ha sido una experiencia sumamente enriquecedora. La capacidad de escuchar y aportar nuevas ideas en momentos críticos, sumada al apoyo continuo y a la acertada orientación durante estos años, ha sido fundamental para el desarrollo de este trabajo de investigación. Este reconocimiento es extensivo a otros miembros del Departamento que se han interesado por este trabajo y que han contribuido también a su consecución. Entre ellos quisiera destacar a los profesores Eduardo Alonso, Antonio Lloret y Alberto Ledesma.

Agradezco también a quienes desde la distancia se han interesado por este trabajo, especialmente a los miembros del Instituto de Materiales y Suelos de la Universidad Nacional de San Juan. Agradezco a Juan Manuel Fiore por el apoyo y la confianza inicial en este proyecto, como así también por su estímulo a lo largo de estos años.

Una mención especial merece mi compañero y amigo Leonardo Guimarães, tanto por su inestimable colaboración en el desarrollo de aspectos específicos de esta Tesis, como así también por su permanente aliento y apoyo, que han representado firmes puntales durante estos años. A Jean Vaunat le agradezco su permanente interés y su efectiva ayuda durante este tiempo. A Enrique Romero le quiero expresar mi agradecimiento por sus comentarios y discusiones. Aprovecho estas líneas para agradecer también a Albert, por su disposición a resolver los problemas informáticos; y a Mari Carmen, Eva, Mar y Oscar por su colaboración en la gestión de los diversos trámites administrativos a lo largo de estos años.

Este trabajo ha sido posible gracias al apoyo económico recibido por parte de diferentes instituciones. En primer lugar mi gratitud para quienes inicialmente posibilitaron mis estudios, ellos son: la Universidad Nacional de San Juan y la Agencia Española de Cooperación Internacional, a través del programa de becas MUTIS. También quiero agradecer el apoyo económico recibido durante estos años por parte de ENRESA, a través del CIMNE.

Quiero agradecer también a aquellos integrantes del proyecto FEBEX con los que he interactuado más activamente. Mi reconocimiento a María V. Villar, Ana M. Fernández, Pedro L. Martín y Pedro Rivas del CIEMAT por el interés que han tenido en este trabajo y por las valiosas sugerencias realizadas. También mi reconocimiento a los miembros de AITEMIN y del CSIC-Zaidín de Granada. Agradezco al grupo de la ULC (Universidad de la Coruña) y de la UPM (Universidad Politécnica de Madrid) por los comentarios al trabajo y también por las fructíferas discusiones. Finalmente agradezco a Fernando Huertas de ENRESA y a Pascual Farías por el interés mostrado por este trabajo.

A mis compañeros de doctorado les agradezco los buenos momentos compartidos durante estos años como así también las discusiones y mesas de café, de las que tanto he aprendido. Me gustaría recordar a aquellos con los que he tenido el gusto de compartir despacho: Clemente, Italo, Ángel, Jordi, Alexandra, Christian, Carlos L., Carlos Ch., Carlos B., Jesús, Beatriz y Olga. Como así también al resto de compañeros del departamento: Roberto, Salvatore, Xavi, Mauricio, Fermín, Luciano., Luciano C., Guillermo, Claudia, Juan, Iván, Domingo, Chen, Kantha, Alejandro, Daniela, Ernesto, Daniel, José María, Sergio y Abel. Agradezco también a mis amigos de al UPC: Augusto, Omar, Adolfo y Gustavo. Finalmente quiero agradecer especialmente a Mabel por su ayuda en las correcciones de este documento.

Quiero expresar mi gratitud hacia toda la familia que se quedó en Argentina y que desde allá me alentó en todo momento. Agradecer especialmente a mis padres, María Estrella y Gabriel, como así también a Alicia y Carlos por su apoyo incondicional durante estos años y por su afecto, los he tenido a todos muy presentes a pesar de la distancia. Finalmente quiero agradecer a mis compañeras de aventura: a mi esposa Lichi y a mis hijas Catalina y Julia. A ellas va merecidamente dedicada esta Tesis. Su compañía, comprensión y especialmente el cariño que me han brindado durante este tiempo me han permitido concluir este trabajo.

TABLE OF CONTENTS

CHAPTER I 1

INTRODUCTION 1

1.1 BACKGROUND AND OBJECTIVES OF THE THESIS 2

1.2 THESIS LAYOUT 8

CHAPTER II 9

A DOUBLE-STRUCTURE THM FORMULATION 9

2.1 PREFACE 10

2.2 THEORETICAL FRAMEWORK 12

2.2.1 INTRODUCTION 12

2.2.2 BALANCE EQUATIONS 17

2.2.2.1 Solid Mass Balance Equation 17

2.2.2.2 Water Mass Balance Equation 18

2.2.2.3 Air Mass Balance Equation 20

2.2.2.4 Energy Balance Equation 20

2.2.2.5 Momentum Balance (Equilibrium) 22

2.2.3 CONSTITUTIVE EQUATIONS 23

2.2.3.1 Thermal Constitutive Equations 23

2.2.3.2 Hydraulic Constitutive Equations 24

2.2.3.3 Mechanical Constitutive Equation 25

2.2.3.4 Phase Physical Properties 25

2.2.4 EQUILIBRIUM RESTRICTIONS 25

2.2.5 MASS TRANSFER BETWEEN MEDIA 26

2.3 NUMERICAL IMPLEMENTATION 26

2.4 APPLICATION CASES 28

2.4.1 CONSOLIDATION OF FISSURED CLAYS 28

2.4.2 MULTIPHASE FLOW IN A HETEROGENEOUS MEDIUM 31

2.5 CONCLUSIONS AND REMARKS 37

CHAPTER III 39

A DOUBLE STRUCTURE MECHANICAL MODEL
FOR EXPANSIVE MATERIALS 39

3.1 PREFACE 40

3.2 MODEL FORMULATION 42

3.2.1 INTRODUCTION 42

3.2.2 MACROSTRUCTURAL MODEL 45

3.2.3 MICROSTRUCTURAL MODEL 48

3.2.4 INTERACTION BETWEEN STRUCTURAL LEVELS 50

3.2.4.1 Loading and Unloading Direction 52

3.2.4.2 Plastic Flow Direction 54

3.2.4.3 Plastic Modulus 56

3.3 ELASTO-PLASTIC STRESS-STRAIN RELATIONS 58

3.3.1 EQUILIBRIUM BETWEEN WATER POTENTIALS 58

3.3.2 NON-EQUILIBRIUM BETWEEN WATER POTENTIALS 62

3.4 NUMERICAL IMPLEMENTATION 66

3.4.1 INTRODUCTION 66

3.4.2 MODEL INTEGRATION 68

3.4.2.1 Elastic Stress Integration 71

3.4.2.2 Intersection with the Yield Surface 73

3.4.2.3 Elasto-Plastic Stress Integration 75

3.4.2.4 Yield Surface Drift Correction 75

3.4.2.5 Sub-Stepping Strategy 77

3.4.2.6 Integration of the Generalized Plasticity Model 78

3.5 APPLICATION CASES 80

3.5.1 SWELLING PRESSURE TEST 80

3.5.2 CYCLIC WETTING/DRYING TEST 83

3.6 CONCLUSIONS AND REMARKS 85

CHAPTER IV 87

APPLICATIONS OF THE DOUBLE STRUCTURE FRAMEWORK 87

4.1 PREFACE 88

4.2 EXPERIMENTAL VALIDATION OF THE MECHANICAL MODEL 89

4.2.1 INTRODUCTION 89

4.2.2 PROPERTIES AND FABRIC OF THE MATERIAL 89

4.2.3 EXPERIMENTAL RESULTS 91

4.2.4 MODEL RESULTS 98

4.3 THM RESPONSE OF THE FEBEX BENTONITE 105

4.3.1 OVERHEATING EPISODE 105

4.3.2 OVERHEATING MODELLING 107

4.4 ANALYSIS OF THE HYDRATION PROCESS OF AN EXPANSIVE MATERIAL 112

4.4.1 INTRODUCTION 112

4.4.2 MECHANICAL MODEL 114

4.4.3 HYDRAULIC MODEL 114

4.4.4 MODELLING 115

4.5 CONCLUSIONS AND REMARKS 119

CHAPTER V 121

THERMO-HYDRO-MECHANICAL ANALYSIS OF A LARGE SCALE HEATING TEST 121

5.1 PREFACE 122

5.2 MOCK-UP TEST. 'OPERATIONAL STAGE' MODEL 124

5.2.1 INTRODUCTION 124

5.2.2 ANALYSIS OF THE MOCK-UP TEST HYDRATION 126

5.2.2.1 General 126

5.2.2.2 Thermal Problem 130

5.2.2.3 Hydraulic Problem 130

5.2.2.4 Mechanical Problem 134

5.3 ANALYSIS OF THE MOCK-UP TEST HYDRATION INCLUDING NON-STANDARD FLOW MODELS 134
5.3.1 INTRODUCTION 134
5.3.2 PRELIMINARY ANALYSES 138
5.3.2.1 Threshold Gradient 139
5.3.2.2 Thermo-Coupling Effects 143
5.3.2.3 Micro-Fabric Evolution 147
5.3.3 DISCUSSION 151
5.4 ANALYSIS OF THE MOCK-UP TEST USING A DOUBLE STRUCTURE FRAMEWORK 153
5.4.1 INTRODUCTION 153
5.4.2 HYDRATION AND SWELLING OF EXPANSIVE CLAYS 153
5.4.2.1 Expansive Clay Behaviour 153
5.4.2.2 Conceptual Models 159
5.4.3 MOCK-UP DOUBLE STRUCTURE MODEL 162
5.4.3.1 Introduction 162
5.4.3.2 Model Laws and Parameters 163
5.4.3.3 Model Results 163
5.5 CONCLUSIONS 179

CHAPTER VI 181

CLOSURE 181
6.1 REMARKS AND GENERAL CONCLUSIONS 182
6.2 FUTURE WORK 185

REFERENCES 187

APPENDIX A.1 209

A.1.1 CONSOLIDATION OF FISSURED CLAYS. CLOSED FORM SOLUTION. 210
A.1.2 MASS TRANSFER MODELS 212

APPENDIX A.2 215

A.2.1 GENERALIZED PLASTICITY MODEL. PARTICULAR CASE 216
A.2.1.1 MODEL FORMULATION 216
A.2.1.2 APPLICATION CASE 218
A.2.2 BBM. MODEL COMPLEMENTARY EQUATIONS 220
A.2.3 DOUBLE STRUCTURE CONSIDERATIONS 222
A.2.4 GENERALIZED PLASTICITY MODEL. PLASTIC FLOW DIRECTION 225
A.2.5 ELASTIC MODEL 226
A.2.6 HYDRAULIC EQUILIBRIUM BETWEEN PORES STRUCTURES 227
A.2.6.1 AUXILIARY EXPRESSIONS FOR THE MACROSTRUCTURAL MODEL 227
A.2.6.2 AUXILIARY EXPRESSIONS FOR THE GENERALIZED PLASTICITY MODEL 229
A.2.7 HYDRAULIC NON-EQUILIBRIUM BETWEEN PORES STRUCTURES 230
A.2.7.1 AUXILIARY EXPRESSIONS FOR THE MACROSTRUCTURAL MODEL 230
A.2.7.2 AUXILIARY EXPRESSIONS FOR THE GENERALIZED PLASTICITY MODEL 231
A.2.8 P-MATRIX 232
A.2.8.1 DEFINITIONS 232
A.2.8.2 "P-MATRIX" PROPERTIES. 232
A.2.9 ONE PLASTIC MECHANISM ACTIVE 232

APPENDIX A.3 235

A.3.1 MIXTURES OF CLAY PELLETS AND CLAY POWDER 236
A.3.1.1 BASIC RELATIONS 236
A.3.1.2 ELASTIC MODEL 238

APPENDIX A.4 241

A.4.1 OBC MODEL OF MOCK-UP TEST 242

A.4.1.1 INTRODUCTION 242

A.4.1.2 CONSTITUTIVE EQUATIONS 242

A.4.1.2.1 Thermal 242

A.4.1.2.2 Hydraulic 244

A.4.1.2.3 Mechanical Problem 249

A.4.1.3 EQUILIBRIUM RESTRICTIONS 252

A.4.1.4 PHASE PHYSICAL PROPERTIES 253

A.4.1.5 MODELLING 254

A.4.1.5.1 Initial Conditions 255

A.4.1.5.2 Boundary Conditions 255

A.4.1.5.3 Model Results 256

A.4.2 SENSITIVITY ANALYSES 269

A.4.3 MOCK-UP DOUBLE STRUCTURE MODEL 276

A.4.3.1 MODEL LAWS AND PARAMETERS 276

Notation

$\mathbf{D}_e$	elastic matrix
$\mathbf{D}_{ep}$	elasto-plastic matrix
e	void ratio
e_M	macrostructural level void ratio
e_m	microstructural level void ratio
F_{LC}	*BBM* yield surface
F_{NL}	Neutral Line
f_β	interaction function for β mechanism
G	plastic potential
G_t	shear modulus
g	a lode angle function
$\mathbf{H}$	hardening modulus matrix
$\mathbf{H}^c$	critical softening matrix.
$\overline{\mathbf{H}}$	effective hardening matrix
$\mathbf{I}$	identity matrix
$\mathbf{i}^i_{\alpha j}$	non-advective mass flux (i=w,a; α=l,g; j=1,2)
$\mathbf{i}_{cj}$	non-advective heat flux (j=1,2)
J	2nd stress invariant of deviatoric stress tensor
J_h	hydraulic gradient
J_o	threshold hydraulic gradient
J_c	critical hydraulic gradient
$\mathbf{j}^i_{Ej}$	advective energy flux in α phase with respect to a fixed reference system (j=1,2)
$\mathbf{j}'^i_{Ej}$	advective energy flux in α phase with respect to the solid phase (j=1,2)
$\mathbf{j}^i_{\alpha j}$	total mass flux of i-species in α phase with respect to a fixed reference system (j=1,2)
$\mathbf{j}'^t_{\alpha j}$	total mass flux of i-species in α phase with respect to the solid phase (j=1,2)
$\mathbf{K}_{\alpha j}$	permeability tensor (α=l,g; j=1,2)
$\mathbf{k}_j$	intrinsic permeability tensor (j=1,2)
$k_{r\alpha j}$	α phase relative permeability (α=l,g; j=1,2)
K	global bulk modulus

K_s	macrostructural bulk modulus for changes in suction
K_T	macrostructural bulk modulus for changes in temperature
K_M	macrostructural bulk modulus for changes in mean stress
K_m	microstructural bulk modulus for changes in mean stress plus suction
k_c	parameter describing the increase in cohesion with suction
LC	Loading-Collapse yield surface (BBM)
lc	plastic mechanism related to BBM
$\mathbf{m}$	auxiliary unit vector $\mathbf{m}^T = (1,1,1,0,0,0)$
$\mathbf{m}_{LC}$	flow rule direction of BBM
$\mathbf{m}_\beta$	flow rule direction of mechanism β
M	slope of critical state line
MC	microstructural contraction path
MS	microstructural swelling path
mc	plastic mechanism related to MC path
ms	plastic mechanism related to MS path
$\hat{p}$	microstructural effective stress
p	mean net stress
p_c	reference stress
p_0	net mean yield stress at current suction and temperature
p_0^*	net mean yield stress for saturated conditions at reference temperature
p_{0T}^*	net mean yield stress for saturated conditions at current temperature
p_r	reference stress
$\mathbf{q}_{\alpha j}$	volumetric flux of α phase with respect to the solid ($\alpha=l,g;\ j=1,2$)
r	parameter defining the maximum macrostructural soil stiffness
$S_{\alpha j}$	volumetric fraction of pore volume occupied by α phase ($\alpha=l,g;\ j=1,2$)
S_{rl}	residual saturation
S_{ls}	maximum saturation
s_o	osmotic suction
s_t	total suction
T	temperature (T_0 = reference temperature)
T_v	time factor
t	time

$\mathbf{u}$	solid displacement vector
u_j	excess pores pressures (j=1,2)
V, V_v	volume, volume of pores
V_s	volume of solids
V_{vM}, V_{vm}	V_v of macrostructure and microstructure
$\boldsymbol{\alpha}_{sM}$	elastic vector associated with macrostructural suction
$\boldsymbol{\alpha}_{sm}$	elastic vector associated with microstructural suction
$\boldsymbol{\alpha}_T$	elastic vector associated with temperature
α	parameter related to the plastic potential
α_0	parameter for elastic thermal strain
α_1	parameter that relates p_o^* with T
α_2	parameter for elastic thermal strain
α_3	parameter that relates p_o^* with T
α_m	parameter controlling the microstructural soil stiffness
α_s	parameter controlling the soil stiffness (*BBM*)
α_{sp}	parameter controlling the soil stiffness (*BBM*)
$\boldsymbol{\beta}_{sM}$	elasto-plastic vector associated with macrostructural suction
β	indicates the direction of the microstructural stress path (β=C =>MC path , β=S =>MS path)
β_m	parameter controlling the microstructural soil stiffness
χ	F_{NL} slope
ΔT	temperature increment (T- T_0)
$\boldsymbol{\varepsilon}$	strain vector. $\left\{\varepsilon_x, \varepsilon_y, \varepsilon_z, \gamma_{xy}, \gamma_{xz}, \gamma_{yz}\right\}^T$
$\dot{\boldsymbol{\varepsilon}}^e$	elastic strain increment due to stress changes
$\dot{\boldsymbol{\varepsilon}}_s^e$	elastic strain increment due to suction changes
$\dot{\boldsymbol{\varepsilon}}_T^e$	elastic strain increment due to temperature changes
ε_{vm}	elastic volumetric strain at microstructural level
ε_v^p	total plastic volumetric strain
ε_{vi}^p	plastic volumetric strain related to i plastic mechanism (i= lc, β)
$\boldsymbol{\gamma}_{sM}$	elasto-plastic vector associated with macrostructural suction
$\boldsymbol{\gamma}_{sm}$	elasto-plastic vector associated with microstructural suction

$\boldsymbol{\gamma}_T$	elasto-plastic vector associated with temperature
η	stress ratio
κ_i	macrostructural elastic stiffness parameter for changes in mean stress
κ_s	macrostructural elastic stiffness parameter for changes in suction
κ_m	parameter controlling the microstructural soil stiffness
$\lambda_{(s)}$	macrostructural stiffness parameter for changes in net mean stress for virgin states of soil at suction s
λ_o, λ_d	retention curve parameters
μ	Poisson's coefficient
$\mu_{\alpha j}$	dynamic viscosity of α phase (α=l,g; j=1,2)
∇	gradient vector
θ	Lode's angle
$\theta^i_{\alpha j}$	($=\rho_{\alpha j}\omega^i_{\alpha j}$)mass of i-species in α phase per unit volume of α phase (i=w,a; α=l,g; j=1,2)
$\omega^i_{\alpha j}$	mass fraction of i-species in α phase (i=w,a; α=l,g; j=1,2)
ρ	parameter that relates cohesion and T
ρ_s	solid density
$\rho_{\alpha j}$	mass of α phase per unit of volume of α phase (α=l,g; j=1,2)
$\boldsymbol{\sigma}_t$	total stress vector. $\left\{\sigma_x,\sigma_y,\sigma_z,\tau_{xy},\tau_{xz},\tau_{yz}\right\}^T_t$
$\boldsymbol{\sigma}$	net stress vector ($\boldsymbol{\sigma}_t - \mathbf{I}p_g$)
$\boldsymbol{\sigma}^*$	stress vector at the image point
$\hat{\boldsymbol{\sigma}}$	generalized stress vector
ω_β	variable related to β mechanism (= +1 for MC path, or = -1 for MS path)
ζ	parameter controlling the rate of increase of macrostructural soils stiffness with suction.

Abbreviations and acronyms

BBM	Barcelona Basic Model
BExM	Barcelona Expansive Model
CIEMAT	Centro de Investigaciones Tecnológicas , Energéticas y Medio Ambientales (Spanish Centre of Technology, Energy, and environmental research)
CSIC-Zaidín	Consejo Superior de Investigaciones Científicas- Estación experimental del Zaidín. Spain (Spanish national agency of scientific research-experimental station at Zaidín)
Dou	Double structure case (*mock-up* model)
ENRESA	Empresa Nacional de REsiduos Radiactivos, S.A., Spain (Spanish national company for radioactive waste)
FEBEX	Full-scale Engineered Barriers in Crystalline Host Rock
MiE	Microstructure Evolution Case (*mock-up* model)
OBC	Operational Base Case (*mock-up* model)
RH	Relative Humidity
ThG	Threshold Gradient Case (*mock-up* model)
THM	Thermo-Hydro-Mechanical
THMG	*THM* plus geochemical
ToE	Thermo-osmotic Effect Case (*mock-up* model)
ULC	University of La Coruña
UPM	Universidad Politécnica de Madrid (Technical University of Madrid)

CHAPTER I

INTRODUCTION

1.1 BACKGROUND AND OBJECTIVES OF THE THESIS

The study of low permeability media has been a subject of intense research activity. The utilization of such type of materials for the isolation of waste materials underlies many of these research works. However, it is possible perhaps to identify their use as buffer in the design of high level radioactive waste disposal as the main motivation of many investigations tending to explore the *THM* (Thermo-Hydro-Mechanical) behaviour of low permeability materials. Additionally, the study of these materials is a matter of great interest in other fields, such as, petroleum exploitations, geotechnical problems and geothermal applications. The term 'low permeability' is generally applied to media with a hydraulic permeability to water of approximately 10^{-8} [m/s] and less (Neuzil, 1986).

A characteristic of low permeability materials is that the time scales are larger compared with other materials. This implies that some phenomena, generally ignored due to its small influence, can play a more relevant role when these media are studied (Carrera, 1991). Swelling clays correspond to special low permeability materials in which the physico-chemical phenomena occurring at clay particle level are dominant. In the last few years, more specific testing programmes have been performed leading to a better understanding of expansive clays behaviour. Particularly helpful have been the works in which information related to the clay fabric has been provided, revealing a strong influence of the pore structure on the *THM* behaviour of expansive materials (Villar, 2000; Cui *et al.,* 2001; Lloret *et al.*, 2003; Marcial *et al.*, 2003; Musso *et al.*, 2003).

Focusing on the problem of radioactive waste repository, most conceptual designs envisage placing the canisters, containing the nuclear waste, in horizontal drifts or vertical boreholes in deep geological media. Three groups of rocks are mainly considered as hosted formation: crystalline rocks, argillaceous rocks and salt rock. The empty space surrounding the canisters is filled by an engineered barrier often made up from compacted swelling clay. In this multi-barrier disposal concept both, the geological barrier (host rock) and the engineering barrier (backfill) should be media with very low permeability in order to achieve the required degree of waste isolation (Gens, 2003). Other functions that the barriers would accomplish are: to provide mechanical stability for the waste canister (by absorbing stresses and deformations) and to seal discontinuities in the emplacement boreholes and drifts, among others.

Significant *THM* phenomena take place in the engineering barrier and in the near field due to the combined actions of the heating arising from the canister, and the hydration coming from the surrounding rock. A crucial aspect of this problem is that many of the *THM* phenomena occurring simultaneously are strongly coupled and interact with each other in a complex way. Therefore, coupled analyses of the relevant *THM* phenomena are generally required to achieve a good understanding of these problems. In this context, coupled *THM* formulations, and the numerical codes based on them, have been widely used in the design and performance assessment studies of nuclear waste disposal (Olivella *et al.*, 1994; Gawin *et al.*, 1995; Thomas & He 1995; Gatmiri & Delage 1997, Navarro, 1997; Gens *et al.* 1998; Alonso *et al.* 1998). Regarding the inclusion of geochemical variables in the analyses, coupled *THMG* formulations have been increasingly applied in the numerical simulations of engineered barriers (Guimarães *et al.*, 1999; Thomas *et al.*, 2001; Gens *et al.*, 2003).

A common feature of the approaches cited above is the assumption of the porous medium as a single porosity material and the adoption of average properties over the elementary representative volume. But, in many cases, the low permeability media is characterized by the presence of more than one kind of voids. For instance, in many compacted soils the fabric is composed of an assembly of quasi-saturated aggregates forming a rather open structure that must be distinguished from the clay microstructure itself. In other cases, the double structure is directly related to the material used, for example in seals composed of high-density pellets with or without powder that fills the pore spaces between them. Moreover, the use of blocks to construct barriers and seals provides a further example where the blocks and the joints between them correspond to quite different structural arrangements. Sometimes the host geological medium can also be considered as a double structure material; for instance in the case of fractured rock, where the distinction between matrix and joints is basic to achieve a good representation of the phenomena. Additionally, the necessity to improve single porosity models can also be found in other fields, such as: in the study of the consolidation in fissured clays, in the exploitation of freshwater-bearing reservoirs, in geothermal system, and in petroleum reservoirs in stratified or fractured media.

In all these cases the inclusion of the different voids levels in the analyses plays a crucial role to a better understanding and explanation of the material behaviour and, evidently, when modelling is considered. Moreover, the parallel progress in: i) a deeper experimental knowledge of the materials behaviour; ii) a more compressive information about the response of low permeability media at field scale, iii) robust and accurate numerical methods for the solution of partial differential equations, and iv) potent computers, would allow the development and use of advanced formulations and constitutive models to be closer to the actual conditions and to the real material features. Consequently, this Thesis is mainly oriented to include the effect of the material fabric in the analysis and the modelling of the *THM* behaviour of low permeability media. Two main aims can be clearly distinguished: the first one is the suggestion of a relatively simple approach for double structure media and, the second one is its experimental validation. There are other additional objectives connected with these two main ones. A brief introduction to these aims is explained below.

Related to the first aim of the Thesis, a general *THM* double structure formulation developed for porous media in which two distinctive types of voids are present has been proposed. The availability of such formulation that expresses in a mathematical way the various *THM* phenomena deemed relevant, in each structural level and their main interactions, is one of the basic requirements to advance in the knowledge of the double structural material behaviour. The purpose is to extend an existing fully coupled *THM* single porosity formulation (Olivella *et al.* 1994) to the case of double structure media with the aid of the double porosity theory (Barenblatt *et al.,* 1960; Aifantis, 1980; Huyarkon, 1986; among others). In this context, the double structure medium can be idealized as a complex of two domains (one for each structural level considered in the conceptual model) linked through a leakage term. The proposal concerns the development of a double structure approach able to handle non-saturated, non-isothermal multiphase flow coupled with the medium deformations. Additionally, the possibility to integrate specific constitutive models for each one of the voids levels considered is left open. The final goal is the implementation of the formulation in a finite element code in order to solve coupled *THM* analysis.

The analyses performed in this Thesis are mainly oriented to the study of the coupled *THM* process in clay barriers. So, the study of the expansive soil behaviour is a subject of central attention. Due to the strong influence of the mechanical problem on the swelling clay behaviour, the mechanical constitutive law is a key element in the modelling of these materials. The mechanical model can be viewed as the nucleus of the double structure formulation for these materials. A general approach to analyse the mechanical behaviour of expansive clays was proposed by Gens & Alonso (1992). A fundamental characteristic of this framework is the explicit distinction of two structural levels within the material: the macrostructure, which accounts for the larger scale structure of the material and the microstructure, associated to the active clay responsible for the swelling behaviour. These two basic structural levels actually exist in many expansive soils and their inclusion in the analyses, in some cases, is crucial to understand and reproduce features of the swelling clay behaviour.

Elasto-plastic models based on the Gens & Alonso (1992) approach have been widely used as a conceptual framework to describe the behaviour of swelling materials and also to perform analyses at point integration level (Alonso *et al.* 1994, Alonso 1998; Alonso *et al.* 1999, Thomas & Cleall 1999; Lloret *et al.*, 2003). However, their inclusion and exploitation in a finite element program to solve actual boundary value problems has never been done until now. This is another of the objectives of this Thesis. A series of modifications and developments have been introduced in the model, in order to formulate the constitutive law in a more suitable form for its implementation in a numerical finite element code. With this objective, concepts of generalized plasticity theory have been proposed in the formulation of the model.

Another important aspect of the mechanical model is that the macroscopic response of the expansive soils is accomplished by considering several plastic mechanisms that can act jointly (or not). So, the governing stress-strain equations may be derived in a formal framework which considers that during loading more than one inelastic mechanism can be active. In this Thesis, concepts of multidissipative materials presented in Rizzi *et al.* (1996) have been introduced to derive the governing stress-strain relations. Additionally, in the more general case, the water potentials associated to each pores level of the clay fabric can be different. The inclusion of the non-equilibrium between water potentials could allow the explanation and the reproduction of the typical behaviour of some expansive soils. Therefore the suggested approach and its implementation in the finite element code are able to deal with such conditions of hydraulic non-equilibrium between pores level.

A critical step in the implementation of a mechanical model in a finite element program is the development of a proper algorithm to update the stresses and the internal variables of the model. An essential requisite is the accuracy of the integration scheme, in order to obtain reliable results. Considering that the mechanical law is highly non-linear and that the objective is the application of the model to solve complex *THM* and geotechnical problems, it is advisable that the integration scheme should also be efficient and robust. Taking into account these conditions, an algorithm based on the schemes proposed by Sloan's (1987, 2001) has been developed according to the particular characteristic of the double structure model. A great advantage of Sloan's schemes is that they have been widely tested in geotechnical problems, evincing their accuracy, robustness and efficiency.

The second main aim of the Thesis is related to the experimental validation of the proposed double structure approach. In that sense, experimental data generated in the framework of the FEBEX (Full-scale Engineered Barriers Experiment) project have been used in different Chapters of the Thesis. The aim of the FEBEX project is to study the behaviour of the components of an engineered barrier and the near-field of a high-level radioactive waste repository in crystalline rock (granite). The works performed in the context of FEBEX project have been very useful to achieve a better understanding of the behaviour of such kind of system. In this Thesis, the experimental data of the project have been used in two main aspects: firstly, the data of laboratory tests have been used to identify the main parameters of the constitutive laws related to the thermal and hydraulic problems and, also, to validate the mechanical constitutive law. Secondly, a large scale heating test has allowed the application of the approach to an actual case in which experimental information of the main *THM* variables are available. They are briefly described below.

Perhaps the main difficulty related to the validation of a non-standard mechanical model is the availability of experimental results that allows testing the performance of the constitutive law under different stress paths and tests conditions. In spite of the great interest focused on the study of expansive clays, it is not so easy to find in the literature a complete set of laboratory tests which allow the validation of a *THM* model as that presented in this Thesis. In that context, the laboratory works performed in the framework of the FEBEX project offered valuable information to this end. The experimental program includes comprehensive study of clay fabric, in which a clear bimodal pore distribution of the bentonite has been identified (Villar, 2000; Lloret *et al.*, 2003). Regarding the mechanical behaviour, two main types of tests were carried out: i) oedometer tests, with a wide combination of generalized loading paths; and ii) swelling pressure tests, in which the stress paths followed during wetting have been recorded (Lloret *et al.,* 2003). Although these tests do not cover all the features of the FEBEX bentonite, an effort to validate the double structure mechanical model (at least in a qualitative manner) can be attempted. Therefore, the intention is to analyse and to reproduce the main stress paths with the aim to achieve a more complete understanding of the clay behaviour under a unified and consistent framework. Additionally, availability of a set of model parameters obtained from experimental results is a crucial aspect to undertake reliable finite element simulations. On the other hand, an accidental overheating that took place in a large-scale heating test of the same project offers the possibility to check the performance of the model when a complex thermo-hydro-mechanical path is involved. The analysis of this event is particularly interesting since the FEBEX bentonite exhibits an irreversible response when the *THM* conditions prevailing before overheating are recovered. Finally, the validation of the model may be completed considering other expansive materials and other stress paths.

The *mock-up* test, a large-scale heating experiment of the FEBEX project, has also given interesting information to advance in the knowledge of expansive clays submitted to heating and hydration. It is an ongoing experiment under controlled *THM* conditions, in which the barrier is made up from blocks of compacted FEBEX bentonite (FEBEX Project, 2000). The evolution of the main *THM* variables of this experiment has been critically analysed and special attention has been placed on the explanation of the apparent decay observed in the hydration rate at advanced stages of the test. Models based on single porosity formulation could not explain this unexpected behaviour of the barrier, showing growing departures between model predictions and test data as the experiment went on (Samper *et al.*, 2001, Sánchez & Gens 2001). These discrepancies affect strongly the reliability of the long-term

prediction, specially that related to the computed time to reach the full saturation of the barrier. As it is well-known, this is a crucial unknown due to its strong impact on the long-term performance of the system and due to its influence on the repository lifetime (Güven, 1990).

Single porosity models are not able to handle properly the effect that the structure of the swelling clays could play in the hydration process. During this process the clay fabric exhibits a dynamic character (Dixon *et al.*, 1999; Cui *et al.*, 2001) that could affect strongly the kinetics of hydration, especially if confined conditions prevail. So, an objective of this Thesis is the inclusion of the clay-fabric effect in the analysis of the *mock-up* test evolution. To do that, a numerical analysis of the experiment has been performed using the double structure approach. The aim is to use a more suitable framework to simulate this problem in which two different pore levels (the macro and micro structure of FEBEX bentonite) can be clearly distinguished. This approach will allow adopting a conceptual model for the hydration of the FEBEX bentonite closer to the actual behaviour. Another aim of the simulation is to use the full version of the double structure *THM* approach to solve an actual test in which measurements are available. Thus, the validation of the double structure approach is pursued in this analysis.

In the Thesis an effort to analyse other features of the low permeability media has also been made. As commented initially, the behaviour of low porosity media is characterized by the fact that some phenomena (which are generally ignored) could play a more relevant role. Two of these phenomena can be comprised generically under the name of 'non-hydraulic flow phenomena', which include the effects of the non-Darcian behaviour and those in which the fluid flow is due to other driving forces apart from the hydraulic gradient (Neuzil *et al.*, 1986). The possibility that 'non-hydraulic flow phenomena' were responsible for the unexpected behaviour of the *mock-up* test has been explored. The aim is to propose two simple models of the *mock-up* test which incorporate two non-hydraulic flow phenomena. One of them includes a flow law with a threshold hydraulic gradient (Low 1961; Dixon *et al.*, 1999; Cui *et al.* 2001 among others) and the other considers the thermo-osmosis phenomenon (Djeran, 1993; Mitchell, 1993; Soler, 1999). The main objective of these simulations is to discuss the role that both phenomena could play in the unforeseen tendencies observed in the barrier. The intention is to use the numerical code as a tool to explore the expected response of the test when these hypotheses are taken into account and compare the models results of the main *THM* variables with the *mock-up* test measurements. Furthermore, the inclusion of these non-hydraulic flow phenomena in the simulations together with the double structure analyses performed, will allow a wider perspective of the problem observed in the barrier in the light of different phenomena that could explain, with physical bases, the evolution of this large scale heating test.

The suggested double structure *THM* formulation is general and it is not limited to study problems in which expansive materials are involved. It could be applied to analyse other kind of problems, some of them are presented in this Thesis. For instance, the problem of consolidation in fissured clays has been considered. In this material the macroscopic response under consolidation is due to the simultaneous contribution of the fissured network and of the clay pores, which have quite different properties. The existence of fissures network in an argillaceous medium shortens the path for the water flow, reducing the time for the complete consolidation. The availability of an analytical solution to this problem has allowed the numerical verification of the formulation.

Another case presented in this work is related to the petroleum exploitation by means of a water-flooding process. This problem has a particular interest when the formation of the petroleum reservoir presents a preferential flow path. The consideration of this preferential flow path is essential to a proper analysis of the problem. In this work the problem has been analysed as a multiphase flow case in which the consideration of two flow domains (formations reservoir and preferential flow path) have been incorporated at formulation level. An additional interest of this case is that the same problem was solved using a single porosity formulation in which the preferential flow path was considered explicitly in the model mesh (Guimarães, 2002; Guimarães *et al.*, 2003). So, these analyses give the opportunity to compare the performance of two different approaches that allow the inclusion of heterogeneities in a formation.

As a summary, the two main aims of this Thesis are:

- The proposal of a general *THM* approach for double structure media.

  The major effort in the developments has been directed towards the study of expansive materials. A *THM* formulation and a mechanical model, especially suitable for these materials, have been suggested.

- The experimental validation of the formulation and of the constitutive models.

  These tasks have been mainly supported by the experimental information produced in the context of the FEBEX project. In that sense, the works have been oriented to integrate all the valuable information (laboratory tests and large scale heating tests) generated in this project in order to analyse the *THM* behaviour of the FEBEX bentonite.

Other goals pursued in the Thesis correspond to:

- The application of the formulation to other kind of problems involving double structure materials. Problems related to petroleum engineering and consolidation of fissured clays have been simulated.

- The numerical analysis of other typical phenomena of low permeability media, such as, threshold gradient and thermo-osmosis effects.

- The development of an integration algorithm for the implementation of the expansive mechanical model in a finite element code.

1.2 THESIS LAYOUT

The Thesis is organized in six Chapters and four Appendixes. Each Chapter contains its own summary, introduction and conclusions. A common list with the cited references is presented after Chapter VI. The main contents of each Chapter are introduced as follows:

- Chapter II presents the main concepts related to the *THM* formulation for double structure media. The balance equations are presented in detail together with other general aspects related to the structure of the approach. The Chapter closes with two application cases; one of them is related to the consolidation of fissured clays and the other to the petroleum extraction in a heterogeneous media. Appendix A.1 gives additional information to this Chapter presenting some complementary topics.

- Chapter III introduces the mechanical constitutive model for expansive materials. A detailed description of the derivation of the strain rate equations is presented, followed by the presentation of some aspects related to the implementation of the model in the finite element CODE_BRIGHT program. Two application cases are presented, in which the capabilities of the model to reproduce and explain the responses of expansive materials are tested. Additional aspects are given in Appendix A.2.

- Chapter IV is devoted to the experimental validation of the approach. First the validation of the mechanical expansive model is presented. The results of the FEBEX laboratory tests are reproduced and interpreted using the double structure model. In the second part of the Chapter the mechanical model has been applied to reproduce a complex *THM* path due to an unexpected overheating event that took place in a large scale heating test. The final application case corresponds to the study of the hydration of a double structure material made up of a mixture of clay pellets and clay powder.

- Chapter V includes three different parts clearly distinguished. The first one introduces the *mock-up* test together with the first numerical analyses of the barrier evolution and the identification of the apparent hydration problems observed in the test. The second part presents the most significant results of the preliminary studies carried out in order to identify the sources of the hydration problems. And the third one is related to the simulation of the problem using the full *THM* double structure approach. Appendix A.4 presents additional information related to this Chapter.

- Chapter VI collects the main conclusion of the Chapters together with some suggestions for future works.

CHAPTER II

A DOUBLE-STRUCTURE *THM* FORMULATION

SUMMARY

The study of Thermo-Hydro-Mechanical (*THM*) problems in porous media is generally dealt with assuming that they possess a continuous distribution of one type of voids. However, there are some media in which, for a proper tackling of the problem, it is crucial to consider the different structural levels involved in the material fabric. In that context, this Chapter presents a coupled *THM* formulation developed to handle problems in porous media with two dominant structures of voids. Additionally, the formulation is especially suitable for cases in which the material exhibits a strong coupling between the mechanical and hydraulic problem in both media. The proposed framework assumes the presence of two porous media linked through a mass transfer term between them. In its more general form, the proposed approach allows the consideration of non-isothermal multiphase flow, coupled with the mechanical and the thermal problems. The double structure formulation has been implemented in a finite element code and it has been used to analyse a variety of problems. However, the main objective of the developments is the analysis of the near field components of a radioactive waste disposal, although the formulation is general enough and it can be applied to other kind of problems. As an example, applications related to a geotechnical problem and to a petroleum engineering case are presented in this Chapter.

2.1 PREFACE

Often, clays used as barriers in isolation schemes exhibit a double structure. For example, in many compacted soils (especially when compacted on the dry side) the fabric is composed by an assembly of quasi-saturated aggregates forming a rather open structure that must be distinguished from the clay microstructure itself. In other cases, the double structure is directly related to the material manufacture, for instance in seals composed of high-density pellets with or without powder that fills the pore spaces available due to the packing of the pellets. Figure (2.1) presents a picture of this man-made material. Moreover, the use of blocks to construct barriers and seals provides a further example where the blocks and the joints between them correspond to quite different structural arrangements. Not only that, but sometimes the host geological medium can also be considered as a double structure material, for instance in the case of fractured rock, where the distinction between matrix and joints is basic to achieve a good representation of the problem. Finally, the need to improve single porosity models can also be found in other kind of engineering problems. For instance, the consolidation process in fissured clays, the study and exploitation of freshwater reservoirs, as well as geothermal and petroleum reservoirs in stratified or fractured media require double structure formulations in some cases.

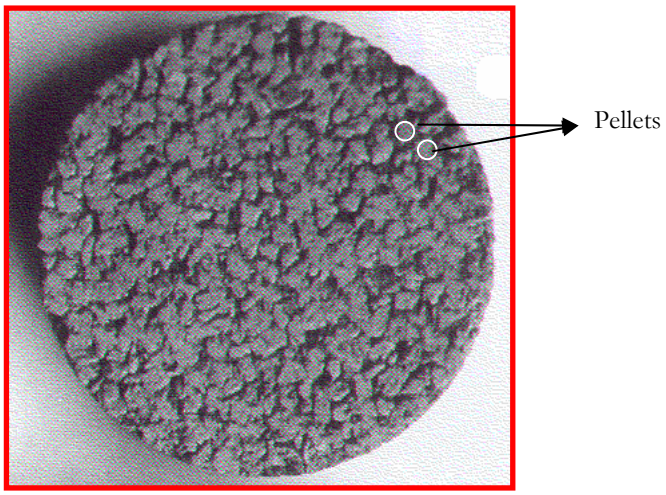

Figure 2.1. Sample made up from a mixture of clay pellets (Alonso & Alcoverro, 1999).

Generally the analysis of problems as those listed above is performed adopting a single porosity theory and average material properties over the elementary representative volume. Therefore, these kind of media are known as 'single porosity'. However, there are different techniques that allow the treatment of these problems in a more appropriate way. For instance, models based on double porosity theory can be used to solve problems in media in which the assumption of single porosity is not valid, as it is explained later on. Homogenizations techniques (*e.g.* Sanchez Palencia, 1980) have also been used to handle problems in double porosity media. The contributions of Murad & Cushman (1997, 2000) and Ichikawa *et al.* (2002) can be mentioned as reference works for clayey materials.

In this Thesis, a general coupled *THM* double structure formulation that can be potentially applied to the types of problems mentioned above has been developed. An existing fully coupled *THM* formulation for single porosity media (Olivella e*t al.*, 1994) has been extended to double structure media with the aid of the double porosity theory (Barenblatt *et al.,* 1960; Warren & Root, 1963; Aifantis, 1980; Huyarkon *et al.*, 1983; among others). The initial Barenblatt's model considers the porous medium as two interacting continuous media coupled through a leakage term, which controls the mass transfer between the two porous media. This simple idea allows applying many of the concepts and laws known for the single porosity medium to problems in which it is necessary to discriminate the different void levels involved.

The double porosity theory has been extensively used in different fields. The earlier applications are related to the modelling of ground water and oil flow in fractured reservoirs. In this line, Barenblatt *et al.* (1960) and Warren & Root (1963) used the double porosity theory in order to model saturated flows in non-deformable media. Later, the theory was extended to deformable media by Aifantis (1980) and was widely applied to model the consolidation phenomena in fissured clays (Khalili & Valliapan, 1991; Musso & Federico, 1993; Khalili *et al.*, 1999; Callari & Federico, 2000; among others), as well as to problems in deformable fractured media (Wilson & Aifantis, 1982; Bai *et al.,* 1994; Ghafouri & Lewis, 1996). The double porosity theory has been extended to the case of multiphase flows in applications related to petroleum production in fractured media (Lewis & Ghafouri, 1997). Recently the effect of temperature has also been considered in dual porosity media (Master *et al.,* 2000 and Khalili *et al.*, 2000).

The double porosity models have also been widely used to solve solute-transport problems in which the matrix diffusion is a relevant phenomenon (*e.g.* Carrera *et al.*, 1997). Another alternative way to model the double structure present in some natural media is using approaches based on double-permeability models, which have been used in the simulation of many thermal-hydrologic problems (for example, Birkholzer & Tsang, 2000). On the other hand, double structure concepts have also been used in the description of the behaviour of swelling materials (Alonso *et al.,* 1991; Gens & Alonso, 1992; Alonso, 1998).

Concerning the treatment of the mechanical problem in double porosity formulations different assumptions have been made up to now. For instance, due to the specific characteristics of some problems, the compressibility of the fissured media can be ignored and only the deformations of the matrix domain are considered (Ghafouri & Lewis, 1996; Lewis & Ghafouri, 1997 and Master *et al.,* 2000). In such case, it is assumed that the contribution of the discontinuity to the global deformations is small and it is neglected. A common hypothesis considered in the consolidation processes in fissured clays is that the behaviour of the whole medium is elastic and average mechanical properties of the media are used (Khalili & Valliapan, 1991; Musso & Federico, 1993; and Khalili *et al.,* 1999). In these works a distinction between intact and fissured bulk modulus of the material is made. A similar approach has also been used in some works related to the modelling of the coupled problem of deformation and flow in fractured rock mass (Wilson & Aifantis, 1982 and Bai *et al.,* 1994). Although these assumptions are described as different, they share the common point that only one mechanical law is defined. In contrast, in the formulation presented in this Thesis the possibility to consider specific mechanical models for each medium is left open. Special attention is also placed on the *THM* couplings involved in the governing equations.

The aim is the development of a general framework for double structure media in which different mechanical constitutive models can be incorporated for each structural level. Regarding the hydraulic and thermal problem the proposed approach is able to handle non-saturated multiphase flow in each media under non-isothermal conditions. The formulation has been implemented in the finite element code, CODE_BRIGHT (Olivella *et al.*, 1996) and it has been used to analyse a variety of problems. Special attention is placed on problems associated with the behaviour and design of unsaturated clay barriers and seals, as presented in Chapters IV and V.

This Chapter is organized as follows: first a brief introduction of the *THM* formulation and some aspects of the developed double structure approach are presented. Afterwards, the main governing equations of the problem are introduced. The Chapter closes with two application cases. More details related to the concepts presented in the Chapter are given in Appendix A.1.

2.2 THEORETICAL FRAMEWORK

2.2.1 INTRODUCTION

Olivella *et al.* (1994) proposed a fully coupled *THM* formulation for single porosity media. It is a macroscopic approach developed in the context of the continuum theory for porous media (Bear, 1972). The formulation incorporates basic thermal, hydraulic and mechanical phenomena, which can be briefly summarized as:

- Thermal: heat conduction, heat advection for all phases, and phase changes
- Hydraulic: liquid advection, gas advection, water vapour and dissolved air diffusion, water evaporation and air dissolution.
- Mechanical: dependence of strains on stresses, suction and temperature changes.

The problem is approached using a multi-phase, multi-species formulation that expresses mathematically the main *THM* phenomena expressed above in terms of:

- Balance equations.
- Constitutive equations.
- Equilibrium restrictions.

Table 2.1 summarizes these main equations and also the main variables proposed originally by Olivella *et al.* (1994). They assume that the porous media is made up of three phases: solid, liquid and gas. The liquid phase contains water and dissolved air whereas the gas phase is made up of dry air and water vapour (the dry air is considered as a single species in spite of the fact that it is a mixture of gasses).

The formulation proposed by Olivella *et al.* (1994) and the finite element code developed on it (CODE_BRIGHT) have been widely validated and employed with useful results in many *THM* applications (Olivella, 1995; Olivella *et al.*, 1996; Alonso & Alcoverro, 1999; FEBEX Project, 2000; Guimarães 2002; among others). However, for materials in which the assumption of a single continuous porosity is not realistic, a double structure approach presented herein is proposed.

A good schematic representation of the double porosity theory is presented in Ghafouri & Lewis (1996), which is reproduced in Figure (2.2). The fractured porous media is divided into two overlapping but distinct continuum, the first represents flow and deformation in the porous matrix (medium '1') while the second represents flow in the fissures (medium '2'). The coupling between both sub-domains is controlled by the leakage term. Medium 1 is composed by the solid and the pores matrix, while medium 2 correspond to the voids of the fractures. Porosity, fluid pressure, permeability, degree of saturation and other properties are considered separately for each continuum. In this conceptual model the flow problem has two global variables (for the case of saturated flow), which are the fluid pressures associated to each medium. In this case it is assumed that two structures of interconnected pores exist, with different properties and fluid that flows through them. The formulation proposed in this Thesis is able to handle this kind of a problem.

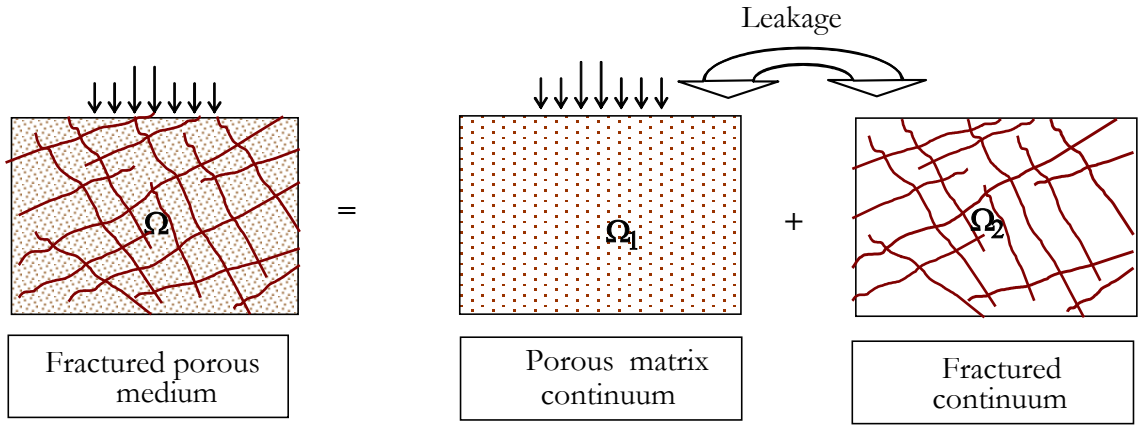

Figure 2.2. Schematic representation of double porosity concepts (Ghafouri & Lewis, 1996)

For some problems it is generally assumed that the fluid can not flow through the porous matrix and the storage capacity of the medium 1 is handled considering the water mass transfer between the two media as a local problem. In that case, there is a global unknown associated to the fluid pressure (in the scheme of Figure 2.2 generally the unknown is the fluid pressure in the fissure network) and for each node of the mesh, a local problem is solved to obtain the mass transfer between media (*i.e.* Huyarkon *et al.*, 1983). Figure (2.3) presents a conceptual representation of this model in a fractured porous medium. In this case the main flow is through the fracture and different geometrical shapes can be adopted to idealize the porous matrix domain. In this Figure, the parallel fracture model and the spherical one are presented. More details are given in Section 2.2.5 and Appendix A.1.

Table 2.1. Equation and Variable Summary (Olivella *et al.*, 1994)

Equation Name	**Variable**
Balance Equations	
Solid mass balance	ϕ
Water mass balance	P_l
Air mass balance	P_g
Energy balance	T
Momentum balance	$\dot{\mathbf{u}}$
Constitutive Equations	
Fick's law (vapour and air)	$\mathbf{i}_g^w$; $\mathbf{i}_l^a$
Dracy's law (liquid and gas)	$\mathbf{q}_l$; $\mathbf{q}_g$
Fourier's law	$\mathbf{i}_c$
Mechanical constitutive model	$\boldsymbol{\sigma}$
Liquid density	ρ_l
Gas law	ρ_g
Equilibrium restrictions	
Henry's law	ω_l^a
Psychrometric law	ω_g^w
Constrains	
$\dot{\boldsymbol{\varepsilon}} = \frac{1}{2}\left(\nabla \dot{\mathbf{u}} + \nabla \dot{\mathbf{u}}^t\right)$	$\dot{\boldsymbol{\varepsilon}}$
$\omega_l^w + \omega_l^a = 1$	ω_l^w
$\omega_g^w + \omega_g^a = 1$	ω_g^a
$s_l + s_g = 1$	s_g
$\mathbf{i}_l^w + \mathbf{i}_l^a = 0$	$\mathbf{i}_l^w$
$\mathbf{i}_g^w + \mathbf{i}_g^a = 0$	$\mathbf{i}_g^a$

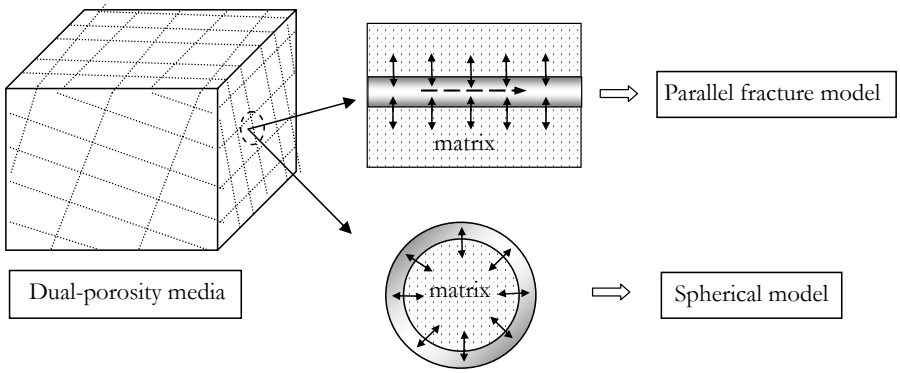

Figure 2.3. Schematic representation of double porosity concepts (Huyarkon *et al.* 1983).

A similar conceptual model can be adopted for expansive materials in which two different structures of pores can be generally distinguished. For instance, in the case of the material presented in Figure (2.1) the medium 1 is related to the solid particles of the clay pellets and the voids inside the pellets, and the medium 2 is associated with the macrostructure formed by the pellets and the macropores between pellets. Figure (2.4) presents an equivalent schematic representation of this concept.

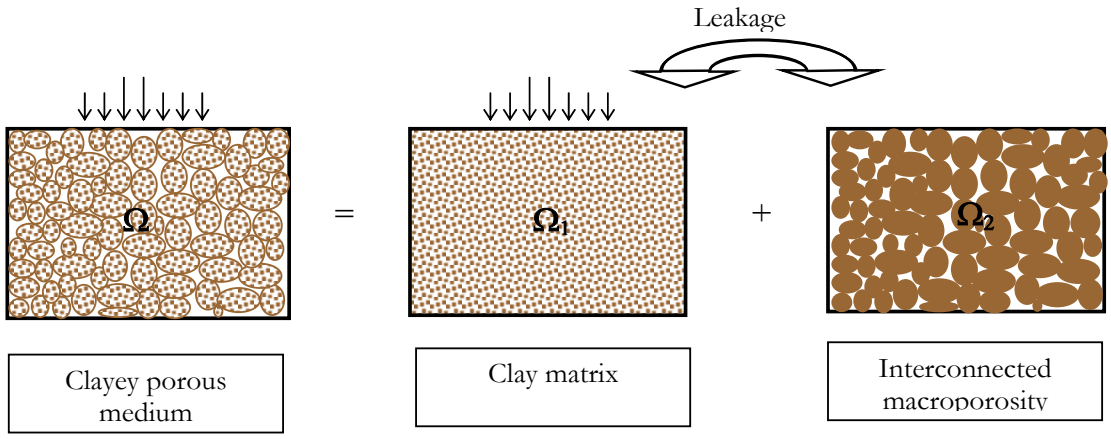

Figure 2.4. Schematic representation of double porosity concepts.

Different pores levels can also be identified in expansive clays, as it can be observed in Figure (2.5). And double porosity concepts can be applied to describe and simulate its behaviour. For instance, in the work of Alonso (1998), the hydration of this kind of material has been modelled using a double structure approach in which the water mass transfer between macro and micro pores has been considered as a local term.

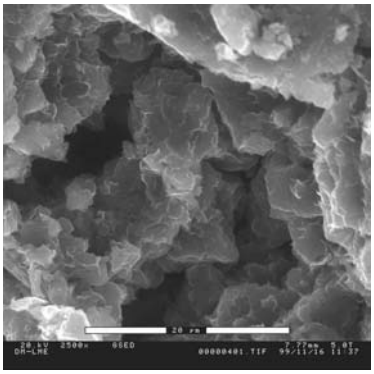

Figure 2.5. Micrograph of a compacted bentonite sample (dry density = 1.72 Mg/m^3) obtained using an environmental electron microscope (Lloret *et al.*, 2003).

Before introducing the main governing equations, some aspects of the formulation are summarized in advance, as follows:

- Two overlapping porous media have been considered in the more general case, with the definitions of two different global porosities.

$$a)\ \phi_1 = \frac{V_{v1}}{V}; \qquad b)\ \phi_2 = \frac{V_{v2}}{V}; \qquad c)\ \phi = \phi_1 + \phi_2 \tag{2.1}$$

  where ϕ_1 and ϕ_2 are the porosities related to medium one (1) and two (2) respectively, whereas ϕ is the global porosity. V_{v1} and V_{v2} are the volume of voids related to each medium (one and two) and V is the total volume.

- Multiphase, non-saturated flow in each domain is considered.

- Mass transfer processes between media are controlled through leakage terms.

- Stress-small strain constitutive laws can be defined for each porous medium.

- Thermal equilibrium between the phases and the media is assumed, this implies that only one energy balance equation is required.

- The relevant *THM* phenomena are considered in a coupled way.

- The boundary flow conditions can be prescribed on both media independently.

The theoretical framework maintains the three main parts introduced by Olivella *et al.* (1994), which are presented in the following Sections

2.2.2 BALANCE EQUATIONS

The compositional approach has been adopted to establish the mass balance equations. This approach consists of balancing the species (mineral, water and air) rather than the phases (solid, liquid and gas). In this way the phase change terms do not appear explicitly, which is particularly useful when equilibrium is assumed. In the notation, the subscript is used to identify the phase (*s* for solid, *l* for liquid and *g* for gas) and the superscript indicates the species: *w* for water and *a* for air. No symbol is attributed to the mineral species because it has been assumed that it coincides with the solid phase. The rest of the notation is indicated along this Chapter and in the Notation (pag. *xiii*).

In this approach, the macroscopic balance of any thermodynamic property π (per unit mass) is expressed by:

$$\frac{\partial}{\partial t}(\rho\pi) + \nabla.(\mathbf{j}_\pi) - f^\pi = 0 \tag{2.2}$$

where ρ is the mass density of the species per unit volume containing π, $\mathbf{j}_\pi$ is the total flux of π with respect to the reference system and f^π is the rate of production/removal of π per unit of volume. The total flux ($\mathbf{j}_\pi$) is expressed in relation to a fixed reference system, thus, this total flux may be decomposed into two components: an advective one (phase motion) and a non advective one (motion of the specie inside the phase), *i.e.*:

$$\mathbf{j}_\pi = \rho\pi\mathbf{v}_\pi + \mathbf{i}_\pi \tag{2.3}$$

where $\mathbf{v}_\pi$ is the advective volumetric flux and $\mathbf{i}_\pi$ is the non advective flux π.

2.2.2.1 SOLID MASS BALANCE EQUATION

The balance of the mineral (solid phase) can be expressed as (Olivella *et al.*, 1994):

$$\frac{\partial}{\partial t}\left(\rho_s(1-\phi)\right) + \nabla\cdot\left(\rho_s(1-\phi)\dot{\mathbf{u}}\right) = 0 \tag{2.4}$$

where ρ_s is the solid density and $\dot{\mathbf{u}}$ is the solid velocity vector.

A more convenient form of the balance equations is obtained considering the definitions of material derivate with respect to the solid velocity; which can be expressed generically as:

$$\frac{D(\circ)}{Dt} = \frac{\partial(\circ)}{\partial t} + \dot{\mathbf{u}}.\nabla(\circ) \tag{2.5}$$

Using this definition, the solid mass balance (Equation 2.4) can be expressed as:

$$\frac{D\phi}{Dt} = \frac{(1-\phi)}{\rho_s}\frac{D\rho_s}{Dt} + (1-\phi)\nabla.\dot{\mathbf{u}} = \frac{(1-\phi)}{\rho_s}\frac{D\rho_s}{Dt} + (1-\phi)\dot{\mathrm{E}}_v \tag{2.6}$$

where $\dot{\mathrm{E}}_v = \nabla.\dot{\mathbf{u}}$ is the increment of the total volumetric strain referred to the whole medium. In other words, an expression for the variation of porosity with time is obtained from solid balance. The first term refers to porosity changes due to variations in solid density and the second term reflects the porosity variations caused by volumetric deformation of the soil skeleton. Considering Equation (2.1.c), Equation (2.6) can be expressed as:

$$\begin{aligned}\frac{D\phi}{Dt} &= \frac{D\phi_1}{Dt} + \frac{D\phi_2}{Dt} = \frac{(1-\phi)}{\rho_s}\frac{D\rho_s}{Dt} + (1-\phi_1-\phi_2)\left(\dot{\mathrm{E}}_{v1} + \dot{\mathrm{E}}_{v2}\right) = \\ &= \frac{(1-\phi)}{\rho_s}\frac{D\rho_s}{Dt} + \dot{\mathrm{E}}_{v1} + \dot{\mathrm{E}}_{v2} - (\phi_1+\phi_2)\dot{\mathrm{E}}_v\end{aligned} \tag{2.7}$$

It has also been assumed that the total volumetric deformation can be written as the sum of contributions for each medium i.e. $\dot{\mathrm{E}}_v = \dot{\mathrm{E}}_{v1} + \dot{\mathrm{E}}_{v2}$. Note that $\dot{\mathrm{E}}_{v1}$ and $\dot{\mathrm{E}}_{v2}$ are the increment of the volumetric strain of the medium 1 and 2 referred to the total volume of the medium. In order to obtain porosity evolution for each medium Equations (1.a) and (1.b) are recalled and differentiated with respect to time, thus leading to:

$$a)\ \frac{D\phi_1}{Dt} = \dot{\mathrm{E}}_{v1} - \phi_1\dot{\mathrm{E}}_v; \qquad b)\ \frac{D\phi_2}{Dt} = \dot{\mathrm{E}}_{v2} - \phi_2\dot{\mathrm{E}}_v \tag{2.8}$$

With these definitions, adding Equations (2.8.a) and (2.8.b) and the solid density term, the global Equation (2.7) is recovered. It should be noted that these equations are simply a decomposition of contributions to the total variations of porosity.

2.2.2.2 WATER MASS BALANCE EQUATION

The water mass balance equations are presented for the general case of two overlapping flow domains (Figure 2.4). In this context, the total mass of water per unit volume in the porous medium *j* is expressed as: $\left(\theta^w_{lj}S_{lj} + \theta^w_{gj}S_{gj}\right)\phi_j$ (j=1, 2) where θ^w_{lj} and θ^w_{gj} are the masses of water per unit volume of liquid and gas respectively. $S_{\alpha j}$ is the volumetric fraction of pore volume occupied by the alpha phase (α=*l*,*g*).

The water flux in each phase of a medium *j* is expressed as:

$$\mathbf{j}_{lj}^{w} = \mathbf{i}_{lj}^{w} + \theta_{lj}^{w}\mathbf{q}_{lj}^{w} + \theta_{lj}^{w}S_{lj}\phi_j\,\dot{\mathbf{u}} = \mathbf{j}'^{w}_{lj} + \theta_{lj}^{w}S_{lj}\phi_j\,\dot{\mathbf{u}}\,; \qquad j=1,2 \tag{2.9}$$

$$\mathbf{j}_{gj}^{w} = \mathbf{i}_{gj}^{w} + \theta_{gj}^{w}\mathbf{q}_{lj}^{w} + \theta_{gj}^{w}S_{gj}\phi_j\,\dot{\mathbf{u}} = \mathbf{j}'^{w}_{gj} + \theta_{gj}^{w}S_{gj}\phi_j\,\dot{\mathbf{u}}\,; \qquad j=1,2 \tag{2.10}$$

where $\mathbf{j}_{lj}^{w}$ and $\mathbf{j}_{gj}^{w}$ denote the total mass fluxes of water in the liquid and gas phases, with respect to a fixed reference system, $\mathbf{i}_{lj}^{w}$ and $\mathbf{i}_{gj}^{w}$ are the non-advective fluxes of water in the liquid and gas phases. The other terms are advective and take into account the motion of the phase. The second part of the expressions corresponds to the distinction between the relative motion of the species water ($\mathbf{j}'_j$) with respect to the solid phase, and the absolute motion $\mathbf{j}_j$ with respect to a fixed reference system.

With these definitions, and considering double porosity concepts, the total water mass balance in each medium can be expressed as:

$$\frac{\partial}{\partial t}\left(\theta_{lj}^{w}S_{lj}\phi_j + \theta_{gj}^{w}S_{gj}\phi_j\right) + \nabla.\left(\mathbf{j}_{lj}^{w} + \mathbf{j}_{gj}^{w}\right) + (-1)^{j+1}\Gamma^{w} = f_j^{w}\,; \qquad j=1,2 \tag{2.11}$$

f_j^{w} is the external mass supply of water per unit volume of *j* medium and Γ^{w} is the term related to the water mass exchange between the two media, which is explained in more detail in Section 2.2.5.

In this form (Equation 2.11) the dependence of the storage term on porosity variations does not appear explicitly. To make it appear and also in order to obtain a more convenient form for programming purposes, the material derivate with respect to the solid velocity field is applied (Equation 2.5) once the fluxes given by (2.9) and (2.10) are introduced and the divergence operator applied. This leads to:

$$\begin{aligned}&\phi_j\frac{D}{Dt}\left(\theta_{lj}^{w}S_{lj} + \theta_{gj}^{w}S_{gj}\right) + \left(\theta_{lj}^{w}S_{lj} + \theta_{gj}^{w}S_{gj}\right)\frac{D\phi_j}{Dt} + \left(\theta_{lj}^{w}S_{lj} + \theta_{gj}^{w}S_{gj}\right)\phi_j\,\dot{\mathrm{E}}_v + \\ &+\nabla.\left(\mathbf{j}'^{w}_{lj} + \mathbf{j}'^{w}_{gj}\right) + (-1)^{j+1}\Gamma^{w} = f_j^{w} \qquad\qquad j=1,2\end{aligned} \tag{2.12}$$

Now, Equation (2.8) permits to express this Equation as a function of volumetric strain rate in each medium because the total volumetric strain rate term cancels out:

$$\begin{aligned}&\phi_j\frac{D}{Dt}\left(\theta_{lj}^{w}S_{lj} + \theta_{gj}^{w}S_{gj}\right) + \left(\theta_{lj}^{w}S_{lj} + \theta_{gj}^{w}S_{gj}\right)\left[\left(\frac{(1-\phi)}{\rho_s}\frac{D\rho_s}{Dt}\right)^{(2-j)} + \dot{\mathrm{E}}_{vj}\right] + \\ &+\nabla.\left(\mathbf{j}'^{w}_{lj} + \mathbf{j}'^{w}_{gj}\right) + (-1)^{j+1}\Gamma^{w} = f_j^{w} \qquad\qquad j=1,2\end{aligned} \tag{2.13}$$

2.2.2.3 AIR MASS BALANCE EQUATION

As pointed out above, it is considered the dry air as single specie and the gaseous phase is a mixture of air and water vapour. Air is also dissolved in the liquid phase. The total air content in medium j is expressed as: $\left(\theta_{lj}^{a} S_{lj} + \theta_{gj}^{a} S_{gj}\right)\phi_j$; where θ_{lj}^{a} and θ_{gj}^{a} are the masses of air per unit volume of liquid and gas respectively in the medium. The air flux in each phase of a medium is expressed as:

$$\mathbf{j}_{lj}^{a} = \mathbf{i}_{lj}^{a} + \theta_{lj}^{a}\mathbf{q}_{lj}^{a} + \theta_{lj}^{a} S_{lj}\phi_j \dot{\mathbf{u}} = \mathbf{j}'^{a}_{lj} + \theta_{lj}^{a} S_{lj}\phi_j \dot{\mathbf{u}}; \qquad j = 1,2 \tag{2.14}$$

$$\mathbf{j}_{gj}^{a} = \mathbf{i}_{gj}^{a} + \theta_{gj}^{a}\mathbf{q}_{lj}^{a} + \theta_{gj}^{a} S_{gj}\phi_j \dot{\mathbf{u}} = \mathbf{j}'^{a}_{gj} + \theta_{gj}^{a} S_{gj}\phi_j \dot{\mathbf{u}}; \qquad j = 1,2 \tag{2.15}$$

$\mathbf{j}_{lj}^{a}$ and $\mathbf{j}_{gj}^{a}$ denote the total mass fluxes of air in the liquid and gas phases, with respect to a fixed reference system, $\mathbf{i}_{lj}^{a}$ and $\mathbf{i}_{gj}^{a}$ are the non-advective fluxes of water in the liquid and gas phases. The other terms are advective and take into account the motion of the phase. They are considered in a similar way as water fluxes. With these definitions and considering double porosity concepts, the total water mass balance in each medium can be expressed as:

$$\frac{\partial}{\partial t}\left(\theta_{lj}^{a} S_{lj}\phi_j + \theta_{gj}^{a} S_{gj}\phi_j\right) + \nabla.\left(\mathbf{j}_{lj}^{a} + \mathbf{j}_{gj}^{a}\right) + (-1)^{j+1}\Gamma^{a} = f_j^{a}; \qquad j = 1,2 \tag{2.16}$$

f_j^{a} is the external mass supply of air per unit volume of *j* medium and Γ^{a} is the term related to the air mass exchange between the two media.

The final Equations for the air mass balance are obtained, once the porosity variations are introduced in the same way as done before for water balance, as follows:

$$\begin{aligned} &\phi_j \frac{D}{Dt}\left(\theta_{lj}^{a} S_{lj} + \theta_{gj}^{a} S_{gj}\right) + \left(\theta_{lj}^{a} S_{lj} + \theta_{gj}^{a} S_{gj}\right)\left[\left(\frac{(1-\phi)}{\rho_s}\frac{D\rho_s}{Dt}\right)^{(2-j)} + \dot{\mathrm{E}}_{vj}\right] + \\ &\nabla.\left(\mathbf{j}'^{a}_{lj} + \mathbf{j}'^{a}_{gj}\right) + (-1)^{j+1}\Gamma^{a} = f_j^{a} \qquad j = 1,2 \end{aligned} \tag{2.17}$$

2.2.2.4 ENERGY BALANCE EQUATION

The balance of energy is expressed in terms of internal energy. In this approach a thermal equilibrium between the phases is assumed; therefore the temperature is the same for all the phases and only one equation of total energy for a medium is required. Adding the internal energy of each phase, of each medium, the total energy for unit volume of a porous medium is obtained.

The most important processes for energy transfer in a porous medium are conduction, advection and phase change (Olivella *et al.,* 1994). Using the specific internal energies and the species mass fluxes, the energy fluxes due to the motion of phases can be written as:

$$\mathbf{j}_{E_s} = E_s \rho_s (1-\phi)\dot{\mathbf{u}} \tag{2.18}$$

$$\mathbf{j}_{E_{lj}} = \mathbf{j}'^{w}_{lj} E^{w}_{lj} + \mathbf{j}'^{a}_{lj} E^{a}_{lj} + E_{lj}\rho_{lj} S_{lj}\phi_j \dot{\mathbf{u}} = \mathbf{j}'_{E_{lj}} + E_{lj}\rho_{lj} S_{lj}\phi_j \dot{\mathbf{u}}; \qquad j = 1,2 \tag{2.19}$$

$$\mathbf{j}_{E_{gj}} = \mathbf{j}'^{w}_{gj} E^{w}_{gj} + \mathbf{j}'^{a}_{gj} E^{a}_{gj} + E_{gj}\rho_{gj} S_{gj}\phi_j \dot{\mathbf{u}} = \mathbf{j}'_{E_{gj}} + E_{gj}\rho_{gj} S_{gj}\phi_j \dot{\mathbf{u}}; \qquad j = 1,2 \tag{2.20}$$

where $\mathbf{j}'_{El}$ and $\mathbf{j}'_{Eg}$ are the advective energy fluxes with respect to the solid phase. ρ_{lj} and ρ_{gj} are the liquid and gas phase densities of the medium, E_s is the solid specific internal energy; E_{lj} and E_{gj} are specific internal energies corresponding to the liquid and gas phases respectively, that is the internal energy per unit mass of phase of the medium.

Concerning the double porosity extension, an additional hypothesis is made. Thermal equilibrium between both media is assumed; consequently, only one equation is needed for the energy balance. If either the characteristic of the problem or the experimental evidence justifies the necessity of a more detailed treatment of this equation, different temperatures in the two media can be considered. For example, in the work of Khalili *et al.* (1999) an approach considering different temperatures in either media is proposed. Using the definitions above, the energy balance equation is expressed as:

$$\begin{aligned} &\frac{\partial}{\partial t}\left[E_s \rho_s (1-\phi)\right] + \frac{\partial}{\partial t}\left[\sum_{j=1}^{2}\left(E_{lj}\rho_{lj}S_{lj}\phi_j + E_{gj}\rho_{gj}S_{gj}\phi_j\right)\right] + \\ &+\nabla.\left[\mathbf{i}_c + \mathbf{j}_{Es} + \sum_{j=1}^{2}\left(\mathbf{j}_{Elj} + \mathbf{j}_{Egj}\right)\right] = \sum_{j=1}^{2} f_j^E \qquad j = 1,2 \end{aligned} \tag{2.21}$$

$\mathbf{i}_c$ is the conductive heat flux, f_j^E are the energy supply per unit volume of medium *j*. This Equation is also transformed following a similar procedure to the explained one in Section 2.2.2.2, the final form of the energy balance equation is given by:

$$\sum_{j=1}^{2}\phi_j\frac{D}{Dt}\left(E_{lj}\rho_{lj}S_{lj}+E_{gj}\rho_{gj}S_{gj}\right)+\left(1-\phi\right)\frac{D}{Dt}E_s\rho_s+$$
$$+\left(\sum_{j=1}^{2}\left(E_{lj}\rho_{lj}S_{lj}+E_{gj}\rho_{gj}S_{gj}\right)-E_s\rho_s\right)\frac{\left(1-\phi\right)}{\rho_s}\frac{D\rho_s}{Dt}+\sum_{j=1}^{2}\left(E_{lj}\rho_{lj}S_{lj}+E_{gj}\rho_{gj}S_{gj}\right)\dot{\mathrm{E}}_{vj}+ \qquad (2.22)$$
$$+\nabla.\left[\mathbf{i}_c+\mathbf{j}_{Es}+\sum_{j=1}^{2}\left(\mathbf{j}_{Elj}+\mathbf{j}_{Egj}\right)\right]=\sum_{j=1}^{2}f_j^E \qquad j=1,2$$

2.2.2.5 MOMENTUM BALANCE (EQUILIBRIUM)

The balance of momentum for the porous medium reduces to the equilibrium equation for total stresses, if inertial terms are neglected:

$$\nabla.\boldsymbol{\sigma}+\mathbf{b}=0 \qquad (2.23)$$

where $\boldsymbol{\sigma}$ is the stress tensor and $\mathbf{b}$ the vector of body forces. This assumption is usually accepted because both velocities and accelerations are small, yielding terms that are negligible in comparison with the stress terms (Gens & Olivella, 2001). Through an adequate constitutive model, the equilibrium equation is transformed into a form expressed in terms of the solid velocities, fluid pressures and temperatures. The assumption of small strain rate is also made. Additionally, it is assumed that the total stresses are macroscopic and the same in the two media. In contrast, strains, which are caused by net stress changes (total stress minus fluid pressure), suction changes and temperature changes, are different in each medium.

A possible decomposition of strains is:

$$\dot{\boldsymbol{\varepsilon}}=\sum_{j=1,2}\dot{\boldsymbol{\varepsilon}}_j=\sum_{j=1,2}\dot{\boldsymbol{\varepsilon}}_j^{e}+\dot{\boldsymbol{\varepsilon}}_j^{p}+\dot{\boldsymbol{\varepsilon}}_j^{o}\;; \qquad j=1,2 \qquad (2.24)$$

where $\dot{\boldsymbol{\varepsilon}}_j^{e}$ is the elastic strain rate due to stress, $\dot{\boldsymbol{\varepsilon}}_j^{p}$ is the plastic strain rate and $\dot{\boldsymbol{\varepsilon}}_j^{o}$ identifies generically the strain rate due to changes in fluid pressures or temperature. Deformations due to viscoplastic or creep behaviour can be added in Equation (2.24). Hence, $\dot{\boldsymbol{\varepsilon}}$ is the total strain rate, which is related with solid velocities through the compatibility conditions that can be written as:

$$\dot{\boldsymbol{\varepsilon}}=\frac{1}{2}\left(\nabla\dot{\mathbf{u}}+\nabla\dot{\mathbf{u}}^{t}\right) \qquad (2.25)$$

The equilibrium of total stresses stands for the whole medium while strains will decompose in different contributions for each medium and this depends on the mechanical constitutive model adopted. The general form of the constitutive equation is described below and, particular models are used in the application examples.

2.2.3 CONSTITUTIVE EQUATIONS

The constitutive equations establish the link between the unknowns and the dependent variables. There are several categories of dependent variables depending on the complexity with which they are related to the unknowns. Here, some of the basic constitutive laws are presented, divided in thermal, hydraulic and mechanical. In spite of this distinction between the three basic components of the problem, the constitutive equation provides in fact the links that couple the various phenomena considered in the formulation (Gens & Olivella, 2001). The governing equations are finally written in terms of the unknowns when the constitutive equations are substituted in the balance equations.

2.2.3.1 THERMAL CONSTITUTIVE EQUATIONS

Heat conduction is assumed to be governed by Fourier's law:

$$\mathbf{i}_c = -\lambda \nabla T \tag{2.26}$$

where λ is the thermal conductivity of the whole porous medium. For instance, empirical observations (FEBEX Report, 2000) have shown that a reasonable approximation for FEBEX bentonite can be obtained by adopting the geometric mean of the thermal conductivities of the three phases; in that case:

$$\lambda = \lambda_s^{(1-\phi)} \lambda_l^{\phi S_l} \lambda_g^{\phi(1-S_l)} = \lambda_{sat}^{S_l} \lambda_{dry}^{(1-S_l)} \tag{2.27}$$

where:

$$\lambda_{sat} = \lambda_s^{(1-\phi)} \lambda_l^{\phi}; \qquad \lambda_{dry} = \lambda_s^{(1-\phi)} \lambda_g^{\phi} \tag{2.28}$$

and:

$$S_l = \frac{S_{l_1}\phi_1 + S_{l_2}\phi_2}{\phi} \tag{2.29}$$

More details about the thermal constitutive laws can be found elsewhere (Olivella *et al.,* 1994; Gens & Olivella, 2001; CODE_BRIGHT User's Manual, 2004).

2.2.3.2 HYDRAULIC CONSTITUTIVE EQUATIONS

In the case of two overlapping flow domains, advective fluxes of fluid phase in each medium will be computed using generalized Darcy's law (Bear, 1972) which is expressed as:

$$\mathbf{q}_{\alpha j} = -\mathbf{K}_{\alpha j}\left(\nabla P_{\alpha j} - \rho_{\alpha j}\mathbf{g}\right); \qquad \alpha = l, g \;;\; j = 1,2 \tag{2.30}$$

where P_α is the pressure of α phase in the *j* medium. $\mathbf{K}_\alpha$ is the permeability tensor of α phase in the *j* medium, evaluated as:

$$\mathbf{K}_{\alpha j} = \mathbf{k}_j \frac{k_{r\alpha j}}{\mu_{\alpha j}}; \qquad \alpha = l, g \;;\; j = 1,2 \tag{2.31}$$

where $\mathbf{k}_j$ is the intrinsic permeability tensor for medium *j*, that depends on its pore structure, generally, through the medium porosity. Different laws are available to model this dependence, which may be selected according with the problem handled. μ_{α_j} is the dynamic viscosity of the α phase in the medium *j*. Finally, $k_{r\alpha_j}$ is the α phase relative permeability of medium *j*. Also for this model there is many laws available (CODE_BRIGHT User Manual's, 2004). In general terms, for each medium it can be expressed as a function of the phase degree of saturation.

$$k_{r\alpha j} = f\left(S_{r\alpha j}\right); \qquad \alpha = l, g \;;\; j = 1,2 \tag{2.32}$$

The non-advective fluxes of species inside the fluid phases in each porous medium are computed through Fick's law, which expresses them in terms of gradients of mass fraction of species through a hydrodynamic dispersion tensor:

$$\mathbf{i}^i_{\alpha j} = -\mathbf{D}^i_{\alpha j}\nabla\omega^i_{\alpha j}; \qquad i = w, a; \quad \alpha = l, g; \quad j = 1,2 \tag{2.33}$$

where $\mathbf{D}^i_\alpha$ is the dispersion tensor of the medium, and ω the mass fraction of *i* species in α phase (Olivella *et al.,* 1994; CODE_BRIGHT User's Manual, 2004).

Finally, the retention curve establishes the link between the saturation degree of the medium and the water potential.

2.2.3.3 MECHANICAL CONSTITUTIVE EQUATION

A general expression for this law is presented here. Generically, a *THM* constitutive equation, showing explicitly the contributions of strains, temperature and fluid pressures can be expressed as:

$$\dot{\boldsymbol{\sigma}}_j = \mathbf{D}_j \dot{\boldsymbol{\varepsilon}}_j + \mathbf{f}_j \dot{s}_j + \mathbf{t}_j \dot{T}_j ; \qquad j = 1,2 \tag{2.34}$$

where $\boldsymbol{\sigma}_j$ is the constitutive stress (net or effective stress), $\boldsymbol{\varepsilon}_j$ is the strain vector, s_j is a variable related to the fluid pressures, $\mathbf{D}_j$ is the constitutive stiffness matrix, $\mathbf{f}_j$ is the generic constitutive vectors relating the changes in the fluid pressures and stresses and $\mathbf{t}_j$ is the constitutive vector relating stresses and temperature.

Note that although the total stress is common for medium 1 and 2, the constitutive stress may be different because the fluid pressures may be different. Therefore, the two equations corresponding to the two media considered reduce to a single equation (to be introduced in the equilibrium of stresses, Equation 2.23) as the sum of strains is performed and the equation is solved for the total stress. Different mechanical laws can be incorporated to describe the material behaviour, in Chapter III a mechanical model for expansive materials is presented in detail.

2.2.3.4 PHASE PHYSICAL PROPERTIES

The properties of the fluid phases appear in the balance equations and in the constitutive law. In general, they depend on the composition of the phases and on the state variables (temperature and fluid pressures). Some of them are introduced in Appendix A.4. A complete description of the adopted laws can be found elsewhere (Olivella, 1995; Gens & Olivella, 2001 and CODE_BRIGHT User's Manual, 2004).

2.2.4 EQUILIBRIUM RESTRICTIONS

It is assumed that phase changes are rapid in relation to the characteristic times typical of these types of problems. Therefore, they can be considered in local equilibrium, giving rise to a set of equilibrium restrictions that must be satisfied at all times. Also, the adopted compositional approach has the advantage that the phase change terms do not appear explicitly and the number of equations is thereby reduced. Equilibrium restrictions are given for the concentration of water vapour in gas phase, which is computed through the psychometric law; and for the concentration of dissolved air in liquid phase, which is evaluated by means of Henry's law (Appendix A.4; Olivella, 1995).

2.2.5 MASS TRANSFER BETWEEN MEDIA

In Equations (2.11) and (2.16) the term Γ^i (i=*w,a*) controls the mass transfer between media. A simple model for this term can be expressed as:

$$\Gamma^i = \gamma\left(\Psi_1 - \Psi_2\right) \tag{2.35}$$

where γ is the leakage parameter and Ψ_j (j=1, 2) represents the thermodynamic force involved in the mass transfer. When water mass transfer is considered, the total water potential (which for the more general case corresponds to the chemical water potential) is the variable involved in Equation (2.35). In some cases, due to the characteristics of the problems, variables related to the total water potential can be adopted as main responsible of the mass transfer process. For instance, in the examples presented in Section 2.4.1 and Section 2.4.2 the fluid pressures are adopted as the variables which control the mass transfer between media. On the other hand, in the work of Ma & Hueckel (1992) a special case of mass transfer of water between macro and micro structure of a clayey material has been modelled as driven by temperature differences. Here, this term is presented in a generic form. In each application and according with the specific characteristics of the problem, the thermodynamic force involved in the mass transfer is specified.

According to Barenblatt *et al.* (1960), the process of liquid transfer between media takes place essentially under a sufficiently smooth change of pressure, and therefore it can be assumed that this pressure is quasi-stationary, hence the name of quasi-steady models (*e.g.* Equation 2.35). In some works, the leakage parameter (γ) is associated to geometric characteristics of the media, such as: the specific surface of the matrix block (Barenblatt *et al.,* 1960); or the number of fractures and the fracture intervals (Warren & Root, 1963); or the average size of clay bocks (Callari & Federico, 2000). More details are presented in Appendix A.1. A more refined treatment of this term can be made through unsteady models (*i.e.* Huayakorn *et al.,* 1983). Considering the schematic representation of Figure (2.3), in the unsteady models, the fluid interaction at the interface between both media is considered solving a 1-D diffusion equation for an idealized geometry of the matrix pores (Streltsova-Adams, 1978; Huyakorn *et al.,* 1983, Kazemi *et al.,* 1976). In the formulation proposed herein, the two kinds of models can be potentially used; the selection will depend on the requirements of each problem.

2.3 NUMERICAL IMPLEMENTATION

The formulation has been implemented in the finite element program CODE_BRIGHT, which is a tool designed to analyze numerically coupled *THM* problems in geological media. One unknown (state variable) is associated with each of the balance equations presented. The unknowns are obtained by solving the system of PDE's (Partial Differential Equations) numerically in a coupled way. From state variables, dependent variables are calculated using the constitutive equations or the equilibrium restrictions.

The same procedure suggested in Olivella *et al.* (1996) has been followed for the numerical treatment of the different terms of the balance equations. The first step is the approximation of the material derivate with respect to the solid as an eulerian derivate, owing to the assumption of small strain rate. Herein, the Equation (2.13) is presented as an example:

$$\begin{aligned} &\phi_j \frac{\partial}{\partial t}\left(\theta^w_{lj} S_{lj} + \theta^w_{gj} S_{gj}\right) + \left(\theta^w_{lj} S_{lj} + \theta^w_{gj} S_{gj}\right)\left[\left(\frac{(1-\phi)}{\rho_s}\frac{\partial \rho_s}{\partial t}\right)^{(2-j)} + \dot{\varepsilon}_{vj}\right] + \\ &+\nabla.\left(\mathbf{j}^w_{lj} + \mathbf{j}^w_{gj}\right) + (-1)^{j+1}\Gamma^w = f^w_j \qquad\qquad j = 1,2 \end{aligned} \tag{2.36}$$

In a similar way the other balance equations have been considered. Details related to the discretization of the problem and the numerical technique used can be found in Olivella *et al.* (1996). In summary, it can be mentioned that the numerical approach can be viewed as divided into two parts: spatial and temporal discretization. Galerkin finite element method is used for the spatial discretization while finite differences are used for the temporal discretization. The discretization in time is linear and an implicit scheme is used. Finally, since the problem presented here is non-linear, the Newton-Raphson method was adopted as iterative scheme.

As a main feature of the numerical approach it can be mentioned that it can use a wide library of elements with segments, triangles, quadrilaterals, tetrahedrons, triangular prisms and quadrilateral prisms. Linear interpolation functions and quadratic interpolation functions for some elements are also available. Analytical integration is used for segments, triangles and tetrahedrons. Numerical integration is used for quadrilateral, triangular prisms (6 points) and quadrilateral prisms (8 points). For the mechanical problem, selective integration is used for quadrilateral and quadrilateral prisms (this means that the volumetric part is integrated with a reduced quadrature of 1 point). Finally, for all elements the flow equations are solved using element-wise and cell-wise approximations (Olivella, 1995; Olivella *et al.*, 1996).

Finite differences and an implicit scheme are used for time integration. The program has an automatic discretization of time. Reduction of time increment may be caused by excessive variation of unknowns per iteration or to excessive number of iterations to reach convergence or if the correction is larger than in the previous iteration (more details in CODE_BRIGHT User's Manual, 2004). CODE_BRIGHT is a FORTRAN code.

Regarding the boundary conditions of the mechanical problem, forces and displacement rate can be enforced in any spatial direction and at any node. In the hydraulic problem, mass flow rate of water and dry gas can be prescribed at any node, and liquid/gas pressure can be also enforced at any node. Finally, regarding the thermal problem, heat flow and temperature can be prescribed at any node of the mesh (Olivella, 1995; CODE_BRIGHT User's Manual, 2004).

2.4 APPLICATION CASES

To illustrate the performance of the formulation, two application cases will be presented in this section. The first one corresponds to the verification of the numerical implementation of the formulation using an analytical solution available for the consolidation phenomena on fissured clays. In the second case, the modelling of a multiphase flow problem related to petroleum engineering is analysed and compared with known results of this problem.

2.4.1 CONSOLIDATION OF FISSURED CLAYS

In highly fissured clays two kinds of voids can be clearly distinguished: the voids associated to the fissures system and the pores corresponding to the clay matrix. In this material the macroscopic response under consolidation is due to the simultaneous contribution of the fissures network and of the clay pores, which have quite different properties. This implies that conventional consolidation theories, such as: Terzaghi's theory (for one dimensional consolidation) or Biot's theory (for three dimensional consolidation) have several limitations to reproduce the material response, because they consider average material properties (such as: porosity, permeability and compressibility). This has motivated the use of more sophisticated and proper formulations that allow the consideration of the specific characteristics of this problem (Khalili & Valliapan, 1991; Musso & Federico, 1993; Khalili *et al.,* 1999 and Callari & Federico, 2002).

There are analytical solutions obtained using concepts of double porosity. In this work, the closed form obtained by Musso & Federico (1993) has been used in order to verify the numerical implementation of the formulation in the CODE_BRIGHT program. The Musso & Federico (1993) model considers saturated flow in two overlapping media, with one fluid pressure associated to each medium: P_1 for the fissure network and P_2 for the clay pores. Figure (2.6) shows the scheme presented by Callari & Federico (2000) in which the two media and the respective fluid pressures can be distinguished. Both media are linked through a leakage term and the rate of fluid transfer is proportional to the fluid pressures differences.

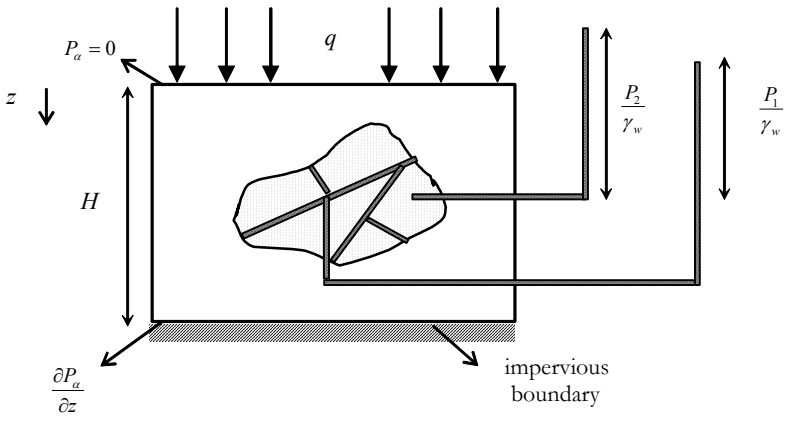

Figure 2.6. Scheme of the consolidation phenomena on fissured clays (Callari & Federico, 2000).

Concerning the mechanical problem, in the analytical solution it is assumed a reversible behaviour of the whole porous medium with an elastic law that expresses the dependence of volumetric deformations on the mean effective stress, p (Musso & Federico, 1993; Callari & Federico, 2000). For the case of double poro-elastic media, it can be defined as:

$$p = p_t - \left(\delta_1 P_1 + \delta_2 P_2\right) \tag{2.37}$$

where p_t is the total mean stress, δ_1 and δ_2 are two coefficients evaluated in the formulation by these authors as (Musso & Federico, 1993):

$$\delta_1 = 1 - \frac{K}{K^*} \tag{2.38}$$

$$\delta_2 = \frac{K}{K^*}\left(1 - \frac{K^*}{K_s}\right) \tag{2.39}$$

where K^* is the drained bulk modulus of the porous medium without fissures (matrix), K_s is the bulk modulus of the grains and K is the drained bulk modulus. The model recovers the case of single porosity medium in the absence of fissures, $K=K^*$ and $\delta_1 = 0$.

Regarding the flow problem, it is assumed that the seepage flow in each medium is governed by Darcy's law, with constant permeability in each medium. Considering these assumptions and neglecting gravity and inertial forces, the governing equations for the case of one-dimensional consolidation under a uniform load are obtained from the general balance of water equation (Equation 2.11 for saturated conditions). After some algebraic operations, the two partial differential equations which express the continuity of flows coupled with the mechanical problem can be written in terms of the excess of pore pressures p_1 and p_2:

$$\frac{k_1}{\gamma_w}\frac{\partial^2 p_1}{\partial z^2} = \left(m_v\delta_1^2 + \gamma\right)\frac{\partial p_1}{\partial t} + \left(m_v\delta_1\delta_2 - \gamma\right)\frac{\partial p_2}{\partial t} + \gamma'\left(p_1 - p_2\right) \tag{2.40}$$

$$\frac{k_2}{\gamma_w}\frac{\partial^2 p_2}{\partial z^2} = \left(m_v\delta_1\delta_2 - \gamma\right)\frac{\partial p_1}{\partial t} + \left(m_v\delta_2^2 + \gamma\right)\frac{\partial p_2}{\partial t} - \gamma'\left(p_1 - p_2\right) \tag{2.41}$$

where k_1 is the permeability of the fissured network, k_2 the permeability of the clay matrix, z is the vertical coordinate, m_v the oedometric compressibility, γ' is the leakage parameter (detailed in Appendix A.1) and γ is evaluated through:

$$\gamma = \frac{1}{K_*}\left(1 - \frac{K}{K_*}\right) \tag{2.41}$$

The one-dimensional consolidation coefficient (C_v) of the porous system is obtained as:

$$C_v = \frac{k_2}{\gamma_w m_v} \tag{2.43}$$

Physical interpretation of the phenomenological coefficient and properties of the double porosity materials can be found in Wilson & Aifantis (1982). Regarding the experimental determination of the main material parameters, tests conducted at different scales were proposed in order to identify them.

The closed form solution obtained by Musso & Federico (1993) is expressed in terms of the non-dimensional excess of pores pressures (u_1 and u_2), defined as a ratio of excess of pores pressures over the uniform pressure increment (q). Details are introduced in the Appendix A.1, here only the final expression to evaluate the global consolidation ratio (U) is presented:

$$U = \int_0^1 \left(1 - \delta_1 u_1 - \delta_2 u_2\right) dZ \tag{2.44}$$

$$Z = \frac{z}{H} \tag{2.45}$$

where u_1 and u_2 are evaluated with Equations (A1.1) and (A1.2) respectively (Appendix A.1), and H is the thickness of the consolidating material. The solution can be represented in terms of U versus the time factor (T_v) for different values of the non-dimensional parameter (λ_f), which is a measure of the degree of the medium fracturation, which are expressed as:

$$T_v = \frac{C_v t}{H^2} \tag{2.46}$$

$$\lambda_f = \frac{H}{s_b} \tag{2.47}$$

where s_b is a linear dimension that characterizes the size of the clay blocks.

Figure (2.7) presents the numerical results using CODE_BRIGHT, together with the analytical solution. The one-dimensional solution for the single porosity consolidation of the intact material is also presented. As expected in double porosity materials, the consolidation occurs faster than in the case of single porosity media. The comparisons between numerical outputs and analytical results indicate a very good performance of the model.

The three characteristic stages of consolidation in fissured clays can be identified (Khalili *et al.,* 1999): the first stage is controlled by the network of fissures with a fast initial drainage, the second corresponds to a transition stage with a gradual transfer of fluid from the clay pores to

the fissures system, and the third period involves the delayed dissipation of the excess of pore pressure of the clay matrix. It can be seen that the second stage is more or less marked depending on the value of λ_f. In the case of highly fissured media (high λ_f) the fissures shortens the length of the path of water, thus reducing the time for complete consolidation, with a global response controlled by the fissures network.

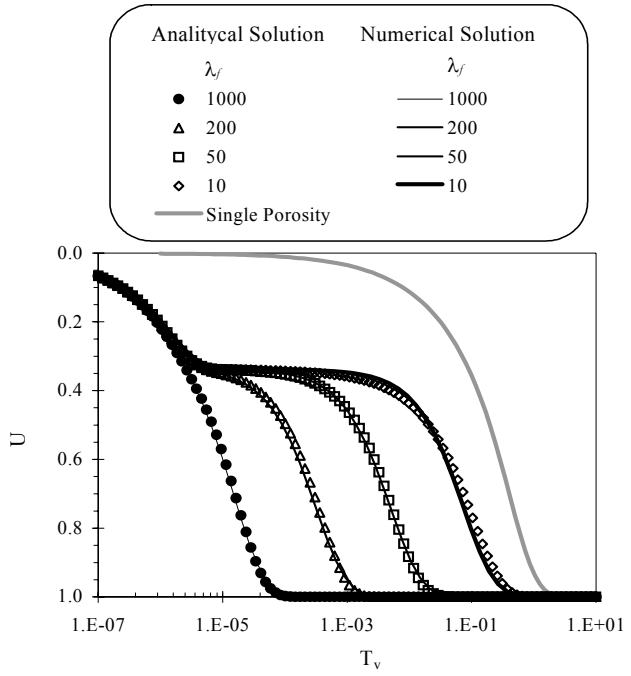

Figure 2.7 Comparisons between model results and analytical solutions for the problem of consolidation in double porosity media.

2.4.2 MULTIPHASE FLOW IN A HETEROGENEOUS MEDIUM

As commented above, the double porosity theory is especially well suited to deal with problems in porous media in which the fluid flow is characterized by the presence of a preferential path, either due to the existence of a more permeable layer, in the case of stratified media, or due to the presence of joints and discontinuities, in the case of a fractured medium. A multiphase flow problem related to petroleum engineering in a porous medium with a preferential flow path is analysed in this section. It is a very simple model and it is mainly oriented to check the capabilities of the formulation to handle this kind of problem in which various fluid pressures are the unknowns. An additional advantage of this case is given by the fact that the problem under study was previously solved using this same program (CODE_BRIGHT) with a single porosity model, in which a more permeable layer has been explicitly considered in the model mesh (Guimarães, 2002; Guimarães *et al.*, 2002). It provides an opportunity to compare the performance of these two different kinds of approaches.

Water-flooding is one of the main oil recovery processes being applied in many reservoirs around the world. A problem usually associated with this exploitation technique is the presence of a preferential path for water flow from the injector well to the producer well. Bailey *et al.* (2000) present a detailed study on the different problems observed when the oil production is stimulated injecting water (generally sea water) in the injector well.

One of the major aspects which influence the producer well performance, in multilayer media, is the layer permeability contrasts. In that work (Bailey *et al.,* 2000) different diagnostic plots are proposed to help the determination of the specific kind of problem by making comparisons with known behaviour patterns. Figure (2.8) presents one extreme case, which corresponds to the presence of a fracture or a very high permeability layer. This picture shows the diagnostic log-log plot of Water/Oil Ratio (*WOR*) versus time. The very rapid increase in the *WOR* observed after the day 1000 is attributed to the fast flow of water through a preferential path (for example a fault or fracture) which can occur at any time during the well story. According to Bailey *et al.* (2000), values of *WOR* between 1 to 10 are normal when water-flooding technique is applied in stratified media. When *WOR* becomes larger than 10 the well exploitation is not normally economically profitable and some remedial actions are necessary.

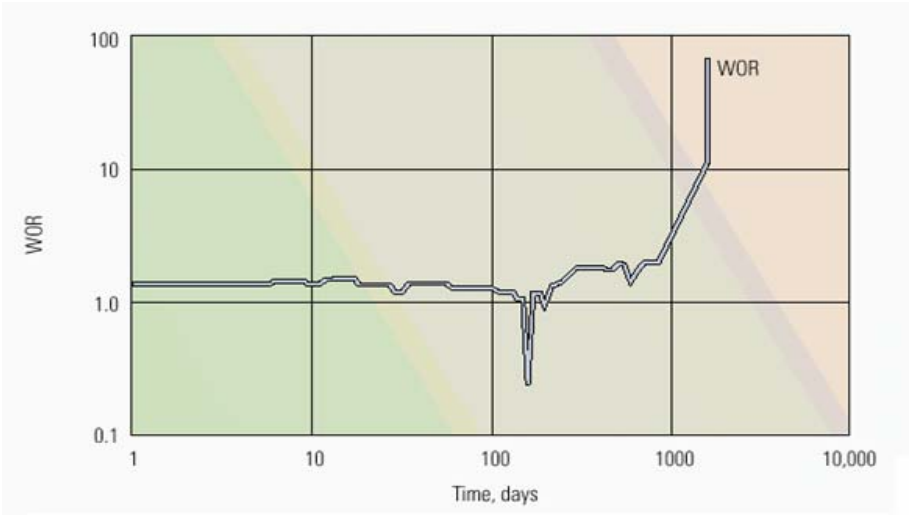

Figure 2.8. Diagnostic plot indicating the presence of a preferential flow path (Bailey *et al.,* 2000).

The double structure formulation presented in this Chapter can simulate naturally this kind of problem, because it is able to handle multiphase flow and also to consider two different flow domains, with different material properties in each one. In this case, one medium of the double porosity model can correspond to the formation (oil reservoir) with a low permeability and the other medium can be related to a fracture or a layer with a high permeability, associated to the preferential flow path. There is not need to consider in a discrete way this last medium in this kind of approach, because it is considered at a formulation level.

A problem of this type was simulated by Guimarães (2002) and Guimarães, *et al.* (2003); and was mainly oriented to analyse the influence on the water-flooding process of the chemical reactions between the different kinds of waters involved in the problem. As explained by Sorbie & Mackay (2000), as well as displacing oil, the injection water (*IW*) will also displace and mix either with the connate water (*CW*), in the mobile oil zone of the reservoir, or with the aquifer water, depending on where the injection well is completed.

Generally the *IW* and the *CW* are chemically incompatible inducing a massive precipitation of minerals in the porous matric (especially in the proximities of the well producer) and inducing also the accumulation of incrustations on the well tubing (Sorbie & Mackay, 2000; and Guimarães, 2002). The presence of preferential paths is also very important when these chemical reactions are studied, because they induce a mixing of the incompatible waters in the proximity of the well producer more quickly and also accelerate the obstruction of the tubing well due to the minerals precipitation (Guimarães, 2002).

Figure (2.9) presents a scheme of the problem solved by Guimarães (2002) in which a high permeable layer is placed in between the more impermeable layers of the reservoir. In that work it was also assumed that the flow is mainly horizontal, adopting a vertical component of the permeability 10 times lower than the horizontal one (*i.e.* $k_h = k_v * 10$). The problem was solved using a 2D model with 8000 (200x40) rectangular elements with a size of 2m x 0.25m. The more permeable layer was explicitly considered in the mesh with its different permeability.

Here, the intention is to solve the same problem using a double structure multiphase approach with two liquids phases: water (w) and oil (o) in each medium (reservoir and more permeable layer). The problem has been simulated using a 1D double porosity model with 200 segment elements, with the same horizontal size considered in Guimarães (2002) (*i.e.* 2m).

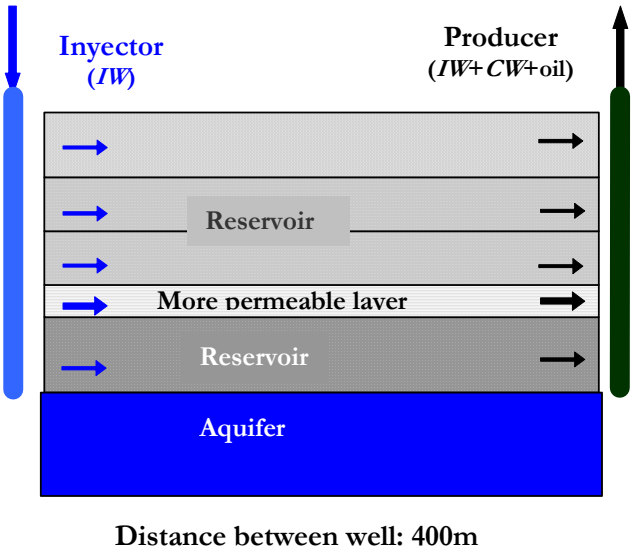

Figure 2.9. Scheme of the analyzed problem.

In order to compare the performance of both models (the single and the double porosity models) the initial conditions and properties have been adopted as close as possible to the ones assumed by Guimarães (2002). In that sense the porous media have been considered as non-deformable and a constant temperature of 25º C during the analysis has been assumed. Additionally, neither the vapour water nor the dissolved air is taken into account.

The laws for liquid phase density adopted by Guimarães (2002) have been considered, which are indicated as follows:

$$\rho_w = 1002,6 \exp(4,3\times10^{-4}(P_w - 0.1)) \tag{2.48}$$

$$\rho_o = 870 \exp(4,81\times10^{-4}(P_o - 0.1)) \tag{2.49}$$

A constant value for the water viscosity (μ_w) of 8.2x10^{-10} MPa.s and a constant oil viscosity (μ_o) of 1.7x10^{-8} MPa.s have been adopted. The same retention curve and relative permeability law have been adopted for the different layers of the reservoir (including the more permeable layer), which are presented in Figures (2.10) and (2.11) respectively. A version of the van Genuchten model has been adopted for the water retention curve, given by:

$$S_e = \frac{S_w - S_{wr}}{S_{ws} - S_{wr}} = \left[1 + \left(\frac{P_o - P_w}{P}\right)^{\frac{1}{1-\lambda_o}}\right]^{\lambda_o} \quad ; \quad S_o = 1 - S_w \tag{2.50}$$

$$S_{ws} = 0.8; \quad S_{wr} = 0.2; \quad P = 0.1; \quad \lambda_o = 0.6$$

where S_w is water degree of saturation and S_o is the oil degree of saturation. S_{ws}, S_{wr}, P and λ_o are model parameters. Power laws have been adopted for the relative permeability models, which are given by:

$$\begin{array}{ll} k_{rw} = S_e^{\,n}; & k_{ro} = (1 - S_e)^n \\ n = 2 & n = 2 \end{array} \tag{2.51}$$

The problem has been solved considering two flow domains, with the following intrinsic permeability of the media: for the preferential path, a value of k_{o2} = 2.5x10^{-12} m^2 has been adopted, which is the same value of permeability adopted for the more permeable layer in the work of Guimarães (2002), and, for the reservoir, an average value of k_{o1} = 4.0x10^{-13} m^2 has been assumed.

A very low value of the leakage parameter has been adopted, γ' = 1.0x10^{-20} kg s^{-1} m^{-3} MPa^{-1}. As in that work, it is considered that the injector well does not reach the aquifer. A uniform value of porosity of 0.2 has been adopted for both media.

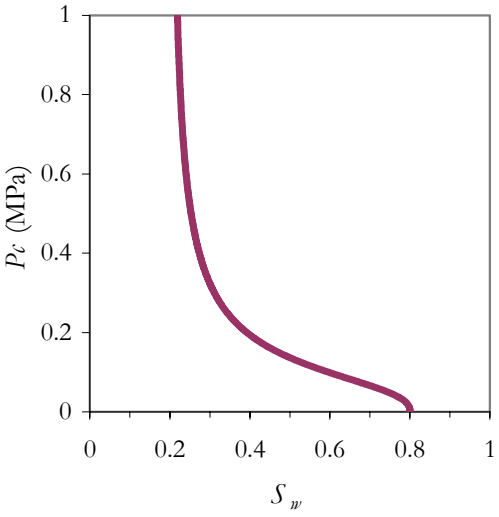

Figure 2.10. Adopted retention curve

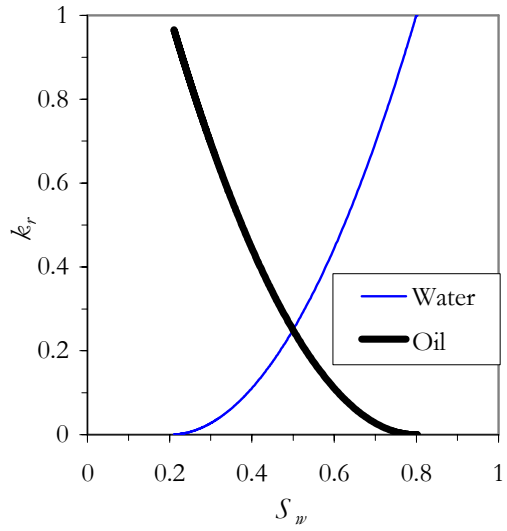

Figure 2.11. Adopted relative permeability curves

The same initial conditions assumed by Guimarães (2002) have been adopted, that is, an initial water pressure (P_w) of 30 MPa and an initial oil pressure (P_o) of 30.3 MPa. This implies a constant and uniform capillary pressure (P_o-P_w) of 0.3 MPa in all the mesh and for both media. According with the water retention curve adopted, this capillary pressure corresponds to an initial water saturation degree of 0.31. Regarding the boundary conditions in the injector well, the water is injected at a pressure of 38 MPa. As in Guimarães (2002), it is assumed that in the producer well the water and the oil have the same pressure of 30.3 MPa. These boundary conditions are prescribed on both media.

Figures (2.12) and (2.13) present the results obtained by Guimarães (2002) using the 2D single porosity model. Figure (2.12) shows the time evolutions of the fractional flows, which are typical indicators used in petroleum engineering, and have been evaluated through the following expressions:

$$f_w = \frac{Q_w}{Q_w + Q_o}; \qquad f_o = \frac{Q_o}{Q_w + Q_o}; \qquad f_w + f_o = 1 \tag{2.52}$$

where the fractional flows for the water (f_w) and for the oil (f_o) are written in function of the total (*i.e.* sum of both media) volumetric flows in the producer well (Q_w and Q_o). According to Guimarães (2002), for the given conditions of this problem, the *WOR* can be estimated as the ratio between the water and the oil fractional flows (*i.e.* $WOR = f_w/f_o$). Figure (2.13) shows the time evolution of this parameter. On the other hand, Figures (2.14) and (2.15) present the same plots when the 1D double porosity model is used. It can be observed that the results obtained using these two different approaches are very similar.

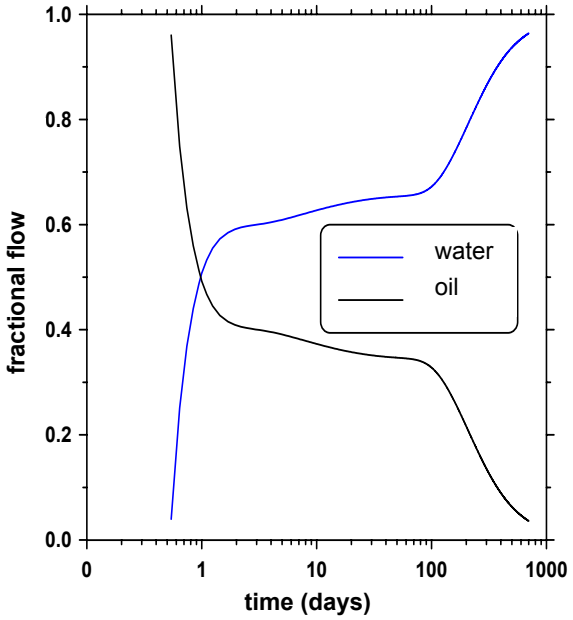

Figure 2.12. Evolution of fractional flows in well producer. 2D single porosity model (Guimarães, 2002).

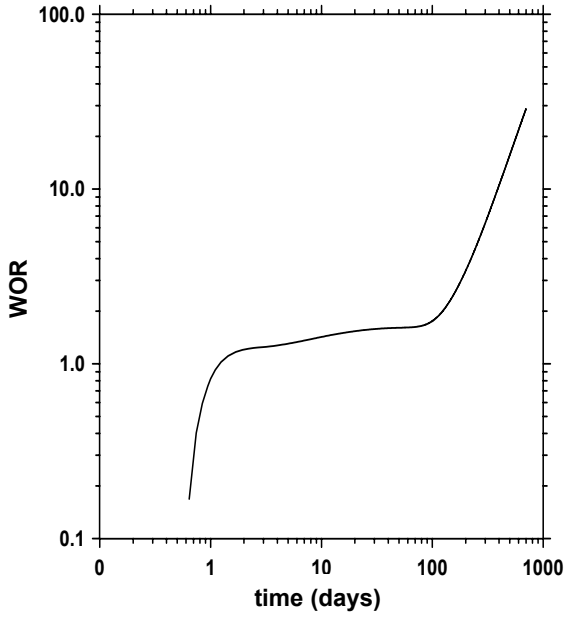

Figure 2.13. Evolution of the water/oil ratio in well producer. 2D single porosity model (Guimarães, 2002).

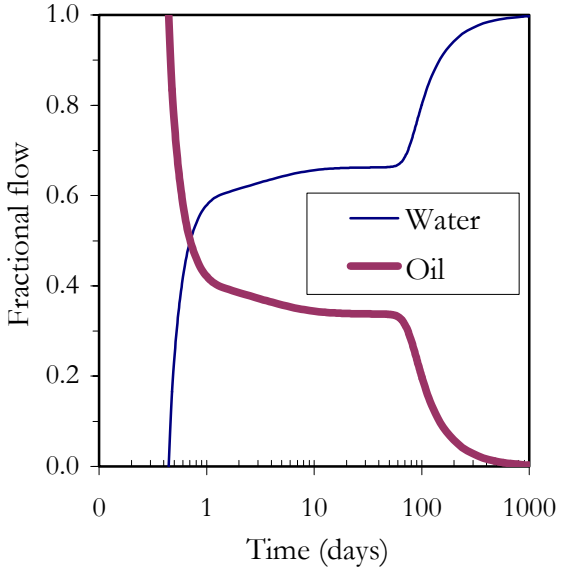

Figure 2.14. Evolution of fractional flows in well producer. 1D double porosity model.

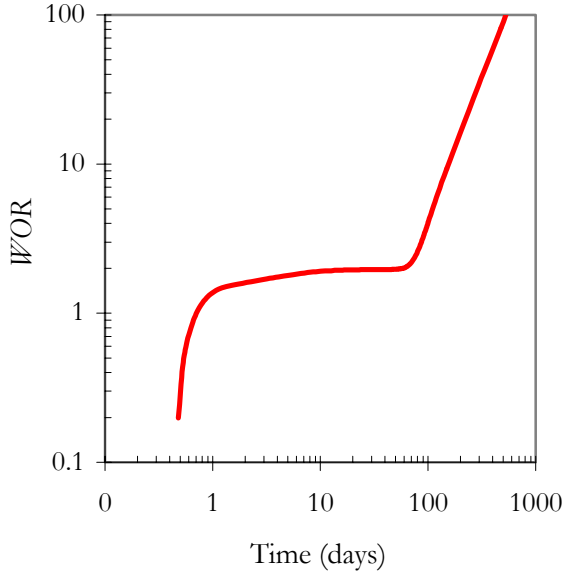

Figure 2.15. Evolution of the water/oil ratio in well producer. 1D double porosity model.

It can be noted (Figure 2.14) that the water production always increases with respect to the oil production. But, from the day 100 on, the water production augments strongly and, probably, the oil production is not economically profitable. The evolution of the *WOR* parameter (Figure 2.15) shows a similar tendency to the one observed in the diagnostic plot presented in Figure (2.8), that is, a sudden increment in the *WOR* value indicating the presence of a preferential flow path for the water flow. This behaviour is ascribed to the presence of the more permeable layer in the reservoir, which connects the injector and the producer wells. In the case analyzed, the slope of the *WOR* is not so abrupt, compared to the one observed in the diagnostic plot, because here the preferential path corresponds to a permeable layer, and not to a fault or fracture.

Considering the performance of the model, it can be mentioned that the application of the multiphase double porosity approach to solve this problem is very useful. When single porosity models are applied to solve problems like the presented here, the uses of 2D models are constrained in order to consider explicitly the more permeable medium. Instead, the application of a double porosity approach has the advantage that the more permeable medium can be considered at a formulation level and, therefore, a 1D model can be used to simulate the problem. In spite of the fact that in a double porosity model the number of unknowns per node increases, the diminution in the total number of degree of freedom is very significant. For instance in the example analysed here, 200 linear segments are used in the 1D double porosity model instead of the 8000 bilinear rectangles necessary in the 2D single porosity model. This advantage is even more noticeable when areal analyses of the water-flooding process are performed (Figure 2.16), because the development of an expensive 3D model is compulsory in the case of single porosity formulation when a preferential path is present.

2.5 CONCLUSIONS AND REMARKS

The availability of a coupled *THM* formulation that expresses, in a mathematical way, the various *THM* phenomena deemed relevant and their main interactions is a basic requirement for a good understanding and representation of complex *THM* problems. In many cases, the use of a double porosity formulation is more realistic because it is possible to take explicitly into account the different phenomena that take place in each voids level of the medium, with their respective constitutive laws, parameters and also their mutual interactions. In this Chapter a *THM* formulation for a medium with a double structure of pores has been presented.

The formulation presented is an open and general approach able to incorporate different constitutive laws for the mechanical, hydraulic and thermal problem of each structural level considered. The formulation has been implemented in the finite element code CODE_BRIGHT and it has been used to solve a variety of problems related to double structure media, some of them presented in this Chapter and also in Chapters IV and V.

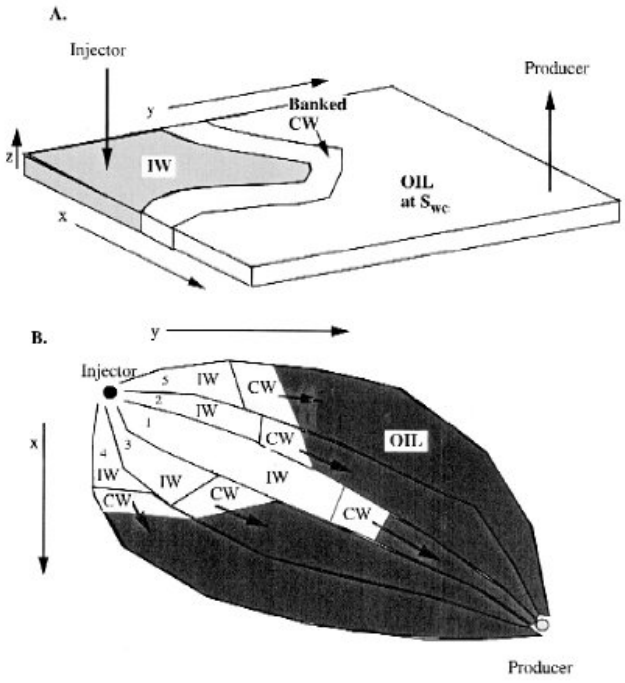

Figure 2.16. Scheme of an areal (2D) water-flood showing the flooding partner (Sorbie & Mackay, 2000).

Two application cases have been presented in this Chapter. The first one corresponds to the numerical verification of the implementation of the formulation in the computed code. The problem of fissured clays consolidation has been analysed, a good performance of the model has been observed when the computing outputs are compared with the results of the analytical solution available for this problem. The second case is devoted to the study of a multiphase flow problem related to petroleum engineering. The water-flooding process in a reservoir exploitation is analysed assuming a preferential flow path in the formation. The results obtained in this case show the potential of the formulation to simulate these kinds of problems.

In this Chapter the general structure of the *THM* formulation has been presented. The following Chapter focus on the mechanical constitutive law. A double structure model for expansive soil will be presented in detail.

CHAPTER III

A DOUBLE STRUCTURE MECHANICAL MODEL FOR EXPANSIVE MATERIALS

SUMMARY

The behaviour of expansive materials is a subject of central attention in this Thesis. Due to the strong influence of the mechanical problem on the swelling clay response, the mechanical constitutive law is a key element in the *THM* analyses and it can be viewed as the nucleus of the double structure formulation for these materials. The constitutive model presented in this Thesis is built on a conceptual approach for unsaturated expansive soils in which the fundamental characteristic is the explicit consideration of two pore levels. The distinction between the macro and micro structure provides the opportunity to take into account the dominant phenomena that affect the behaviour of each structural level and the main interactions between them. The microstructure is associated to the active clay minerals, while the macrostructure accounts for the larger scale structure of the material. The model has been formulated considering concepts of classical and generalized plasticity theories. The generalized stress-strain rate equations are derived within a framework of multidissipative materials, which provides a consistent and formal approach when there are several plastic mechanisms. The model is formulated in the space of stresses, suction and temperature; and it has been implemented in a finite element code. The approach has been applied to explain and reproduce the behaviour of expansive soils in different problems for which experimental data are available. In this Chapter two application cases are presented: in the first one, the response of a moderately expansive soil in a swelling pressure test is simulated, and in the second one, the behaviour of an expansive soil under wetting/drying cycles is reproduced. Additionally, the model has been used in all the modellings of Chapters IV and V.

3.1 PREFACE

The study of expansive soils has been a subject of increasing interest in recent research (Bernier *et al.,* 1997; Al-Mukhtar *et al.,* 1999; Villar *et al.* 1999; Dueck & Börgesson, 2001; Komine & Ogata 1994; Al-Rawas & Mc Gown, 1999; Cuisinier & Masrouri 2001; Marcial *et al.* 2002). A major aspect is the possible use of those materials as engineered barriers and seals in radioactive waste repositories. Many disposal concepts consider the barrier made up from highly expansive compacted clay, in an initially unsaturated state. During its lifetime the barrier will undergo processes of heating, induced by the heat-emitting waste, and of hydration, from water coming from the host rock (which is generally in a saturated state). This scenario has led to a growing interest in the knowledge of the behaviour of unsaturated expansive soils under a wide range of testing conditions; in particular the *THM* behaviour has received special attention (Wiebe *et al.,* 1998; Romero, 1999; Villar, 2000; Sultan *et al.,* 2002; Romero *et al.,* 2003; Villar *et al.,* 2003.b; Villar & Lloret, 2003). However, the interest on these materials is not limited to nuclear waste disposal applications, but they are present in other engineering problems such as shallow and deep foundations, slopes with stability problems, desiccation and formation of fissures in soils in arid regions, and clay based liners for waste isolation from the environment.

Comprehensive modelling of unsaturated expansive clays is a complex problem. The swelling behaviour of these clays has often been reproduced through relatively simple and empirical laws, which relate the material response to suction changes and applied stresses. The weakness of this kind of ad-hoc laws is that it can be generally used only for the stress paths and conditions from which they are derived. However, there are a few formulations that integrate the main aspects of behaviour in a unified framework (Gens & Alonso, 1992; Alonso *et al.*, 1999, Cui *et al.*, 2002b). In that context, the general model proposed by Gens & Alonso (1992) can be considered as a reference framework to analyse the behaviour of unsaturated expansive materials. In that work, particular attention is placed on the clay fabric and how it can be integrated the different structural levels present in an expansive soil in the constitutive modelling.

The fabric of expansive clays has been actively studied (Atabeck, 1991; Push, 1982; Romero 1999; Cui *et al.,* 2002a; Lloret *et al.,* 2003) observing a marked double structure. In those tests a clear bimodal pores distribution, which is characteristic of expansive clays, can be observed (in Chapter IV, results of mercury intrusion porosimeter tests of the FEBEX bentonite are presented). As commented in Gens & Alonso (1992), the presence of two dominate pores levels is very common in natural and compacted clays. More details about the typical fabric types can be found in Gens & Alonso (1992). These two dominant pore sizes can be associated with two basic structural levels (Figure 3.1):

- the macrostructure, composed by arrangements of clay aggregates, with macropores between them, and,

- the microstructure, which corresponds to the active clay minerals and their vicinity.

The model introduced in this Chapter is based on the general framework proposed by Gens & Alonso (1992) and considers some of the improvements proposed by Alonso *et al.* (1999). That expansive model, known as *BExM* (Barcelona Expansive Model) has been widely used as a conceptual framework to analyse swelling materials and also to perform numerical analyses at point integration level. However, its inclusion and use in a finite element code to solve actual boundary value problems have never been done until now.

In this Thesis a series of modifications and developments have been performed in order to enhance the constitutive law and also to formulate the model in a more suitable form for its implementation in a finite element code. One of the aims is to provide a more general mathematical framework in order to achieve a more general interpretation of the phenomena that take place in expansive clays when they are subjected to complex *THM* paths. With this objective, concepts of generalized plasticity theory have been included in the formulation of the model. The macroscopic response of the expansive soils is accomplished by the consideration of several plastic mechanisms that can act jointly or not at different stages of the analysis. The governing small strain-stress equations have been derived in the framework introduced by Rizzi *et al.* (1996), which provides a consistent and formal mathematical structure when there are several sources of energy dissipation.

Another aspect dealt with in this Chapter is the extension of the model to take into account the effects of non-hydraulic equilibrium between the two structural levels considered. This implies the inclusion of another variable in the formulation, named generically microstructural suction which is not in equilibrium with the capillary suction (macrostructural suction). The inclusion of this phenomenon in the modelling has allowed explaining and reproducing typical behaviour of some expansive soils.

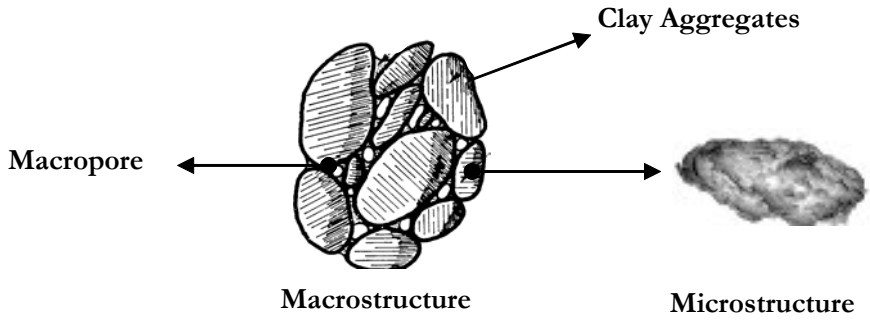

Figure 3.1. Schematic representation of the two structural levels considers.

Finally, a crucial step in the implementation of the mechanical model in the CODE_BRIGHT finite element program is the development of a proper algorithm to update the stresses and the internal variables of the model. An essential requisite is the accuracy of the integration scheme, in order to obtain reliable results. Since the stresses should be integrated many times in the course of a typical non-linear problem simulation, the scheme should not only be accurate but also efficient and robust.

Taking into account the conditions commented above, an algorithm based on Sloan's (1987, 2001) scheme, has been developed for the particular conditions of the double structure model. A great advantage of those schemes is that they have been widely tested in geotechnical problems, evincing their accuracy, robustness and efficiency.

The Chapter starts with a brief introduction of the mathematical framework adopted to handle the problem and also with the main aspects related to the two structural levels considered. Then a detailed explanation about the derivations of the strain rate equations is presented, followed by the presentation of some aspects related to the implementation of the model in the CODE_BRIGHT finite element program. Two application cases are presented, in which the capabilities of the model to reproduce and explain experimentally the responses of expansive materials are tested. Finally, the main conclusions are presented. Some complementary aspects of the model are introduced in the Appendix A.2. In the notation bold faces indicate tensors. Stresses ($\boldsymbol{\sigma}$) and strains ($\boldsymbol{\varepsilon}$) are first order tensors, and stiffness and compliance matrices are second order tensors.

3.2 MODEL FORMULATION

3.2.1 INTRODUCTION

The microstructure is the seat of the basic physical-chemical phenomena occurring at clay particle level. These phenomena are the main responsible of the expansive soils behaviour (Gens & Alonso, 1992). This level plays a crucial role in the interpretation of the behaviour exhibited by expansive materials. On the other hand, deformations due to loading and collapse will have a major effect at the macrostructural level. This macrostructural behaviour can be described by concepts and models of unsaturated non-expansive soils, such as the elasto-plastic Barcelona Basic Model (*BBM*) developed by Alonso ***et al.*** (1990).

In expansive soils there are other mechanisms, in addition to the ones included in the *BBM*, which can induce plastic strains (Gens & Alonso, 1992). For example, Figure (3.2) shows the behaviour of compacted expansive clay subjected to a cyclic suction-controlled oedometer test with suctions between 0.2 and 1.7 MPa (Pousada, 1984). In this test the sample is subjected alternatively to wetting and drying paths under constant vertical stress. It can be observed that the material exhibits a clear non-linear behaviour, with irreversible accumulated deformations at the end of each cycle. The results obtained by Day (1994) in a cyclic test of suction reversals (Figure 3.3) also show a marked inelastic behaviour. This is again a compacted clay, but here the amplitude of the suction cycles is larger, because the sample was dried under atmospheric conditions during the summer months in southern California. It is important to highlight that both samples were compacted under static conditions, and that the constant vertical stress applied during the test was relatively low. In this situation, it is expected that observed plastic deformations should developed inside the macrostructural yield surface of the *BBM*. This inelastic behaviour can be associated with the interactions between the two structural levels. This plastic mechanism considers that microstructural changes can modify the global arrangement of aggregates in an irreversible way (Gens & Alonso, 1992). In Alonso ***et al.*** (1999), it has shown that the *BExM* is able to explain and to reproduce the cyclic behaviour of expansive soils.

More experimental studies related to the soil behaviour under suction cycles can be found in the literature (for example: Subba Rao & Satyadas, 1987; Chen *et al.,* 1987; Dif & Bluemel, 1991; Alonso *et al.*, 1995; Al-Homoud *et al.,* 1995; Basma *et al.*, 1996; Tripathy *et al.*, 2002). Different techniques of suction control and different stress paths were applied by different authors. Analysing these tests, it can be identified that the irreversible behaviour appears independently of the applied suction (as in Figures 3.2 and 3.3), the transition between elastic and plastic behaviour is not easy to identify (it is a gradual process). Therefore, it is difficult to determine the initiation of the yielding.

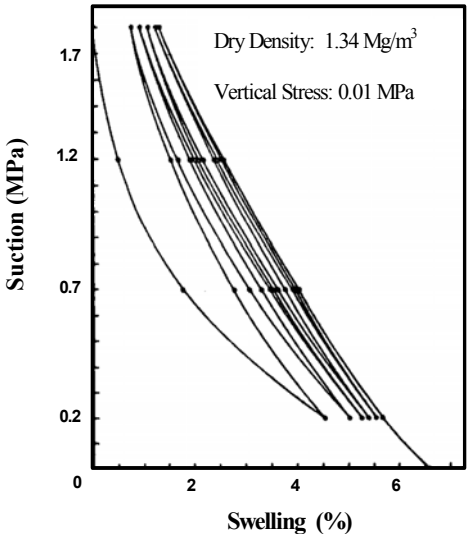

Figure 3.2 Accumulation of swelling strain in cyclic controlled suction test, Pousada (1984)

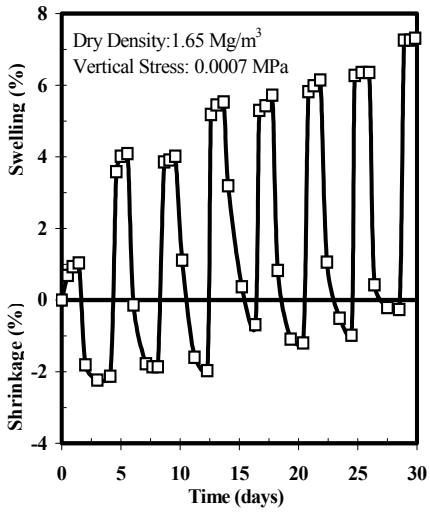

Figure 3.3 Evolution of shrinkage and swelling strains in non-controlled suction reversal test, Day (1994)

In this Thesis the elasto-plastic model related to the interaction mechanism between both structures is formulated in the framework of the generalized plasticity theory. In this theory the yield function is not defined or, at least, it is not defined in an explicit way. This theory is well suited if generalized stress reversals need to be modelled and also when there are several sources of energy dissipation (Pastor *et al.,* 1990; Zienkiewicz *et al.,* 1985; Lubliner & Auricchio, 1996; Simoni & Sherfler, 2001; de Borst & Heeres, 2002). Initially it was developed as a new theory, as a simplification of the classical elasto-plasticity in which it is not necessary to define the yield surfaces and plastic potentials (Lubliner & Auricchio, 1996). Afterwards it was shown that classical elasto-plasticity could be considered as a particular form of the new theory (Lubliner, 1991; Heeres, 2001). Generalized plasticity model was applied to materials that show irrecoverable deformations upon reloading (Lubliner, 1991), and also to the behaviour of soils under cyclic loading when they exhibit irreversible deformation in loading, unloading and reloading (Zienkiewicz *et al.* 1985; Pastor *et al.,* 1990). These are also typical aspects of behaviour patterns observed in expansive soils under generalized stress paths including suction and stress changes.

There are significant advantages in using generalized plasticity theory to model the plastic mechanism related to the interaction between both pores structures. Some of them are:

- No clear evidence exists concerning the shape of the internal yield surfaces corresponding to the interaction mechanisms between the two structural levels. Furthermore, their experimental determination does not appear to be easy.

- The effect of drying/wetting cycles on the behaviour of expansive soils is a matter of great practical importance. Generalized plasticity is especially well adapted to deal with this type of generalized cyclic loading.

- It is a formulation suitable for implementing it in numerical codes in a simple, robust and structured manner.

- It provides sufficient flexibility to incorporate additional microstructural phenomena such as non-equilibrium microstructural suction, or geochemical variables such as osmotic suction and cation exchange (Guimarães *et al.,* 2001).

The behaviour of the macrostructure is modelled in the context of classical plasticity (*BBM*). This is the proper framework because the yield surface associated to its behaviour could be generally inferred by the usual methodology of classic plasticity. Regarding the plastic behaviour induced by the microstructural effects, for which it is not easy to detect the yielding initiation, the option proposed here is to use the more general framework of generalized plasticity theory. Moreover, in the case that these yield surfaces can be experimentally defined, there are no problems to include them in the simulation, since the classical plasticity theory is a particular case of the generalized plasticity (Lubliner *et al.* 1993). For example, Appendix A.2 (Section A.2.1) presents a hypothetical case in which yield surfaces are considered.

The model is formulated in terms of the three stress invariants (p, J, θ), suction (s) and temperature (T). Where p is the mean net stress, J is the square root of the second invariant of deviatoric stress tensor and θ is the lode angle. The expressions for the evaluation of the invariants are introduced in Appendix A.2 (Section A.2.2). The vector of generalized stresses is identified with a hat symbol on top of it:

$$\hat{\boldsymbol{\sigma}} = \{T, s, p, J, \theta\}^T$$

In the following sections, the main aspects of the three parts of the model are introduced. The complete model formulation requires the definition of laws for:

- The macrostructural level.

- The microstructural level.

- The interaction between the structural levels.

3.2.2 MACROSTRUCTURAL MODEL

The inclusion of this structural level in the analysis allows the consideration of phenomena that affect the skeleton of the material (such as macrostructural collapses), which have a strong influence on the macroscopic response of expansive materials. This model is able to reproduce many of the basic patterns of behaviour observed in non-expansive soils (Alonso *et al.*, 1990). In that sense, it is a proper law to model the macrostructural behaviour. Although *BBM* allows small reversible swelling in the elastic zone, it can not be considered a proper model to reproduce large and irreversible deformations typically observed in expansive clays.

The *BBM* considers two independent stress variables to model the unsaturated behaviour: the net stress ($\boldsymbol{\sigma}$), computed as the excess of the total stresses over the gas pressure ($\boldsymbol{\sigma}_t$-$\mathbf{I}p_g$), and the matric suction (s), computed as the difference between gas pressure and liquid pressure (p_g-p_l). As explained in Alonso *et al.* (1990), the *BBM* considers the following typical behaviours observed in unsaturated soils: contribution of suction to stiffening the soil against external load, development of small reversible expansion strains due to wetting (suction decrease) at low confining stress, development of irreversible strains (collapse) due to wetting at high confining stress, dependence of the amount of collapse with confining stress, and dependence of the shear strength on suction (an increase of suction implies an increment in the apparent cohesion of the material), among others.

The *BBM* is an elasto-plastic strain hardening model, which extends the concept of critical state for saturated soils to the unsaturated conditions. In the *BBM* the yield surface depends not only on the stress level and on the history variables (as in a critical state model) but also on the matric suction, as it can be observed in Figure (3.4). A basic point of the model is that the size of the yield surface increases with suction. The trace of the yield function on the isotropic p-s plane is called the *LC* (Loading-Collapse) yield curve, because it represents the locus of activation of irreversible deformations due to loading increments or wetting (collapse compression), Figure (3.5). In this figure the two paths reach the same final *LC,* therefore, they induce the same plastic volumetric deformations. The position of the *LC* curve is given by the value of the hardening variable p_o^*, which is the pre-consolidation yield stress of the saturated state (Alonso *et al.,* 1990).

Concerning the effects of temperature over the behaviour of expansive clays, increasing laboratory information has been available since the last few years. The contributions are mainly addressed to the study of thermal effects in saturated conditions (Demars & Charles, 1982; Baldi *et al.,* 1988; Hueckel & Baldi, 1990; Lignau *et al.,* 1996; Tanaka *et al.* 1997; Komine & Ogata, 1998; Delage *et al.* 2000; Sultan *et al.,* 2002; Cekerevack & Laloui, 2004; among others), while the information related to the effect of temperature under unsaturated conditions is more scarce but growing (Saix, 1991; Wiebe *et al.,* 1998; Romero, 1999; Romero *et al.,* 2003; Villar *et al.,* 2003; Villar & Lloret, 2003). A similar tendency is observed in the development of the constitutive models, that is, most of them have been proposed to handle the non-isothermal behaviour of clay under saturated conditions (Hueckel & Baldi, 1990; Hueckel & Borsetto, 1990; Modaressi & Laloui, 1997; Cui *et al.* 2000, Graham *et al.,* 2001; Laloui & Cekerevack, 2003). As a thermo-mechanical law for non-saturated conditions it can be mentioned the model proposed by Gens (1995).

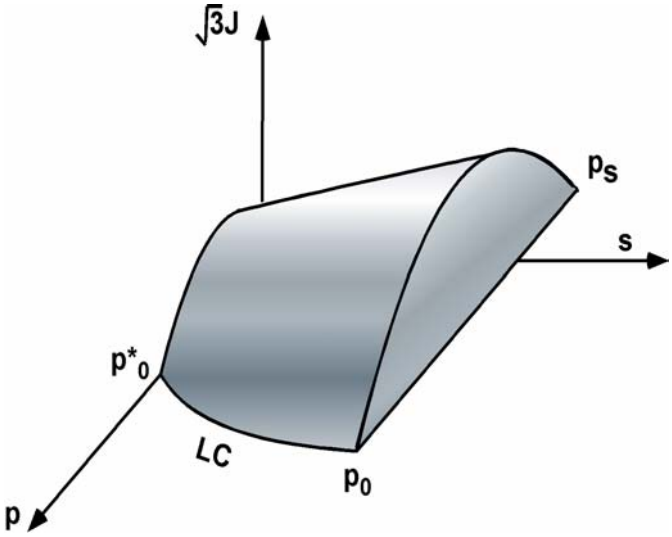

Figure 3.4. Three dimensional representation of the *BBM* yield surface

The model developed by Gens (1995) has been adopted to include the effect of temperature in the *BBM* (Garcia Molina *et al.*, 1996). This model incorporates the thermal effect on the *BBM* framework considering that the elastic component of the strain induced by temperature changes is only volumetric and including also a dependence of the pre-consolidation pressure (hardening parameter of the model) on temperature. In this way, it is assumed that temperature increases reduce the size of the yield surface and the strength of the material. This is a well-established fact for saturated conditions (Hueckel & Baldi, 1990; Hueckel & Borsetto, 1990) which can also be extended to the unsaturated conditions, as was confirmed in recent experimental studies performed by Romero *et al.* (2003) and Villar & Lloret (2003).

The model equations used in this Thesis have been extended from the ones proposed by Alonso *et al.* (1990) and Gens (1995) to the general 3-D non-isothermal case. In those contributions a detailed description of the *BBM* can be found. In Appendix A.2 (Section A.2.2) the more relevant equations of the model are introduced, here only a brief reference to some of them is made.

A version of the modified Cam Clay model (Roscoe & Burland, 1968) is the saturated law adopted as a boundary condition of the unsaturated formulation. The yield surface (F_{LC}) can be expressed as:

$$F_{LC} = 3J^2 - \left[\frac{g(\theta)}{g(-30^o)}\right]^2 M^2 \left(p + p_s\right)\left(p_0 - p\right) = 0 \tag{3.1}$$

where M is the slope of the critical state, p_o is the apparent unsaturated isotropic pre-consolidation pressure, $g(\theta)$ is a function of the Lode angle and p_s considers the dependence of shear strength on suction and temperature.

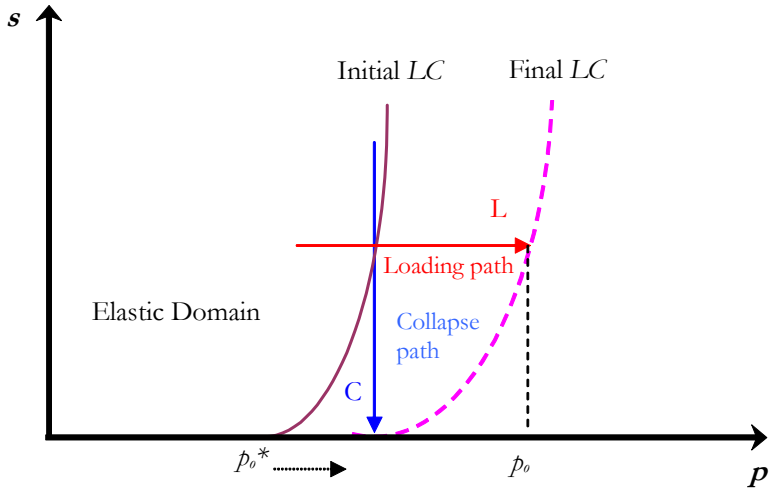

Figure 3.5. Movements of the *LC* yield curve due to load (*L*) or collapse (*C*) paths.

The hardening law is expressed as a rate relation between the volumetric plastic strain and the saturated isotropic pre-consolidation stress (p^*_0, Figure 3.4), according to:

$$\frac{\dot{p}^*_0}{p^*_0} = \frac{(1+e)}{(\lambda_{(0)} - \kappa)} \dot{\varepsilon}^p_v \tag{3.2}$$

where e is void index, κ is the elastic stiffens parameter for changes in net mean stress and $\lambda_{(0)}$ is the stiffness parameter for changes in net mean stress for virgin states of the soil in saturated conditions.

Regarding the direction of the plastic strain increment, a non-associated flow rule in the plane s=constant and T=constant is suggested (Alonso *et al.,* 1990 and Gens, 1995). The plastic potential (G) adopted is given by:

$$G = \alpha 3J^2 - \left[\frac{g(\theta)}{g(-30^o)}\right]^2 M^2 (p + p_s)(p_0 - p) = 0 \tag{3.3}$$

where α is determined from the condition that the flow rule predicts zero lateral strains in a K_0 stress path (Alonso *et al.,* 1990).

3.2.3 MICROSTRUCTURAL MODEL

It is assumed that physico-chemical phenomena occurring at this level are basically reversible and that the microstructural fabric does not have a preferential orientation (Gens & Alonso, 1992). The deformations arising from microstructural phenomena are considered elastic and volumetric. The microstructural volumetric strain depends on the microstructural effective stress ($\hat{p}$) defined as (Alonso, 1998):

$$\hat{p} = p + \chi s_t \tag{3.4}$$

being:

$$s_t = s + s_o \tag{3.5}$$

where p is the net mean stress and s_o the osmotic suction. Alonso (1998) suggests a general expression for χ: $\chi = (S_l)^n$, where n is a coefficient and S_l is the degree of saturation. In the following Sections, it is assumed that χ is a constant ($\chi > 0$) and that the total suction (s_t) is equal to the matric suction (s) because the effect of the osmotic suction is not considered in this Thesis. In Guimarães *et al.* (2001) and Guimarães (2002) the formulation is extended to include geochemical variables such as osmotic suction and cation exchange. As explained in Gens & Alonso (1992), the simple case in which χ is equal to 1 implies that the principle of effective stresses rules the microstructural behaviour.

An additional assumption is made in the current formulation that hydraulic equilibrium exists between the water potentials of both structural levels. Section 3.3.2 presents the extension of the constitutive model to handle problems in which this hypothesis is released.

In the *p-s* plane the line corresponding to constant microstructural effective stresses is referred to as the Neutral Line (F_{NL}) since no microstructural deformation occurs when the stress path moves on it (Figure 3.6).

$$\hat{p} = \text{constant} = p + \chi s = \hat{p}_{NL} \tag{3.6}$$

where $\hat{p}_{NL}$ is a reference microstructural effective stress. The increment of microstructural elastic strain is expressed as a function of the increment of the microstructural effective stress:

$$\dot{\varepsilon}^{e}_{vm} = \dot{\varepsilon}_{vm} = \frac{\dot{\hat{p}}}{K_m} = \frac{\dot{p}}{K_m} + \chi \frac{\dot{s}}{K_m} \tag{3.9}$$

where the subscript m refers to the microstructural level, the superscript e refers to the elastic component of the volumetric (subscript v) strains (ε) and K_m is the microstructural bulk modulus (Appendix A.2, Section A.2.3).

The Neutral loading Line (*NL*) divides the *p-s* plane into two parts, defining two main generalized stress paths, which are identified as:

$$\dot{\hat{p}} > 0 \Rightarrow \text{microstructural contraction path } (MC) \tag{3.7}$$

$$\dot{\hat{p}} < 0 \Rightarrow \text{microstructural swelling path } (MS). \tag{3.8}$$

In the previous version of the model, Alonso *et al.* (1999), the path indicated in Equation (3.7) was called "suction increase" or "drying path", and the path indicated in Equation (3.8) was called "suction decrease" or "wetting path". Herein, the names microstructural contraction and microstructural swelling path have been adopted, respectively.

Regarding the effects of temperature at this level, only the global (macroscopic) thermal response of the material is considered at the macrostructural level (in the *BBM* model). It can be mentioned that, although the experimental evidence in this field are becoming more common, it seems that there is not enough data to develop a constitutive model. In that sense it is interesting to mention the experimental study of Villar *et al.* (2003), in which the non-isothermal behaviour of two different expansive clays are compared. The different behaviours observed in the experimental response of the two clays are ascribed to the dissimilar response of the microstructure in each material when temperature is involved. Even if it is possible to give a qualitative explanation of some processes occurring at clay particle induced by thermal effects, more laboratory data are necessary in order to propose a consistent model.

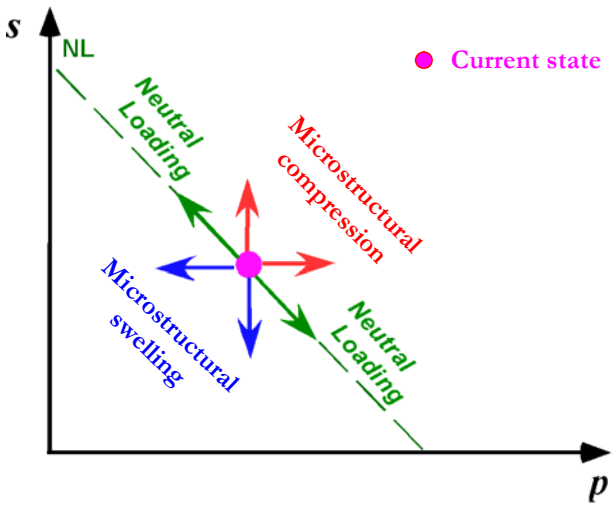

Figure 3.6. Definition of microstructural swelling and contraction directions.

3.2.4 INTERACTION BETWEEN STRUCTURAL LEVELS

Gens & Alonso (1992) include the interaction between the two structural levels as a basic point of their approach, to achieve a more comprehensive description of expansive soil behaviour. According to that work, it is assumed that the microstructural behaviour is not affected by the macrostructure but the opposite is not true, *i.e.* macrostructural behaviour can be affected by microstructural deformations, generally in an irreversible way. An assumption of the model is that the irreversible deformations of the macrostructure are proportional to the microstructural strains according to an interaction function *f*. In Alonso *et al.* (1994) and Alonso *et al.* (1999), a mathematical formulation of the model based on classic plasticity was put forward. In Appendix A.2.1 some details of this model are presented.

According to Gens & Alonso (1992), the plastic macrostructural strain induced by microstructural effects can be evaluated by the expression:

$$\dot{\varepsilon}_{v\beta}^{p} = f\,\dot{\varepsilon}_{vm} \tag{3.10}$$

where $\varepsilon_{v\beta}^{p}$ is the macrostructural plastic strain coming form the interaction mechanisms between both structures Two interaction functions f are defined: f_c for microstructural contraction paths and f_S for microstructural swelling paths. In the case of isotropic load, the interaction functions depends on the ratio p/p_o. Figure (3.7) presents a generic representation of the interaction functions.

The ratio p/p_o is a measure of the degree of openness of the macrostructure. When this ratio is low it implies a dense packing of the material (Figure 3.8). It is expected that under the latter condition (dense macrostructure) the microstructural swelling (*MS* path) affects strongly the global arrangements of clay aggregates, inducing large macrostructural plastic strains. So, the higher values of the f_s function correspond to low values of p/p_o. In this case the microstructure effects induce a more open macrostructure, which implies a macrostructural softening. On the other hand, when the microstructure contracts (*MC* path) the larger (induced) macrostructural plastic strains occur with open macrostructures, that is, values of p/p_o close to 1. Under this path the clay tends to a more dense state, which implies a hardening of the macrostructure. This coupling between both plastic mechanisms is considered mathematically assuming that:

$$\dot{\varepsilon}_{v}^{p} = \dot{\varepsilon}_{vLC}^{p} + \dot{\varepsilon}_{v\beta}^{p} \tag{3.11}$$

That is, the hardening variable of the macrostructure p_o^* (Equation 3.2), depends on the total plastic volumetric strains (ε_v^p), which is obtained from the sum of plastic volumetric strains induced by the *BBM* yielding (ε_{vLC}^{p}), plus the ones coming form the interaction mechanisms between both structures (denoted generically as $\varepsilon_{v\beta}^{p}$).

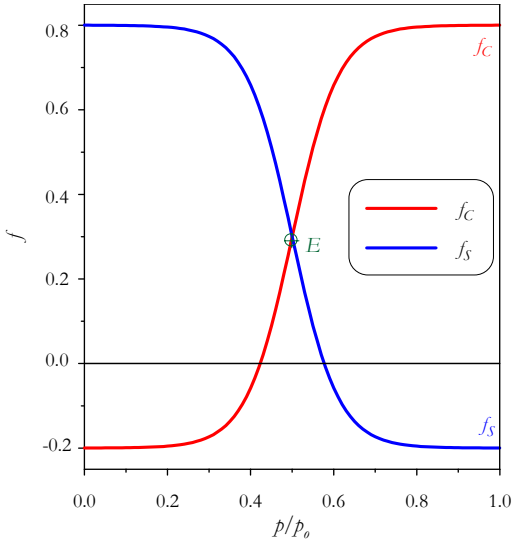

Figure 3.7. Interaction functions

In Figure (3.7) the point in which two interaction curves meet, indicated as E, is the equilibrium point (Alonso ***et al.,*** 1999). This point represents the state of the material for which no cumulative deformations are observed after cycles of suction changes. To the left of this point (low load), cycles of suction result in a net expansion of the material. In this case, for the same microstructural deformations, the plastic macrostructural strains of expansion dominate over the plastic macrostructural strains of contraction. The opposite case occurs to the right of the E point (high load). In section 3.6.2 an application case related to cyclic load is presented and discussed.

This mechanical law can model the macropore invasion induced by microstructure expansion, when conditions of high confinement prevail (reported by Komine & Ogatta, 1994) considering negative values of the function f_S for high values of p/p_o (Alonso ***et al.,*** 1999).

There are several experimental works oriented to identify the different phenomena and mechanisms included in this model, as well as, to determine the model parameters. In this line, it can be mentioned the work of Alonso ***et al.*** (1994), Garcia-Escudero (2001), Alonso ***et al.*** (2001), Lloret ***et al.*** (2003) and Villar ***et al.*** (2004).

It is noted that the material response will depend strongly on the direction of the microstructural stress path with respect to the NL that separates two regions of different material behaviour. A proper modelling requires the definition of specific elasto-plastic laws for each domain in order to describe correctly the material behaviour according to the microstructural stress path followed (MC or MS). Generalized plasticity theory can deal with such conditions, allowing the consideration of two directions of different behaviour and the formulation of proper elasto-plastic laws for each region.

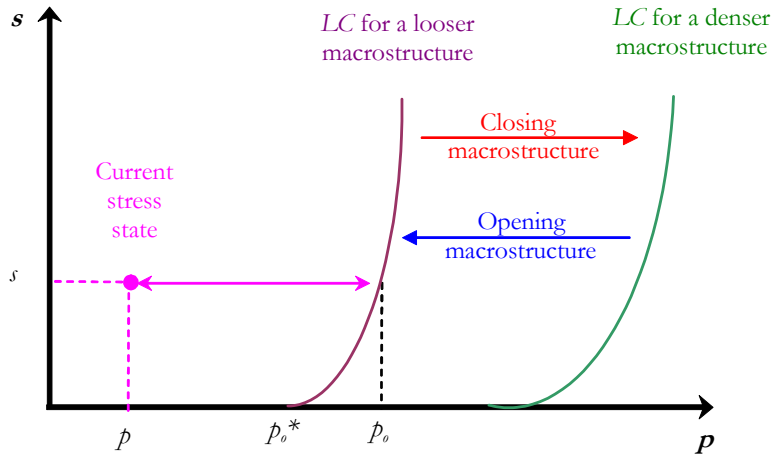

Figure 3.8.Movements of the *LC* yield curve due to microstructural effects.

According to the generalized plasticity theory, for a complete model definition, it is necessary to provide:

- a loading and unloading direction,
- a plastic flow direction, and,
- a plastic modulus.

3.2.4.1 LOADING AND UNLOADING DIRECTION

At every point of the stress space two vectors may be defined, one indicates the microstructural compression direction and the other the microstructural swelling direction (equivalent to loading/unloading in conventional stress/strain formulations). The Neutral Line is considered as reference for the microstructural behaviour dividing the generalized stress space into two regions. From Equation (3.6), the neutral line is defined as (Figure 3.9):

$$F_{NL}: \quad p + \chi s - \hat{p}_{NL} = 0 \tag{3.12}$$

Then, the microstructural compression direction can be obtained as:

$$\hat{\mathbf{n}}_C = \frac{\partial F_{NL}}{\partial \hat{\boldsymbol{\sigma}}} = \{0, \chi, 1, 0, 0\}^T \tag{3.13}$$

The opposite direction defines the microstructural swelling direction, which is expressed by:

$$\hat{\mathbf{n}}_S = \frac{\partial F_{NL}}{\partial \hat{\boldsymbol{\sigma}}} = \{0, -\chi, -1, 0, 0\}^T \tag{3.14}$$

In order to provide a generic expression for the plastic mechanisms induced in *MC* or *MS* paths, β will indicate the type of path followed. The following general expression is obtained:

$$\hat{\mathbf{n}}_\beta = \frac{\partial F_{NL}}{\partial \hat{\boldsymbol{\sigma}}} = \omega_\beta \{0, \chi, 1, 0, 0\}^T \tag{3.15}$$

where:

$$\omega_\beta = 1 \qquad if \quad \beta = C \qquad (MC \text{ path}) \tag{3.16}$$

$$\omega_\beta = -1 \qquad if \quad \beta = S \qquad (MS \text{ path}) \tag{3.17}$$

Given a generalized stress state and a generalized stress increment, the criterion to identify the microstructural stress path can be specified as (Figure 3.9):

Microstructural compression criterion:

$$\hat{\mathbf{n}}_C^T \cdot \dot{\hat{\boldsymbol{\sigma}}}^e > 0 \qquad (MC \text{ path}) \tag{3.18}$$

Microstructural swelling criterion:

$$\hat{\mathbf{n}}_S^T \cdot \dot{\hat{\boldsymbol{\sigma}}}^e > 0 \qquad (MS \text{ path}) \tag{3.19}$$

Neutral loading:

$$\hat{\mathbf{n}}_\beta^T \cdot \dot{\hat{\boldsymbol{\sigma}}}^e = 0 \qquad (NL \text{ path}) \tag{3.20}$$

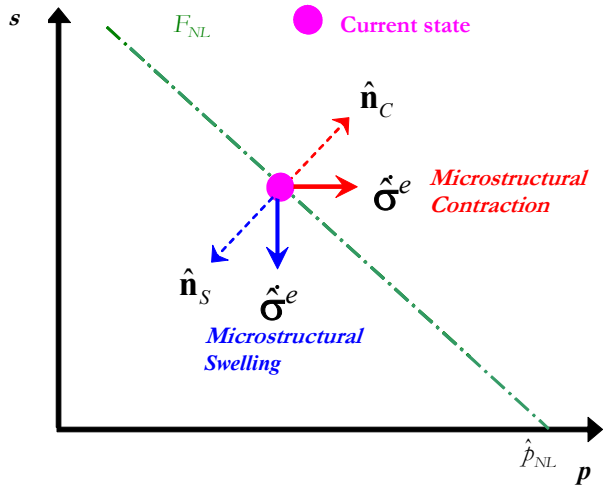

Figure 3.9. Definition of microstructural swelling and contraction directions.

where $\dot{\hat{\boldsymbol{\sigma}}}^e$ is the elastic generalized stress increment, that is, generalized strain increment (deformations, suction and temperature) times elastic tensors (more details are given in Section 3.3.1). The dot means matrix product (single contraction in index notation).

3.2.4.2 Plastic Flow Direction

The concept of image point is applied to define the flow rule for a generic state. The image point is obtained as a projection of the current stress state on the *BBM* yield surface (Figure 3.10). It is assumed that the current stress ratio η, θ, s and T are maintained constant during projection. The normal to the plastic potential at the image point ($\mathbf{n}_{G^*}$) is defined as:

$$\mathbf{n}_{G^*} = \left(\frac{\partial G}{\partial p^*}, \frac{\partial G}{\partial J^*}, \frac{\partial G}{\partial \theta^*} \right)^T \tag{3.21}$$

The equations used to evaluate this vector and the projection are included in Appendix A.2. (Section A.2.4).

In order to define the flow rule it is necessary to take into account the component of the macrostructural behaviour induced by microstructural strains due to the coupling mechanism. For a given microstructural path (*MC* or *MS*), the macrostructural response (expansion or compression) depends on the sign of the interaction function f_β. If f_β is positive the effect on the macrostructure goes in the same direction as the microstructural deformation. When f_β is negative, the opposite occurs. As an example, a microstructural compression path is examined. This path leads to a contracting behaviour of the microstructure. Therefore if f_ε is positive, the

macrostructure will also contract and a macrostructural hardening will take place. In contrast, if f_c is negative, there will be expansive macrostructural strains and a macrostructural softening will occur.

To take into account these two possibilities, the flow rule for microstructure compression paths is finally given as:

$$\mathbf{m}_C = \frac{f_C}{|f_C|}\mathbf{n}_{G^*} \tag{3.22}$$

where $\mathbf{m}_c$ is the plastic flow direction. Similar considerations for microstructure swelling paths lead to:

$$\mathbf{m}_S = -\frac{f_S}{|f_S|}\mathbf{n}_{G^*} \tag{3.23}$$

A general form of the plastic flow direction can therefore be written as:

$$\mathbf{m}_\beta = \omega_\beta \frac{f_\beta}{|f_\beta|}\mathbf{n}_{G^*} \tag{3.24}$$

The flexibility offered by the generalized plasticity theory to define the flow rule is also a good reason to select this theory to formulate a constitutive model, especially when complex paths involving loading reversals are considered.

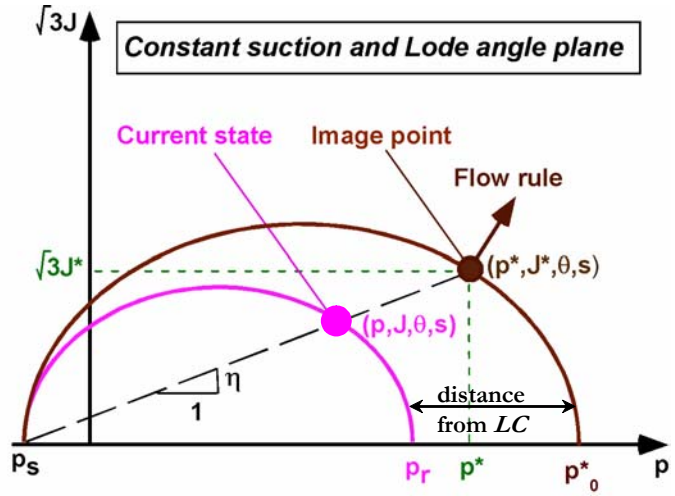

Figure 3.10. Reference pressure and Flow rule

3.2.4.3 PLASTIC MODULUS

The plastic modulus H_β is defined adopting a similar structure as the one proposed by Pastor *et al.* (1990), that is:

$$H_\beta = H_\beta^1 H_\beta^2 H_\beta^3 \tag{3.25}$$

Where:

- H^1_β is the term that contains the main variables that control the coupling between both structures. It can be defined as:

$$H_\beta^1 = \frac{K_m}{f_\beta} \tag{3.26}$$

When the stress path is isotropic f_β depends on p/p_o. However, if a deviatoric stress component is applied f_β depends on the p_r/p_o ratio and the following equation should be used to determine the distance to the *LC* surface:

$$p_r = p + \left[\frac{g(-30^o)}{g(\theta)}\right]^2 \frac{3J^2}{M^2(p+p_s)} \tag{3.27}$$

where p_r is a reference mean net stress for a non isotropic stress state. Figure (3.10) presents a schematic representation for this case.

- H^2_β is the term that considers the history of the material associated to this particular mechanism. When it is assumed that irreversible macrostructural plastic strains are always induced by the microstructural effective stresses change, this factor is given by:

$$H_\beta^2 = 1 \tag{3.28}$$

This implies that there is no elastic domain associated with the interaction mechanism. In this case a history variable ($\hat{p}_{NL}$), related to the last generalized microstructural stress attained by the material, is considered (Figure 3.9). At this point it is possible to introduce different evolution laws that take into account the history of the material. For example, a hypothetical case with an elastic domain has been modelled in Appendix A.2 (Section A.2.1) In that case there were two yield surfaces, one for each microstructural stress path (*MC* or *MS*), delimiting the elastic behaviour. That is, a conceptual model similar to the one adopted in the *BExM*.

- H^3_β is a factor that ensures the correct scaling of the plastic deformations, and it is defined as:

$$H^3_\beta = \left\| \mathbf{m}_\beta \right\| \tag{3.29}$$

where $\left\| \bullet \right\|$ is the Euclidean norm of the vector.

Finally, the plastic strain increment induced by β mechanisms is integrated in the model considering these three basic elements of the generalized plasticity theory (Appendix A.2, Section A.2.6). For instance, the equation for the plastic strain increment related to the stress increment is introduced, which is expressed as:

$$\dot{\boldsymbol{\varepsilon}}^p_\beta = \dot{\lambda}_\beta \, \mathbf{m}_\beta \tag{3.30}$$

where the scalar $\dot{\lambda}_\beta$ is defined in a similar way as in Pastor *et al.* (1990):

$$\dot{\lambda}_\beta = \frac{\mathbf{n}^T_\beta \cdot \dot{\boldsymbol{\sigma}}}{H_\beta} \tag{3.31}$$

where $\mathbf{n}_\beta = \dfrac{\partial F_{NL}}{\partial \boldsymbol{\sigma}}$. Considering Equations (3.12), (3.24-26) and (3.28-31), for the component of plastic strain arising from the interaction mechanisms, the volumetric plastic strain increment due to p increment is given by:

$$\dot{\varepsilon}^p_{v\beta} = f_\beta \frac{\dot{p}}{K_m} m_{v\beta} \tag{3.32}$$

where:

$$m_{v\beta} = \frac{\omega_\beta}{\left\| \mathbf{m}_\beta \right\|} \frac{f_\beta}{\left| f_\beta \right|} \frac{\partial G}{\partial p^*} \tag{3.33}$$

That is, the coupling defined by Equations (3.9) and (3.10) for a p increment is considered in Equation (3.32). The mechanism active β is identified in accordance with the criterion of microstructural contraction/swelling established in Section 3.2.4.1 (Equations 3.18-20).

In summary, the mechanical law has been formulated considering an elasto-plastic model to describe the macrostructural behaviour (formulated in the context of classical plasticity), a nonlinear elastic model to describe the microstructural behaviour and a generalized plasticity model to include the irreversible effects induced by the coupling between both structural levels.

3.3 ELASTO-PLASTIC STRESS-STRAIN RELATIONS

When dealing with soils in unsaturated conditions two stress fields have been adopted: net stresses and suction. The thermal effects have been included considering the temperature difference, ΔT ($\Delta T=T-T_0$), with respect to a reference temperature (T_0) (Gens, 1995). As commented above, the hypothesis of hydraulic equilibrium between the two pores structures has been made. However, the more general case corresponds when this hypothesis is removed. Therefore, the potentials of the water stored at each structural level are no longer in equilibrium and it is necessary the evaluation of two suctions, one related to the macro structure and one associated to the microstructure. Although this latter case is the general one and includes, as a particular case the hypothesis of hydraulic equilibrium, the derivation of the set of governing stress-strain relations is made by steps, considering first the case when the hypothesis of water potential equilibrium is assumed and, afterward, when this hypothesis is relaxed. So, the aim of the following sections is to obtain the elasto-plastic tensors related to the increment of strains, suction and temperature; which define the stress-strain relations.

3.3.1 EQUILIBRIUM BETWEEN WATER POTENTIALS

When non-equilibrium between the potentials of the water stored at each structural level occurs, a process of mass transfer is induced in order to re-establish the equilibrium. The assumption of instantaneous equilibrium corresponds when the characteristic time of the local water transfer between media is so fast, compared with other processes (such as advection), that equilibrium between water potentials can be considered. It also implies that the suctions associated at each water potentials are equal and, therefore, only one variable must be computed. So, in the model formulation, the generic name of suction is used for both, but it has different physical meaning depending on the structural level considered

The behaviour of the soil described by the double structure model can be regarded as the consequence of joint action of several mechanisms that can act simultaneously. In this Thesis, some concepts of multi-dissipative materials introduced by Rizzi *et al.* (1996) have been considered to take into account that different mechanisms can induce plastic deformations.

A first step is the assumption of an additive decomposition of the strains into elastic and plastic components, so, the total strain increment can be expressed as:

$$\dot{\boldsymbol{\varepsilon}} = \dot{\boldsymbol{\varepsilon}}^{e} + \sum_{n=1}^{i=na} \dot{\boldsymbol{\varepsilon}}_{n}^{p} \tag{3.34}$$

where *na* is the number of active plastic mechanisms that correspond to one subset of the total plastic possible mechanisms. The model has three inelastic mechanisms: *lc*, due to yield of the *BBM*, and *mc* or *ms* when one of the two interaction mechanisms is active (two is the maximum number of simultaneous active plastic mechanisms, *i.e. lc* plus *mc* or *ms*).

In classical plasticity theory, it is assumed that the material behaves either as an elastic or a plastic solid. The yield surface defines the transition from elasticity to plasticity, stress states inside the yield surface are considered as elastic ($F < 0$).

In generalized plasticity theory the state of the material is determined from the control variables: generalized stresses, strains and a finite number of internal variables. A process of loading is defined as elastic if the set of internal variables remains unchanged (Lubliner, 1991).

In the case of elastic loading, the stress increment is related to the increment of strains, suction and temperature by the following relation:

$$\dot{\boldsymbol{\sigma}} = \mathbf{D}_e \cdot \dot{\boldsymbol{\varepsilon}}^e + \boldsymbol{\alpha}_s \dot{s} + \boldsymbol{\alpha}_T \dot{T} \tag{3.35}$$

where $\mathbf{D}_e$ is the global elastic matrix which considers the elastic component of the two structural levels. $\boldsymbol{\alpha}_s$ and $\boldsymbol{\alpha}_T$ are the elastic vectors associated to suction and temperature, respectively. The expressions of the elastic tensors are introduced in Appendix A.2 (Section A.2.5).

When a loading process is inelastic, the plastic strain rates are assumed to be governed by a flow rule. For the macrostructural model, the strain increment can be expressed as:

$$\dot{\boldsymbol{\varepsilon}}^p_{LC} = \dot{\lambda}_{LC} \frac{\partial G}{\partial \boldsymbol{\sigma}} = \dot{\lambda}_{LC} \mathbf{m}_{LC} \tag{3.36}$$

where $\dot{\lambda}_{LC}$ is the plastic multiplier associated to the *lc* plastic mechanism, and $\mathbf{m}_{LC}$ is the flow rule direction (normal to the plastic potential Equation 3.2).

In this expansive model the material behaviour is described by elasto-plastic mechanisms that can be activated during the loading process. The set of active plastic mechanisms is not known in advance. Therefore it is necessary to use an iterative procedure to find them (Simo & Hughes, 1988; Carol & Prat, 1999). A possibility is to assume that all the plastic mechanisms are initially active (Carol & Prat, 1999). In this Thesis, it is assumed that both plastic mechanisms are initially active, that is: *lc* and β (*i.e.* *mc* or *ms*).

Regarding the *lc* plastic mechanism it is assumed that, once yield occurs (that is $F_{LC} = 0$) the stresses must remain on the yield surface during a plastic deformation. This constrain it is enforced by the consistency condition, which implies that: $\dot{F}_{LC} = 0$. After some algebra on the consistency condition (Appendix A.2, Section A.2.6.1), the following equation is obtained:

$$\dot{\lambda}_{LC}\left(H_{LC} + H^c_{LC}\right) + \dot{\lambda}_{\beta}\left(h_{\beta} + h^c_{\beta}\right) = \dot{e}_{LC} + \dot{s}_{LC} + \dot{t}_{LC} \tag{3.37}$$

where $\dot{\lambda}_{LC}$ and $\dot{\lambda}_{\beta}$ are the unknowns. H_{LC}, H^{e}_{LC}, h_{β} and h^{e}_{β} are moduli related to the *lc* and β plastic mechanisms, while $\dot{e}_{LC}$, $\dot{s}_{LC}$ and $\dot{t}_{LC}$ are variables linked to the increment of strains, suction and temperature. In Appendix A.2 (Section A.2.6.1) all the details of Equation (3.37) are included.

For the β plastic mechanism, a procedure similar to the one suggested by Pastor *et al.* (1990) has been followed to obtain the equation with the unknowns $\dot{\lambda}_{LC}$ and $\dot{\lambda}_{\beta}$ (Appendix A.2, Section A.2.6.2). It can be written as:

$$\dot{\lambda}_{LC}\, h^{e}_{LC} + \dot{\lambda}_{\beta}\left(H_{\beta} + H^{e}_{\beta}\right) = \dot{e}_{\beta} + \dot{s}_{\beta} + \dot{t}_{\beta} \tag{3.38}$$

where h^{e}_{LC}, H_{β} and H^{e}_{β} are moduli related to the plastic mechanisms (*lc* and β). $\dot{e}_{\beta}$, $\dot{s}_{\beta}$ and $\dot{t}_{\beta}$ are variables linked to the increment of strains, suction and temperature. In Appendix A.2 (Section A.2.6.2) all the expressions necessary to evaluate Equation (3.38) are presented.

The system formed by Equations (3.37) and (3.38) can be written as:

$$\begin{cases} \dot{\lambda}_{LC}\,\overline{H}_{LC} + \dot{\lambda}_{\beta}\,\overline{h}_{\beta} = \dot{e}_{LC} + \dot{s}_{LC} + \dot{t}_{LC} \\ \dot{\lambda}_{LC}\,\overline{h}_{LC} + \dot{\lambda}_{\beta}\,\overline{H}_{\beta} = \dot{e}_{\beta} + \dot{s}_{\beta} + \dot{t}_{\beta} \end{cases} \tag{3.39}$$

which can be expressed in a compact form, as:

$$\overline{\mathbf{H}}.\dot{\boldsymbol{\lambda}} = \dot{\mathbf{e}} + \dot{\mathbf{s}} + \dot{\mathbf{t}}\ ; \qquad \overline{\mathbf{H}} = \mathbf{H} + \mathbf{H}^{e} \tag{3.40}$$

where:

$$\overline{\mathbf{H}} = \begin{bmatrix} \left(H_{LC} + H^{e}_{LC}\right) & \left(h_{\beta} + h^{e}_{\beta}\right) \\ h^{e}_{LC} & \left(H_{\beta} + H^{e}_{\beta}\right) \end{bmatrix}; \qquad \mathbf{H} = \begin{bmatrix} H_{LC} & h_{\beta} \\ 0 & H_{\beta} \end{bmatrix} \tag{3.41}$$

$$\dot{\boldsymbol{\lambda}} = \begin{Bmatrix} \dot{\lambda}_{LC} \\ \dot{\lambda}_{\beta} \end{Bmatrix}; \qquad \dot{\mathbf{e}} = \begin{Bmatrix} \dot{e}_{LC} \\ \dot{e}_{\beta} \end{Bmatrix} \tag{3.42}$$

$$\dot{\mathbf{s}} = \begin{Bmatrix} \dot{s}_{LC} \\ \dot{s}_{\beta} \end{Bmatrix}; \qquad \dot{\mathbf{t}} = \begin{Bmatrix} \dot{t}_{LC} \\ \dot{t}_{\beta} \end{Bmatrix} \tag{3.43}$$

The hardening modulus matrix (**H**) is symmetric when there is reciprocity in the hardening rules of both mechanisms (reciprocal hardening implies that $H_{ij}=H_{ji}$ for i≠j), Rizzi *et al.* (1996). So, the presented model has non-reciprocal hardening (h_β can be non-zero), because the only coupling between both plastic mechanisms is given by the hardening law of the *BBM* (Equations 3.2 and 3.11).

According to Rizzi *et al.* (1996), there is a unique increment of $\boldsymbol{\varepsilon}$ for any increment of $\boldsymbol{\sigma}$ if, and only if, **H** is a *P-matrix* (as defined in Appendix A2, Section A.2.8). When this condition is satisfied, the flow rule of the multidissipative materials exhibits hardening, otherwise it exhibits softening. Finally, for **H** = 0 the behaviour is perfectly plastic. For the general case of non-associative plasticity, there is a unique increment of $\boldsymbol{\sigma}$ for any increment of $\boldsymbol{\varepsilon}$ if, and only if, $\overline{\mathbf{H}}$ is a *P-matrix*. $\mathbf{H}^c$ is the critical softening matrix.

The assumption that $\overline{\mathbf{H}}$ is a *P-matrix* implies that each diagonal element of the **H** matrix plus the corresponding diagonal element of the $\mathbf{H}^c$ matrix is greater than zero (*i.e* $\left(H_{LC}+H^c_{LC}\right)>0$ and $\left(H_\beta+H^c_\beta\right)>0$). Therefore, the condition of $\overline{H}>0$ is satisfied for each plastic mechanism. The solution of the system (3.39) requires the inversion of the $\overline{\mathbf{H}}$ matrix which would be a *P-matrix,* obtaining:

$$\dot{\boldsymbol{\lambda}}=\overline{\mathbf{H}}^{-1}.\left(\dot{\mathbf{e}}+\dot{\mathbf{s}}+\dot{\mathbf{t}}\right) \tag{3.44}$$

After some algebra, the following expressions are obtained:

$$\begin{cases}\dot{\lambda}_{LC}=\dfrac{\overline{H}_\beta}{\left|\overline{\mathbf{H}}\right|}\left(\dot{e}_{LC}+\dot{s}_{LC}+\dot{t}_{LC}\right)-\dfrac{\overline{h}_\beta}{\left|\overline{\mathbf{H}}\right|}\left(\dot{e}_\beta+\dot{s}_\beta+\dot{t}_\beta\right)\\ \dot{\lambda}_\beta=\dfrac{\overline{H}_{LC}}{\left|\overline{\mathbf{H}}\right|}\left(\dot{e}_\beta+\dot{s}_\beta+\dot{t}_\beta\right)-\dfrac{\overline{h}_{LC}}{\left|\overline{\mathbf{H}}\right|}\left(\dot{e}_{LC}+\dot{s}_{LC}+\dot{t}_{LC}\right)\end{cases} \tag{3.45}$$

The choice of the plastic mechanisms assumed initially active should be verified by checking that they are actually active (Simo & Hughes, 1988; Carol & Prat, 1999). If one of them is not active, the problem becomes a single dissipative model.

The net stress increment can be expressed as:

$$\dot{\boldsymbol{\sigma}}=\mathbf{D}_e\cdot\left(\dot{\boldsymbol{\varepsilon}}-\dot{\boldsymbol{\varepsilon}}^e_s-\dot{\boldsymbol{\varepsilon}}^e_T-\sum_{n=1}^{na}\dot{\boldsymbol{\varepsilon}}^p_n\right)\quad\dot{\boldsymbol{\sigma}}=\mathbf{D}_e\cdot\left(\dot{\boldsymbol{\varepsilon}}-\dot{\boldsymbol{\varepsilon}}^e_s-\dot{\boldsymbol{\varepsilon}}^e_T-\sum_{n=1}^{na}\dot{\boldsymbol{\varepsilon}}^p_n\right) \tag{3.46}$$

where $\dot{\boldsymbol{\varepsilon}}^e_s$ and $\dot{\boldsymbol{\varepsilon}}^e_T$ are the elastic strain increments due to suction and temperature changes.

After some algebra (Appendix A.2, Section A.2.6) the following general form is obtained:

$$\dot{\boldsymbol{\sigma}} = \mathbf{D}_{ep} \cdot \dot{\boldsymbol{\varepsilon}} + \boldsymbol{\gamma}_s \dot{s} + \boldsymbol{\gamma}_T \dot{T} \tag{3.47}$$

where $\mathbf{D}_{ep}$ is the global elasto-plastic matrix, $\boldsymbol{\gamma}_s$ and $\boldsymbol{\gamma}_T$ are the elasto-plastic vectors associated to suction and temperature, respectively. In the case of two active plastic mechanisms these tensors may be evaluated with:

$$\mathbf{D}_{ep} = \mathbf{D}_e \cdot \left[\mathbf{I} - \frac{1}{\left|\overline{\mathbf{H}}\right|} \left(\overline{H}_\beta \mathbf{m}_{LC} \cdot \mathbf{n}_{LC}^T - \overline{b}_\beta \mathbf{m}_{LC} \cdot \mathbf{n}_\beta^T + \overline{H}_{LC} \mathbf{m}_\beta \cdot \mathbf{n}_\beta^T - \overline{b}_{LC} \mathbf{m}_\beta \cdot \mathbf{n}_{LC}^T \right) \cdot \mathbf{D}_e \right] \tag{3.48}$$

$$\begin{aligned} \boldsymbol{\gamma}_s = \boldsymbol{\alpha}_s + \boldsymbol{\beta}_s - \frac{1}{\left|\overline{\mathbf{H}}\right|} \mathbf{D}_e \cdot \Big\{ & \overline{H}_\beta \mathbf{m}_{LC} \left[l + l_\beta + \mathbf{n}_{LC}^T \cdot \left(\boldsymbol{\alpha}_s + \boldsymbol{\beta}_s \right) \right] - \overline{b}_\beta \mathbf{m}_{LC} \mathbf{n}_\beta^T \cdot \left(\boldsymbol{\alpha}_s + \boldsymbol{\beta}_s \right) + \\ & \overline{H}_{LC} \mathbf{m}_\beta \mathbf{n}_\beta^T \cdot \left(\boldsymbol{\alpha}_s + \boldsymbol{\beta}_s \right) - \overline{b}_{LC} \mathbf{m}_\beta \left[l + l_\beta + \mathbf{n}_{LC}^T \cdot \left(\boldsymbol{\alpha}_s + \boldsymbol{\beta}_s \right) \right] \Big\} \end{aligned} \tag{3.49}$$

$$\begin{aligned} \boldsymbol{\gamma}_T = \boldsymbol{\alpha}_T - \frac{1}{\left|\overline{\mathbf{H}}\right|} \mathbf{D}_e \cdot \Big[& \overline{H}_\beta \mathbf{m}_{LC} \left(d + \mathbf{n}_{LC}^T \cdot \boldsymbol{\alpha}_T \right) - \overline{b}_\beta \mathbf{m}_{LC} \mathbf{n}_\beta^T \cdot \boldsymbol{\alpha}_T + \\ & \overline{H}_{LC} \mathbf{m}_\beta \mathbf{n}_\beta^T \cdot \boldsymbol{\alpha}_T - \overline{b}_{LC} \mathbf{m}_\beta \left(d + \mathbf{n}_{LC}^T \cdot \boldsymbol{\alpha}_T \right) \Big] \end{aligned} \tag{3.50}$$

In Appendix A.2 (Sections A.2.5 and A.2.6) all the equations necessary to compute the elastic and elasto-plastic tensors are presented in detail. For other cases, for example when only the *lc* plastic mechanism is active, a procedure similar to the one presented in Gens (1995) has been followed (Appendix A.2.9). On the other hand, when the interaction mechanism β is active only, the stress-strain rate equations have been obtained according to the concepts of generalized plasticity presented in Pastor *et al.* (1990) (Appendix A.2.9).

3.3.2 NON-EQUILIBRIUM BETWEEN WATER POTENTIALS

Starting from an equilibrium state, if a perturbation induces non-equilibrium between the water potentials of the two pores levels, transfer of water mass between them occurs until the initial equilibrated state is recovered. As commented in Chapter II, there are different alternatives to model such kind of process. The simpler model related to the mass transfer of water can be expressed through Equation (2.35) as:

$$\Gamma^w = \gamma \left(\Psi_M - \Psi_m \right) \tag{3.51}$$

γ is the leakage parameter and Ψ_j is the water potential associated to each media, macro and micro structure (j=*M*,*m* respectively).

The evaluation of the water potential can be made considering the chemical potential of the water. Expressions based on the chemical potential of an ideal gas are generally used to its evaluation. The chemical potential of an ideal gas is derived from the Gibbs free energy and can be expressed as (Appelo & Postma, 1993):

$$\mu_i = \mu_i^0 + RT\ln(a) \qquad where \qquad a = P_i / P^0 \tag{3.52}$$

With Equation (3.52) the chemical potential (μ_i) of the gas *i* can be evaluated at the current gas pressure (P_i) and under isothermal conditions (T). μ^0_i is the reference chemical potential of the gas at the reference pressure P^0 (and Temperature), R is the gas constant (8.314 J/deg.mol), and *a* is the activity.

Expressions like (3.51) have been extended to other substances and conditions in which the activity is defined likewise from a concentration measured. Several approaches adopt the liquid chemical potential as the thermodynamic force to model the process of mass transfer with satisfactory results (*e.g.* Navarro & Alonso, 2001; Loret *et al.,* 2002). However, it is important to have in mind that Equation (3.52) has been derived for a perfect gas, its extension to other liquids or solids is an assumption (Appelo & Postma, 1993). On the other hand, in compacted expansive clays the microstructural water is highly affected by the psychico-chemical phenomena occurring at clay particle level, especially by the presence of exchangeable cations. These conditions are far from the ideal ones and it seems not simple to find the expression for the chemical potential of the microstructural water. Some attempts to its evaluation have been made recently by Fernandez (2004) for the case of the FEBEX bentonite, but it seems not easy to manipulate numerically these expressions, at least for the moment.

In Gens & Olivella (2001) a well-established alternative approach is presented to evaluate the water potential. The total water potential, Ψ, can be defined as the variation of the Gibbs free energy of water per unit change of mass when the rest of the thermodynamical variables remain constant. Therefore, the potential can be envisaged as the energy required (under isothermal conditions) to extract a unit mass of water and take it to a reference state. Total water potential controls the mass transfer of water. When two water volumes are in contact and there is no flow, it necessarily means that the water potentials are the same in the two zones (Gens & Olivella, 2001). The total water potential can be divided into four different components:

$$\Psi = \Psi_{gravitational} + \Psi_{gas\ \ pressure} + \Psi_{matric} + \Psi_{osmotic} \tag{3.53}$$

The gravitational potential is related to the difference in elevations. The gas pressure potential is linked to the applied gas pressure. The osmotic potential is associated to the differences in solute concentration. Finally, the matric potential is a measure of the attraction that a soil matrix has for liquid moisture. Only the matric and osmotic potentials affect the mechanical response of unsaturated soils.

As commented in (Gens & Olivella, 2001), the concept of suction is generally used instead of potential. Suction is equal to potential but with the opposite sign. Therefore matric suction is $s = -\Psi_{matric}$ and osmotic suction is $s_o = -\Psi_{osmotic}$. The sum of these two suctions is the total suction (Equation 3.5). The matric suction is often equated to the capillary pressure ($s = p_g - p_l$). This definition has only real meaning in the framework of the capillary model of soil and is not directly applicable to many soils, as for example the expansive clays, in which active clay fractions are significant. In these materials, when conditions of high suctions prevail, it is not certain that the water is in a state of true tension. So, the high negative pore pressures that frequently arise from the capillary equation reflect the degree of attraction of the water by the soil matrix and are often more related to the physico-chemical effects than to some virtual capillary meniscus existing in the soil (Gens & Olivella, 2001). These concepts have been used in this Thesis, considering the suction of each pores level as the main driving forces involved in the mass water transfer.

The inclusion of the mass transfer of water allows a more general representation of the behaviour of expansive soils. For example, a characteristic response of this phenomenon is the exhibition of more than one swelling stage under hydration (Alonso ***et al.,*** 1991; Volckaert ***et al.***, 2000; Navarro & Alonso, 2000). Figure (3.11) shows the typical output of this kind of behaviour in terms of the swelling pressure. The tests were carried out over three different samples, which had a clear double structure. They were made up from a mixture of clays pellets and clay powder. The tests were performed in the context of the Reseal project, Volckaert ***et al.*** (2000). Despite of the observed differences (due to the different densities and mixtures composition of the samples), the tests exhibit a typical behaviour with two main swellings in all cases. The initial swelling corresponds to the hydration of the clay powder and also of the more external clay of the pellets. The second swelling is due to the hydration of the more inaccessible clay, inside the pellets. The framework presented in this Thesis can deal with this kind of phenomena. In Chapter IV (Section 4.4) a detailed analysis of this problem is presented, which focuses also on the strong *HM* (Hydro-Mechanical) coupling observed between the two structural levels existent in this kind of material.

The process of water mass transfer can be modelled according with the concepts and framework presented in Chapter II. Regarding the mechanical model, it is necessary its extension to include the non-balanced microstructural suction. That is, there are two different suctions: the macrostructural suction (s_M) (which is the matric suction) and the microstructural suction (s_m). Thus, in the case of an elastic loading, the stress increment is related to the increment of strains, temperature, macrostructural and microstructural suction by the following relation:

$$\dot{\boldsymbol{\sigma}} = \mathbf{D}_e \cdot \dot{\boldsymbol{\varepsilon}} + \boldsymbol{\alpha}_{s_M} \dot{s}_M + \boldsymbol{\alpha}_{s_m} \dot{s}_m + \boldsymbol{\alpha}_T \dot{T} \tag{3.54}$$

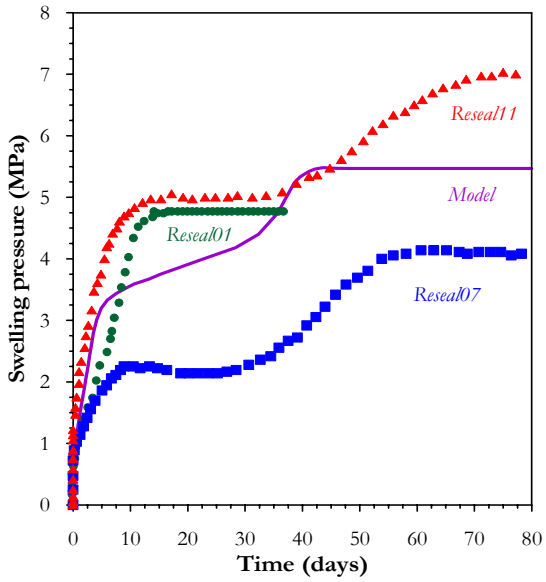

Figure 3.11. Time evolution of the swelling pressure. Test data from Volckaert *et al.* (2000)

In the case of plastic loading, assuming that both plastic mechanisms are initially active (*lc* and β) the system (3.39) is now given by:

$$\begin{cases} \dot{\lambda}_{LC}\overline{H}_{LC} + \dot{\lambda}_{\beta}\overline{h}_{\beta} = \dot{e}_{LC} + \dot{s}^{M}_{LC} + \dot{s}^{m}_{LC} + \dot{t}_{LC} \\ \dot{\lambda}_{LC}\overline{h}_{LC} + \dot{\lambda}_{\beta}\overline{H}_{\beta} = \dot{e}_{\beta} + \dot{s}^{M}_{\beta} + \dot{s}^{m}_{\beta} + \dot{t}_{\beta} \end{cases} \tag{3.55}$$

in a compact form it can be expressed as:

$$\overline{\mathbf{H}}.\dot{\boldsymbol{\lambda}} = \dot{\mathbf{e}} + \dot{\mathbf{s}}^{M} + \dot{\mathbf{s}}^{m} + \dot{\mathbf{t}} \tag{3.56}$$

where the two new terms are:

$$\dot{\mathbf{s}}^{M} = \begin{Bmatrix} \dot{s}^{M}_{LC} \\ \dot{s}^{M}_{\beta} \end{Bmatrix}; \qquad \dot{\mathbf{s}}^{m} = \begin{Bmatrix} \dot{s}^{m}_{LC} \\ \dot{s}^{m}_{\beta} \end{Bmatrix} \tag{3.57}$$

Following a procedure analogous to the one presented in section 3.4.2.3, the expressions for the case in which two plastic mechanisms are active are obtained. The net stress increment can be expressed as:

$$\dot{\boldsymbol{\sigma}} = \mathbf{D}_e \cdot \dot{\boldsymbol{\varepsilon}} + \boldsymbol{\gamma}_{s_M} \dot{s}_M + \boldsymbol{\gamma}_{s_m} \dot{s}_m + \boldsymbol{\alpha}_T \dot{T} \tag{3.58}$$

With respect to the $\mathbf{D}_{ep}$ matrix (Equation 3.48) and the $\boldsymbol{\gamma}_T$ vector (Equation 3.50) there are no changes for this condition. The two elasto-plastic vectors associated to the macrostructural and microstructural suction are evaluated as:

$$\begin{aligned}\boldsymbol{\gamma}_{sM} = \boldsymbol{\alpha}_{sM} - \frac{1}{\left|\overline{\mathbf{H}}\right|}\mathbf{D}_e \cdot \Big\{ & \overline{H}_\beta \mathbf{m}_{LC}\left[\mathit{l} + \mathbf{n}_{LC}^T \cdot \boldsymbol{\alpha}_{sM}\right] - \bar{h}_\beta \mathbf{m}_{LC}\mathbf{n}_\beta^T \cdot \boldsymbol{\alpha}_{sM} + \\ & \overline{H}_{LC}\mathbf{m}_\beta \mathbf{n}_\beta^T \cdot \boldsymbol{\alpha}_{sM} - \bar{h}_{LC}\mathbf{m}_\beta\left[\mathit{l} + \mathbf{n}_{LC}^T \cdot \boldsymbol{\alpha}_{sM}\right]\Big\}\end{aligned} \tag{3.59}$$

$$\begin{aligned}\boldsymbol{\gamma}_{sm} = \boldsymbol{\alpha}_{sm} + \boldsymbol{\beta}_{sm} - \frac{1}{\left|\overline{\mathbf{H}}\right|}\mathbf{D}_e \cdot \Big\{ & \overline{H}_\beta \mathbf{m}_{LC}\left[\mathit{l}_\beta + \mathbf{n}_{LC}^T \cdot \left(\boldsymbol{\alpha}_{sm} + \boldsymbol{\beta}_{sm}\right)\right] - \bar{h}_\beta \mathbf{m}_{LC}\mathbf{n}_\beta^T \cdot \left(\boldsymbol{\alpha}_{sm} + \boldsymbol{\beta}_{sm}\right) + \\ & \overline{H}_{LC}\mathbf{m}_\beta \mathbf{n}_\beta^T \cdot \left(\boldsymbol{\alpha}_{sm} + \boldsymbol{\beta}_{sm}\right) - \bar{h}_{LC}\mathbf{m}_\beta\left[\mathit{l}_\beta + \mathbf{n}_{LC}^T \cdot \left(\boldsymbol{\alpha}_{sm} + \boldsymbol{\beta}_{sm}\right)\right]\Big\}\end{aligned} \tag{3.60}$$

In Appendix A.2 (Sections A.2.4 and A.2.6) all the expressions necessary to evaluate the elastic and elasto-plastic matrixes and vectors are presented in detail.

3.4 NUMERICAL IMPLEMENTATION

3.4.1 INTRODUCTION

The standard technique in non-linear finite element analysis is to consider a piecewise linear approximation of the problem. In a general scheme, for any given global iteration of any discrete increment considered in the linearization, the main variables of the problem are evaluated for each node of the mesh. In a general *THM* problem these main variables are: the displacement field, the fluids pressures and the temperature. Another main step, in non-linear analyses, is the updating of the stresses and the internal variables at each quadrature point of the finite element discretization.

The strain-stress rate equations (used in the updating of stresses) are formulated as a system of ordinary differential equation (as the one presented in the previous Sections). This system can be solved using proper integration procedures, also known as stress integration method. Several numerical integration schemes have been proposed in order to implement elasto-plastic models in finite elements codes. Two main families of algorithms can be distinguished: the ones based on the explicit forward Euler scheme and the algorithms based on the implicit backward Euler method.

Schemes based on the explicit method have been extensively used for the stress integration of elasto-plastic models. For example, the algorithms proposed by Wissman & Hauck (1983), Sloan (1987) and the schemes built on this latter one (Sloan & Booker, 1992; Garcia Molina *et al.,* 1996; Abbo, 1997, Potts & Zdravković, 1999; Sloan *et al.,* 2001; Sheng *et al.,* 2002). In the next sections more details about these schemes are presented. Now it can be mentioned that

the more refined versions of these algorithms combine sub-stepping techniques with automatic sub-stepping control, error control and yield surface drift correction. An advantage of this kind of schemes is that they are not iterative, which have a particular benefit when highly non-linear models are considered. Moreover, these schemes use the standard form of the elasto-plastic law, so, only the first derivates of the yield surface and plastic potential are required. From a computational point of view this is an aspect of a great interest (reduction of CPU time). Finally, if these advantages are combined with the possibility to maintain a strong control over the errors in the stresses, this algorithm becomes very attractive for its implementation in a finite element code, especially when it is oriented to deal with highly non-linear elasto-plastic models and complex problems.

A complete discussion about the different implicit stress integration methods can be found in several books, as for example Crisfield (1991) and Simo & Hughes (1998). Regarding their applications to soils mechanic models the works of Borja & Lee (1990), Borja (1991), Potts & Ganendra (1992, 1994), Abbo (1997), Vaunat *et al.* (2000) and Tamagnini *et al.* (2002) can be highlighted. Generally speaking, in the implicit backward Euler methods the integration of the 'elasto-plastic problem' is split into two parts: an 'elastic-predictor problem' and a 'plastic-corrector problem'. Three main advantages of this method can be mentioned: it does not require the intersection with the yield surface to be computed when the stress state changes from an elastic to a plastic state, the stresses satisfy automatically the yield criterion (to a specified tolerance) and, it provides all the information required to evaluate the consistent tangent matrix (second order terms; Simo & Taylor, 1985), which gives a quadratic rate of convergence for the global Newton-Raphson scheme. In an implicit method the rate equations are evaluated at unknown stress state and the resulting system of non-linear equations must be solved iteratively at each integration point of the mesh. If a Newton-Raphson scheme is used to solve this system, the second derivates of yield surface and plastic potential may be implemented. The computation of these second derivates (in relation to the stresses) is a shortcoming of the implicit scheme; due to the CPU time consumed on their evaluation, especially from complex models such as the ones used generally in soil mechanics. Furthermore, the implicit scheme is less reliable because the convergence of Newton-Rapshon algorithms is not always guaranteed, especially when highly non-linear problems are considered (Abbo, 1997). Finally, some problems observed in geotechnical applications (*i.e.* in footing problems, Abbo, 1997) alert that special care and strategies are required to ensure convergence, such as sub-stepping techniques combined with very small load steps. These last problems emerge as a strong weakness if the implementation of the model is devoted to solving complex boundary value problems.

As commented by Abbo (1997), it is somewhat surprising that although the successful implementation of an elasto-plastic model in finite elements is critically dependent on the selection of the stress integration algorithm, not many woks can be found in which the performance of the two kinds of schemes are compared. This is even more marked for the case of geotechnical models (perhaps due to their major complexity). There are relatively few contributions addressed to this objective. In this line, Potts & Ganendra (1992, 1994) performed a critical comparison between the explicit sub-stepping scheme of Sloan (1987) and the return mapping algorithm of Ortiz & Simo (1986). A critical state model was used in the analyses, whose complexity is quite representative of a standard geotechnical constitutive law. They conclude that both algorithms give accurate results but, the explicit sub-stepping algorithm is better, because it is more robust and efficient than the implicit return mapping

scheme. At similar conclusions arrive Yamaguchi (1993) when complex constitutive laws are considered. But perhaps the more interesting work in this sense is the one performed by Abbo (1997). He focuses the analyses in the comparisons of the spent CPU time and in the accuracy of the stresses for two different algorithms: the explicit modified Euler one (Sloan's scheme) and the implicit backward Euler return scheme. Rounded forms of the Tresca and Mohr-Coulomb constitutive laws were used in the comparisons. These are relatively simple models compared with the typical ones used in geotechnical problems. According to Abbo (1997), both schemes provide an economical means of integrating rounded Tresca and Mohr-Coulomb constitutive laws. Each procedure requires a similar amount of CPU time and give stresses of a similar accuracy. With respect to the explicit modified Euler scheme, he added two advantages: one is related to the possibility to control the errors in the stresses (to a desired level), and the second one is related to its robustness, mainly due to the no-iterative characteristic of this scheme. Finally, another interesting aspect compared by Potts & Zdravković (1999) is related to the flexibility of the two schemes to include new phenomena or more complex versions of the model in the program. According with their experience, the sub-stepping explicit algorithm is more open and suitable to this end, whereas the software to deal with implicit schemes is more rigid and it is constitutive model dependant.

Some work can be found in the literature concerning the capability of the two kinds of schemes to handle elasto-plastic models in which there is more than one dissipation source. The explicit schemes have been widely used to integrate these kinds of models (*i.e.* Potts & Zdravković, 1999) and, in respect of the implicit scheme; the work of Simo & Hughes (1988) is a good reference. It seems that these two algorithms can deal with multidissipative models without major problems.

3.4.2 MODEL INTEGRATION

Either an explicit or an implicit scheme can be used to integrate the double structure model presented in the previous Sections. In recent work (Heeres, 2001; de Borst & Heeres, 2002) the implicit integration algorithms have been extended to handle non-standard elasto-plastic models (such as the generalized plasticity law presented here). Since the stresses must be integrated many times on the course of a typical non-linear problem simulation, the selection of a specific algorithm should be based on the accuracy of the solution and also on its robustness and efficiency.

In the case of CODE_BRIGHT the Newton-Rapshon method is used for the global solution of the problem (at mesh level). In this scheme, it is necessary to update stresses and internal variables once for each iteration, for each time increment and for each gauss point of the discretization. In addition, there are other two strong constraints, one of them is that the double structure model is highly non-linear, and the other is that the final objective is to solve complex *THM* coupled boundary value problems. These facts stress the necessity to count on a competent and tested algorithm to integrate this model.

A refined explicit Euler method with automatic sub-stepping and errors control has been used to implement the expansive model. Based on the consideration presented in the Section before, the main reasons to adopt this scheme for this model are the following:

- It is possible to control the integration errors so as lie near a prescribed error tolerance. A strong control over the errors in the stresses integration process is feasible.

- It is a robust and efficient scheme. These qualities have been checked for highly non-linear elasto-plastic models and also to solve complex geotechnical boundary value problems.

- It provides an open and flexible framework to accommodate new versions of the model. It is quite straightforward to incorporate other irreversible mechanisms in the elasto-plastic law.

The addition to this model of irreversible effects induced by geochemical variables, such as, osmotic suctions and cation exchange (Guimarães *et al.* 2001, Guimarães 2002), has provided the possibility to check the last item mentioned in the previous paragraph. Their implementations in the code were reasonably direct and could be done in a consistent and a modular way in the existing program structure.

Although lots of works related to the stresses integration methods can be found, comprehensive computational details of the algorithms are seldom given. This is not the case of the selected scheme, because exhaustive information in this respect can be found in many of the cited work. Due to that, only the main aspects of the implemented scheme are presented here, more details are given elsewhere (Sloan, 1987; Abbo, 1997; Sloan *et al.,* 2001). The algorithm is based on the original one proposed by Sloan (1987), with the extension to unsaturated conditions proposed by Garcia Molina *et al.* (1996) and taking into account some of the subsequent improvements suggested for this algorithm. The scheme has been extended to the specific characteristics of the double structure model. As main features it can be mentioned that it can deal with more than one plastic mechanism active (in which one of then can be a generalized plasticity model) and it can include the effects of strains, suctions (micro and macro) and temperature in the stress integration process.

The implemented algorithm has been developed for the case in which an elastic domain can be present. That is, similar to the *BExM* (Alonso *et al.*, 1999) presented in Appendix A.2 (Section A.2.1). In this case four different situations can be distinguished in relation to the current stress state and the irreversible mechanisms active. The first one (case I) is related to a purely elastic response of the material, which corresponds to a stress state inside the shaded area zone in the scheme of Figure (3.12). The second case (II) is associated to a plastic response of the material due to *LC* yielding (*BBM* model). Now the stress state is on the *LC* yield surface and the irreversible coupling mechanisms (β) are not active. The third case (III) is related to one interaction mechanism (β) active and with the stress state inside the *LC* yield curve. Finally, the fourth case (IV) is associated to a plastic behaviour of the material with two plastic mechanisms, *i.e.* the *lc* mechanism plus one coupling mechanism (β) active.

In order to explain the mechanics of how the developed algorithm integrates the elasto-plastic law, firstly a simpler situation is considered. A case in which one plastic mechanism is activated in the transition from the elastic to plastic behaviour is first explained (for example

the transition between case I and II has been considered). The other cases are introduced afterwards.

The control variables of the problem are strains, macro suction, micro suction and temperature. With the only objective to facilitate the explanation, the generic name of generalized strains is assigned to them. The initial estate of the material is given by the initial stresses, the initial values of hardening parameters (p_o^* and $\hat{p}_{NL}$) and the initial values of the history variables (e_m and e_M).

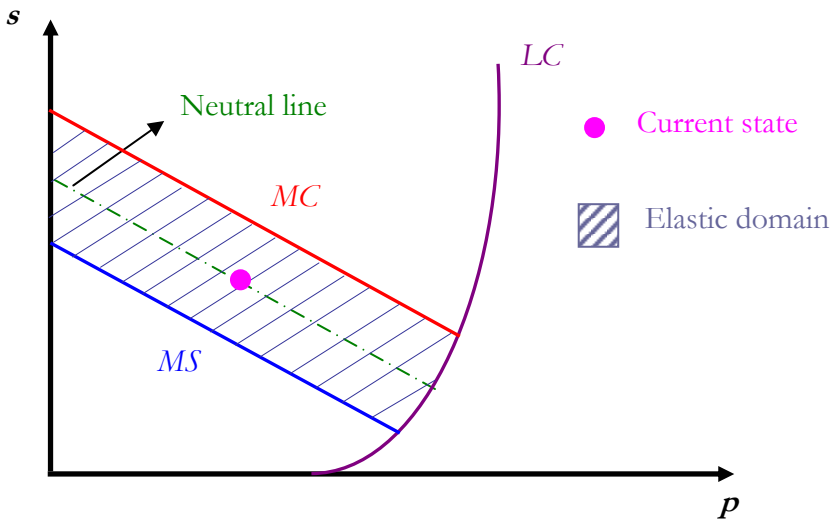

Figure 3.12. Graphical summary of the double structure elasto-plastic model with the yield surfaces associated to the interaction mechanisms

During a typical iteration of a non-linear problem, at each integration point, the initial state and the increment in the generalized strains are known. The stresses must be numerically updated in order to be in accordance with these generalized strains increment. To do that, an initial stage is the division of the given generalized strains increment into a number of sub-steps. This sub-stepping is done following the standard approach of Sloan's algorithm, that is, defining a pseudo time τ :

$$\tau = \frac{(t - to)}{\Delta t} \qquad 0 \le \tau \le 1 \tag{3.61}$$

where t_o is the time at the start of the considered increment (global system) and $(t_o + \Delta t)$ is the time at the end of this increment. In Section 3.4.2.5 the implemented sub-stepping strategy is introduced.

Afterwards four main stages are followed, indicated as follows:

- *Elastic stress integration:* it is assumed that the generalized strains sub-increment is entirely elastic. The stresses are updated integrating the elastic generalized strains-stress law over this sub-increment. At the end of the sub-increment, it is checked if the trial stress state is outside the yield surface, if not, no plastic yield occurs and the stress state is updated with the trial stress state. Exit.

- *Intersection with the yield surface*: if the trial stress state causes plastic yielding, the intersection point between the trial stress path and the yield surface is found. The stresses are updated with the elastic part of the generalized strains sub-increment. The other portion of the generalized strains sub-increment is integrated in the plastic stress updating.

- *Elasto-plastic stress integration*: the stresses are updated integrating the elasto-plastic law over the sub-increment of the generalized strains considered. At the end of the sub-increment, it is checked (and corrected if it is necessary) if the stresses are on the yield surface according to the procedure indicated as follows.

- *Yield surface drift correction*: if the final stress state is found outside the updated yield surface, the stress state is projected back to the yield surface using a drift correction method. Exit.

3.4.2.1 ELASTIC STRESS INTEGRATION

In the first version of the Sloan's scheme (Sloan, 1987) a Hooke's law is adopted to the elastic part of the model. In this case the evaluation of the trial stress vector is obtained straightforwardly multiplying the strains increment vector by the constant elastic matrix. On the other hand, the integration of a non-linear elastic law of an elasto-plastic model is not a trivial task, mainly due to its influence on the evaluation of the yield surface intersection. Sloan *et al.* (2001) extends the original Sloan's scheme for the case of critical state model. In this case the stress dependence of the elastic parameters K and G implies a non-linear elastic behaviour. For this case, in order to find the trial stress state, Sloan *et al.* (2001) propose the use of more proper secant moduli (of K and G), instead of the tangent ones.

A different decision has been taken here to integrate the non-linear elastic model. The same modified Sloan's scheme with errors control and sub-stepping used in the elasto-plastic update is applied to integrate the elastic part of the model. This provides the possibility to integrate the elastic and elasto-plastic part of the constitutive law with the same degree of accuracy and efficiency. It is interesting to remind that the elastic law is highly non-linear, because the elastic operators depend on stresses, suctions (macro and micro) and temperature. Moreover, the elastic contribution of the microstructure must be added, with a high non-linear dependence of the microstructural stiffness on stresses and micro suction (Equation A2.23). In Sloan's algorithm the size of each sub-increment may vary through the integration process, depending on the non-linearity of the constitutive relations. This allows finding accurately and efficiently the updated stresses and also the intersection point with the yield surface, when the elastic part of model is highly non-linear.

Considering a pseudo time sub-increment in the range $0 \leq \Delta\tau_n \leq 1$, and using the subscript n-1 and n to denote quantities computed at the pseudo time τ_{n-1} and $\tau_n = \tau_{n-1} + \Delta\tau_n$, the values of the generalized strains for this sub-increment are given by:

$$\Delta\boldsymbol{\varepsilon}_n = \Delta\tau_n \Delta\boldsymbol{\varepsilon} \; ; \qquad \Delta s_M = \Delta\tau_n s_M \; ; \qquad \Delta s_m = \Delta\tau_n s_m \; ; \qquad \Delta T = \Delta\tau_n T \tag{3.62}$$

With the explicit Euler method and for the more general case (Equation 3.54), the increments of stresses at the end of the pseudo time step $\Delta\tau_n$ are evaluated through:

$$\Delta\boldsymbol{\sigma}_1 = \mathbf{D}_{e\left|\boldsymbol{\sigma}_{n-1}, r_{n-1}\right.} . \Delta\boldsymbol{\varepsilon}_n + \boldsymbol{\alpha}_{sM\left|\boldsymbol{\sigma}_{n-1}, s_{M_{n-1}}, r_{n-1}\right.} \Delta s_M + \boldsymbol{\alpha}_{sm\left|\boldsymbol{\sigma}_{n-1}, s_{m_{n-1}}, r_{n-1}\right.} \Delta s_m + \boldsymbol{\alpha}_{T\left|\boldsymbol{\sigma}_{n-1}, T_{n-1}, r_{n-1}\right.} \Delta T \tag{3.63}$$

The estimated value of stresses and internal variables are obtained from:

$$\boldsymbol{\sigma}_n = \boldsymbol{\sigma}_{n-1} + \Delta\boldsymbol{\sigma}_1 \tag{3.64}$$

$$r_n = r_{n-1} + \Delta r_1 \tag{3.65}$$

In this case, the internal variables (r) correspond to the history variables: e_M and e_m. A more accurate estimation of the stresses increment at the end of the interval $\Delta\tau_n$ can be found using the modified Euler procedure:

$$\Delta\boldsymbol{\sigma}_2 = \mathbf{D}_{e\left|\boldsymbol{\sigma}_n, r_n\right.} . \Delta\boldsymbol{\varepsilon}_n + \boldsymbol{\alpha}_{sM\left|\boldsymbol{\sigma}_n, s_{M_n}, r_n\right.} \Delta s_M + \boldsymbol{\alpha}_{sm\left|\boldsymbol{\sigma}_n, s_{m_n}, r_n\right.} \Delta s_m + \boldsymbol{\alpha}_{T\left|\boldsymbol{\sigma}_n, T_n, r_n\right.} \Delta T \tag{3.66}$$

The following estimation of the stresses and internal variables can be made with:

$$\tilde{\boldsymbol{\sigma}}_n = \boldsymbol{\sigma}_{n-1} + \frac{1}{2}\left(\Delta\boldsymbol{\sigma}_1 + \Delta\boldsymbol{\sigma}_2\right) \tag{3.67}$$

$$\tilde{r}_n = r_{n-1} + \frac{1}{2}\left(\Delta r_1 + \Delta r_2\right) \tag{3.68}$$

The local error measure is found by taking the difference between a modified Euler solution, which is of second order accuracy, and an Euler solution, which is of first order accuracy (Sloan, 1987; Abbo, 1997). It therefore corresponds to an estimation of the local truncation error. The relative error measure (R_n) can be obtained using any convenient norm, as:

$$R_n = \frac{1}{2}\frac{\left\|\Delta\boldsymbol{\sigma}_2 - \Delta\boldsymbol{\sigma}_1\right\|}{\left\|\tilde{\boldsymbol{\sigma}}_n\right\|} \tag{3.69}$$

The updating of the current sub-increment is accepted if R_n is not greater than some prescribed tolerance, *STOL*, or it is rejected otherwise. In this latter case ($R_n > STOL$) a reduction of the sub-increment is made according with Section 3.4.2.5, and the integration process is repeated considering the new (reduced) generalized strain sub-increment. This loop is repeated until the prefixed value of error tolerance is fulfilled. More details are given in Section 3.4.2.5.

When the acceptance condition is satisfied (*i.e.* $R_n \leq STOL$), previous to updating the stresses, it is necessary to check if the new stress state remains inside the elastic domain. In Section 3.4.2.2 the procedure followed to check this condition is introduced. According to Sloan ***et al.*** (2001), in the case of purely elastic generalized strains sub-increment, the stresses and internal variables can be updated whether using Equations (3.64) and (3.65) or Equations (3.67) and (3.68). These two latter ones have been used for the case in which the integrated stress state is inside the yield surface, obtaining:

$$\boldsymbol{\sigma}_n = \tilde{\boldsymbol{\sigma}}_n \tag{3.70}$$

$$r_n = \tilde{r}_n \tag{3.71}$$

Finally the size of pseudo time sub-interval is automatically adjusted according to Section 3.4.2.5, and a new sub-step can be started.

3.4.2.2 INTERSECTION WITH THE YIELD SURFACE

At the end of each elastic sub-increment it is checked if the stress state has changed from elastic to plastic (case I to case II). This happens if:

$$F_{n-1} = F_{|\boldsymbol{\sigma}_{n-1}, r_{n-1}|} < 0 \qquad \textit{and} \qquad F_n = F_{|\boldsymbol{\sigma}_n, r_n|} > 0 \tag{3.72}$$

In this case, to determine the portion of the stress increment that lies within the yield surface, it is necessary to find a scalar μ such as:

$$\boldsymbol{\sigma}_{in} = \boldsymbol{\sigma}_{n-1} + \mu\Delta\boldsymbol{\sigma}_1 \tag{3.73}$$

$$F_{in} = 0 \tag{3.74}$$

For an elastic to plastic transition μ lies within the range $0 < \mu < 1$. A value of μ equal to zero (0) implies a purely plastic deformation during the sub-step, whereas when it is equal to one (1) indicates a purely elastic response during the sub-step. Therefore μ gives the portion of the generalized strains sub-increment that moves the stresses from $\boldsymbol{\sigma}_{n-1}$ to the intersection with the yield surface $\boldsymbol{\sigma}_{in}$. In the numerical implementation of the algorithm, the exact condition (Equation 3.74) is replaced by a transition given by $\left| F_{in} \right| < FTOL$, were $FTOL$ is a small positive tolerance. The yield surface tolerances recommended as suitable by Sloan *et al.* (2001) have been used in the analyses (the values are typically in the range 10^{-6} to 10^{-9}).

The value of μ is obtained solving the non-linear Equation (3.74). The Newton-Rapshon scheme proposed by Sloan (1987) has been extended for the double structure model:

$$\begin{aligned}
&\boldsymbol{\sigma}_{k} = \boldsymbol{\sigma}_{k-1} + \mu_{k} \Delta\boldsymbol{\sigma} \\
&\mu_{k+1} = \mu_{k} + \Delta\mu_{k+1} \\
&\Delta\mu_{k+1} = -\frac{F_{k}}{\left(\partial F/\partial\boldsymbol{\sigma}\right)_{k}^{T} \Delta\boldsymbol{\sigma} + \left(\partial F/\partial s\right)_{k} \Delta s_{M} + \left(\partial F/\partial T\right)_{k} \Delta T}
\end{aligned} \tag{3.75}$$

The iterative procedure is started by assuming $\boldsymbol{\sigma}_0 = \boldsymbol{\sigma}_{n-1}$ and a seed value for μ_1, and continues until a relative error in the norm of stresses, defined by the following Equation, is less than some specified tolerance $ITOL$ (generally close to 10^{-9}).

$$\frac{\left\| \boldsymbol{\sigma}_{k+1} - \boldsymbol{\sigma}_{k} \right\|}{\left\| \boldsymbol{\sigma}_{k} \right\|} < ITOL \tag{3.76}$$

The Newton-Raphson is an efficient method to find the intersection point with the yield surface, generally it converges rapidly (typically about 5 iterations) but, as commented, the convergence is not guaranteed in this method. Therefore, this method has been combined with a bisection algorithm. This is a less efficient algorithm than the Newton-Raphson one, but unconditionally convergent for continuous yield functions (Sloan *et al.,* 2001). In the numerical implementation of the algorithm, if the Newton-Raphson method does not converge after 10 iterations, the alternative bisection method is used. But, according with the experience of the cases modelled in this Thesis, this situation rarely occurs and generally the intersection is found with a few number of Newton-Raphson iterations (less than six).

Once Equation (3.76) is satisfied the stresses and internal variables are updated using the following Equations (3.77 and 3.78) respectively; and the plastic part of the generalized strains increments (1-μ) is integrated according to Section 3.4.2.3.

$$\boldsymbol{\sigma}_n = \boldsymbol{\sigma}_k \tag{3.77}$$

$$r_n = r_k \tag{3.78}$$

3.4.2.3 ELASTO-PLASTIC STRESS INTEGRATION

The case analysed here corresponds to a stress state on the yield surface and in which one of the irreversible mechanisms β are not active (case II). For this case, the elasto-plastic law stress integration procedure is analogous to the one explained for the elastic part of the model, Section 3.4.2.1. Now the elastic operators of the Equation (3.63) and (3.66) are replaced by the elasto-plastic one (using tensors equivalent to 3.48, 3.50, 3.59 and 3.60). Once the errors criteria for the elasto-plastic integration are fulfilled (*i.e.* $R_n \leq STOL$, with R_n given by Equation 3.69), the stresses and the internal variables are updated (Equations 3.70 and 3.71, respectively). Depending on whether the sub-increment stress integration is accepted or rejected, the pseudo time is automatically adjusted for the next sub-step. Some details about the sub-stepping strategy are introduced in Section 3.4.2.5. Finally, at the end of each elasto-plastic sub-step it is necessary to check if the stress state is on the yield surface. The procedure explained in the next section is used to this end.

3.4.2.4 YIELD SURFACE DRIFT CORRECTION

In this scheme it is possible that the accepted updated stresses (at the end of the sub-increment) do not satisfy the yield criterion, therefore $\left| F_n \right| > FTOL$. As such departures are cumulative during the integration process, it is necessary to ensure that the stresses are corrected at the end of each sub-increment in order to satisfy the yield condition and, consequently, update accurately the stresses. Different methods to correct the stresses have been proposed in the literature. In the work of Potts & Gens (1985) a comprehensive study related to different techniques used in geotechnical models were performed. In these methods, the stresses are corrected back to the yield surface according with different criteria to projecting back.

The recommended method by Potts & Gens (1985) has been selected here for the model implementation. The method is the one identified as 'correct' in that work and the basic assumption is the consideration of constant total strain during the correction process. This implies that an elastic strain change must be balanced by an equal and opposite change in the plastic strains. As commented by Potts & Gens (1985), this consideration is consistent with the philosophy of displacement finite element procedure. In addition, it is considered that during the correction process the macrostructural suction and the temperature remain constant. A complete description of this technique can be found in Potts & Gens (1985) and in Sloan *et al.* (2001) as well. Only the main equations of the algorithm are presented here.

The problem under consideration can be described as follows: the stress state at the beginning of the sub-increment ($\boldsymbol{\sigma}_{n-1}$) satisfies the yield criterion (because of the correction applied at the end of the last sub-increment), during the current sub-increment the stresses and the hardening parameter have been updated obtaining ($\boldsymbol{\sigma}_n$) and (r^p_n) respectively. Owing to the tendency to drift the predicted stresses does not necessarily lie on the new yield surface, *i.e.* $|F_n| > FTOL$. Therefore, the corrected values of ($\boldsymbol{\sigma}_c$) and (r^p_c) that satisfy the yield criterion ($|F_c| < FTOL$) are found by imposing:

$$\delta\boldsymbol{\varepsilon}^p = \delta\boldsymbol{\varepsilon}^e \tag{3.79}$$

where δ indicates correction. The elastic strains corrections can be obtained as:

$$\delta\boldsymbol{\varepsilon}^e = \left[\mathbf{D}_e\right]^{-1}\left(\boldsymbol{\sigma}_c - \boldsymbol{\sigma}_n\right) \tag{3.80}$$

The plastic strains corrections are proportional to the plastic potential, according to:

$$\delta\boldsymbol{\varepsilon}^p = \mu_c \frac{\partial G}{\partial \boldsymbol{\sigma}} \tag{3.81}$$

where μ_c is an unknown scalar. Combining Equations (3.80) and (3.81) and considering the changes in the hardening parameter, the next set of equations is obtained:

$$\boldsymbol{\sigma}_c = \boldsymbol{\sigma}_n - \mu_c \mathbf{D}_e \frac{\partial G}{\partial \boldsymbol{\sigma}} \tag{3.82}$$

$$r^p_c = r^p_b + \mu_c \delta r^p \frac{\partial G}{\partial \boldsymbol{\sigma}} \tag{3.83}$$

In the case of *BBM* model, δr^p corresponds to the correction associated to the hardening variable p^*_o. The corrected stresses state must satisfy the yield criterion according to:

$$F_c = F\left|\left(\boldsymbol{\sigma}_n - \mu_c \mathbf{D}_e \frac{\partial G}{\partial \boldsymbol{\sigma}}\right), \left(r^p_b + \mu_c \delta r^p \frac{\partial G}{\partial \boldsymbol{\sigma}}\right)\right| = 0 \tag{3.84}$$

Expanding Equation (3.84) as a Taylor's series and neglecting terms in μ^2_c, the equation for the unknown scalar is obtained (Potts & Gens, 1985):

$$\mu_c = \frac{F_{|\boldsymbol{\sigma}_n, r_n^b|}}{\left(\frac{\partial F}{\partial \boldsymbol{\sigma}}\right)^T \mathbf{D}_e \frac{\partial G}{\partial \boldsymbol{\sigma}} - \left(\frac{\partial F}{\partial r^b}\right)^T \delta r^b \frac{\partial G}{\partial \boldsymbol{\sigma}}} \tag{3.85}$$

Once μ_c is known, the corrected values of stresses and internal variables can be evaluated. It is possible that this scheme must be applied repeatedly until the yield condition ($|F_c| < FTOL$) is satisfied.

3.4.2.5 SUB-STEPPING STRATEGY

The stepping procedure suggested by Sloan *et al.* (2001) has been adapted to integrate this model (Sánchez & Guimarães, 2002). As a main feature of this strategy it can be mentioned that once the local error has been computed for a given step, the size of the next step is evaluated considering this error estimation. Therefore, the size of the each sub-interval is adjusted according with the information of the last step. This error control allows varying automatically the size of the interval over the course of the integration, depending on the non-linearity of the model.

The sub-increment strategy and the main stages of the integration can be summarized in 10 stages, introduced as follows:

- 1. The integration scheme is started with the known initial state (stresses and internal variables) and the generalized strains increment.
- 2. An initial pseudo time step is assumed $\Delta\tau_1$ (a value of 0.5 is typically adopted).
- 3. The generalized strains sub-increment is obtained from Expressions (3.62).
- 4. The integration procedure indicated in Section 3.4.2.1 or 3.4.2.3 is performed depending on whether it is an elastic or an elasto-plastic integration.
- 5. The relative error measure (R_n) is computed (Equation 3.69) and q is evaluated with:

$$q = 0.95\sqrt{STOL / R_n} \qquad \text{with the constrain:} \quad 0.2 \le q \le 1.2 \tag{3.86}$$

- 6. Regardless of whether the sub-increment is accepted or not, the next pseudo time step is automatically adjusted with:

$$\Delta\tau_{n+1} = q\Delta\tau_n \tag{3.87}$$

- 7. After a successful elastic sub-increment, it is necessary to check if the updated stress state remains inside the yield surface (Section 3.4.2.2).

    - If the sub-increment is purely elastic the stresses and history variables are updated according to Equations (3.70) and (3.71). Then the pseudo time is checked according to stage 10.

    - If the stresses sub-increment cross the yield surface, stresses and internal variables are updated with the elastic portion (Equations 3.77 and 3.78). The plastic part of the sub-increment is integrated according to Section 3.4.2.3.

- 8. After a successful elasto-plastic sub-increment, it is necessary to correct the drift of the yield surface according to Section 3.4.2.4. Then the pseudo time is checked according to stage 10.

- 9. After a refused sub-increment (elastic or elasto-plastic) a new sub-increment is re-started with a smaller step-size (Equation 3.87) and with reduced generalized strains sub-increments according to Expressions (3.62). This loop is repeated until a successful sub-increment size is obtained. Here, an additional control is imposed in order to avoid lots of iterations. The users can establish a maximum number of iterations to reach a successful integration, after that, the integration process is aborted and a reduction of the time increment is imposed over the global system. This strategy yields good results, especially when complex highly non-linear problems are modelled.

- 10. The sub-stepping integration continues until the entire increment of the generalized strains is applied, this is verified through:

$$\sum \Delta\tau = \tau = 1 \tag{3.88}$$

3.4.2.6 INTEGRATION OF THE GENERALIZED PLASTICITY MODEL

The scheme used to integrate the generalized plasticity model is an adaptation of the elasto-plastic one explained above. As commented, the generalized plasticity theory offers different alternatives to model the elasto-plastic behaviour. The hypothesis that there is not an elastic region associated to this mechanism ($H^m{}_\beta=1$) is presented here. In the Appendix A.2.1.2 the particular case in which an elastic domain exists is introduced.

Firstly, the case of a stress state inside the *LC* yield curve is introduced (case III). For each sub-step, the procedure starts with a known initial state (stresses and internal variables) and the evaluation of the generalized strains increment according to Equation (3.62). After that, the Loading/Unloading criteria given by Equations (3.18) to (3.20) are expressed in a proper way for numerical purposes, *i.e.* in terms of tolerances:

$$\hat{\mathbf{n}}_C^T \cdot \dot{\hat{\boldsymbol{\sigma}}}^e > CTOL \rightarrow \text{Microstructural Compression path } (MC) \tag{3.89}$$

$$\hat{\mathbf{n}}_S^T \cdot \dot{\hat{\boldsymbol{\sigma}}}^e > CTOL \rightarrow \text{Microstructural Swelling path } (MS). \tag{3.90}$$

$$\left.\begin{array}{l} \hat{\mathbf{n}}_C^T \cdot \dot{\hat{\boldsymbol{\sigma}}}^e < CTOL \\ \hat{\mathbf{n}}_S^T \cdot \dot{\hat{\boldsymbol{\sigma}}}^e < CTOL \end{array}\right\} \rightarrow \text{Neutral Loading } (NL) \tag{3.91}$$

where $\dot{\hat{\boldsymbol{\sigma}}}^e$ is the elastic generalized stress sub-increment and *CTOL* is a tolerance associated to the loading criteria of the coupling mechanism between structures. The values of *CTOL* are typically in the range 10^{-7} to 10^{-9}.

The stress integration scheme adopted corresponds to an elasto-plastic law. That is, the procedure explained in the Section 3.4.2.1 but replacing the elastic operator of Equations (3.63) and (3.66) by the elasto-plastic ones, which may be evaluated depending on the active plastic mechanism *mc* or *ms* (using tensors equivalent to 3.48, 3.50, 3.59 and 3.60). At the end of the sub-increment the error is computed according to Equation (3.69). The updating of the current sub-increment is accepted if R_n is not greater than some prescribed tolerance, *STOL* ($R_n < STOL$), or it is rejected otherwise. If the step is accepted and the stress state remains inside the *LC* yield curve, the stresses and internal variables ($\hat{p}_{NL}$ and e_m) are updated. If not, the sub-increment is re-started, following a procedure similar to the explained in Section 3.4.2.5.

The generalized plasticity model is integrated with the same degree of accuracy and efficiency that the *BBM* elasto-plastic law. From an algorithm point of view, the main difference, in relation to the elasto-plastic law updating, is that the yield surface drift correction (Section 3.4.2.4) is omitted in the generalized plasticity integration. This is a proper choice when the yield surface can not be identified or it is not clearly defined, as it generally happens with the coupling mechanisms considered here. This task (yield drift correction) should be done many times on the course of a typical simulation. It does not seem reasonable to spend much CPU time to return to one yield surface that is not well known. In any case, the implementation performed contemplates the possibility to consider an elastic domain limited by yield surfaces, for cases in which the frontier between elastic and elasto-plastic behaviour could be experimentally determined. In the Appendix A.2 (Section A.2.2.1) an example is presented in which the activation and deactivation of the plastic mechanisms occur at some stage of the simulation.

At the end of each sub-step it is necessary to check if the stress state lies within the *LC* yield surface. A procedure analogous to the one explained in the Section 3.4.2.2 is followed for this case. The algorithm used to find the intersection point with the yield surface is similar to system presented in Equations (3.75). The difference now is that the hardening parameter of the *BBM* model changes due to the coupling mechanism between structures. Considering this fact, the algorithm used is the following:

$$\begin{aligned}
&\boldsymbol{\sigma}_{k} = \boldsymbol{\sigma}_{k-1} + \mu_{k}\Delta\boldsymbol{\sigma} \\
&\mu_{k+1} = \mu_{k} + \Delta\mu_{k+1} \\
&\Delta\mu_{k+1} = -\frac{F_{k}}{\left(\partial F/\partial\boldsymbol{\sigma}\right)_{k}^{T}\Delta\boldsymbol{\sigma} + \left(\partial F/\partial s\right)_{k}\Delta s_{M} + \left(\partial F/\partial T\right)_{k}\Delta T + \left(\partial F/\partial r^{h}\right)_{k}\Delta r^{h}}
\end{aligned} \tag{3.92}$$

The iterative procedure is started assuming $\boldsymbol{\sigma}_0 = \boldsymbol{\sigma}_{n\text{-}1}$, $r_0 = r_{n\text{-}1}$ and a seed value for μ_1. The iterative procedure continues until a relative error in the norm of stresses, defined by Expression (3.76), is less than some specified tolerance *ITOL* (generally close to 10^{-9}).

For the same reason introduced in Section 3.4.2.2, this Newton-Raphson algorithm is combined with a bisection algorithm. If the Newton-Raphson method does not converge after 10 iterations, the alternative bisection method is used. But, as commented, the performance Newton-Raphson scheme in the cases simulated in this thesis was very good. Once Equation (3.76) is satisfied, the stresses and internal variables are updated using Equations (3.77) and (3.78) respectively. The plastic part of the generalized strains increments (1-μ) is integrated considering the two plastic mechanisms active, as it is explained in the next paragraph.

When two irreversible mechanisms (case IV) are active, that is when *BBM* yielding and β mechanism are active, the integration process used is the one indicated in Section 3.4.2.3. Stresses and internal variables are updated following the modified Euler scheme presented in Section 3.4.2.1, but now the elasto-plastic matrix and vectors correspond to the ones indicated in Equations (3.48, 3.50, 3.59 and 3.60, case IV). At the end of the sub-increment the Expression (3.65) is evaluated. If the step is accepted the stresses and internal variables are updated. If not, the sub-increment is re-started, following a procedure similar to the one explained in Section 3.4.2.5. Finally, at the end of each successful sub-increment, the correction of stresses and internal variables due to the yield surface drift is performed according to a procedure similar to the one introduced in Section 3.4.2.4.

3.5 APPLICATION CASES

The mechanical model has been applied to two different problems related to the behaviour of expansive materials. In the two examples the hypothesis that there is not an elastic region associated to the interaction mechanism is assumed (H^{m}_{β}=1). In Appendix A.2, Chapter IV and V there are more examples in which the model has been used.

3.5.1 SWELLING PRESSURE TEST

The swelling pressure test offers valuable information related to the behaviour of expansive soils. In this section the simulation of a test carried out by Romero (1999) an a sample of Boom clay pellets is presented. In these materials two structural levels can be clearly distinguished: the microstructure associated to the high density pellets (dry density 1.96 Mg/m^3); and the macrostructure that corresponds to the granular-like arrangement of these pellets (dry density 1.37 Mg/m^3) with macropores between the pellets. The corresponding macro and micro void ratios are 0.60 and 0.35, respectively.

The adopted parameters are in the range of the ones determined by Romero (1999). The parameters are presented in Table (3.1). The stiffening of the material with suction has been considered trough Equation A3.14 (Appendix A3). The aim here is not to validate the model, but to check its capability to explain and to reproduce the main tendencies observed in the test (Figure 3.13). The isotropic response of the model is presented. Figure (3.14) shows the computed mean stress-suction path obtained under conditions of constant volume and prescribing the same suctions steps of the test. It can be observed that the model can reproduce satisfactorily the main trends observed during the experiment.

The initial condition (*I*) corresponds to an initial suction of 80 MPa and a low vertical stress, inside the elastic domain. Then a wetting path is followed until values of suctions close to 0.01 MPa (point *W*). Finally the sample is subjected to a drying process, with a maximum suction of 0.4 MPa. Figure (3.15) shows the evolution of the *BBM* hardening parameter during the test and Figure (3.16) displays the evolution of the interaction functions f_c and f_s.

The first stage corresponds to the stage of high suction and low stress. In this region the stresses remains inside the *LC* yield surface and the stress path is defined by the increase of load required to compensate the swelling strains due to suction reduction. During this stage (path *I-C*), the *ms* mechanism is active with positive values of the f_s function. This implies that the induced macrostructural plastic strains (due to *ms* mechanism) are expansive, with a tendency to a more open macrostructure and, consequently, a reduction of p_o^*. The *LC* yield curve moves to the left, from the initial position *LC_I* to the contact condition *LC_C* (*i.e.* a macrostructural softening).

Point *C* identifies the contact point between the stress path and the *LC* curve. Under this condition a collapse of the macrostructure occurs and the stresses tend to reduce to compensate the collapse compressive. This implies a hardening of the material with an important increase of p_o^*. Now the stress path is controlled by the shape of the *LC* curve, with both plastic mechanisms active (*lc* plus β). Finally, during the drying path *W-D* the *mc* mechanism is active with positive values of f_c which induces plastic macrostructural strains of contraction (with a macrostructural hardening). The final state of the sample is a denser macrostructure, with a net increment in the value of p_o^* and a larger elastic domain given by the final position of the yield surface *LC_D*.

Table 3.1

Main parameters of the elasto-plastic constitutive law used in Section 3.5.1

Parameters defining the Barcelona Basic Model for macrostructural behaviour

κ	κ_s	α_s (eq.A3.14)	$\lambda_{(0)}$	p_c (MPa)	r	ζ (MPa^{-1})	p_o^* (MPa)
0.015	0.01	-0.05	0.16	0.05	0.57	6.00	0.10

Parameters defining the law for microstructural behaviour (Equation A2.23)

κ_m
0.010

Interaction functions

$$f_C = -0.10 + 0.20\left(p_r / p_o\right)^{0.5} \qquad f_S = -0.10 + 0.2\left(1 - p_r / p_o\right)^2$$

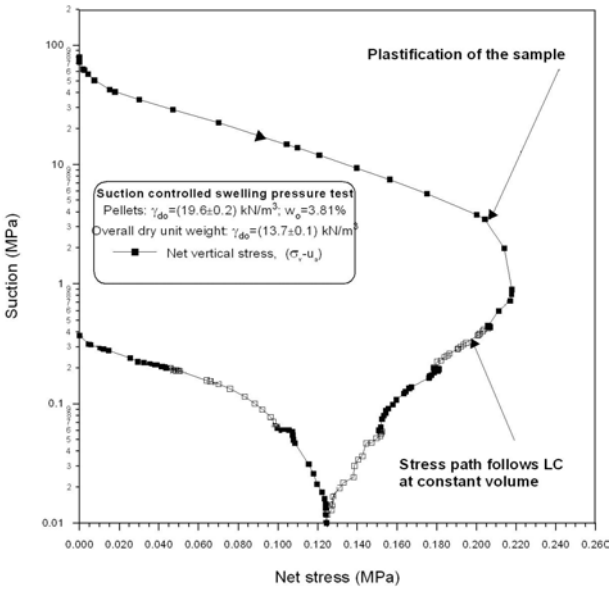

Figure 3.13. Reported stress path. After Romero (1999).

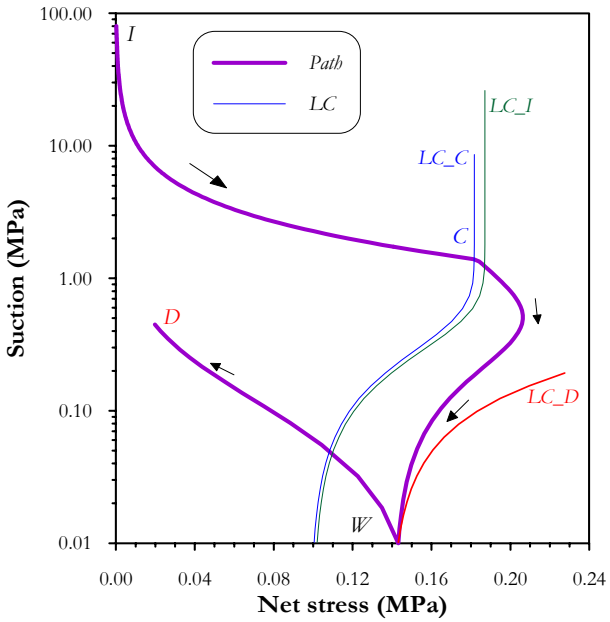

Figure 3.14. Computed stress path, together with the positions of the *LC* curves.

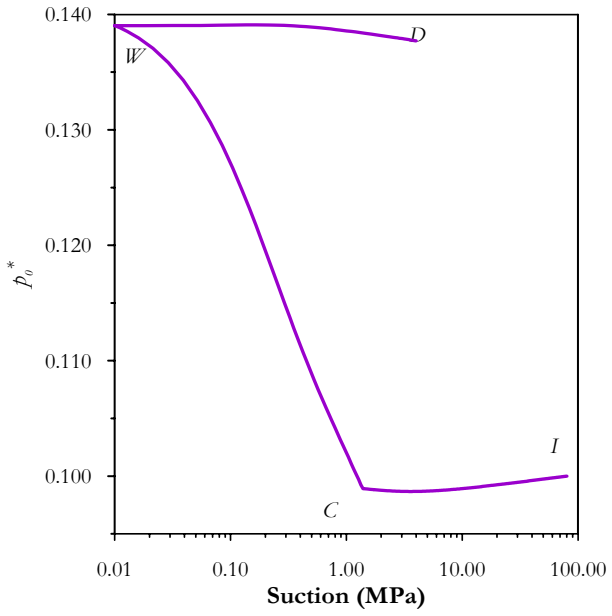

Figure 3.15. Evolution of the hardening parameter, p_0*, during the test.

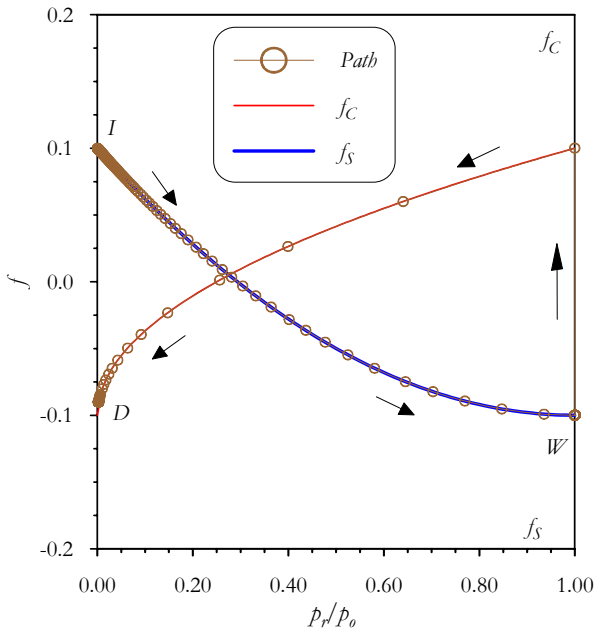

Figure 3.16. Movement of the stress path on the f_C and f_S interaction functions.

3.5.2 CYCLIC WETTING/DRYING TEST

The tests carried out by Pousada (1984) (*i.e.* Figure 3.2) have been selected to analyze the response of expansive clay samples made up from the same fabric and subjected to suction cycles under oedometric conditions at two different vertical stress levels. The tests correspond to samples with a dry density of 1.34 Mg/m^3 and with an initial water content of 24 %, subjected to six wetting-drying suction cycles changing from suction of 0.2 MPa to 1.7 MPa. Table (3.2) shows the values of the various parameters used to model the tests.

The experimentally-observed response of the material, in terms of volumetric deformations, at two different vertical stresses (0.01 MPa and 0.1 MPa) is presented in Figures (3.17) and (3.18). These plots also show the results of the model in terms of: volumetric strains, macro void ratio and micro void ratio. It can be observed that the response obtained is good in qualitative terms, because the model can reproduce the tendency to reduce the swelling capacity of the material when the vertical stress increases, both, in the total strain values and in their irrecoverable components. The reductions in the accumulated strains, when the cycles go on, are also well captured by the model in both tests. This kind of behaviour can be explained considering double structure concepts.

The capability of the *BExM* to simulate the behaviour of swelling clays under cyclic load has been checked in Alonso ***et al.*** (1999). The aim here is to analyse the effect of the applied load on the response of an expansive clay under wetting/drying cycles. As explained in Alonso ***et al.*** (1999), the point *'E'* (in the intersection between the interaction functions), corresponds to the equilibrium conditions reached after a certain number of cycles when the suction cycles develop symmetric paths around it. For both tests presented in Figures (3.17 and 3.18), the suction cycles develop predominantly on the left side of point *E*. This implies net expansions of the samples, which are more marked in the case of the small stress level. This is due to the position of the initial stress with respect to point *E,* which implies a larger movement over the interaction function and, consequently, larger macrostructural strains induced by the interaction mechanism.

Table 3.2

Main parameters of the elasto-plastic constitutive law used in Section 3.6.2

Parameters defining the Barcelona Basic Model for macrostructural behaviour

κ	κ_s	$\lambda_{(0)}$	p_c (MPa)	r	ζ (MPa^{-1})	p_o^* (MPa)	μ
0.050	0.001	0.065	0.01	0.96	0.20	0.75	0.40

Parameters defining the law for microstructural behaviour

α_m (MPa^{-1})	β_m (MPa^{-1})
8.0×10^{-01}	2.0×10^{-02}

Interaction functions

$$f_C = 1.6 + 0.6 \tanh\left(10\left(p / p_o\right) - 0.40\right) \;\; ; \;\; f_S = 1.6 - 0.6 \tanh\left(10\left(p / p_o\right) - 0.40\right)$$

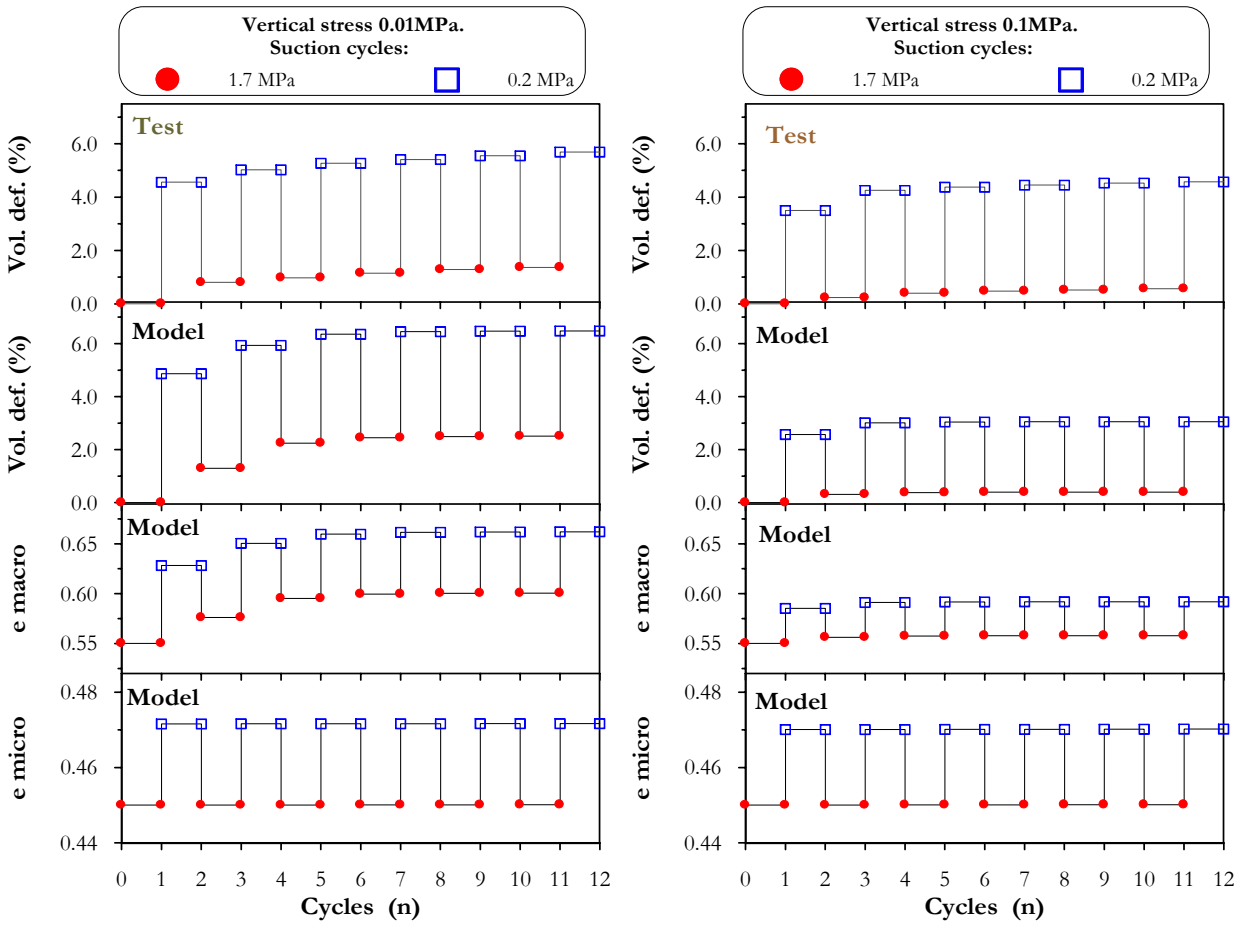

Figure 3.17. σ_v = 0.01MPa. Values of volumetric deformations (reported and computed), macro and micro void indexes induced by suctions cycles (upper graph). Movement of the stress sate on the interaction functions (lower graph).

Figure 3.18. σ_v = 0.1MPa. Values of volumetric deformations (reported and computed), macro and micro void indexes induced by suctions cycles (upper graph). Movement of the stress sate on the interaction functions (lower graph).

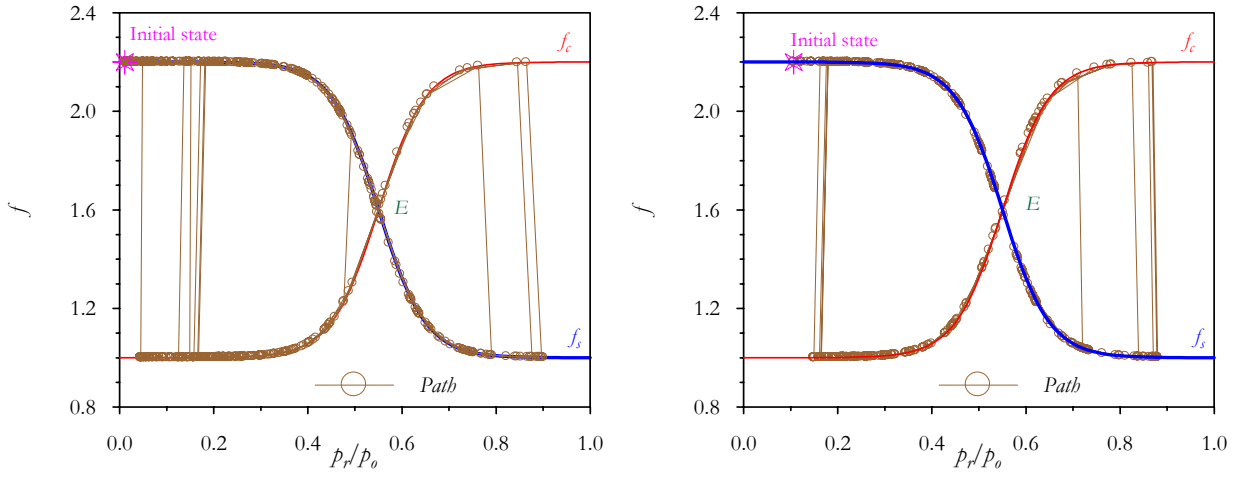

Another interesting aspect is the evolution of the micro and macro void ratios as the cycles take place. The microstructural behaviour is reversible and the changes in the microstructural void ratio are practically independent of the stress level. On the other hand, the macrostructural void ratio is significantly influenced by value of the applied stress. This can be attributed to the increased difficulty of changing the macrostructural arrangement when the material confinement is higher.

3.6 CONCLUSIONS AND REMARKS

A double structure model, based on the general framework for expansive materials proposed by Gens & Alonso (1990) has been presented. In order to be closer to the typical fabric of expansive materials, the existence of two pores structures has been explicitly included in the formulation. The distinction between the macrostructure and microstructure provides the opportunity to take into account the dominant phenomena that affect the behaviour of each structure in a consistent way. For instance, the capabilities of the expansive model to reproduce characteristic phenomena that affect the global arrangements of aggregates, such as macrostructural collapses, have been validated in the application case (Section 3.5.1). The model can handle this kind of behaviour owing to the inclusion of a specific and suitable law for the macrostructural level. On the other hand, the explicit consideration of the microstructure in the formulation allows the integration of phenomena that control the behaviour of clayey material in the analyses properly. Typical response of expansive materials under hydration, such as large swelling strain or high swelling pressure, can be reproduced by the model incorporating simple and well-known laws of clay minerals. Finally, the consideration of the coupling between the two structural levels is a key feature of the model. The model is able to reproduce and explain some typical response of expansive materials thanks to the consideration of irreversible effects in the macrostructure induced by microstructural strains. Irreversible behaviour, such as the one exhibited in the cyclic drying/wetting test, has been simulated and described considering this plastic mechanism in the analyses (Section 3.5.2). In this Thesis, there are other cases in which the inclusion of these irreversible effects in the analyses has played a crucial role to simulate and understand better the behaviour of the expansive materials.

The complex behaviour exhibited by expansive materials under different *THM* conditions requires the development of non-standard models that contemplate the main observed trends. The model has been formulated using concepts of elasto-plasticity for strain hardening materials, as many geotechnical constitutive laws, but, this model is not the typical geotechnical one. A well-known elasto-plastic model for unsaturated soils, which describes the macrostructural behaviour, has been combined with a generalized plasticity model to reproduce the irreversible effects related to the interaction between the two structural levels. The mathematical framework used to formulate the model has been presented in detail. Special attention has been placed on the concepts of the generalized plasticity theory. The difficulty to identify clearly the yield surface of the plastic mechanisms associated to the coupling between the pores structures aims the adoption of this theory. Additionally, the inclusion of generalized plasticity concepts has provided enhanced flexibility that makes it very suitable for practical applications and for the incorporation of new phenomena in the formulation. Finally, the particular case of classical plasticity (when the yield surface can be

identified) can be reproduced without problem within this theory, as confirmed in the application case of Appendix A.2 (Section A.2.1).

The coupled consideration of the elasto-plastic laws has been performed in the context of the formal framework proposed by Rizzi *et al.* (1996) for multidissipative materials. The well-known concepts of classical plasticity for single dissipative materials can be extended using this theory for the cases in which there is more than one source of dissipation. The elasto-plastic tensors related to the increments of strains, macro suction, micro suction and temperature used in the numerical implementation of the model have been derived from this context of multi-dissipative materials. Finally, the elasto-plastic formulation has been extended to consider non-equilibrium between the water potentials associated to each structural level.

The model has been implemented in the finite element program CODE_BRIGHT. Since the stresses should be integrated many times on the course of a typical non-linear simulation, the selection of the algorithm has been based on the accuracy of the solution and also on its robustness and efficiency. The numerical integration of the model has been performed using a refined Euler scheme with automatic sub-stepping and errors control. The algorithm is an adaptation of the Sloan's scheme (Sloan, 1987; Sloan *et al.* 2001) to the specific characteristics of this model. The algorithm has been extended to update stresses and internal variables (hardening and history variables) in terms of the increment in the generalized strains; which are: strains, macrostructural suction, microstructural suction and temperature. Another extension of the scheme is related to the handling of more than one irreversible mechanism (specifically a model based on classical plasticity plus one based on generalized plasticity). The same modified Sloan's scheme has been used to integrate the two elasto-plastic laws and the highly non-linear elastic law. This ensures the integration of the different parts of the model with the same degree of accuracy and efficiency. Sloan's algorithm presents two main characteristics. One of them is that the size of each sub-increment may vary through the integration process depending on the non-linearity of the constitutive relations; this allows finding efficiently the updated stresses. The other main feature of the model is that it offers the possibility to control the errors in the stresses and hardening variables up to a desired level. This permits integrating accurately the constitutive law. The performance of the algorithm in the application cases presented in this Chapter (as in the examples in the following Chapters) was excellent. The robustness exhibited by the scheme is especially remarkable.

Regarding the application cases, the model has simulated satisfactorily the actual response of two expansive materials. The model is able to reproduce the main tendencies observed during hydration under confined conditions of a man-made expansive material. The different stages of the stress path are quite well simulated and a physical interpretation of the observed behaviour within the context of double structure media can be also given. The second application case analyses the behaviour of a compacted expansive clay submitted to several cycles of wetting and drying. It is confirmed that the model can deal with this kind of cyclic generalized load. The central aspects of the tests, such as the tendency to accumulated strains reduction when cycles accumulate or the effect of the applied load on these tests, can be explained naturally by the model considering the two structural levels and the interaction between them.

CHAPTER IV

APPLICATIONS OF THE DOUBLE STRUCTURE FRAMEWORK

SUMMARY

In Chapters II and III the formal aspects of the double structure approach have been introduced. Some application cases have also been presented with the sole aim of checking some capabilities of the mechanical model and of the formulation. In this Chapter the modelling is focused on the study of the expansive materials. The *THM* behaviour of the FEBEX bentonite is a matter of central interest. In the context of the FEBEX project, extensive information related to the behaviour of the FEBEX bentonite has been collected. An attempt to integrate this experimental data and validate the mechanical model underlies the first application case. In the second application, the mechanical model has been applied to explaining and reproducing the response of the FEBEX bentonite subjected to a complex *THM* path. This generalized stress path is the consequence of an accidental overheating that took place in an ongoing large-scale heating test. Finally, in the last application case, the double structure approach has been applied to simulate the hydration process of an expansive material made up from a mixture of clay pellets and clay powder.

4.1 PREFACE

In spite of the great interest centred on the study of the expansive clays behaviour, it is not easy to find a set of experimental tests that allows the identification of the main parameters of a model as the one presented in Chapter III. However, in the framework of the FEBEX project, the laboratory works conducted for the characterization of the FEBEX bentonite offer valuable information to this end. The experimental works carried out allow a good identification of the main properties of this clay. Special attention was also placed on the study of the bentonite fabric, which reveals a clear bimodal pore distribution (Villar, 2000; Lloret ***et al.,*** 2003). Regarding the mechanical characterization, two types of tests have been carried out: i) tests in which a combination of loading paths at constant suction and drying/wetting paths at constant load were applied; and ii) swelling tests under constant volume conditions in order to determine the swelling pressure and the stress path followed during wetting (Lloret ***et al.,*** 2003).

The complex behaviour exhibited by the FEBEX bentonite in those tests could not be explained by standard models of non-saturated soils mechanics, such as, state surface models or Barcelona Basic Model (*BBM*). The mechanical model presented in Chapter III appears as a good option to model this complex *THM* behaviour. As explained in Chapter III, this model includes in the analysis the two structural levels that actually exist and also the main physico-chemical phenomena responsible of the macroscopic response of expansive materials. Therefore, the modelling of the FEBEX bentonite behaviour has been undertaken with the main aim of analysing the results of the tests performed in a unified manner, within a consistent theoretical framework, and also with the objective to validate the double structure model.

In the context of the same project, a large-scale heating test has also offered valuable information to check the capabilities of the model when a complex *THM* path is involved. An irreversible behaviour of the FEBEX bentonite was detected when an accidental overheating took place in the heating test. Numerical analysis has been performed following an equivalent generalized stress-path and the mechanical model has been applied to explain and reproduce the observed behaviour of the FEBEX bentonite.

In the last application case, the double structure approach is applied to analyse the behaviour of an expansive material composed of a mixture of clay pellets and clay powder. This is a material actively studied in the design of high level radioactive waste disposal, because it could be potentially used as a seal or to build up engineering barriers. The simulation is focused on the hydration process of this man-made material under confined conditions. Special attention is placed on the phenomena that affect the response of the material and in the coupling between the mechanical and hydraulic problem when two pores levels are considered.

The Chapter is organized as follows: first the application related to the experimental validation of the model is introduced. The main results of the experimental programme are briefly examined taking into account the role of the soil fabric in controlling the observed mechanical behaviour. After that, the results of the laboratory tests are reproduced and interpreted using the double structure model. The second part of the Chapter is devoted to the analysis of the overheating event. The main aspects of the incident are presented together with the model

results. Afterwards, the simulation of the hydration process of a clay pellet mixture considered as a boundary value problem is presented. Finally, the main conclusions of the Chapter are presented. Appendix A.3 presents some complementary aspects of this Chapter.

4.2 EXPERIMENTAL VALIDATION OF THE MECHANICAL MODEL

4.2.1 INTRODUCTION

Although bentonite pastes have been actively studied in the past (*i.e.* Callaghan & Ottewill, 1974; Kraehenbuehl *et al.,* 1987; Ormerod & Newman, 1983; Warkentin *et al.,* 1957), knowledge concerning the mechanical behaviour of compacted bentonite is still scarce. The microstructure of compacted expansive clays has been studied by Pusch (1982) who observed a double structure made up from clay aggregates and large macrostructural pores. The pore space inside the aggregates was constituted by voids of a much smaller size. The same double structure has been identified in several compacted clays intended for engineered barriers in waste disposal (*i.e.* Atabek *et al.,* 1991 in FoCa clay; Romero *et al.,* 1999 in Boom clay; Pusch & Moreno, 2001, in MX80; Cui *et al.,* 2002a, in a mixture of 70% Kunigel clay and 30% Hostun sand). As indicated in Chapter II, the behaviour of this material is potentially very complex since it results from the interaction between the volume change of aggregates made up from a highly expansive clay mineral (microstructural level) and the rearrangement of the granular-like skeleton formed by the aggregates (macrostructural level). In the next sections the results of an experimental study carried out on FEBEX bentonite heavily compacted to a dry density of up to 1.7 Mg/m^3 are presented, together with the main simulation results.

4.2.2 PROPERTIES AND FABRIC OF THE MATERIAL

The tests were performed on a bentonite from the Cortijo de Archidona deposit in Almería, Southeastern Spain. The conditioning of the bentonite in the quarry, and later in the factory, was strictly mechanical, consisting of homogenisation, removal of rock fragments, drying at 60 °C and crumbling of clods. Finally, the clay was sieved using a 5-mm square mesh to obtain the product to be used in the laboratory (Lloret *et al.,* 2003).

The bentonite has a montmorillonite content higher than 90 percent It also contains variable quantities of quartz and other minerals such as plagioclase, cristobalite, potassium feldspar, calcite and trydimite. The hygroscopic water content of the clay at laboratory conditions (relative humidity 50±10 %, temperature 21±3 °C) is about 13.7±1.3 %. More details about de FEBEX bentonite are presented in Villar (2000), Lloret *et al.* (2003).

As it was mentioned above, the fabric of the compacted soil plays an important role in the observed swelling behaviour of these materials, so it was studied using a variety of techniques. Mercury intrusion porosimetry (MIP) tests were performed to examine the pore size distribution of the statically compacted material used in the experimental programme. Figure (4.1) shows the measured incremental pore volume for two samples compacted to very different values of dry density (ρ_d), 1.5 Mg/m^3 and 1.8 Mg/m^3. It can be observed that the

pore size distribution is clearly bi-modal, very characteristic of this type of materials (Alonso *et al.,* 1987). The dominant values are 10 nm that would correspond to the pores inside clay aggregates and a larger pore size that depends on the compaction dry density and ranges from 10 μm (for ρ_d=1.8 Mg/m^3) and 40 μm (for ρ_d=1.5 Mg/m^3). These larger voids would correspond to the inter-aggregate pores. The boundary between the two pore size families can be seen to be around 0.13 μm, as pores smaller than this magnitude do not appear to be affected by the magnitude of the compaction load. As Figure (4.1) clearly shows, compaction affects mainly the pore structure of the larger inter-aggregate pores.

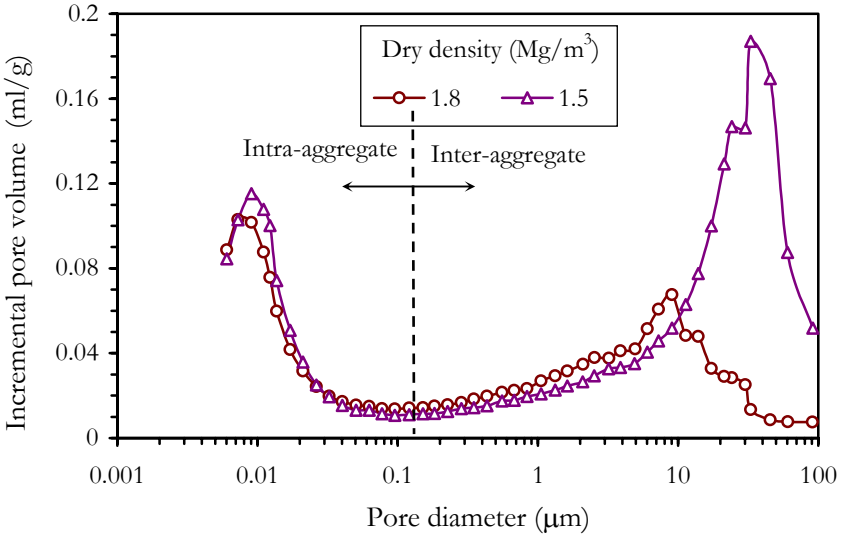

Figure 4.1. Distribution of incremental pore volume for two compacted bentonite samples at different dry densities. Mercury Intrusion Porosimeter test (Lloret *et al.,* 2003).

Figure (4.2) shows the relationship of pore diameter with intruded pore volume for two samples compacted at dry densities, 1.55 Mg/m^3 and 1.73 Mg/m^3. It can be noted that there exists a significant pore volume into which the mercury could not penetrate because of the difference between the void ratio of the soil and the void ratio intruded by the mercury. The magnitude of this volume (e = 0.32) is practically the same for the two specimens. Indeed the intra-aggregate pore volumes are very similar for the two samples with void ratio values around 0.46. The remaining of the pore space corresponds therefore to inter-aggregate pores, accounting for about 37% of the voids (e = 0.28) in the sample with a dry density of 1.55 Mg/m^3 and about 20% (e = 0.11) in the sample with a dry density of 1.73 Mg/m^3. Figure (2.5) shows a micrograph obtained using an environmental electron microscope where the presence of aggregates, the size of inter-aggregate voids and the bimodal distribution of pore sizes are readily apparent. Similar observations have been reported in Cui *et al.* (2002a).

Summarising, all the observable data concerning the fabric of compacted soils indicate a clear presence of two structural levels in the material: a microstructure inside the aggregates and a macrostructure constituted by the ensemble of aggregates and inter-aggregates pores. Microstructure features appear largely independent of compaction effort.

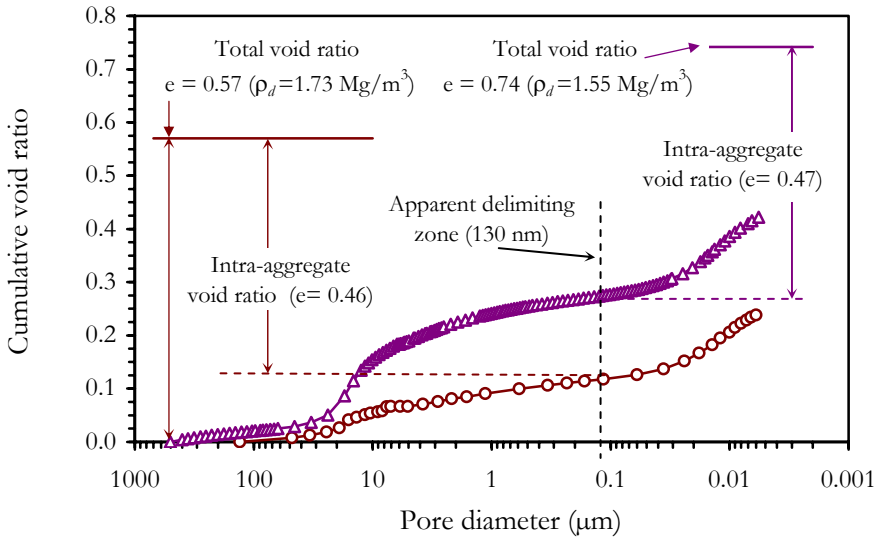

Figure 4.2. Relationship between pore diameter and intruded pore volume for two samples compacted at different dry densities (Lloret *et al.,* 2003).

4.2.3 EXPERIMENTAL RESULTS

The testing programme was performed using oedometers especially designed to apply a very large range of suctions. The highest suction range reached was close to 550 MPa. The maximum vertical stress that could be applied in the apparatus was 10 MPa (Lloret *et al.*, 2003). Oedometer tests with suction control were carried out at CIEMAT and UPC laboratories. The main limitation of oedometer testing is that it does not provide full information on the stress state of the material, as the horizontal confining stress is not usually measured. As a result, difficulties are sometimes encountered in the interpretation of the results and in the comparison with model predictions. In addition, in the case of unsaturated soils, there is also uncertainty regarding the degree of saturation of the soil, which is always unknown, although the retention curves obtained at constant volume may provide approximate water content for every suction value. However, most significant trends and features of soil behaviour may be obtained using this type of tests (Gens & Alonso, 1992), the performance of which is far less complex than that of triaxial tests.

Two types of tests were carried out:

- Tests in which a combination of loading paths at constant suction and wetting and drying paths at constant load were applied.

- Swelling tests under constant volume conditions in order to determine the swelling pressure and the stress path followed during wetting.

The first type of test was carried out at CIEMAT laboratory. Apart form the initial and final equilibration stages, the actions applied on the samples were load increments at constant suction and changes of suction at constant load. Samples were compacted statically to a dry density of 1.70 ± 0.02 Mg/m^3 with the material at hygroscopic water content (close to 14 %.). More details about the experimental technique can be found in Lloret *et al.* (2003).

The initial conditions of the test correspond to a dry density close to 1.70 Mg/m^3 and gravimetric water content near the 14 %. The various load or suction changes were applied in stages as shown in Figure (4.3) (Lloret *et al.,* 2003). In order to use a logarithmic scale a constant value of 0.1 MPa was added to all suction values plotted in this Figure. The same convention has been used in the rest of the Chapter. All tests started at an applied vertical stress of 0.1 MPa and at the compaction suction of about 125 MPa. Afterwards a variation of suction was applied under constant load, except for one specimen in which suction was kept unchanged. Afterwards the load was increased also under constant suction, which was then followed by wetting to saturation (zero suction). Maximum vertical stresses under saturated conditions were either 5 MPa or 9 MPa, depending on the test.

Figure (4.4) shows the variation of void ratio during the initial stage of suction modifications and subsequent loading. The starting points for the loading stages are very different because of the large dependence of volumetric strains on suction applied at low loads. On loading, the stiffness of the bentonite (*i.e.* the slope of the void ratio vs. vertical stress line plotted in semi-logarithmic scale) reduces slightly as the suction applied during loading increases. However, the most noticeable effect of suction is the shifting of the point at which there is a change in the slope of these lines, indicated by a vertical arrow in the Figure (4.4). In the framework of elasto-plasticity this change is interpreted as the crossing of a yield surface and the load at which it takes place can be considered as an apparent pre-consolidation pressure. Large pre-consolidation pressure reductions are apparent at low suction values. Yielding was not reached in tests S1 and S2, and it is assumed that the pre-consolidation stress, for this density, corresponds approximately to the vertical stress value reached during static compaction, about 18 MPa.

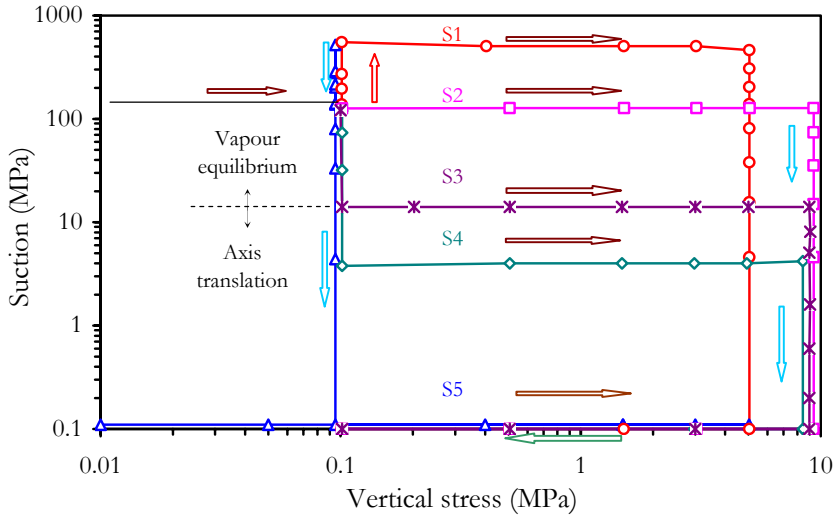

Figure 4.3. Generalized stress paths followed by tests S1 to S5 (Lloret *et al.,* 2003).

The variations of void ratio during the stages at which the vertical stress was maintained constant and suction was varied are presented in Figure (4.5). Large void ratio changes are observed in the specimens where wetting took place at 0.1 MPa, whereas in the samples where wetting took place at 5.1 MPa and, especially, at 9 MPa load, the volume changes are quite small. The effects of applied load are very noticeable.

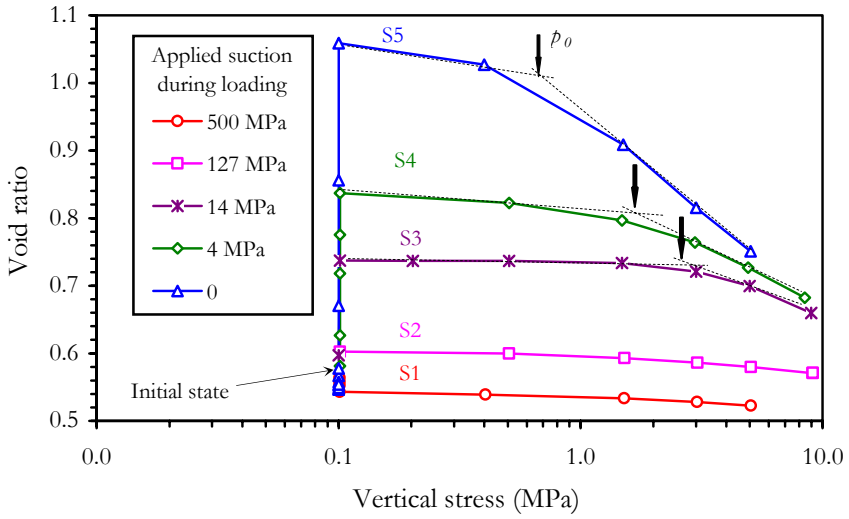

Figure 4.4. Variation of void ratio during the initial stage of suction variation and subsequent loading. Tests S1 to S5.

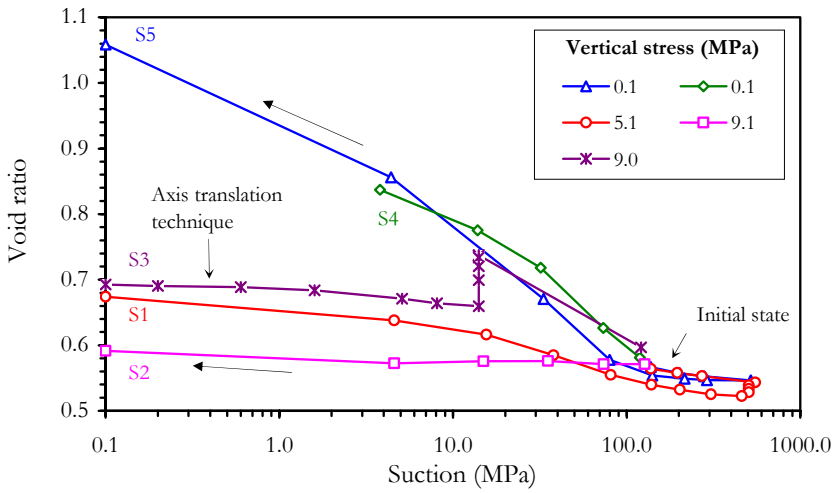

Figure 4.5. Variation of void ration during the stages at which vertical stress is maintained constant and suction varied. Tests S1 to S5.

One of the samples (S5) was subjected to drying at 500 MPa suction before being wetted to a suction of 0.1MPa. The measured void ratio changes are plotted in Figure (4.6). It can be seen that the drying produces very small volumetric strains. However, when wetting is continued towards smaller suction values, a large increase of swelling strains is observed signalling a significant change of behaviour. The comparison of the results from this test with those from test S4 that did not undergo this initial drying/wetting cycle (Figure 4.6) suggests that such a suction cycle does not have any noticeable effects on subsequent behaviour.

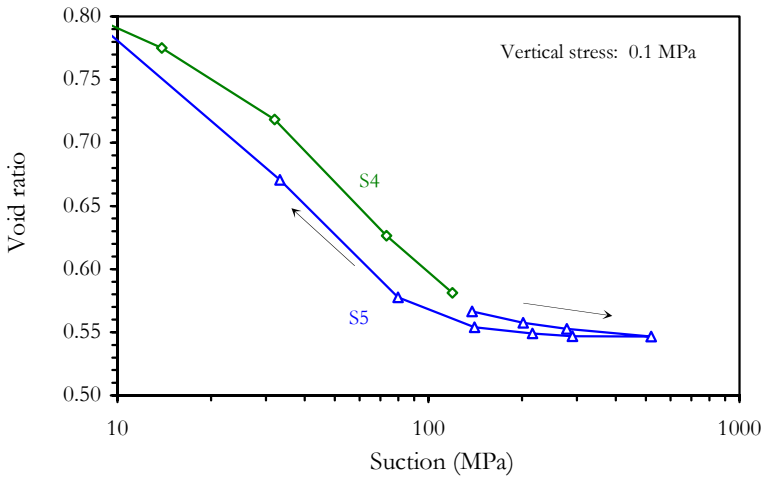

Figure 4.6. Variation of void ratio with suction of test S5 during an initial drying/swelling cycle and subsequent wetting. The results of test S4 are included for comparison.

An important feature of behaviour concerns the possible stress path dependency or independency of the material under generalized stress including suction. In unsaturated non-expansive soils, it is often found that the behaviour is stress path independent if the trajectories only include loading and wetting (suction reduction) stages (Alonso *et al.,* 1987). However, Gens & Alonso (1992) argued that in expansive soils, there would be irreversible macrostructural rearrangements caused by the swelling of the microstructure when wetting the samples. This interaction would be higher when applied stresses are low. As a consequence, this macrostructural changes could result in stress path dependency of volume changes even in the cases where only wetting paths are involved. This issue has been examined in this experimental programme.

Figure (4.7) shows void ratio variation for two specimens that share the initial and final stress points but have followed different stress paths. It can be noted that the final state is different, so there is a measure of stress path dependency. As observed in other cases (Brackley, 1973; Justo *et al.,* 1984), the final void ratio of the sample wetted under low stresses is higher. The disruption of the macrostructure would be more severe in this case because of the larger swelling strains developed during wetting, inducing large macrostructural volume changes that can not be recovered upon subsequent loading. Figure (4.8) shows a similar plot for three other specimens with the same initial and final points where, again, it can be noted that the final void ratio values do not coincide. As before, the sample that was wetted at the lower applied vertical stress (4 MPa) reaches the highest final void ratio.

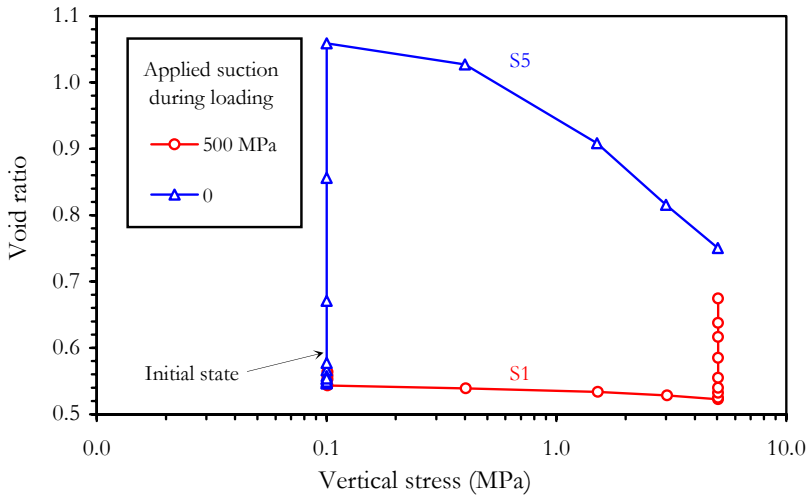

Figure 4.7. Variation of void ratio observed in tests S1 and S5 with the same initial and final stress states.

The swelling tests under constant volume were performed in the UPC laboratory. These tests aimed to reproduce the conditions during hydration of an engineered barrier in underground waste repositories where the compacted bentonite was rigidly constrained by the waste canister and the host rock (more details are introduced in Chapter V). Samples were compacted at an initial dry density of 1.63 ± 0.01 Mg/m^3 at hygroscopic water content (13.7±1.3 %).

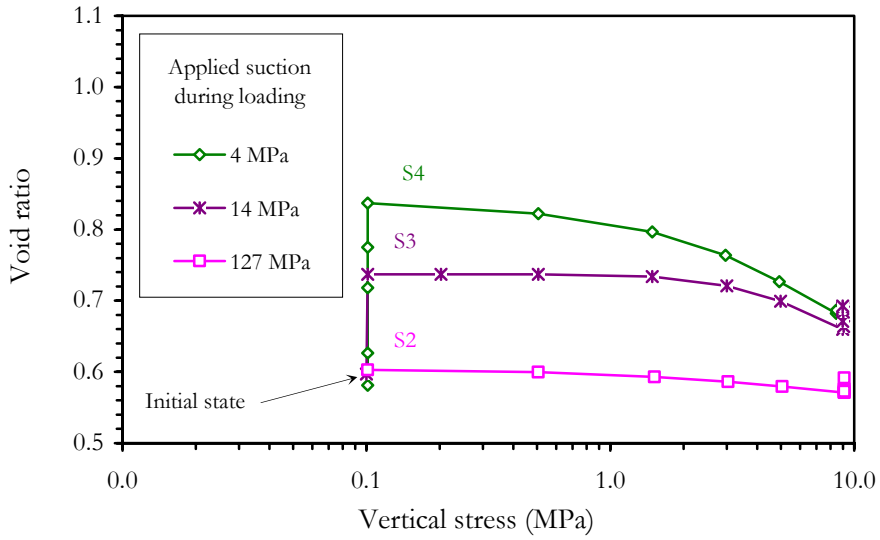

Figure 4.8. Variation of void ratio observed in tests S2, S3 and S4 with the same initial and final stress states.

The main features of the four swelling pressure tests performed in the UPC laboratory are presented in Table (4.1). Initially a suction change was applied to three of the samples in order to achieve a range of initial conditions for the next testing stage. During the swelling pressure phase a condition of no volume change was prescribed and suction was reduced in stages under controlled conditions. In this way it is possible to follow the stress path, in terms of suction *vs.* vertical stress throughout the tests, as shown in Figure (4.9).

Examination of these stress paths provides important information on the stress-strain characteristics of the bentonite in this type of tests (that corresponds to a number of relevant field situations) but, also, on the underlying causes of the observed behaviour. Three zones can be distinguished (Figure 4.9). The first one corresponds to the stage of high suction and low applied loads. In this region the vertical stress remains below the pre-consolidation stress (in elasto-plastic terms, the stress state has not reached the yield locus) and the stress path is defined by the increase of load required to compensate the swelling strains due to suction reduction.

Once the pre-consolidation pressure (yield locus) is attained, the second zone is reached and a drastic change of slope ensues. If the load is sufficiently high, collapse of the macrostructure occurs and the value of vertical stress tends to reduce to compensate the collapse compressive strains. Naturally, the microstructural swelling strains also contribute to the compensation of collapse deformation but, at this stage, they may not be large enough to offset the reduction of vertical stress.

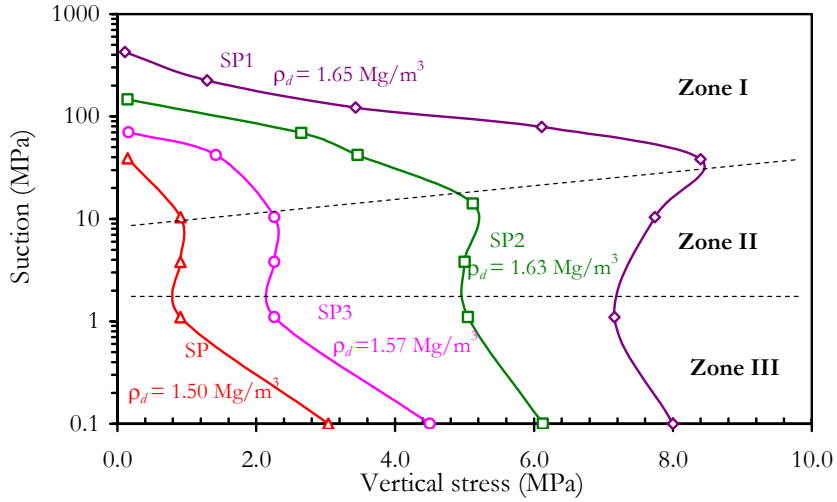

Figure 4.9. Generalized stress paths observed in the swelling pressure tests.

Finally, zone III corresponds to the region of low suctions where microstructural swelling strains exhibit their largest magnitude. Now microstructural strains overcome any possible collapse strains and the vertical stress must rise again to compensate for the large swelling strains. It is interesting to note that, even the rather complex behaviour displayed by the compacted bentonite during the swelling pressure tests can be readily explained in the context of a conceptual framework that considers the interaction between microstructure and macrostructure.

Table 4.1

Main features of the swelling pressures tests performed at the UPC laboratory (Lloret *et al.,* 2003).

Test	Initial conditions		Path before swelling pressure test [σ_v (MPa), s (MPa)]				ρ_d (before test)
			I		II		
	ρ_d (Mg/m^3)	w (%)	σ_v	s	σ_v	s	(Mg/m^3)
SP1	1.62	14.6	0.11	128	0.11	424	1.65
SP2	1.63	13.2	0.15	146			1.63
SP3	1.62	14.6	0.16	128	0.16	70	1.57
SP4	1.63	14.2	0.15	128	0.15	39	1. 50

4.2.4 MODEL RESULTS

In the previous section, the test results have been qualitatively interpreted in terms of a conceptual framework in which two structural levels (macro and micro) interact. Now some of the most characteristic results presented earlier are examined using the double structure elasto-plastic model described in Chapter III. An important advantage of this model is that the variables associated with each level can be followed throughout the test and a more detailed examination of the patterns of behaviour can be made. It should be strongly stressed that the aim of this modelling exercise is not specifically to test the predictive capability of the model but its general performance. In fact, the parameters have been chosen specifically to give a good representation of the experimental observations.

The model is used one-dimensionally, substituting applied vertical stress for mean net stress. Therefore p now denotes net vertical stress. *MC* and *MS* surfaces coincide so that there is always some degree of interaction between micro and macro levels. The parameters used in the modelling are included in Table (4.2). The results of tests S1 and S5 have been used to determine them. Elastic macrostructural parameters have been obtained from the sections of the tests that are inside the *LC* yield curve. The value of the slope of the saturated consolidation line, $\lambda_{(0)}$, has been based on the loading stage of the S5 test. The parameters of the interaction curves have been adjusted to yield the correct amount of stress path dependency and the parameters for the microstructural behaviour have been derived from the swelling stages of tests S1 and S5. Finally the parameters controlling the shape of the *LC* yield surface have been evaluated from the experimental results (Lloret *et al.,* 2003).

The initial values of the microstructural and macrostructural void ratio are 0.45 and 0.11, respectively, in accordance with the observations on the soil fabric. The static compaction stress (18 MPa) gives the initial position of the *LC* yield surface. With the expression used to define the *LC* curve (Equation A2.12), the hardening parameter p_o^* has an initial value of 12 MPa.

Table 4.2

Main parameters of the elasto-plastic constitutive law used in Section 4.2

Parameters defining the Barcelona Basic Model for macrostructural behaviour

κ	κ_s	$\lambda_{(0)}$	p_c (MPa)	r	ζ (MPa^{-1})	p_o^* (MPa)
0.005	0.001	0.080	0.50	0.90	0.20	12

Parameters defining the law for microstructural behaviour

α_m (MPa^{-1})	β_m (MPa^{-1})
2.1x10^{-02}	2.3x10^{-03}

Interaction functions

$$f_C = 1 + 0.9 \tanh\left(20\left(p / p_o\right) - 0.25\right) \;;\; f_S = 0.8 - 1.1 \tanh\left(20\left(p / p_o\right) - 0.25\right)$$

The model is first applied to the analysis of tests S1 and S5. They share the same initial and final generalized stress states but their trajectories are very different (Figure 4.10). In test S1 the specimen was loaded under a high 550 MPa suction up to a 5.1 MPa vertical load and then it was wetted reducing the suction to 0 in stages. In contrast, test S5 is first wetted at a low applied vertical stress value of 0.1 MPa and afterward the sample, already saturated, is loaded to a vertical stress of 5.0 MPa. These two tests, therefore, provide the opportunity to examine the behaviour over a wide range of stress paths. Figure (4.10) shows the computed variation of void ratio over the stress paths followed by the two tests together with the experimental results. It can be observed that major features of behaviour are correctly reproduced including:

- Large swelling strains when the material is wetted at low stresses (Path B-D, Test S5)
- Smaller, but still significant, swelling strains when the soil is wetted under a 5 MPa vertical stress (Path C-E, Test S1)
- Change of the slope of the compression line during loading indicating yield in test S5 (Path D-E). No yield is apparent during the loading at high suction of specimen S1 (Path B-C).
- Final void ratio (point E) is different in the two samples; there is a measure of stress path dependency, at least regarding volumetric strains
- Good reproduction of behaviour is also achieved when considering the experimental results in terms of void ratio *vs.* suction variation (Figure 4.11) although some departures are observed at intermediate stages of the swelling of test S5.

Summarising, the model is capable to offer a good simulation of the observed results and, with the set of parameters adopted, even the quantitative agreement is quite close. Accepting then that the constitutive law is a reasonable representation of the real behaviour, it is interesting to explore the further information that can be obtained from the model so that the behaviour mechanisms underlying the mechanical behaviour of the soil can be better understood.

Figure (4.12) shows the evolution of the microstructural and macrostructural void ratio computed for Test S5. During the swelling stage (path B-D), the microstructural strains are relatively large and they cause even larger irreversible strains in the macrostructure because of the large coupling between the two structural levels that exist at low stresses. During the subsequent loading (path D-E) under saturated conditions the deformation of the macrostructure is significant but it is not due to microstructural strains that are now quite small. This part of the test is basically controlled by the behaviour of the macrostructure. Figure (4.13) shows the parts of the interaction functions involved in the various stages of the test.

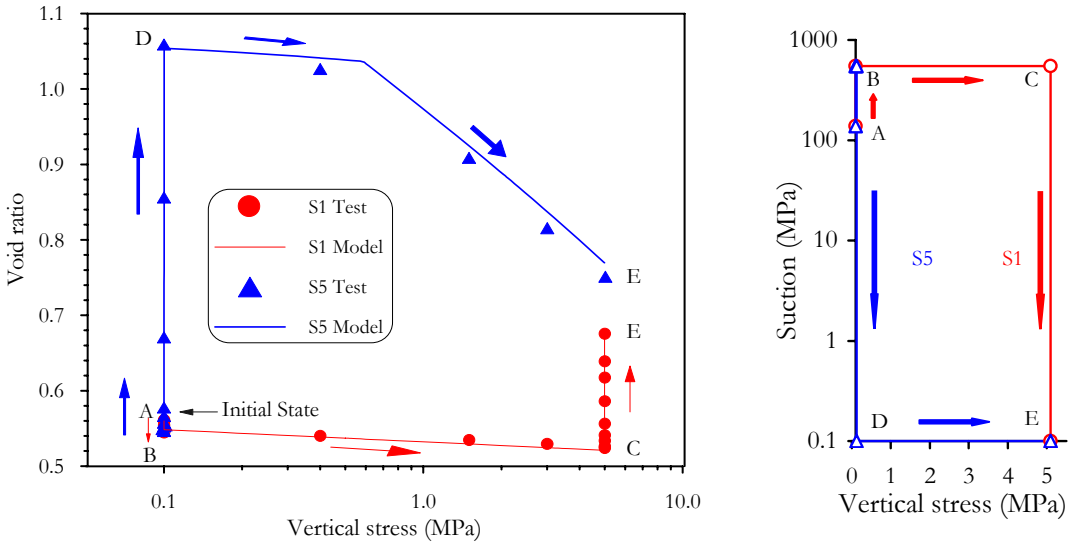

Figure 4.10. Computed variation of void ratio for tests S1 and S5. Experimental results are provided for comparison.

Some of the positions of the *LC* yield curve during the performance of test S5 are shown in Figure (4.14). It can be seen that during swelling (path B-D) the *LC* curve moves to the left in response to the irreversible swelling strains taking place in the macrostructure. Subsequent loading (path D-E) takes the *LC* again to the right to the final load value of 5.0 MPa. Indeed the yield point observed and computed (Figure 4.10) corresponds to the crossing of the *LC* during this loading stage.

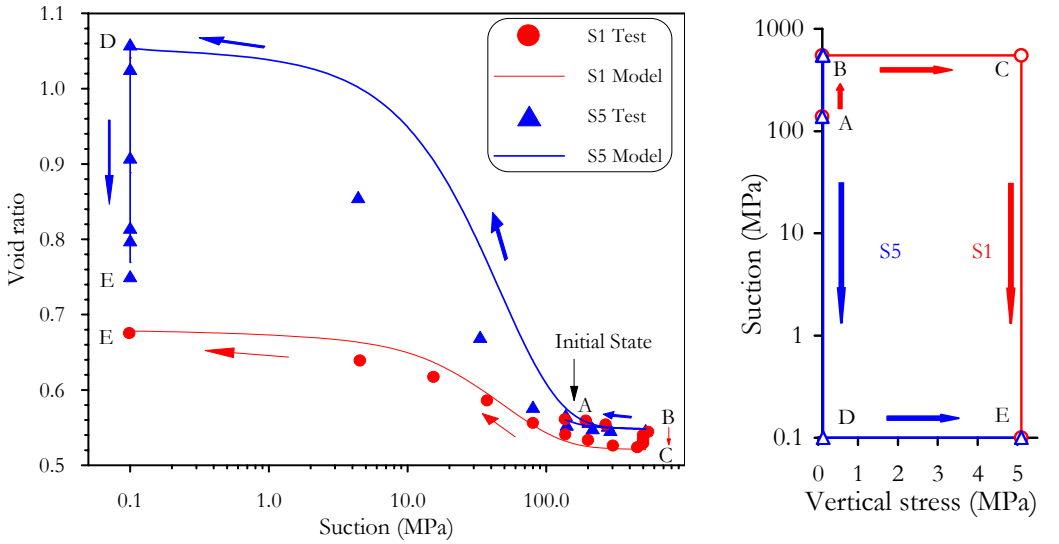

Figure 4.11. Computed variation of void ratio in constant load stages for tests S1 and S5. Experimental results are provided for comparison.

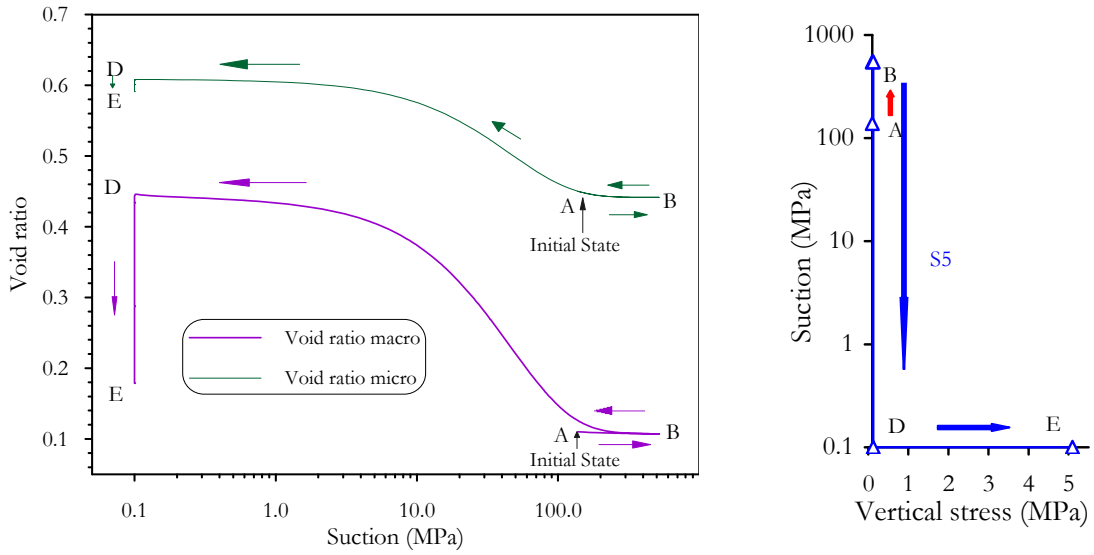

Figure 4.12. Evolution of the computed microstructural and microstructural void ratio. Test S5.

Continuous information on the evolution of the *LC* yield curve can be obtained plotting the evolution of the hardening parameter, p_o^* (Figure 4.15). The reduction of p_o^* during swelling and subsequent increase upon loading are readily apparent.

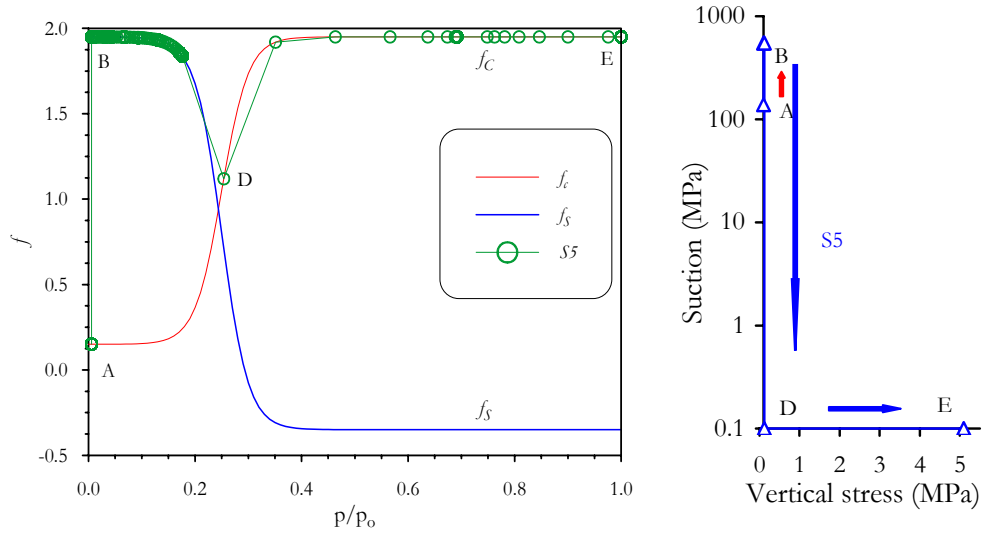

Figure 4.13. Interaction functions involved in the various stages of tests S5.

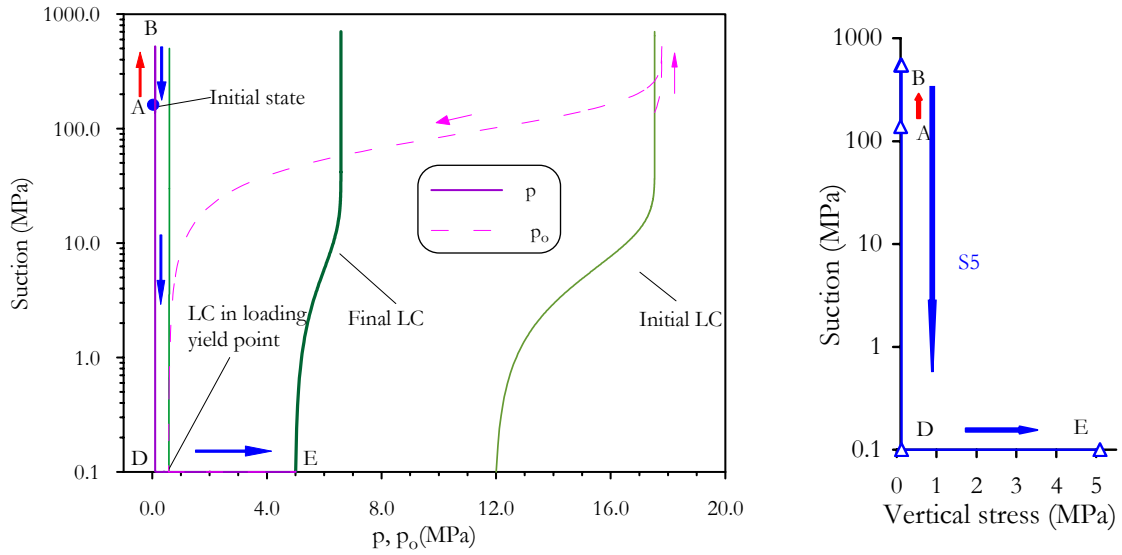

Figure 4.14. Stress path and successive LC yield surfaces for test S5.

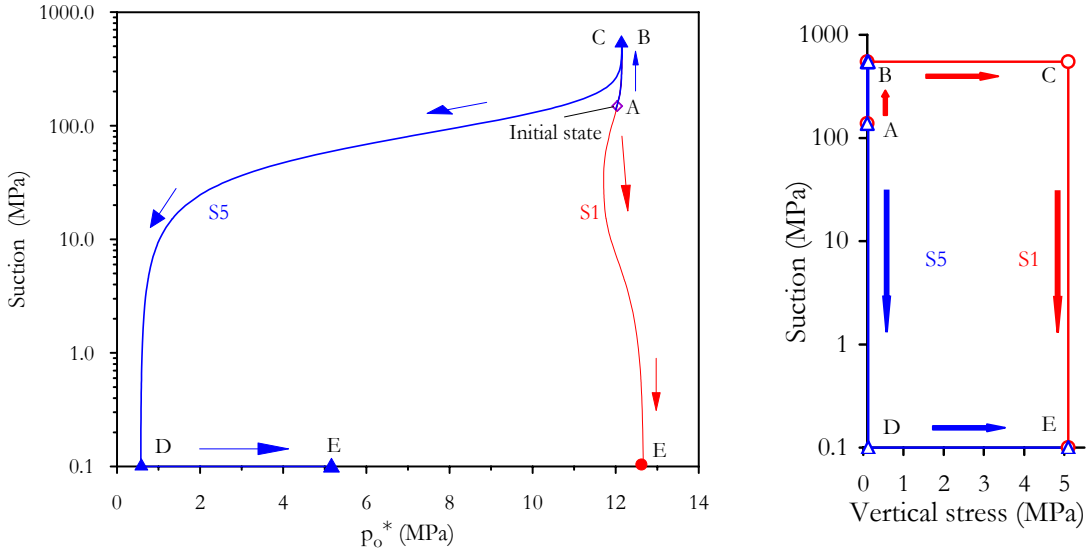

Figure 4.15. Evolution of the hardening parameter p_o^* for tests S1 and S5

The behaviour of sample S1 is quite different (Figures 4.16 and 4.17). During the first stage of drying (path A-B) and subsequent loading (path B-C), the microstructural volumetric strains are very small. The macrostructural strains are also small even during loading because of the high stiffness imparted to the sample by the large 500 MPa suction. During the swelling stage (path C-E) under a 5.1 MPa load, the microstructural strains are significant although smaller than for test S5 because of the higher load applied. The most significant difference is, however, that the macrostructural strains that are induced are quite small because now the stress state is much closer to the *LC* (Figure 4.18), i.e. the sample is in a comparatively looser

state and the potential for macrostructural disruption is much lower. The loading stage (path B-C) takes place inside the *LC* yield surface, so no yield is expected and none was observed. The evolution of the hardening parameter for test S1 has also been plotted in Figure 16. It can be observed that the changes are very slight (indicating a *LC* curve practically stationary) and that the final value of p_o^* is higher than in the case of test S5.

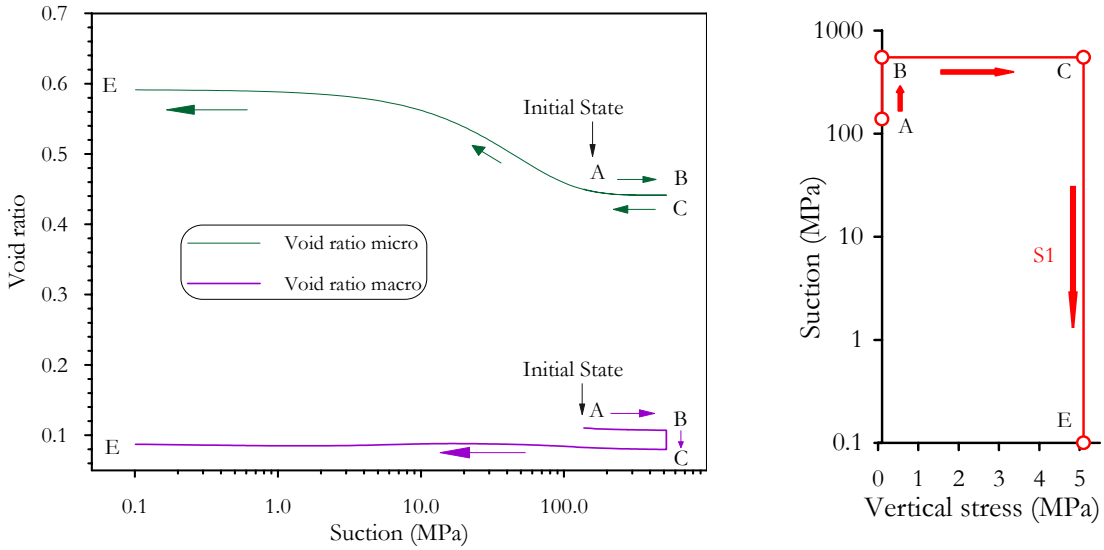

Figure 4.16. Evolution of the computed micro and macrostructural void ratio. Test S1.

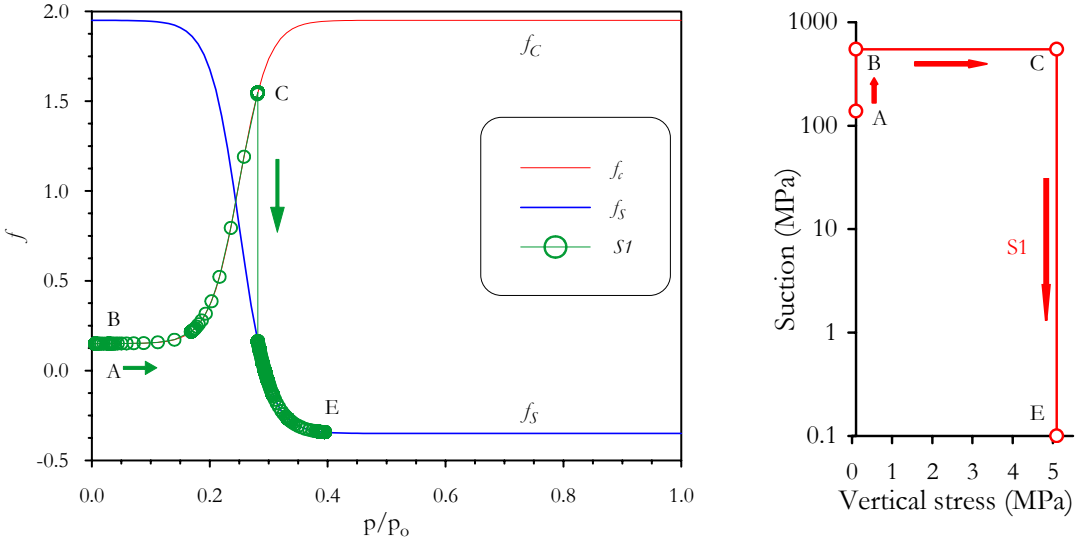

Figure 4.17. Interaction function involved in the various stages of tests S1.

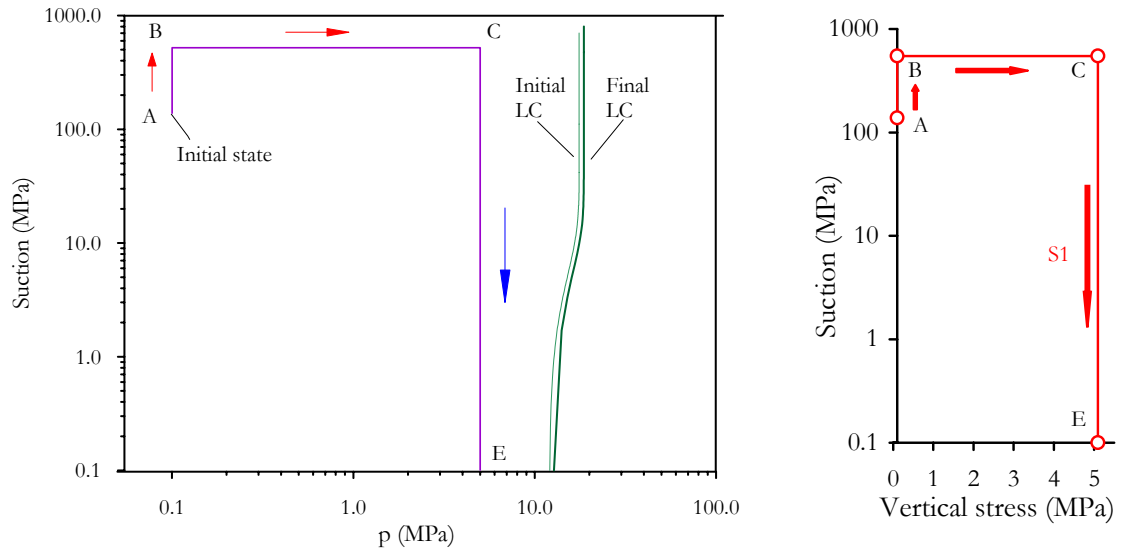

Figure 4.18. Stress path and *LC* yield surfaces for test S1.

Now the basic reason for the stress path dependency of volumetric strains can be readily identified. The basic difference is that in test S5 the large swelling strains take place at low stress values and, consequently, the interaction with the macrostructure is very strong and results in large plastic strains that are not fully recovered upon subsequent loading. In test S1, development of plastic strains in the macrostructure is quite reduced because, when the swelling of the microstructure takes place, the interaction between the two structural levels is small. The different states of the samples at the end of the test are reflected in the different final positions of the *LC* curves (and p_o^* values). Exactly the same analysis could be made regarding the results of tests S2, S3 and S4.

As a final test of the adequacy of the model to represent the behaviour of compacted swelling materials, it has been applied to the modelling of the swelling pressure tests. At a low suction (i.e. 0.2 MPa) it is assumed that the stress path is controlled by the microstructural effective stress. Figure (4.19) shows the results of the model calculations together with the experimental results. Although differences between computed and experimental results can be observed, the model is capable of producing swelling stress paths very similar to the observed ones.

The effect of temperature on the mechanical behaviour of FEBEX bentonite has been studied using oedometer tests with suction control and at constant temperatures: 40ºC and 60ºC (Villar, 1999, Villar *et al.,* 2004). Due to the limited number of experiments performed and due to the temperature range explored, these tests can be considered as a preliminary study. According to this study, the effect of temperature on the pre-consolidation stress is small, so it has been considered that the model parameters relates to this variable are equal to cero (α_1 and α_3 =0), until more experimental data allow their determination. Similar comment is made in relation to the effect of temperature on the shear strength of FEBEX bentonite. There are not laboratory tests in this line.

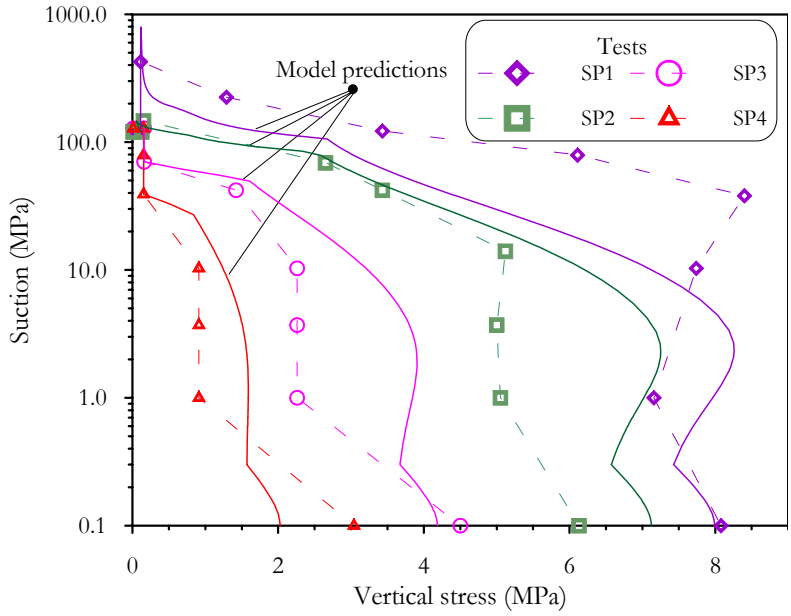

Figure 4.19. Computed stress paths for swelling pressure tests SP1 to SP4. Experimental results are provided for comparison

4.3 *THM* RESPONSE OF THE FEBEX BENTONITE

4.3.1 OVERHEATING EPISODE

A difficulty in validating the type of models described in Chapter III is the lack of experimental results involving complex *THM* stress paths. However, a large-scale heating test that is being carried out in CIEMAT (Madrid) has provided relevant data to evaluate the performance of the model, at least in a qualitative manner. This test is part of the FEBEX project and its main aim is the study of the engineered barrier and the near field components of a high level radioactive waste disposal.

The layout of the test is represented in Figure (4.20). Two electrical heaters (simulating canisters containing heat-emitting waste) were placed in the centre of a steel cylinder 6 m long and with inner diameter of 1.62 m. The space between the heaters and the steel cylinder was filled with a 0.64 m-thick engineered barrier made up from compacted bentonite. The barrier was hydrated uniformly from all around the cylinder with an applied water pressure of about 0.5 MPa. Simultaneously, the barrier was heated maintaining a constant temperature of 100 ºC at the contact between heaters and bentonite. The physical processes involved in the *THM* barrier behaviour are discussed in detail in Chapter V. The *THM* behaviour of the heating test has been successfully modelled and a selection of results involving computations and observations are presented in Chapter V, ENRESA (2000) and Sánchez & Gens (2002).

On day 1391 of the experiment there was an accidental overheating. The heaters reached 300 ºC in some areas and the contact between bentonite and heaters reached about 200 ºC, more than 100 ºC the temperature prescribed in the test. Figures (4.21 to 4.24) present detailed observations of this event. Time zero corresponds to 13:00 hours on 26th November 2000. Some values corresponding to a time of 1000 hours are also shown in levels included in the plots.

Figure (4.21) shows the evolution of temperatures at several radii in the barrier. It can be seen that points close to the heater reach temperatures near 200 ºC. Afterwards the heaters were switched off and the barrier cooled down rapidly to temperatures close to 45 ºC near the heaters. The variation of temperatures away from the heaters is not so strong. Finally the prescribed thermal conditions of the test were re-established, *i.e.* a constant temperature of 100 ºC at the contact between heaters and clay.

Figure (4.22) shows the evolution of relative humidity. Initially, a vapour front crossing the barrier results in a temporary increase of relative humidity. Afterwards the increased temperature causes a net drying of the material with a consequent reduction of relative humidity. After about 1000 hours the relative humidity recovers approximately the values before the overheating event. Figure (4.23) shows the evolution of suction for a point close to the heater derived from the measured values of relative humidity and temperature. It can be observed that suction reduced from 110 MPa to 55MPa due to the passage of a vapour front. Afterwards thermally-induced drying increased the suction to values close to 165 MPa. Finally, there was a tendency to recover the value before the event. The evolution of the radial stress in the barrier is especially interesting (Figure 4.24). Just after overheating, there was a moderate increase of radial stress (from 6.6 MPa to 7.2 MPa) followed by a strong reduction down to around 2 MPa. The radial stress recovered somewhat subsequently but it remained very far from the initial values. There was a large irreversible net reduction of radial stress.

Other experimental observations can be found in which similar trends are detected. For example, in Al-Homoud *et al.* (1995) a reduction of the clay swelling pressure it can be observed in some tests after cycles of drying/wetting. But here the loading is more general as it involves also a thermal cycle. On the other hand, under different conditions, Push & Güven (1990) have been detected experimentally (through microscopic studies) that when smectites are submitted to a strong heating the dehydration of clay platelets implies microstructural contraction and larger voids appear between the clay platelets. According to Push & Güven (1990) this phenomenon is reversible until temperatures close to 150 ºC; when this value is exceeded, this process is enhanced and it becomes partially irreversible. But, it is important to highlight two aspects of this study; the first is that the smectite has been submitted to heating for a long time (*i.e.* six months) and the other one is that the density of the material tested was very low. These two aspects are far from the conditions existing in the *mock-up* test overheating. In any case, it can be foreseen that if a strong drying takes place under conditions of confinement and high pressures, irreversible changes in the clay structure (contraction) may occur.

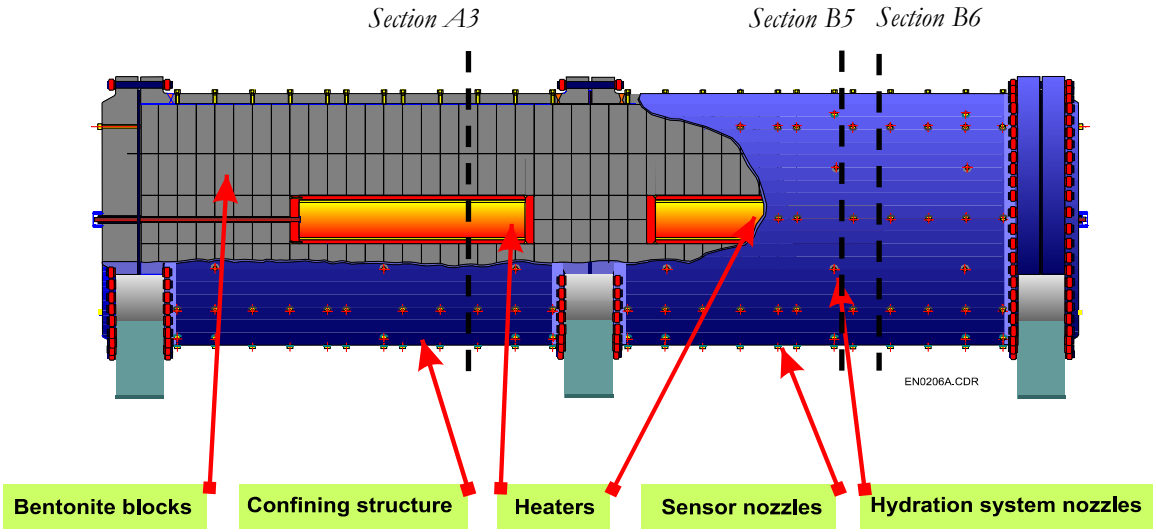

Figure 4.20. Layout of the large scale heating test.

4.3.2 OVERHEATING MODELLING

A full understanding of the phenomena occurring during the overheating event requires a coupled *THM* analysis. A preliminary step, however, is to examine whether the mechanical constitutive model is consistent with the observations of irreversible phenomena indicated above. This examination is described herein. It should be pointed out the following important considerations:

- only the constitutive law is tested, so there are no time effects due to the transient phenomena occurring in the barrier,
- the information ascribed to the constitutive law point corresponds in fact to a zone of the barrier of finite size,
- the aim is not to reproduce the full behaviour of the barrier but to check whether the main features of the observed mechanical behaviour are a natural outcome of the constitutive model.

A synthetic generalized stress path was applied to the constitutive law, corresponding to four major episodes: a wetting due to the passage of a vapour front, an intense drying associated with the increase of temperature, a subsequent cooling due to the switching off of the heaters and, finally, the re-establishment of the prescribed test conditions. The suction and temperature changes are applied under conditions of no volume change mimicking the confined state of the test.

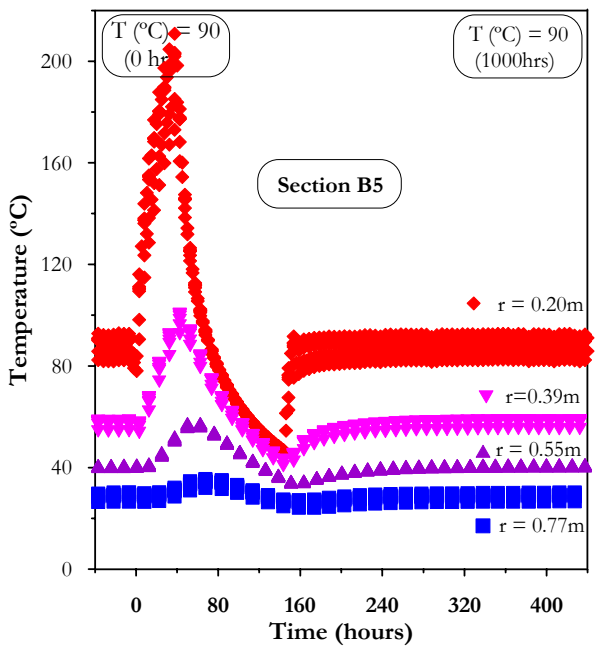

Figure 4.21. Evolution of temperature during and after the overheating event.

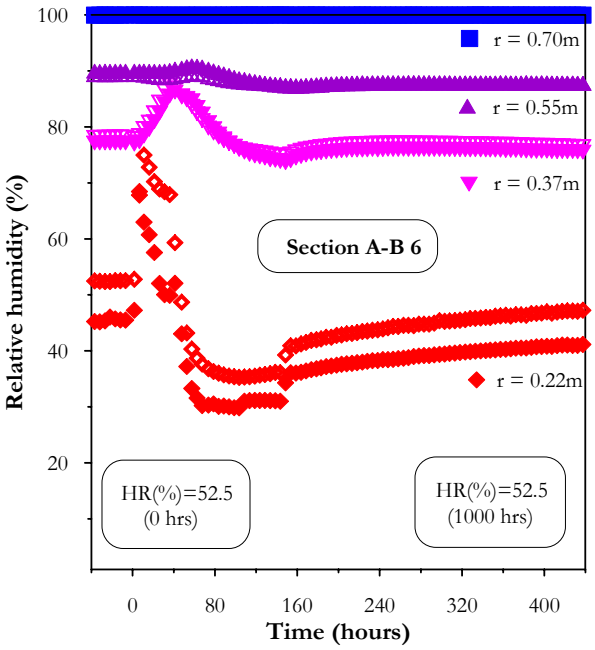

Figure 4.22. Evolution of relative humidity during and after the overheating event.

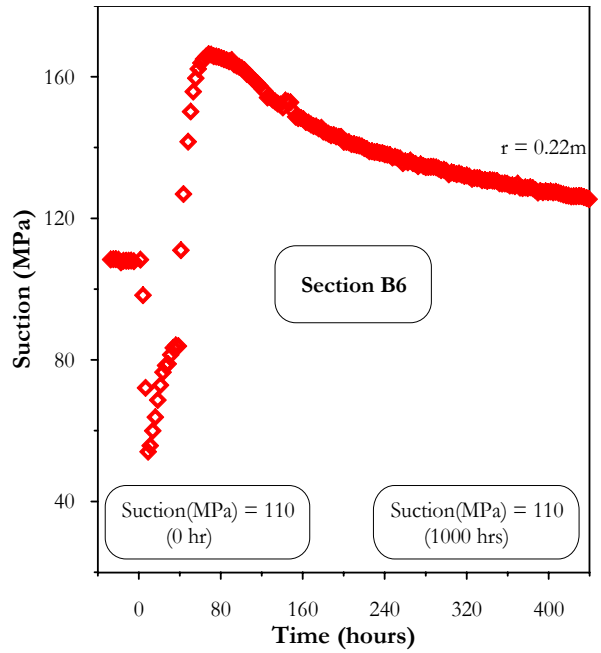

Figure 4.23. Evolution of suction during and after the overheating event.

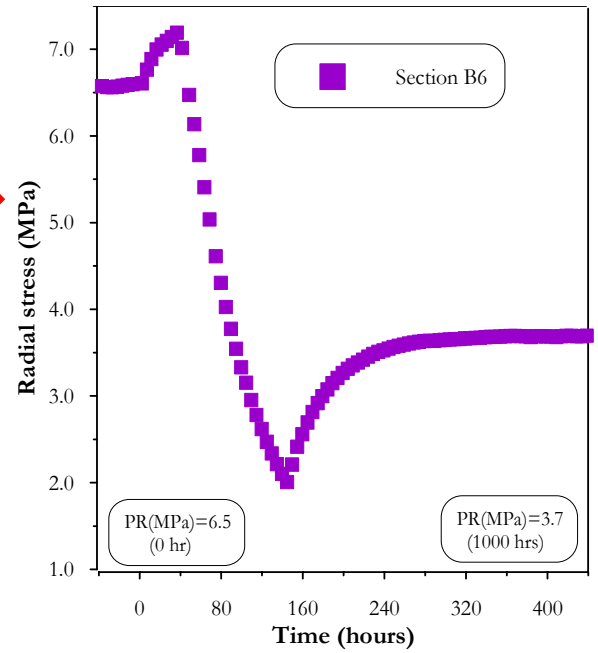

Figure 4.24. Evolution of radial stresses during and after the overheating event

Table (4.3) summarizes the four main loading stages of the overheating episode. The values of suction, temperature and radial stress have been obtained to the experiment records (that is, correspond to average values of the records in the sections involving heaters).

The main parameters used in the simulations are the same as the ones assumed in Section 4.2. A value close to 6.5 MPa has been adopted for p_o^*. According to Gens & Alonso (1992), this hardening parameter depends on the initial density and on the load history. The analysis presented in Chapter V has been taken into account to adopt this value. On the other hand, it the value of the β_m parameter has been reduced in order to adjust slightly the test measurements. This implies a lesser swelling capacity of the material, that could be related to the observed tendency of FEBEX bentonite to decrease the swelling capacity (and swelling pressure) with temperature (Villar *et al.*, 2004). It should be noted that the main objective of this simulation is to explore if the constitutive model can explain the observed behaviour of FEBEX bentonite, there is no intention of checking the quantitative predictive capabilities of the model. Table (4.4) summarizes the values adopted for the model parameters.

Figure (4.25) shows the evolution of radial stress in two representative sections of the barrier during and just after overheating. The four stages are also indicated. Figures (4.26 to 4.28) present the model results when the generalised loading stages are applied. A reasonable correspondence between measured and calculated values of radial pressure is observed. Both interaction functions f_C and f_S are operative at some stage of the process. Figure (4.28) shows the evolution of the *BBM* hardening parameter during the four stages of the test. Finally, Figure (4.29) shows a three-dimensional representation of the four loading stages adopted and the computed values of radial stress.

Table 4.3

Main loading stages of the overheating (average records)

Stage	Description	s (MPa)	T (ºC)	σ_r (MPa)
0	Initial coonditions before overheating.	110	90	6.5 - 7.5
1	Reduction of s (due to vapour front passage) and increase of T, below de maximun value.	55	135	7.5 – 8.0
2	Achievement of the maximun temperature and suction.	165	200	2.0 – 2.5
3	Cooling down of the barrier to the minimun observed temperature.	155	45	2.5 – 3.5
4	Re-establishement of the initial thermal and hydraulic conditions.	110	90	3.5 – 4.0

In the first loading stage the elastic mechanisms associated with suction reduction and temperature increase tend to increase the swelling pressure because they are associated with soil expansion. This expansion is only partially overcome by the *ms* plastic mechanism. In this path the interaction function f_s has negative values, which implies a hardening of the material (that is an increase of p_o^*). Heating continues in the second stage but now it is associated with a drying of the soil (increase of suction). This intense drying dominates and causes a tendency to contract and, consequently, a swelling pressure reduction occurs. During this stage the *mc* mechanism is active and the interaction between the two structural levels produce a densification of the sample (increasing the value of the hardening parameter p_o^*). The irreversible behaviour during this stage has one strong influence on the final response of the bentonite.

The third stage is characterized by a reduction of temperature and a wetting of the material; the latter dominates causing a tendency to expand and hence an increase of swelling pressure. In the final stage, the initial thermal and hydraulic variables are again prescribed, continuing the wetting of the material and increasing the temperature. These two factors, again, lead to a tendency for expansion of the soil and hence an increase of swelling pressure. During the last two stages the *ms* plastic mechanism is active. The interaction between the two structures causes an expansion of the macrostructure and a reduction of p_o^* during the main part or this path. This behaviour tends to change in the later part of this stage, when the stress path reaches negative values of the interaction function.

The final outcome is that the constitutive model response to this complex generalized stress path is a significant reduction in swelling stress that is not recovered when returning to the initial conditions, the same behaviour as the one observed in the heating test.

Naturally, this analysis does not reproduce exactly the conditions of the test, as it involves instantaneous application of the thermal and hydraulic loading without considering the transient phenomena that have occurred in the barrier. It is therefore not surprising that there is a time lag between test observations and constitutive model predictions. In any case, the main objective of proving the capability of the model to reproduce irreversible behaviour when it is submitted to complex *THM* loading paths has been largely achieved. Also a physical explanation has been suggested to explain the observed bentonite behaviour.

Table 4.4

Main parameters of the elasto-plastic constitutive law used in Section 4.3

Parameters defining the Barcelona Basic Model for macrostructural behaviour

κ	κ_s	$\lambda_{(0)}$	p_c (MPa)	r	ζ (MPa^{-1})	p_o^* (MPa)	α_0 (ºC^{-1})
0.005	0.001	0.080	0.50	0.90	0.20	6.5	1.5x10^{-05}

Parameters defining the law for microstructural behaviour

α_m (MPa^{-1})	β_m (MPa^{-1})
2.1x10^{-02}	7.0x10^{-04}

Interaction functions

$$f_C = 1 + 0.9 \tanh\left(20\left(p / p_o\right) - 0.25\right) \;;\; f_S = 0.8 - 1.1 \tanh\left(20\left(p / p_o\right) - 0.25\right)$$

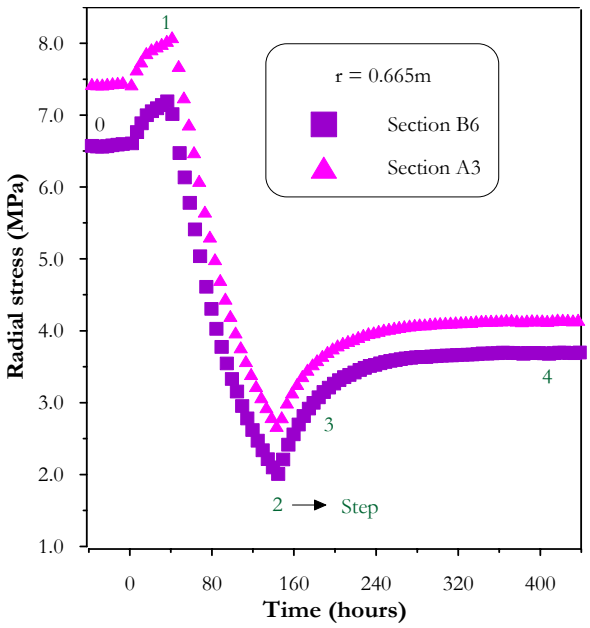

Figure 4.25. Evolution of radial stresses during and after the overheating event.

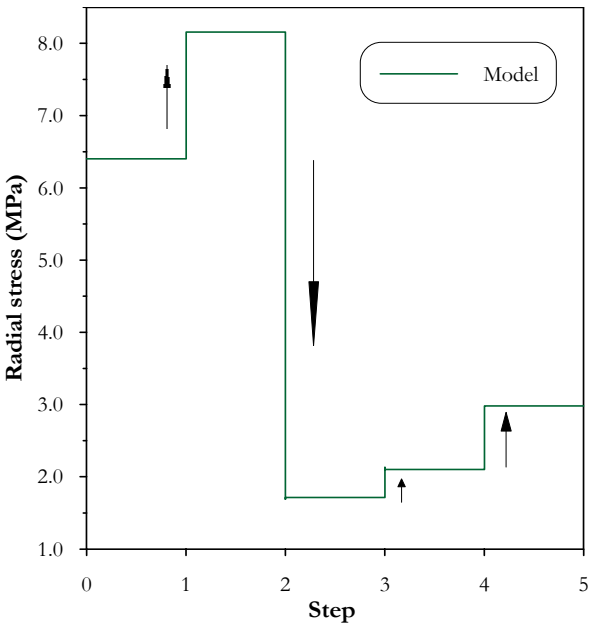

Figure 4.26. Computed values of radial stress during the stress path.

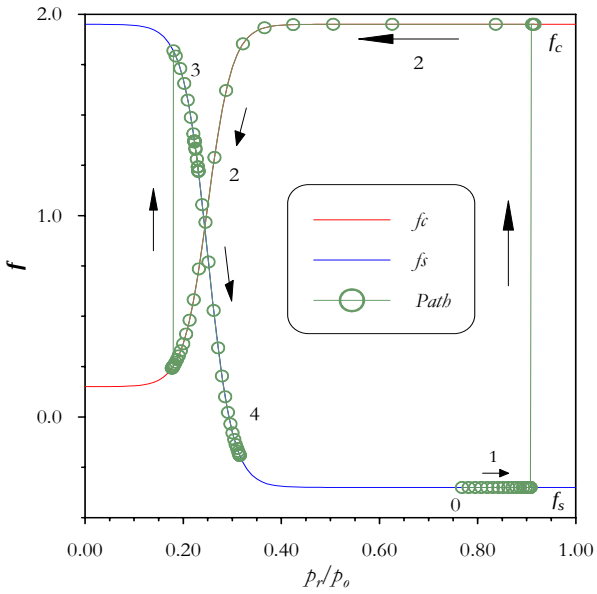

Figure 4.27. Movement of the stress sate on the f_c and f_s interaction functions.

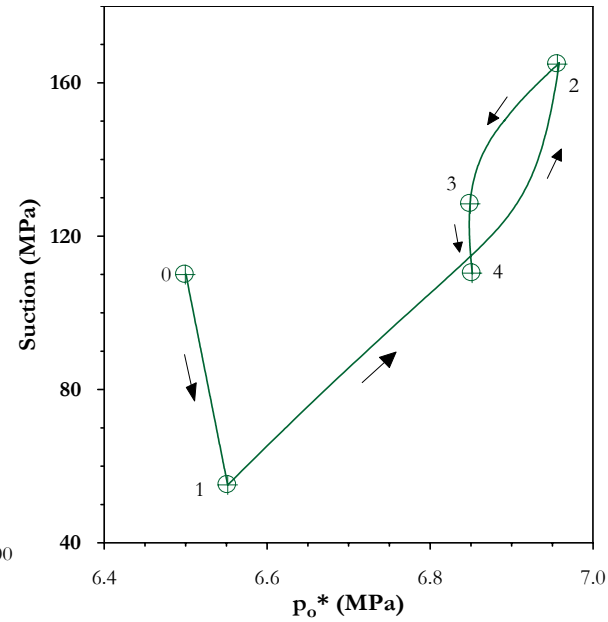

Figure 4.28. Evolution of the hardening parameter during the four loading stages.

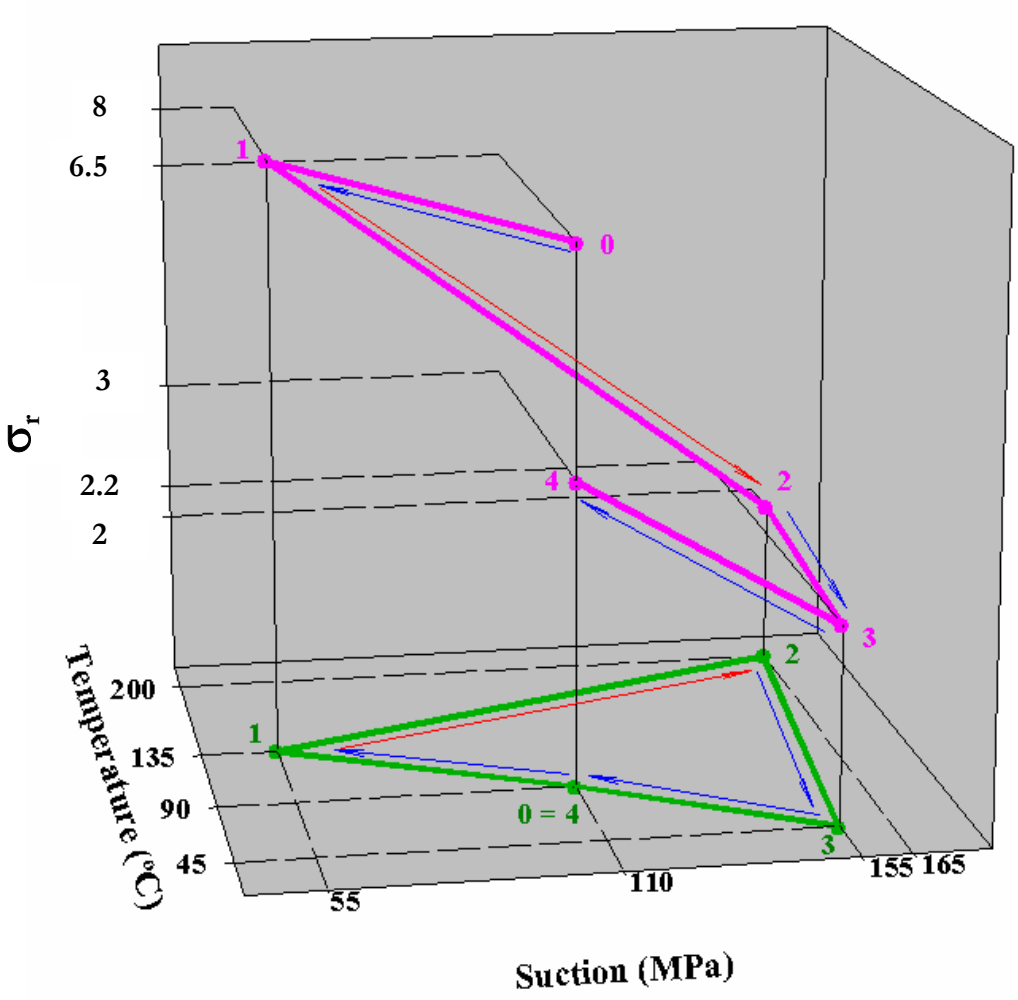

Figure 4.29. Three-dimensional representation of the applied loading stages.

4.4 ANALYSIS OF THE HYDRATION PROCESS OF AN EXPANSIVE MATERIAL

4.4.1 INTRODUCTION

In this section the hydration under confined conditions of a mixture of clay pellets and clay powder is analysed as a boundary value problem using the double structure approach. Expansive materials made of clay pellets or from mixture of clay pellets and clay powder correspond to typical double structure materials. The pellets are generally fabricated at the factory from highly expansive clay, obtaining heavily compacted granulated (generally close to 2.0 Mg/m^3 of dry density).

The clay pellet mixtures have been actively studied in the context of the high level waste repository design (Alonso *et al.,* 1996; Volckaert *et al.,* 2000; Pasquiou, 2001; Romero *et al,* 2003; Hoffmann, 2004; Vallejan, 2004). These mixtures have attractive characteristics that explain the interest in their study as a material for constructing barriers and seals. An interesting advantage of using pellets is that it is possible to achieve target densities of the barrier with a low compaction effort due to the pellets high density. It is also a suitable material when a small or irregular volume should be sealed. On the other hand these mixtures are able to satisfy the properties imposed to engineered barriers and seals, such as: very low permeability, mechanical stability for the waste canister and ability to seal discontinuities in the emplacement boreholes and drifts.

In the context of the Reseal Project (Volckaert *et al.,* 2000) comprehensive experimental studies of pellets mixtures were carried out to determine their hydro-mechanical properties as seal material. The aim of the laboratory tasks were the hydro-mechanical characterization of the mixtures. The temperature effects were not taken into account in these studies. Two different types of clays were considered: FoCa and Serrata clay. Tests with different apparent densities and with different mixtures of clay pellets and clay powder were carried out. Samples of different lengths were also tested.

Most of the hydro-mechanical studies performed have considered the pellet mixture as an equivalent homogeneous material (Volckaert *et al.,* 2000). This assumption has limitations to analyse and reproduce some characteristic material responses. The adoption of a conceptual model for these mixtures is not an easy task. As a first attempt to be closer to the mixture characteristic, a distinction of two main pores structures has been made. In this context the medium 1 corresponds to the clay powder and the medium 2 corresponds to the high density pellets. Obviously there are more pore levels involved in this material, for instance, inside the pellets there are clay aggregates, with their interaggregate and intraaggregate voids that could also be distinguished, as well as the clay platelets. In the analysis presented here the two basic pore levels mentioned above have been considered. The approach can be extended to include more pores levels, if deemed convenient.

This work is focused on the behaviour of these mixtures when they are subjected to hydration under confined conditions. Special attention is placed on the hydro-mechanical coupling of the material. The response of the swelling pressure test is examined. In this experiment the sample has lateral confinement and hydration takes place from one or both ends. Swelling is prevented applying a pressure in order to ensure the constant volume of the sample. These conditions (imbibition under confinement) are close to the ones expected in the actual seals. When a sample of a clay pellet mixture is tested under these conditions it is expected that the water would flow initially through the macropores (the medium with higher permeability) and then it would hydrate the pellets. As the pellets are wetted, they tend to expand and, due to the confined conditions of the test, the macropores tend to close. Finally, a practically homogeneous material is obtained. This implies a dynamic character of the material fabric with one strong coupling between the mechanical and hydraulic problems, because the permeability depends on porosity, which in turn depends strongly on suction and stresses. The constitutive models adopted in the simulation are described below.

4.4.2 MECHANICAL MODEL

In the experiments, this material exhibits the characteristic responses of expansive soils, such as, large swelling strains under wetting, high swelling pressures, macrostructural collapses, more than one swelling stages, and irreversible behaviour, among others (Volckaert *et al.,* 2000, Alonso *et al.,* 1996). The mechanical behaviour is modelled considering two expansive materials, and adopting a mechanical law as the one presented in Chapter III (and Appendix A.2). In the notation the suction of media 1 and 2 are identified as s_1 (p_g- p_{l1}) and s_2 (p_g- p_{l2}) respectively. More details are presented in Appendix A.3.

4.4.3 HYDRAULIC MODEL

It is assumed that there are two porous media (1 and 2), with fluid flow ruled by a generalized Darcy's law (Chapter 2). A constant gas pressure has been assumed. The saturated permeability of the expansive clays shows a strong dependence on porosity. For instance, Figure (4.30) presents experimental data of Serrata clay (Volckaert *et al.,* 2000 and ENRESA, 2000). To include the effects of the porous structure on the media permeability an exponential law in terms of the media porosity has been adopted according to:

$$\mathbf{k}_j = \mathbf{k}_o e^{\left(b\left(\bar{\phi}_j - \phi_o\right)\right)}; \qquad j = 1,2 \tag{4.1}$$

where $\bar{\phi}$ is the local medium porosity (as defined in Appendix A.3), $\mathbf{k}_0$ is the reference permeability tensor at the reference porosity ϕ_0, and b is a model parameter. It is noted that both media have the same parameters; the only difference is given by their respective porosity. This is a key point when the two media tend to the homogenized final conditions.

For the relative permeability model a power law has been assumed, which is expressed as:

$$k_{rl\ j} = \left(S_{l\ j}\right)^n; \qquad j = 1,2 \tag{4.2}$$

The retention curve for expansive clays suggested in FEBEX Project (2000) has been adopted. In this model the dependence of the degree of saturation on suction is expressed as:

$$S_{l\ j} = \left[1 + \left(\frac{s_j}{P_o}\right)^{\frac{1}{1-\lambda_o}}\right]^{-\lambda_o} f_d; \qquad j = 1,2 \tag{4.3}$$

where:

$$f_d = \left(1 - \frac{s_j}{P_d}\right)^{\lambda_d} \quad ; \qquad j = 1,2 \tag{4.4}$$

where P_o and λ_o are model parameters. The function f_d is included in order to model more properly the range of high suctions. P_d is related with the suction at 0 degree of saturation and λ_d is another model parameter; when it is equal to zero the original model (*i.e.* Gens *et al.,* 1998) is recovered. Finally, for the mass water transfer between media a quasi-steady model in terms of media suction has been adopted.

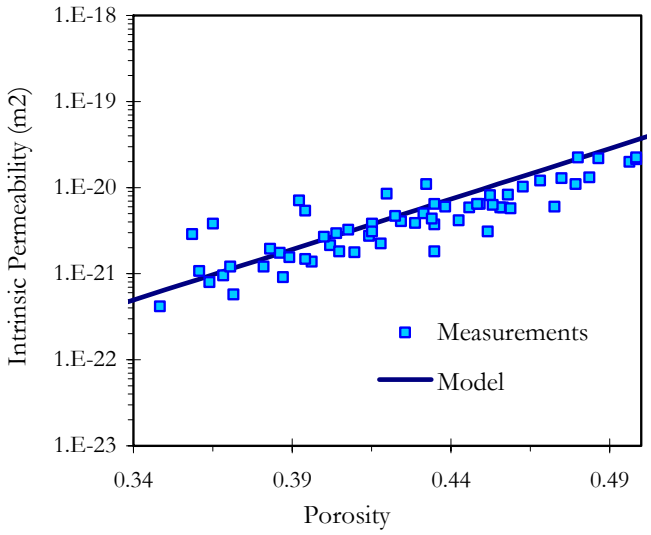

Figure 4.30. Intrinsic permeability of Serrata clay (Volckaert *et al.,* 2000; FEBEX Project, 2000)

4.4.4 MODELLING

The test identified as 'Reseal16' in Volckaert *et al.* (2000) has been considered as a reference for the analysis. A sample of Serrata clay, composed by 50% of clay pellets and 50% of clay powder, with a global density of 1.55 Mg/m^3 was tested in the laboratory. The density of the pellets was 2.05 Mg/m^3 and the solid density was 2.70 Mg/m^3. The sample length was 5 cm with an internal diameter 12 cm. The test was carried out in a cell with hydration from both ends. The experimental data generated in the context of the Reseal and FEBEX projects (Volckaert *et al.,* 2000 and FEBEX Project, 2000, respectively) has been used to identify the model parameters.

In these tests an initial relative humidity close to 22 % was measured (Volckaert *et al.,* 2000). Here it is assumed that the water potentials associated at each pores level are initially in equilibrium and an initial suction of 210 MPa has been adopted for both media. According to the retention curve the initial saturation in medium 2 is S_{l2}=0.59. This implies an initial water

content of the pellets 6.93%, which is a value very close to the reported one (6.37 %). On the other hand, in medium 1 the initial degree of saturation is very low S_{l1}=0.06. According with the experimental data a macro and micro porosity of ϕ_1=0.335 and ϕ_2=0.097 have been adopted, respectively. The simulation of the test has been made solving a boundary value problem with a 1-D model of 100 elements. In Volckaert *et al.* (2000) a comprehensive experimental study of the clay used in the swelling pressure is presented. The parameters and the laws adopted here are in the order of the reported in this work. Table (4.5) contains the parameters of the mechanical model, while the parameters related to the flow problem are included in Table (4.6).

All the swelling pressure tests presented in Volckaert *et al.* (2000) showed more than one swelling step. Three stages can be detected (Figure 4.31): i) an initial stage, associated to the hydration and swelling of the clay powder; ii) a transition stage between the first and the second swelling; and iii) a third stage, corresponding to the final hydration and swelling of the pellets. The model can reproduce this behaviour by distinguishing each swelling phase according with the structural level involved. The first swelling is ascribed to the medium 1 (mainly the clay powder), the second swelling stage is due to the delayed hydration of the expansive pellets, considered in the model through the mass transfer term between media. It can be seen that the model is able to reproduce in a satisfactory way the three observed phases and the results in terms of water intake can be considered also good.

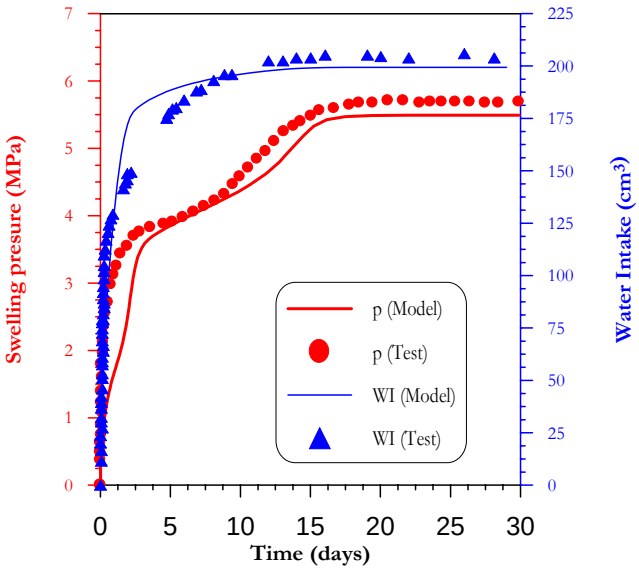

Figure 4.31. Experimental data and numerical results of the swelling pressure and water intake versus time in the swelling pressure test. Test 'Reseal16' (Volckaert *et al.,* 2000)

In Figure (4.32) the time evolution of the suctions for both media are represented for a point located at the hydration boundary (sup.) and at a point near the centre of the specimen, away from the hydration boundary (cent.). Initially the fluid flow takes place predominantly through medium 1. Then, suction in media 1 decreases faster than the suction in media 2. Both suctions tend to equilibrate through the mass water transfer between media.

The variables associated with each level are calculated throughout the test and a detailed examination of the hydro-mechanical coupling can be made. For instance, Figure (4.33) shows the evolution of intrinsic permeability of each medium. Initially, there are large differences between both media, which implies a preferential flow path through the macropores. As the pellets are hydrated (due to the water mass transfer between media), they expand and compress the macropores leading to a more homogeneous material. At the end of the test, the permeabilities of both media tend to converge and the total fluid flow is the sum of two components.

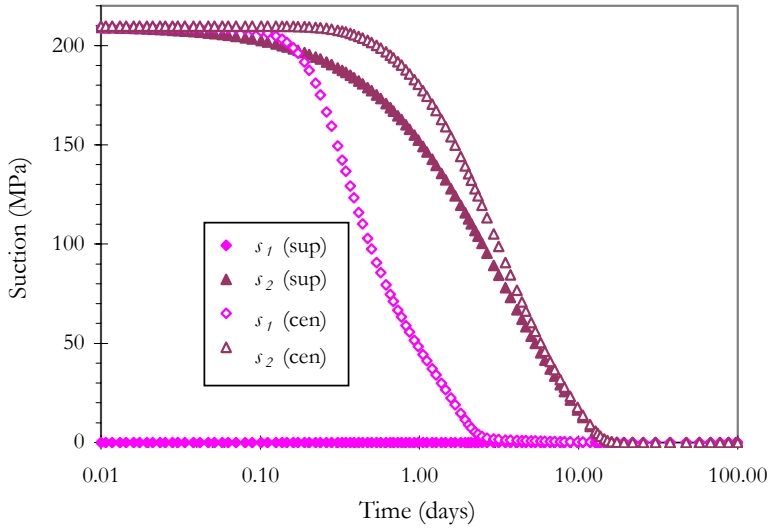

Figure 4.32. Time evolution of the suctions in medium 1 and 2.

Table 4.5

Main parameters of the elasto-plastic constitutive law used in Section 4.4

Parameters defining the Barcelona Basic Model for macrostructural behaviour

κ_{i1o}	α_{s1}	κ_s	μ_1	$\lambda_{(0)}$	M	α	p_c (MPa)	r	ζ (MPa^{-1})	p_o^* (MPa)
0.125	-0.150	0.0135	0.40	0.50	1.5	0.55	0.20	0.80	8.00	6.00

Parameters defining the law for microstructural behaviour

κ_{io}	α_{s2}	μ_2
0.08	-0.150	0.40

Interaction function

$$f_S = -0.20 + 1.0\left(1 - p_r / p_o\right)^3$$

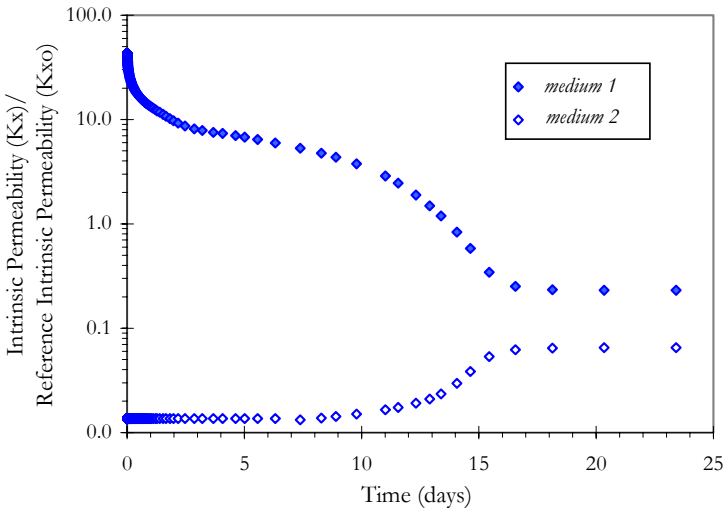

Figure 4.33. Evolution of intrinsic permeability in the two media.

Table 4.6

Parameters related to the flow problem of Section 4.4

Parameters defining the retention curve				
$P_{0\,1}$(MPa)	$P_{0\,2}$(MPa)	$\lambda_{o1}=\lambda_{o2}$	$\lambda_{d1}=\lambda_{d2}$	$P_{s1} = P_{s2}$ (MPa)
50	1000	0.60	2.20	100
Parameters defining the permeability law				
k_0 (m^2)	ϕ_o	b	n	
5.25x10^{-21}	0.40	27	3	
Leakage parameter (kg s^{-1} m^{-3} MPa^{-1}) = 4.0x10^{-7}				

4.5 CONCLUSIONS AND REMARKS

In this Chapter the double structure approach has been applied to different cases. All the examples present a marked double structure and are actual cases in which there are measurements of the main variables of the problem. Regarding the first application case, the mechanical behaviour of compacted bentonite has been explored under different stress paths. Examination of the results has revealed significant features of behaviour such as yield phenomena, dependency of swelling strains on applied stresses, stress path dependency of strains, and compound stress paths in swelling pressure tests. In spite of the complexity of the behaviour, a good insight into the behaviour of the compacted bentonite, and into the basic mechanisms controlling it, has been achieved using an elasto-plastic framework that incorporates the interaction between microstructural and macrostructural fabric levels in a

simplified manner. Most of the main features of the behaviour are correctly reproduced by the model allowing a more detailed examination of the role that the different variables play on the explanation of the overall behaviour of the soil. It is important to highlight that despite the relative complexity of the model only standard tests of non-saturated soil mechanics have been used to identify most parameters.

The second application case corresponds to the study of an overheating episode that took place in a large scale heating test. The clay barrier under study was made up from the same bentonite characterized in the first case. So, practically the same parameters have been used in the simulation. The performance of the constitutive mechanical model is also good in this problem. It has been shown that the model is able to reproduce the major features of the observed mechanical behaviour in response to a complex history involving temperature and suction changes. That is, after a close cycle of changes in the state variables of the problem (temperature and suctions), irreversible changes in the clay fabric implies no-recoverable values of the swelling pressure when confined conditions prevail. The interaction between the two structural levels plays a crucial role in the understating and reproduction of this irreversible mechanism.

Finally the double structure formulation is applied to a problem related with the behaviour of a clearly non-homogeneous material, made up from a mixture of clays pellets and clay powder. The problem exhibits distinctive features connected to the strong coupling between the unsaturated flow (in each pore structure) and the deformation of the two media, characterized by an important swelling of the pellets. It s highlighted, that the aim of this modelling is not to check the predictive capabilities of the formulation, but to explore its suitability to analyze the behaviour of mixtures of clay powder and clay pellets. It has been observed a satisfactory response of the model in the test analyzed. It seems that the relevant physical phenomena, and couplings, are well captured by the double structure framework.

CHAPTER V

THERMO-HYDRO-MECHANICAL ANALYSIS OF A LARGE SCALE HEATING TEST

SUMMARY

In the previous Chapters the efforts have been mainly focused on the development of a double structure approach and on the validation of the mechanical model. In this Chapter several objectives are pursued. One of them is to analyse the *THM* (Thermo-Hydro-Mechanical) evolution of an engineered barrier submitted to heating and hydration simultaneously. The experiment is a large scale heating test, known as ***mock-up*** test, which has been carrying out at the CIEMAT laboratory in Madrid. The analyses are focused on the transient stage of this test. Especial attention is placed on the explanation of the apparently unforeseen decay observed in the hydration rate at advanced stages of the experiment. So, another aim of this Chapter is the identification of the phenomena that could explain, with physical basis, the unexpected behaviour of the clay barrier. Three phenomena identified as: 'threshold gradient', 'thermo-coupling effects' and 'evolution of micro-fabric' will be considered. The test has been analysed considering the potential influence of these processes in the experiment response. Finally, a more detailed analysis of the barrier has been undertaken considering the full *THM* double structure framework presented in the previous Chapters (II, III and IV). Therefore, the validation of the double structure framework is the other objective pursued herein.

5.1 PREFACE

Engineered barriers are basic elements in the disposal concept for high level radioactive waste. Generally the conceptual design considers the repositories placed in deep geological media (natural clays or crystalline rock) and adopts compacted expansive clays as the basic material to build the barrier. This clay-based isolation system has the multiple purposes of providing mechanical stability for the waste canister (by absorbing stresses and deformations); serving as a buffer around it; sealing discontinuities in the emplacement boreholes and drifts; and delaying the water flow from the host rock. This last task is probably one of the most important, because it postpones the contact between water and the waste canister as long as possible; and, in the case of canister failure, it retards the migration of the radionuclides released. At least two key unknowns appear relevant in this matter. One of them is the time to reach the full saturation of the barrier, and the other is which would be the *THMG* (*THM* and Geochemical) barrier conditions in a long-term regime. The first one is the subject of this Chapter. As it is well-known, this is a crucial unknown due to its strong impact on the long-term performance of the system and due to its influence on the repository lifetime (longevity studies, Güven, 1990).

The barrier behaviour is highly complex, since it involves coupled *THM* phenomena that take place due to the simultaneous heating (generated by the waste radioactive decay) and hydration of the barrier (due to the contribution of the surrounding rock). The understanding and explanation of the main *THM* processes and their couplings, in actual conditions, require the contribution of experimental and fundamental studies. Experimental works have been conducted in two main directions: large-scale heating experiments, and laboratory tests. The fundamental studies have been mainly oriented to the development of coupled *THM* formulations and numerical codes based on those formulations.

Regarding the experimental work, in the last few years, several laboratory tests at full-scale (or almost full-scale) have been carried out with the main aim to advance in the knowledge of the behaviour of these kind of systems under actual conditions (FEBEX Project, 2000; Volckaert *et al.*, 2000; Svemar & Push 2000; Fuente-Cantillana *et al.*, 2001; Dixon *et al.*, 2002). These tests replace the waste canisters by electrical heaters and they are mainly aimed to demonstrate the feasibility of the conceptual design under study. Generally, these experiments are well-instrumented with the objective to know their evolution and to evaluate its performance under conditions similar to those expected in the actual repositories. This fact gives the opportunity to check the predictive capability of the numerical codes and to calibrate them as well. In addition, laboratory tests have been mainly conducted to know the materials behaviour and to identify its properties (constitutive laws and parameters).

Concerning theoretical studies, formulations for coupled *THM* finite element analyses have been the subject of increasing attention (Olivella *et al.*, 1994; Gawin *et al.*, 1995; Thomas & He 1995; Gatmiri & Delage 1997). The numerical codes are effective tools to study the behaviour of the barrier and the host medium, because they allow the consideration of different *THM* processes and their couplings in a unified and consistent framework. The inclusion of geochemical variables in the formulations in order to perform coupled *THMG* numerical analyses of engineered barriers is becoming more widespread (Guimarães *et al.*, 1999; Thomas *et al.*, 2001; Gens *et al.*, 2003).

The numerical models are used in different stages in the researches related to an underground laboratory for high-level radioactive waste disposal. During the test design, scoping calculations reveal useful information related to the expected performance of the barrier and the near field under different plausible scenarios. After that, during the operation stage of the experiment, the critical analysis of the comparisons between model output and test data is a helpful exercise to understand better the actual *THMG* processes and also to evaluate the conditions that control the barrier evolution. Finally, numerical simulations emerge as indispensable when the interest is focused on performance assessment involving long-term predictions

In this Chapter, numerical models are used to analyse an ongoing large-scale heating test carried out under *THM* controlled conditions. The evolution of the experiment is critically analysed by comparing the test data and the model results. An apparent decay in the rate of hydration, observed at advanced stages of the experiment, causes significant discrepancies between models output and measurements. These discrepancies affect strongly the reliability of the long-term prediction performed, especially that are related to the time required to reach the full saturation of the barrier. Due to that, the studies have been oriented towards the identification of other processes or phenomena which can clarify and explain, with physical basis, the 'unexpected' barrier behaviour.

A preliminary study envisages three main phenomena that are identified as: threshold gradient, thermo-coupling effects and evolution of micro-fabric. Although the developed models are very simplified, the numerical analyses performed offer valuable information about the barrier response under these hypotheses.

Single porosity models are not able to handle properly the role that the structure of the swelling clays could play on the hydration process. During this process the clay fabric exhibits a dynamic character (Dixon *et al.*, 1999; Cui *et al.*, 2001) that could affect strongly the kinetics of hydration, especially if confined conditions prevail. So, a more detailed analysis of the clay fabric effects in the evolution of the *mock-up* test has been performed with the aid of the double structure concepts. The problem has been analysed numerically in the light of the full *THM* double structure approach presented in Chapter II, III and IV. This seems a more suitable framework to simulate the problem in which two different pore levels (the macro and micro structure of the Febex bentonite) can be clearly distinguished. The use of this approach has allowed the adoption of a conceptual model for the hydration of the swelling clays closer to the actual observed behaviour. The explicit consideration of the two dominant levels of pores could help the understanding of some processes that take place during heating and hydration of the expansive clay.

The main aim of the analyses presented in this Chapter is to discuss the role that different phenomena could play in the unforeseen tendencies observed in the barrier. Here, the numerical code has been used as a tool to explore the expected response of the test when these hypotheses are taken into account. Even though the study presented in this Thesis has been centred on the *mock-up* test, the main conclusions are general enough and they could be extended to explain the behaviour observed in other experiments in which similar conditions and problems in the hydration process have also been detected.

In this Chapter, three different parts can be clearly distinguished: the first one presents the *mock-up* test together with the first numerical analyses of the barrier evolution and the identification of the apparent hydration problems observed in the test; the second one presents the most significant results of the preliminary studies carried out in order to identify the sources of the hydration problems; and the third one is related to the double structure framework proposed to analyse the test. Besides, aspects related to the expansive clay behaviour under hydration and the conceptual model adopted are described. The model results are also an important matter for attention. Finally, the Chapter is closed with the main conclusions of the work. In the Appendix A.4, additional information related to the test and the numerical analyses are presented. Due to the strong connection between the subjects treated in the three mentioned parts already mentioned, it was decided to maintain all the contents in an unique Chapter, in spite of its length.

5.2 *MOCK-UP* TEST. 'OPERATIONAL STAGE' MODEL

5.2.1 INTRODUCTION

The *mock-up* test is being carried out at the CIEMAT laboratory in Madrid, as part of the FEBEX project. The aim of this project is to study the behaviour of the barrier components in the near-field of a high-level radioactive waste repository in crystalline rock (granite). The project is based on the Spanish disposal reference concept, which considers the waste canister placed horizontally in drifts and surrounded by a clay barrier constructed from highly-compacted bentonite blocks. The experimental task of the FEBEX project is made-up of three main parts (FEBEX Project, 2000):

- an *in-situ* test, under natural conditions and at full scale;
- a *mock-up* test, at almost full scale and;
- a series of laboratory tests to complete the information from the two large-scale tests.

The *in-situ* test operates under natural conditions at the underground laboratory managed by NAGRA, at the Grimsel test site in Switzerland. Figure (5.1) represents the test schematically. Its components have been constructed with the actual design dimensions of a repository drift in granite. There are two electrical heaters, which replace the canisters containing heat-emitting waste, surrounded by a 0.69 m thick clay barrier (with a global dry density of 1.60 Mg/m^3). The barrier was build-up with blocks of compacted FEBEX bentonite at a dry density of 1.70 Mg/m^3. The experiment has been extensively monitored, with sensors installed in the bentonite, the granite, the heaters and the service zone. The evolutions of the main *THM* variables have been recorded in different sections of the clay barrier and in boreholes in the host rock. The *THM* variables are: temperature (in clay barrier and host rock), heater power (global variable), relative humidity (in clay barrier), total pressure (in clay barrier and host rock), relative displacement (in clay barrier), fluid pressures (clay barrier and host rock), among others. More details can be found in FEBEX Project (2000). Fundamentally, the objective of the demonstration is expected to be attained in the *in-situ* test.

The *mock-up* test avoids many of the uncertainties arising form the natural system. This is achieved mainly due to the good control of the initial and boundary conditions of the experiment. The physical components of the test consist of five basic units: the confining structure with its hydration system, the clay barrier, the instrumentation, and the system for data acquisition and for heater control. Figure (5.2) shows the test schematically (FEBEX Project, 2000).

The confining structure is a cylindrical steel body with a useful length of 6.00 m and an inner diameter of 1.62 m. The hydration system supplies granitic water under pressure to the periphery of the clay barrier. The main elements of the heating system are two heaters located concentrically in the confining structure. The clay barrier is formed from highly-compacted bentonite blocks. The blocks were fabricated with an average water content of 13.6% and an average dry density of 1.77 Mg/m^3, the final global dry density of the barrier is 1.65 Mg/m^3. This difference in dry density is due to the presence of gaps, between the external perimeter of the clay barrier and the confining structure (mainly in the upper part) and also due to the joints between blocks. Basically, the instrumentation includes sensors installed in the clay barrier, in the heaters and in the confining structure. The main measured variables are: temperature, relative humidity, fluid pressure and total pressure (FEBEX Project, 2000). Figure (5.3) shows the main longitudinal and transversal cross-sections monitored from the test.

A wide experimental program oriented to the full characterization of the materials involved in the design of the clay barriers and the host rock has been carried out at the CIEMAT, CSIC-Zaidín and UPC laboratories. Especial attention has been placed on the study of the main *THM* properties of the FEBEX bentonite and on the examination of its fabric. Many of these tests have been used to develop the constitutive models and also to identify the constitutive law parameters used in the simulations. Some of the analyses have been presented in Chapter IV (identification of the mechanical model parameters) and others will be presented in this Chapter and Appendix A.4.

The modelling of these large scale tests is another fundamental part of the FEBEX project. As commented in Gens *et al.* (1998), during the heating and hydration of a large scale heating test several coupled *THM* phenomena occurs. For instance, hydration takes place from the external boundary inwards driven by the gradient between the applied water pressure and the suction in the bentonite. Hydration will cause a progressive rise in degree of saturation. This affects both the temperature field, due to the modifications of thermal conductivity, and the stress/strain distribution, due to suction changes. On the other hand, in the inner part of the buffer, applied heat causes a temperature rise that moves outwards. Temperature-induced water evaporation causes drying of the bentonite. Vapour coming from the inner part of the barrier will diffuse towards the outer regions where it will condense causing a local rise of degree of saturation. Water transfer is also affected by the dependence of water viscosity on temperature and by porosity changes arising form variations of stresses and suction. Changes in hydraulic conditions influence the temperature field via variations of thermal conductivity and affect also stress/strain field due to pore water pressures and pore gas pressure changes. There are more significant couplings in this problem as explained in the next sections. Thus, it can be concluded that for this kind of problems performance of coupled *THM* analyses are compulsory.

A comprehensive *THM* modelling of the *in-situ* test has been performed (FEBEX Project, 2000, Sánchez & Gens 2001, Sánchez & Gens 2002). The numerical models developed for the *in-situ* test have been supported by the experimental data obtained in the laboratory test and also by the information coming from the *mock-up* experiment. The *in-situ* test model is relatively complex since it integrates information of the clay barrier and also of the host geological medium (fractured granite). The modelling work has been oriented to understand, to explain and to reproduce the evolution of the experiment. Comparisons between measurements and model results have been made for the main *THM* variables of the experiments in all of the instrumented sections and boreholes. Considering that it is a natural system, the obtained results can be considered good enough since the tendencies of the main *THM* variables of the experiment are well captured and also satisfactory quantitative agreements are obtained. A complete analysis of this test, with all the comparisons between records and model results can be found in: FEBEX Final report (2000), Sánchez & Gens (2001) and Sánchez & Gens (2002). Some additional comments related to the modelling of this experiment are introduced in the following Chapter. Regarding the modelling of the *mock-up* test, the main aspects are presented in the following Sections.

5.2.2 ANALYSIS OF THE *MOCK-UP* TEST HYDRATION

5.2.2.1 GENERAL

As a summary of the main characteristics of this test it can be mentioned that:

- the heterogeneities of the natural system (granite formation) are avoided,
- the test has a clay barrier with an unlimited availability of hydration water, supplied at constant and controlled pressure,
- the mass of water introduced into the system is continuously measured and registered,
- the boundary conditions are better defined than in the *in-situ* test,
- the initial conditions are well-known at the beginning of the heating phase,
- the test is very well instrumented, with several sensors located along the barrier which register the evolution of the main *THM* variables, and
- the experiment has two electrical heaters, symmetrical placed in relation to the central section of the test. So, this allows the availability of repetitive measurements.

These facts facilitate the identification of the main processes and couplings that take place in a barrier submitted to heating and hydration. Additionally, the validation of the numerical code developed for the analysis of the near field behaviour is easier, as only the performance of the clay barrier is considered.

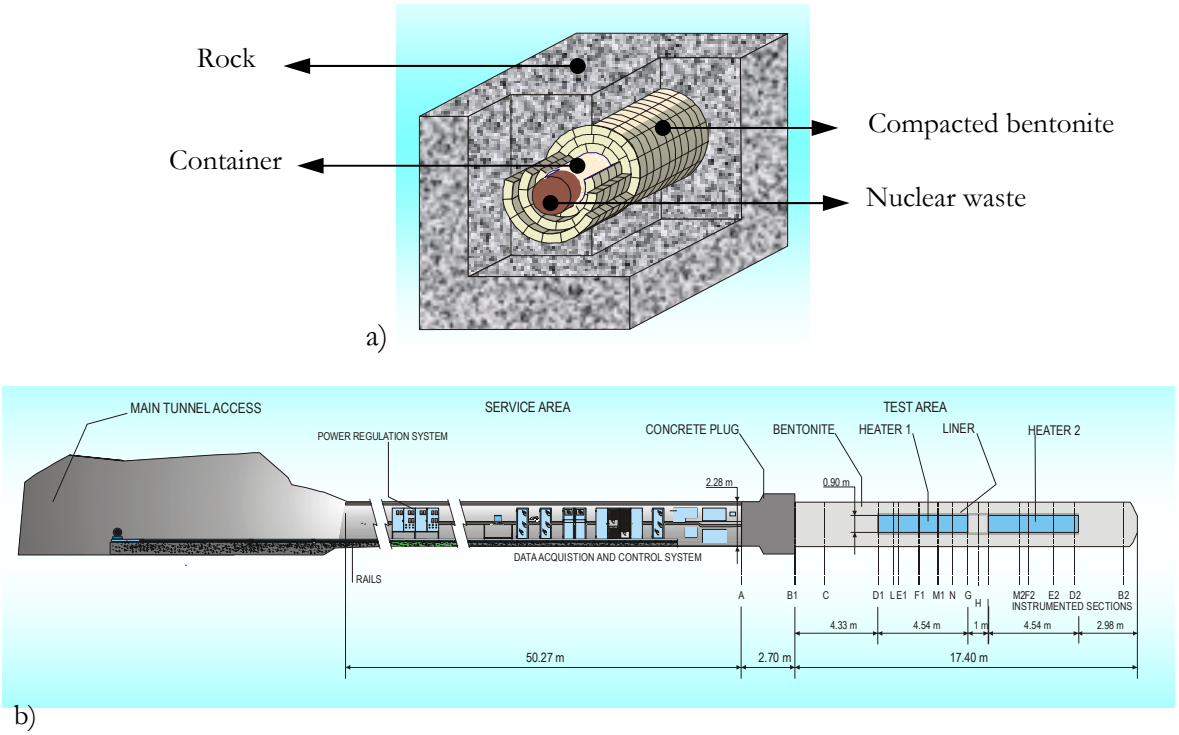

Figure 5.1. a) Scheme of the engineered barrier. b) Scheme of the *in-situ* test.

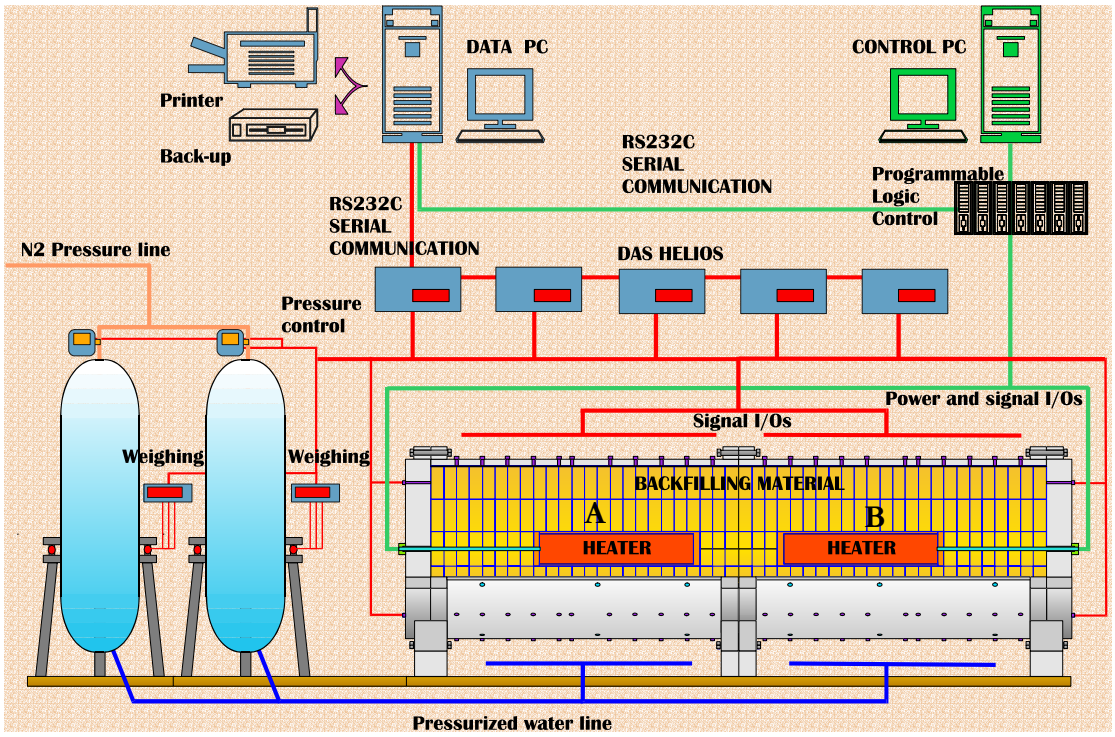

Figure 5.2. Scheme of the *mock-up* test

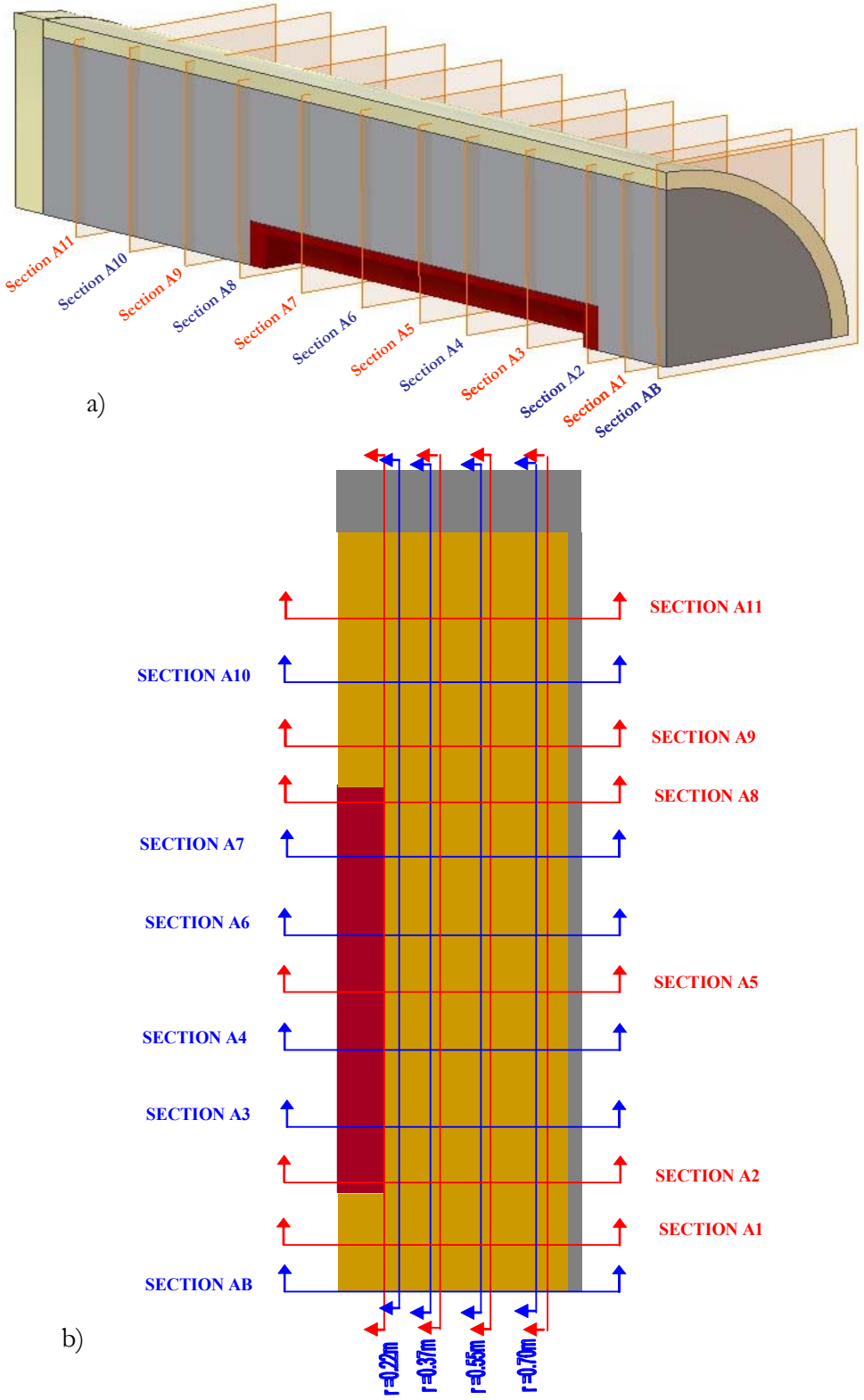

Figure 5.3. a) A 3-D schematic representation of the barrier. b) Longitudinal and transversal cross-sections. The schemes correspond to the Zone A only. In the Zone B, there are other similar instrumented cross sections symmetrically placed respect to Section AB.

The phase of heating and hydration of the test, known as the 'operational stage', started in February 1997 and is ongoing nowadays. Before and during the 'operational stage' of the test, coupled *THM* numerical analyses have been performed using the CODE_BRIGHT finite element program. These modelling works have provided the opportunity to check the predictive capability of the code, as well as to improve and validate the formulation and the constitutive models adopted. The main results of the simulations can be found in FEBEX Project (2000), Sánchez & Gens (2001) and Sánchez & Gens (2002).

The numerical analysis presented in this Chapter considers, as a starting point, the problems detected in the 'OBC' model (Operational Base Case) to reproduce the evolution of the *mock-up* test at advanced stages of hydration. The 'OBC' model considers the bentonite as a single porosity medium (with average material properties). A 2-D axis-symmetric model has been adopted for the numerical analysis. Also the symmetry of the test has been taken into account and one half of the *mock-up* test has been considered (one heater). In the following sections, a brief description of the main results of the 'OBC' model is presented with the objective of explaining the main trends of the *THM* behaviour observed in the *mock-up* test and also of introducing the problems identified in the simulations. More information about the 'OBC' model is presented in the Appendix A.4. Before the presentation of the *THM* behaviour observed in the *mock-up* test, the following aspects related to the analyses are summarized:

- The main longitudinal and transversal cross-sections selected for the analyses are shown in Figure (5.3).

- The analyses have been focused on two characteristic cross-sections. One of them is identified as a 'hot cross-section', and it is in the heater zone (*i.e.* Section A4 and B4, Figure 5.3). The other is identified as a 'cool cross-section', and it is located away from the heater (Section A10 and B10, Figure 5.3). In this way two different patterns of behaviour can be examined. Results involving other sections are presented in Appendix A.4.

- The experimental values shown in the comparisons between model results and experimental data have been supplied by CIEMAT. The last records considered in the comparisons were obtained on 18th September 2003, corresponding to the day 2417 from the starting of the heaters (*i.e.* about 6.62 years).

- The identification of the main constitutive law parameters (from the laboratory data available) were carried out before the operational stage. Some constitutive laws were adjusted (the retention curve and intrinsic permeability) during the first stage of the operational phase (mainly due to the availability of more experimental data), so it can be considered that the 'OBC' model were developed carried out with the information existing on dates close to the day 200 of the test. No more adjustments have been made, nor the overheating episode (Chapter IV) has been considered. This is because the main aim of these analyses is to show the actual magnitude of the discrepancies between model results and experimental data. In that sense the numerical results shown after the day 200 are predictions of the OBC model.

Figures (5.4 to 5.7) present the evolution of the global variables of the problem, which are: the heater power and the water intake. Figures (5.8) show the time evolution of temperature at different points of the barrier, whereas Figures (5.9) present the evolution of the relative humidity at different radii of the barrier for the two selected sections. Finally, Figures (5.10) show the time evolution of stresses in selected positions of the barrier (P_T: tangential stress, P_Z: longitudinal stress and P_R: radial stress). In the following Sections, the main results (experimental and numerical) of the *mock-up* test are analysed considering the different problems (thermal, hydraulic and mechanical) in a separately way.

5.2.2.2 THERMAL PROBLEM

The barrier is heated maintaining a constant maximum temperature of 100 ºC in the contact between heaters and bentonite. It can be stated that the model yields good results regarding the thermal problem. This is reflected either in the evolutions of a global variable (such as the power emitted by the heaters Figure 5.4), or in the measures of the local ones (such as the evolution of temperatures in different points of the test Figures 5.8). It can be noted that there are some small differences in the temperature field, especially in zones close to the heater. They may be an effect of the lower thermal conductivity in the discontinuity that may exist between heater and bentonite. The long-term predictions (20 years) indicates a slow increment of the heater power as the barrier is hydrated (Figure 5.5) due to the increase of thermal conductivity as the saturation augments (Equation A4.2, Appendix A4). Also the temperature at different radii of the barrier increases slowly as hydration goes on (Figure 5.8).

5.2.2.3 HYDRAULIC PROBLEM

The barrier is hydrated uniformly from the periphery, maintaining a practically constant water pressure of about 0.5 MPa. Figure (5.6) shows the time evolution of the water entry in the test and the rate of water intake as well. In Figures (5.9) it can be seen that until the day 900 of the test, approximately, the model offers a good reproduction of the hydraulic variables. Up to that time, the overall behaviour of the test is the expected one: an increasing saturation in the zones close to the hydration boundary and an intense drying in the regions close to the heaters followed by a slow hydration. The behaviour of zones close to a radius of 0.37 m shows an initial wetting, due to the condensation of the water vapour coming form the inner region, and then a drying.

From about the day 900, some differences are observed between the hydraulic behaviour of the test and model predictions. In terms of the water entry, the model results move away progressively, in relation to the experimental data. This fact can be clearly detected in terms of the rate of water intake (Figure 5.6), in which the test data values (from the day 900 of the test) undergo an important reduction in comparison with the values of the 'OBC' model. A recovery of the experimental values can be seen when a non-planned event took place (the overheating episode, close to the day 1381), finally the tendency observed previous to the overheating was recovered, that is, a clear slowing down of the rate of water intake compared with the model predictions.

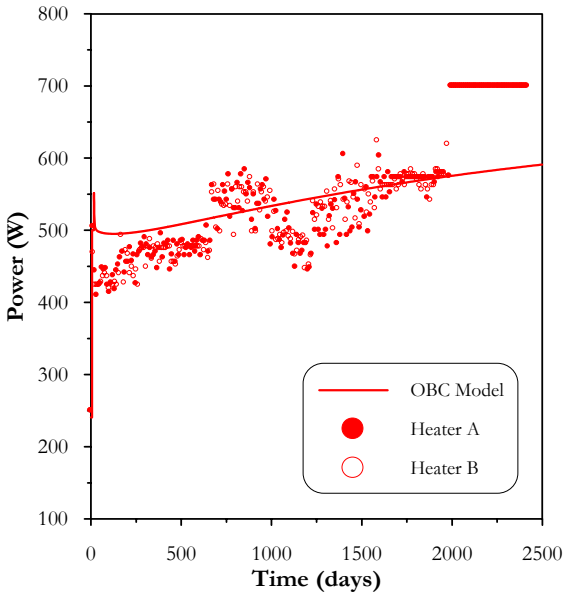

Figure 5.4. Evolution of heater power in the *mock-up* test. Observed and computed values. OBC (Operational Base Case) model.

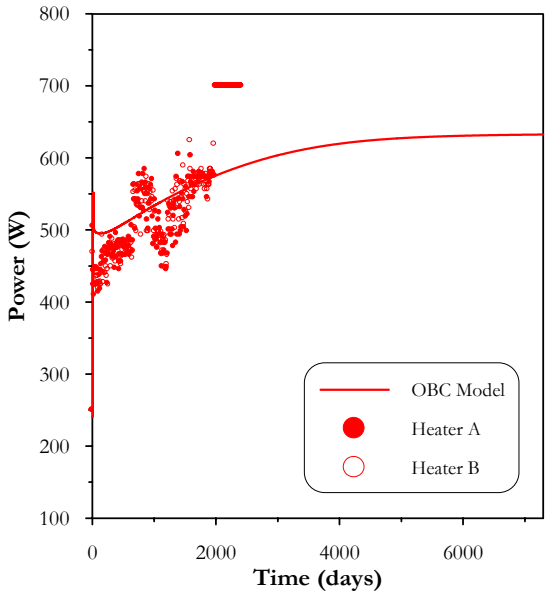

Figure 5.5. Evolution of heater power in the *mock-up* test. Long-term prediction (OBC model).

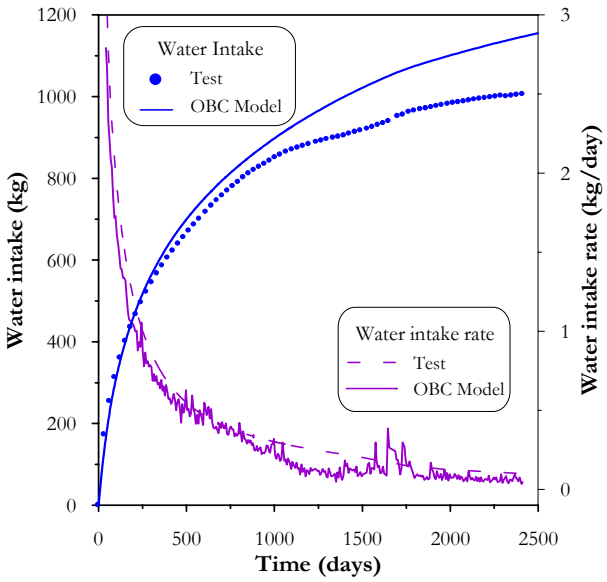

Figure 5.6. Evolution of water entry in the *mock-up* test. Observed and computed values (OBC model).

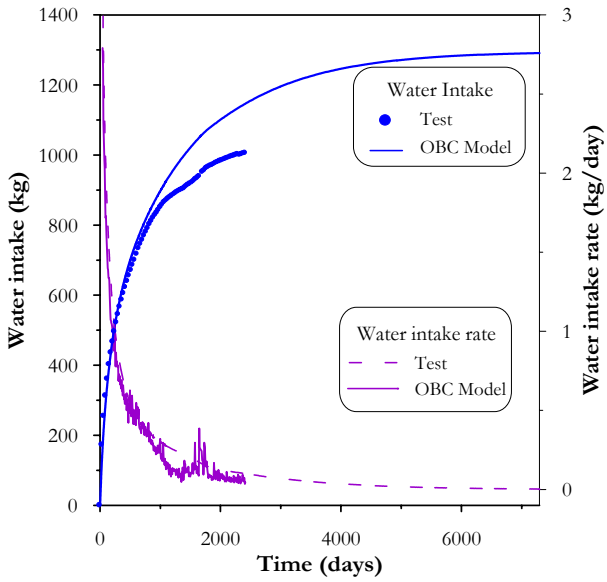

Figure 5.7. Evolution of water entry in the *mock-up* test. Long-term prediction (OBC model).

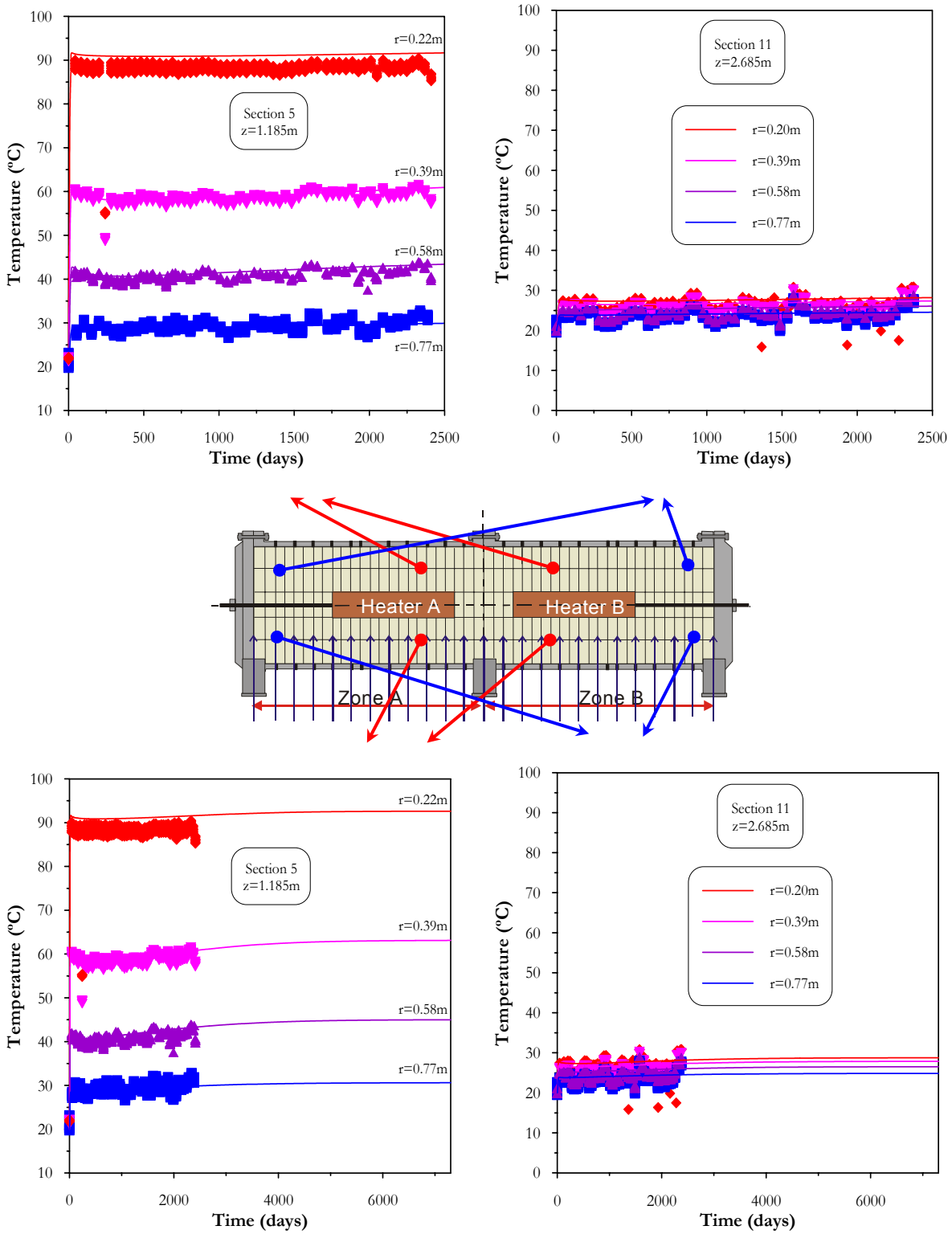

Figure 5.8. Evolution of temperature in the *mock-up* test. Sections A5-B5 ('hot cross-section') and A11-B11 ('cold cross-section'). Observed versus computed values and long-term predictions (OBC model).

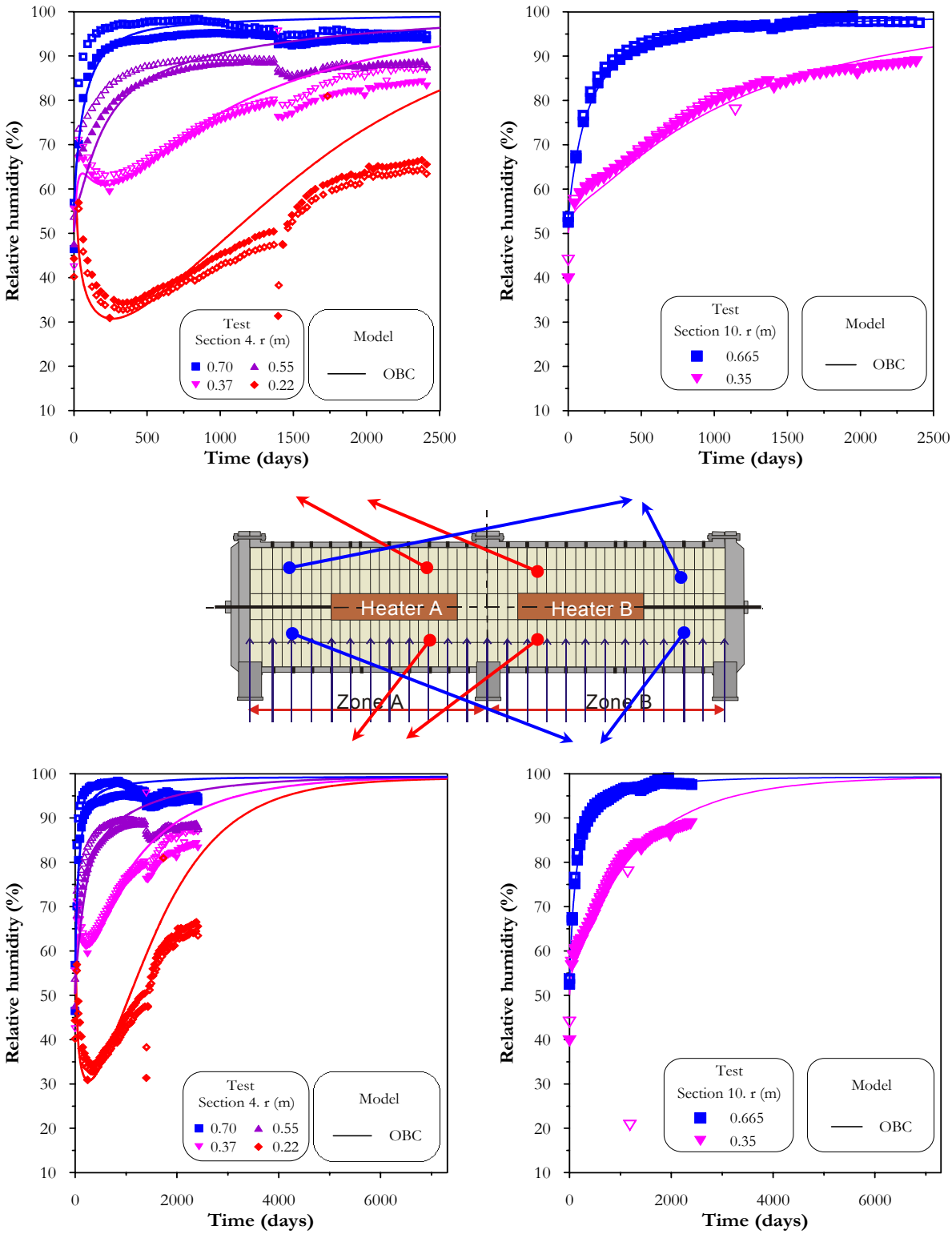

Figure 5.9. Evolution of relative humidity in the *mock-up* test. Sections A4-B4 ('hot cross-section') and A10-B10 ('cold cross-section'). Observed versus computed values and long-term predictions (OBC model).

Regarding the evolution of relative humidity in the heater regions (sections A4 and B4, Figure 5.9) a significant reduction in the rate of relative humidity increase can be observed. The effects of the overheating can be clearly noted in the 'hot cross-section', especially just after this episode. It seems that the transient period induced by the overheating was practically finished after the day 1700. The apparent hydration problems are even more evident when the long-term predictions are observed (Figures 5.7 and 5.9), in which a clear tendency to a very slow hydration rate in all of the measured radii can be detected. On the other hand, when a 'cold cross-section' is examined, the hydration problems are less perceptible (Sections A10 and B10, Figure 5.9). Note that some small differences between model and test results can also be detected in these sections after the day 2000 (approximately).

5.2.2.4 MECHANICAL PROBLEM

Similar trends to the ones observed in the hydraulic problem appear in the mechanical problem. That is, up to the day 900 approximately, in sections involving heater there is a good agreement between predictions and observations. From that moment on, measured stresses respond to the modifications of the hydration pattern, and a tendency to maintain constant values of stresses can be observed. This is ascribed to the strong hydro-mechanical coupling of the problem.

The overheating episode had different influences on mechanical behaviour depending on the considered sections. In sections far from the heaters, the values and tendency registered previous to this event have been recovered practically immediately (Section A10 and B10), whereas in sections involving heaters, a more marked influence on the evolution of the stress field can be observed. In these sections, the tendency to maintain a practically constant stress level (observed previous to this episode) has been recovered after the overheating. But, the stresses are now lower compared with the ones measured before this event (Sections A6 and B6). Arguments based in double structure concepts have been presented in the Chapter IV to explain this behaviour. Finally, in zones near the ends the overheating event has no perceptible effects and the model captures very well the measures values of stresses (Section A12 and B12). The long-term analysis predicts a maximum stress of the order of 10 MPa.

5.3 ANALYSES OF THE MOCK-UP TEST HYDRATION INCLUDING NON-STANDARD FLOW MODELS

5.3.1 INTRODUCTION

The understanding and the explanation of the apparent decay in the rate of the barrier hydration are viewed as an important aspect concerning the performance of reliable long-term predictions.

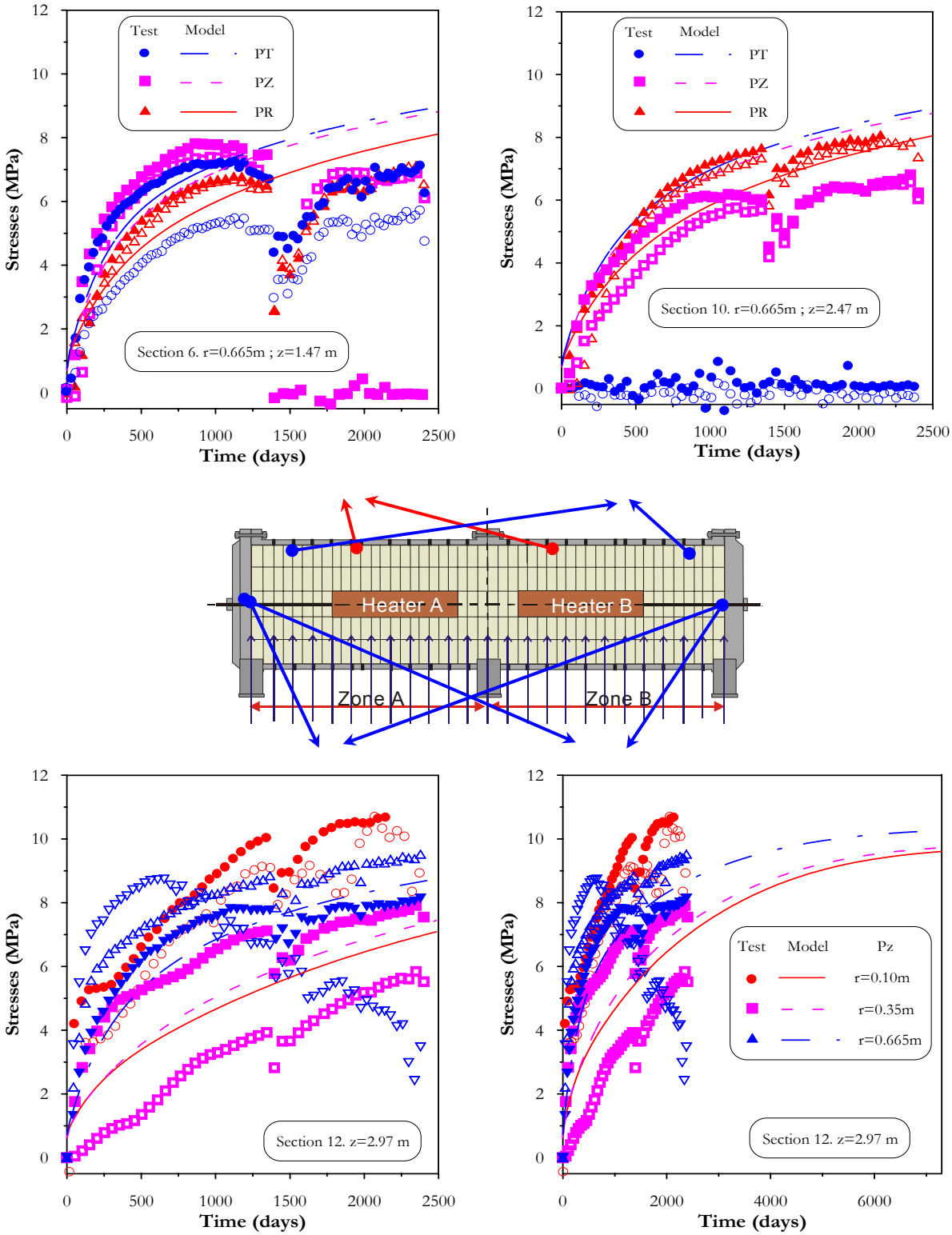

Figure 5.10. Evolution of stresses in the *mock-up* test. Sections A6-B6, and A10-B10 and A12-B12. Observed versus computed values and long-term predictions (OBC model).

In the first place, it was explored whether with minor modifications of the constitutive laws or their parameters was possible to explain and reproduce more closely the global evolution of the test. A wide sensitivity study was carried out to that end, and it was unable to obtain a set of constitutive laws and materials parameters (with physical meaning) consistent with the observations. As a main conclusion of this work it can be mentioned that, although changes in some parameters can lead to better agreements locally in some variables, it does not appear that such strategy can lead to a global explanation of the behaviour that includes all the observations made, both in the hot and in the cool zones. Some of the work performed in this context are described in Appendix A.4 (Section A4.2) and in Sánchez & Gens (2001).

Simulations of the *mock-up* test performed by ULC (University of La Coruña) group have similar problems as those mentioned in the Sections above. Even though the numerical codes are different and the determination of the model parameters was carried out independently, the same tendency is observed, *i.e.*, a growing departure between models predictions and measurements, from 900 days onwards (Samper *et al.*, 2002).

The hypothesis that problems in the hydration system could affect the normal water supply to the barrier has also been considered. It was explored whether there were any problems in the hydration system, or a geotextile blockage had occurred, that could affect the normal hydration of the barrier. It was confirmed experimentally that there was no obstruction in the hydration system or geotextile, and that the water intake was nearly uniform over the entire hydration front (Martin & Villar, 2004). Discarding problems in the water supply and considering that changes in the materials parameters could not explain the unexpected behaviour of the barrier, research was focused on the identification of other processes that could be responsible for the apparent slowing down of barrier hydration. These improvements in the model may also explain the different response observed in the two types of sections analysed.

Obviously the main difference between these two sections is the temperature distribution, as it can be seen in the cross sections of temperature shown in Figures (5.11 to 5.13). It could be thought that the temperature has a strong effect in the clay properties which affects the normal hydration of the barrier. But there are at least three important aspects that lessen the possible direct role played by temperature in the unexpected barrier trends, namely:

- The departure between test and model results is detected when the temperature field is well-established. There are not important changes in the temperature evolution since practically the beginning of the test (Figure 5.8).

- The decay in the hydration rate also affects the external zones of the barrier in sections involving heaters (Figure 5.9). However, for these external radii, there are small temperature differences along a longitudinal external section (Figure 5.13). It can be seen that the temperature differences between sections involving heaters and the outer sections are in the order of 5 ºC. It seems a relatively low variation in order to explain the dissimilar behaviour.

- There are other works that suggest that the phenomenon under consideration here also occur under isothermal conditions, as explained below.

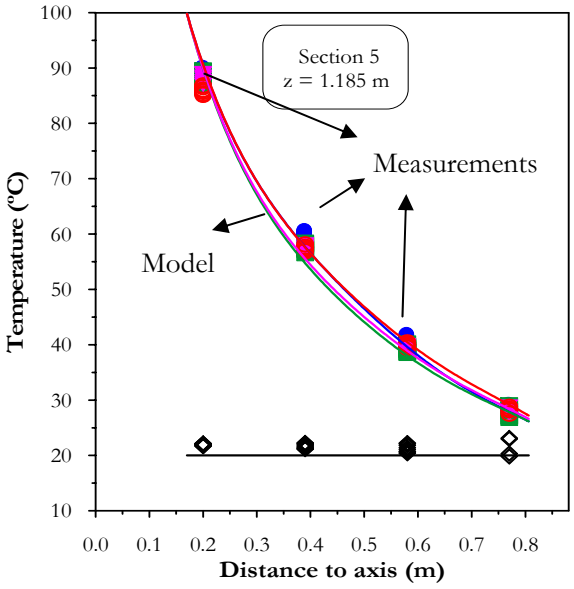

Figure 5.11. Distribution of temperate across the section A5-B5. Observed versus computed values (more details in Figure A4.11).

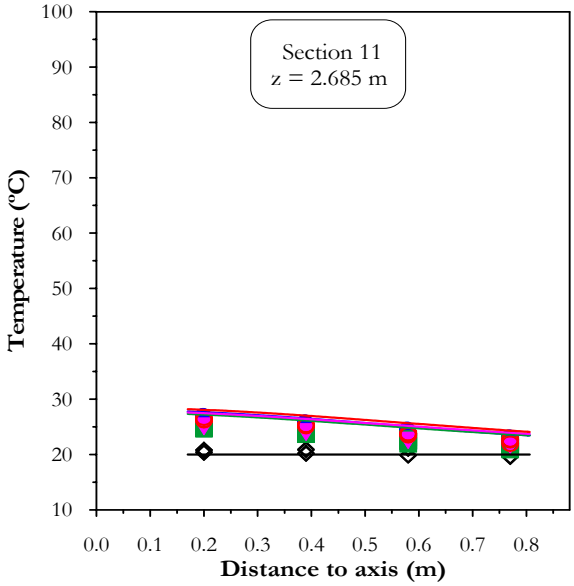

Figure 5.12. Distribution of temperate across the section A11-B11. Observed versus computed values (more details in Figure A4.11).

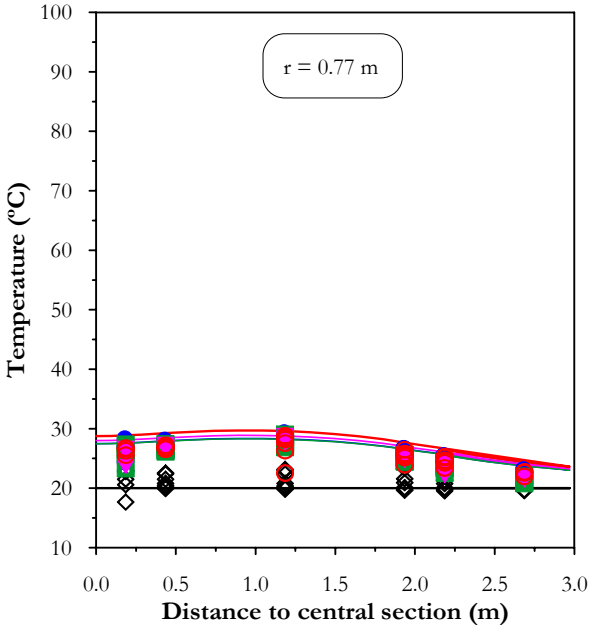

Figure 5.13. Distribution of temperate along the barrier. Observed versus computed values (more details in Figure A4.11).

A lower level of saturation, compared with the expected one, has also been detected in some tests related to the hydration of expansive clays. For instance, this situation has been reported in the isothermal test known as ITT (Dixon *et al.*, 2002; Thomas *et al.*, 2003). The ITT is a large-scale *in-situ* experiment carried out by the AECL (Atomic Energy of Canada Limited). The ITT was monitored for a period of 6.5 years and during its operations it experienced a 35 % decrease in the rate of water supply relative to the one measured prior to experiment installation (Dixon *et al.*, 2002). This decrease had one strong impact on the level of buffer saturation achieved at the end of the test. Values of water content lower than the expected one have been found.

The behaviour of this test was analysed in Thomas *et al.* (2003) through numerical models. The simulations put in evidence that a 'conventional' *THM* formulation (Thomas & He 1997) and model can not match the experimentally measured values. In that sense an unexpected behaviour of the clay barrier is detected (Thomas *et al.*, 2003). Neither the pattern of moisture distribution within the buffer, nor the rate of infiltration has been reproduced (Thomas *et al.*, 2003). Obviously, in this experiment the temperature has no influence due to the isothermal characteristic of the test. Finally, in Cui *et al.* (2001), the hydration of expansive clay, under isothermal conditions, has also been analysed and similar conclusions are foreseen when long time and low hydraulic gradient are involved.

5.3.2 PRELIMINARY ANALYSES

In this section the extension of the *THM* formulation and the numerical code to include other phenomena, not considered in the original ones, are presented. The purpose is to use the code as a tool to investigate the behaviour of the barrier when these phenomena are considered. The aim is to explore the hypothetical influence of these phenomena over the *mock-up* test evolution, especially over the long-term predictions. Initially three phenomena have been studied:

- Threshold gradient
- Thermo-coupling effects.
- Evolution of micro-fabric

The inclusion of geochemical variables in the analyses has also been considered and is discussed in Section 5.3.3.

These studies have been addressed to the development, and to the numerical implementation on the CODE_BRIGHT program, of very simplified models that considered these phenomena separately. The three models have been calibrated with the data available on 30th March 2002, (day 1880 of the test, indicated by a vertical dash line in the following Figures), and the final results of the simulations correspond to 18th September 2003 (day 2417). This implies that the results obtained between these dates are model predictions. It is noted that all the parameters of the OBC model are maintained in these simulations, only the affected by the 'new phenomena' have been modified (if there are any).

1-D axis-symmetrical models have been used in these analyses. Two characteristic sections have been considered: one including heater and the other one without heater. In the first one, a temperature of 100 ºC is prescribed at the contact between heater and bentonite. This is a condition representative of sections such as A4 and B4. In the other section a temperature of 27 ºC is prescribed on the internal part of the barrier. This is a condition similar to the one registered in sections A10 and B10. The results of 1-D 'OBC' model are also included in the Figures to allow the comparisons between the model performances. In order to be closer to the actual conditions of the barrier, all the analyses take into account the overheating episode. In the following sections the main features of these models are briefly presented.

5.3.2.1 THRESHOLD GRADIENT

The threshold gradient phenomenon considers a lower limit of applicability of the Darcy's law. Some experimental evidences show that under low hydraulic gradients (J), Darcy's simple relationship does not rule the liquid flow in some porous media, especially in soils containing active clay minerals. Arguments based on the strong clay-water interactions are suggested to explain this non-Darcian flow behaviour (*i.e.* Bear, 1972; Dixon *et al.*, 1992).

There are many models for the description of this phenomenon (see for example Bear, 1972). A well-known law considers two characteristic gradients, (Figure 5.14): the threshold hydraulic gradient (J_o) and the critical hydraulic gradient (J_c) (*i.e.* Dixon *et al.*, 1992). J_o is the hydraulic gradient below which no flow occurs. J_c is the hydraulic gradient below which flow occurs but it is not Darcian. If the hydraulic gradient is higher than J_c Darcy's law applies.

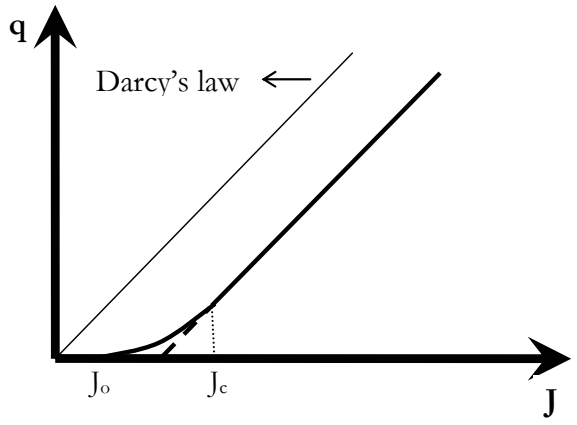

Figure 5.14. Schematic representation of the threshold gradient phenomenon (Dixon *et al.*, 1992).

Some experimental work can be found aimed to explore the validity of the Darcy's law under low gradient in saturated conditions (Hansbo, 1960; Low 1961; Miller & Low, 1963; Russell & Swartzendruber, 1971; Dixon *et al.*, 1992; Dixon *et al.*, 1999). A threshold gradient close to 50 has been reported in some of these works. Russell & Swartzendruber (1971) performed tests in two different media: non-swelling material and porous media containing swelling clay. In

the first type of material a good Darcian proportionality between flux and hydraulic gradient has been found until very low hydraulic gradient (less than 1). The second type of material was a mixture of silt, sand and bentonite clay at 2, 3 and 5 %. It was detected that the Darcian proportionality is lost at small gradients for low clay content (from 3%). This deviation from the Darcy's law is explained considering the high energy of the adsorbed water (Dixon *et al.*, 1992; Cui *et al.*, 2001) and also the pore clogging effect when active clays are present in the porous media (Russell & Swartzendruber, 1971; Cui *et al.*, 2001). On the other hand, Cui *et al.* (2001) detected higher values of critical gradient, close to 7500, in a pressure decrease path for a mixture of sodium bentonite with sand (by a proportion of 7/3 in mass). In Cui *et al.* (2001, 2002b), additional experimental information in this respect is reported.

When low permeability clays are tested, the main problem is the long time required by the experiments. Additionally, special equipment is required and there are also some effects (generally ignored in standard tests) which could play an important role; such as, the bacterial actions, osmosis and counter-gradients (Dixon *et al.*, 1999). An extended experimental technique to overcome these problems is the application of large hydraulic gradients. A drawback of this practice is related to the fact that the applied hydraulic gradients are very far from the one measured (or expected) in actual conditions. So, the experimental results obtained are not realistic in many cases. Figure (5.15) collects the range of hydraulic conductivity and hydraulic gradients reported by Neuzil (1986) and also the tests performed by Dixon *et al.* (1999). It can be observed that the applied hydraulic gradients are relatively high when the materials have low permeability. It is not easy to find in the literature data which allow expanding the information presented in Figure (5.15). Figure (5.16) shows the applied hydraulic gradient and the measured hydraulic permeability of the FEBEX bentonite, for values of dry density between 1.74 and 1.55 Mg/m^3 (Villar *et al.*, 2004).

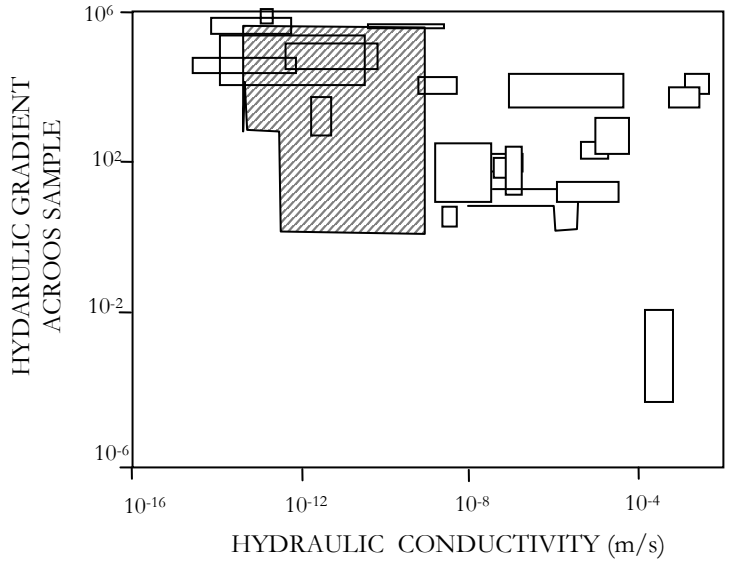

Figure 5.15. Range of hydraulic conductivities and hydraulic gradients reported in the literature, Dixon *et al.* (1999). The shaded area indicates the data obtained by Dixon *et al.* (1999). The other data were collected by Neuzil *et al.* (1986).

In the *mock-up* test there is a strong contrast between the predominant hydraulic gradients in the two sections analysed (Figure 5.17). The section involving heater presents high hydraulic gradients in zones close to the heater, compared with the ones prevailing close to the hydration front, whereas, the hydraulic gradient is more uniform in sections distant to the heater. The lowest hydraulic gradients are in zones near the hydration front. It can be observed that close to the day 900 (when the discrepancies between the model and the test start to appear) the value of the hydraulic gradient is about 2000 in zones near the hydration front.

Note that the ranges of the hydraulic gradients applied experimentally are higher than the hydraulic gradients computed in zones close to the hydration boundary. For this reason it is difficult to state if the apparent decay in the kinetics of hydration of the barrier is due to the existence of a threshold gradient. Moreover, the lack of experimental data at low hydraulic gradient complicates the development of an improved flow model that incorporates this phenomenon. With the sole aim to explore the hypothetical influence of this phenomenon on the barrier behaviour, a very simple model has been proposed, until more experimental data in this respect are available. The model is similar to one presented in Figure (5.14). The following considerations have been taken into account:

- A threshold gradient (J_o) equal 50 (this is a common value found in the literature).
- A critical gradient (J_c) close to 2000. It corresponds to the hydraulic gradient computed in the onset of the discrepancies (at the hydration boundary).
- A power law for the range of hydraulic gradient with non-Darcian's flow

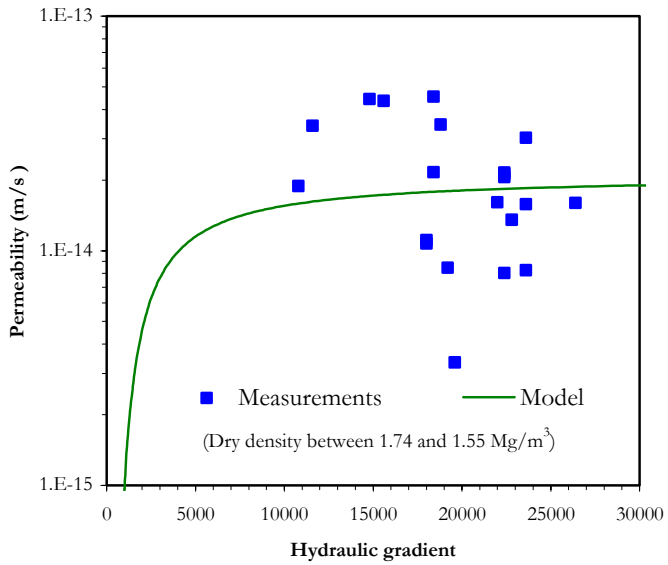

Figure 5.16. Experimental hydraulic gradient *vs.* saturated permeability (Villar *et al.*, 2004).

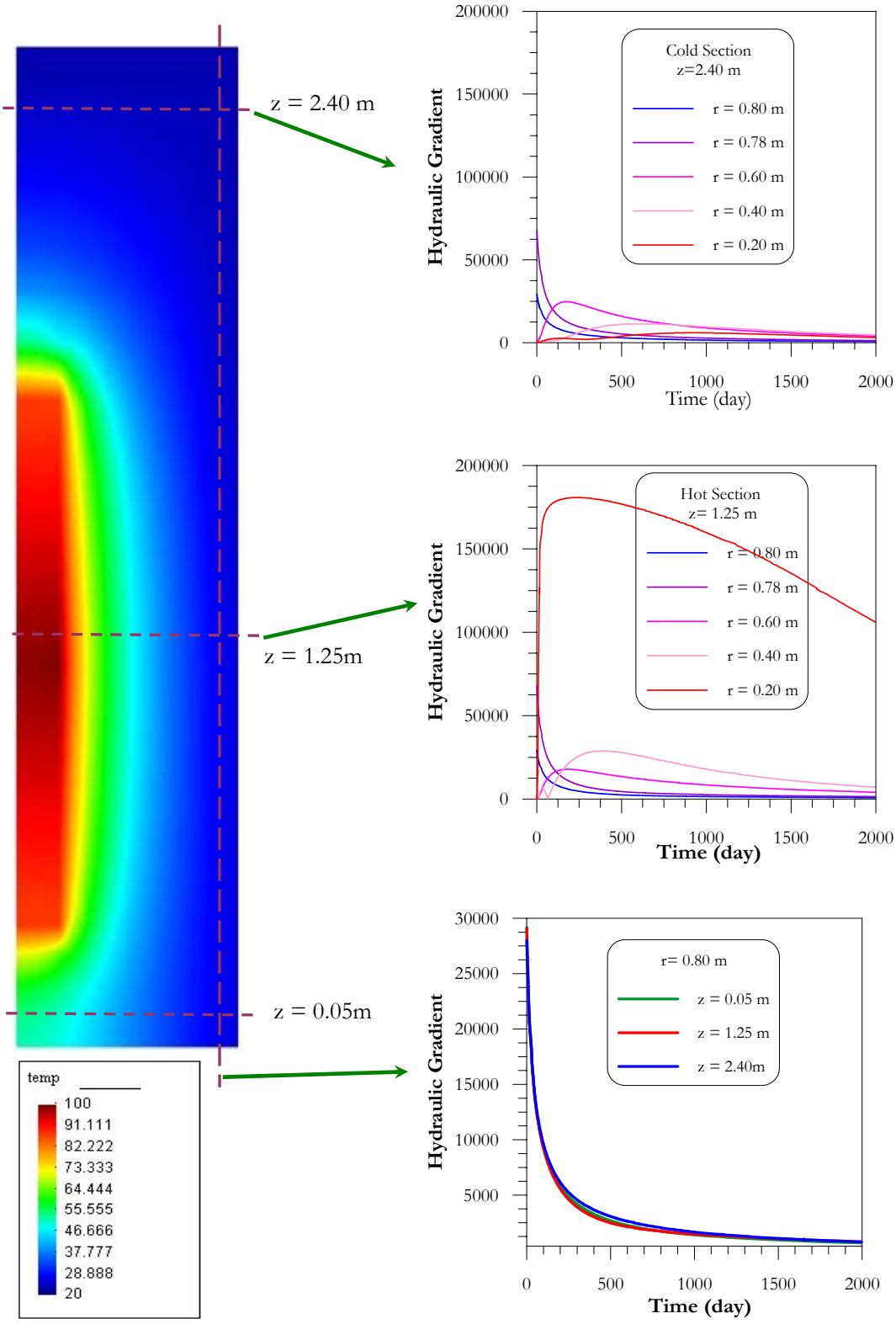

Figure 5.17. Distribution of hydraulic gradient in cross and longitudinal sections.

In Figure (5.16) it can be observed that the model is consistent with the experimental data available for the FEBEX bentonite (*i.e.* for high hydraulic gradient) and for the zone in which there are not measurements (*i.e.* low hydraulic gradient) experimental information obtained in the literature has been considered.

Figures (5.18) and (5.19) show (with solid lines) the results obtained considering the Threshold Gradient (ThG) model in both reference sections. The dash lines correspond to the 'OBC' model. A good agreement between model and test data can be seen in the hot section, in zones close to the heater (Figure 5.18). The tendency to the reduction in the hydration rate is well captured by the model. The model predictions are also good for the results from the day 1880 onwards. In zones near the hydration front the tendency is not so well captured. Regarding the model response in sections A10 and B10, the results are also good. It can be seen that the model predicts (after the dash vertical line) the incipient decay in the more internal radius of these sections. Figures (5.20) and (5.21) present the evolution of water intake and stresses respectively, for the two models analysed. The presence of a threshold gradient implies a lower rate of water intake, compared with the OBC model. This affects the distribution of water in the barrier and due to the strong *HM* coupling the stress field is also influenced.

Figures (5.22) to (5.25) present the long-term predictions. It can be observed that under this hypothesis the barrier does not reach full saturation. Naturally, the relevance of this prediction depends on the existence of a threshold gradient in the FEBEX bentonite and, in this case, on the adequacy of the model and parameters here adopted. Therefore, the result presented should be considered only as an exercise with the object to explore the hypothetical response of the barrier under these assumptions, until the hypotheses regarding the threshold gradient are independently confirmed by experiment.

5.3.2.2 THERMO-COUPLING EFFECTS

The hydraulic gradient is the main force influencing the movement of water in the soils. It is, however, not the only one. Figure (5.26) presents all the different kinds of flow (excepting the electrical component) that can occur in the porous media and the corresponding gradient responsible for the movements. The word 'law' is used for the diagonal terms associated to the direct flow phenomena, and the name 'effect' is reserved for the non-diagonal ones, called 'coupled processes' (*i.e.* Bear, 1972; de Marsily, 1986; Mitchell, 1991, 1993). The Figure also includes the names given to some of these flows.

The 'phenomenological coefficient' that links each flow with the corresponding driving force must be measured experimentally (Djeran, 1993; Mitchell, 1993; Soler, 1999). Generally, the non-diagonal coefficients are relatively small and negligible compared to the diagonal terms and the coupled process can be ignored. However there are certain problems in which, due to their particular conditions, the coupled process may play a more influential role.

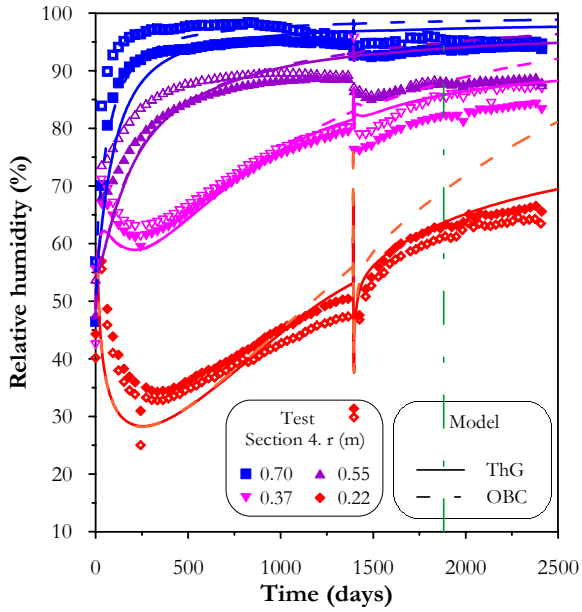

Figure 5.18. Relative humidity. Sections A4-B4. Observed versus computed values of 'ThG' (Threshold Gradient) and 'OBC' models.

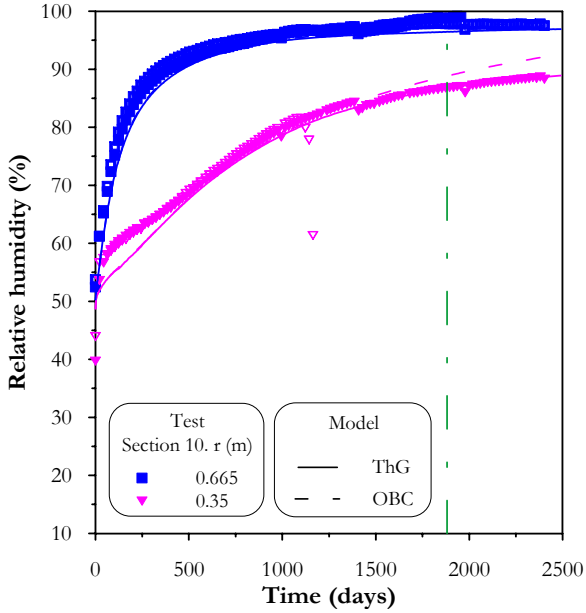

Figure 5.19. Relative humidity. Sections A10-B10. Observed versus computed values of 'ThG' and 'OBC' models.

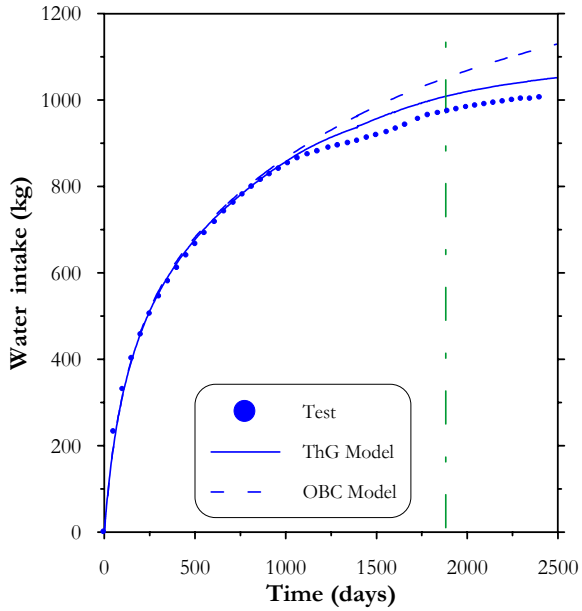

Figure 5.20. Water intake. Observed versus computed values of 'ThG' and 'OBC' models.

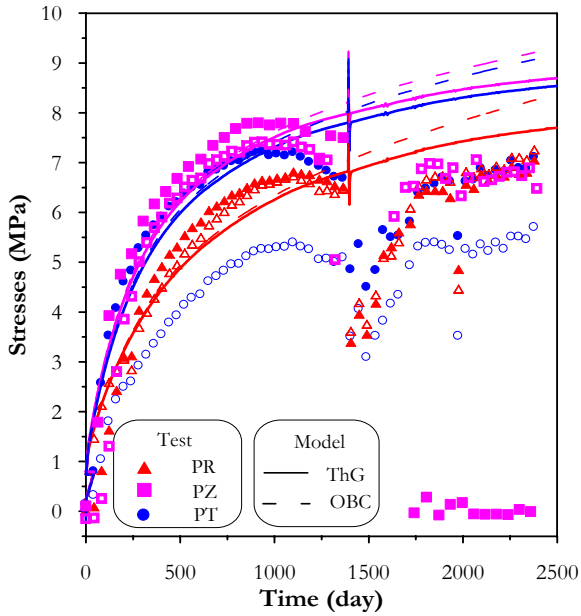

Figure 5.21. Stresses. Observed versus computed values of 'ThG' and 'OBC' models.

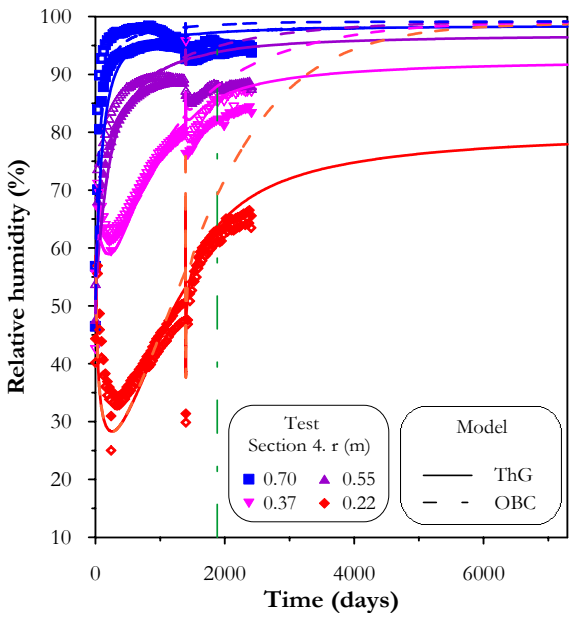

Figure 5.22. Relative humidity. Sections A4-B4. Long-term predictions 'ThG' and 'OBC' models.

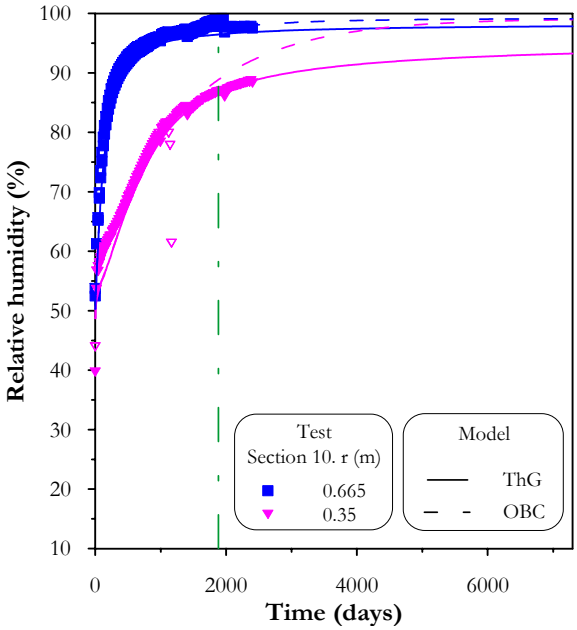

Figure 5.23. Relative humidity. Sections A10-B10. Long-term predictions 'ThG' and 'OBC' models.

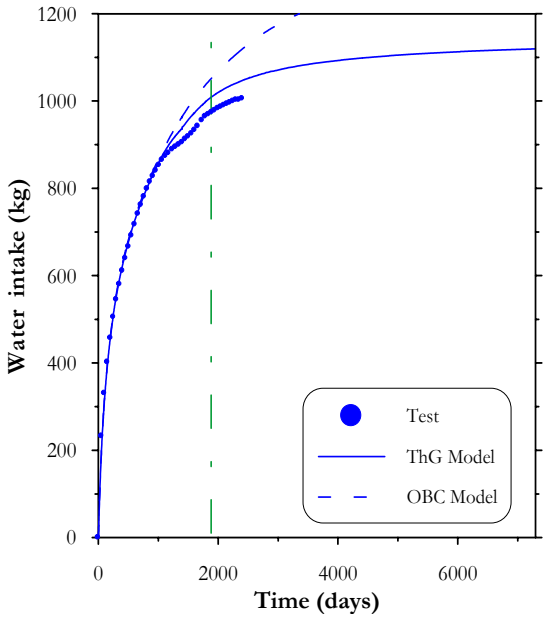

Figure 5.24. Water intake. Long-term predictions 'ThG' and 'OBC' models.

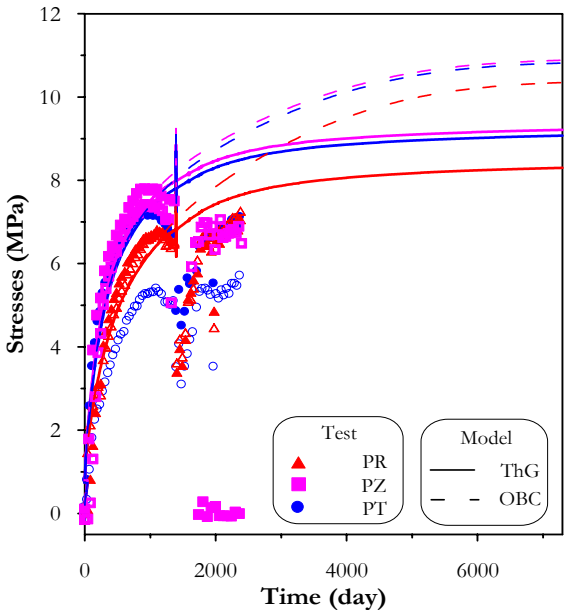

Figure 5.25. Stresses. Long-term predictions 'ThG' and 'OBC' models.

Flow	Gradients		
	Hydraulic Head	**Chemical Concentration**	**Temperature**
Fluid	**Darcy's Law** (Hydraulic Conduction)	**Chemical Osmosis**	**Thermo Osmosis**
Solutes	**Ultra Filtration**	**Fick's Law** (Diffusion)	**Soret Effect** (Thermal Diffusion)
Heat	**Thermo Filtration** (Isothermal Heat Transfer)	**Dufour Effect**	**Fourier's Law** (Thermal Conduction)

Figure 5.26. Direct and coupled flow processes.

The thermal conditions imposed on the *mock-up* test correspond to a practically constant thermal gradient during the test and, in consequence, a constant thermo-osmotic liquid flow associated with it may exist. In contrast, the hydraulic gradient is very high at the beginning of the test, but diminishes with the hydration of the barrier. The liquid flows associated to these two gradients have opposite directions. Generally, the advective flow due to the pressure gradients (Darcy's law) is the dominant flow. However, at advanced stages of the test (when the hydraulic gradient becomes smaller), it is possible that the flow of liquid due to the coupled phenomena (thermo-osmotic flow) could have a noticeable effect on the behaviour of the test in the hot sections, causing a tendency to slow down the hydration in the hot zones close to the heaters.

The magnitude of this effect will depend on the relation between the gradients of the two mechanisms and on the relationship between the phenomenological coefficients associated to either flow. On the other hand, this phenomenon would not influence the cold sections. Figure (5.27) presents a schematic representation of these conditions. K_{HT} is the phenomenological coefficient associated to the thermo-osmotic flow.

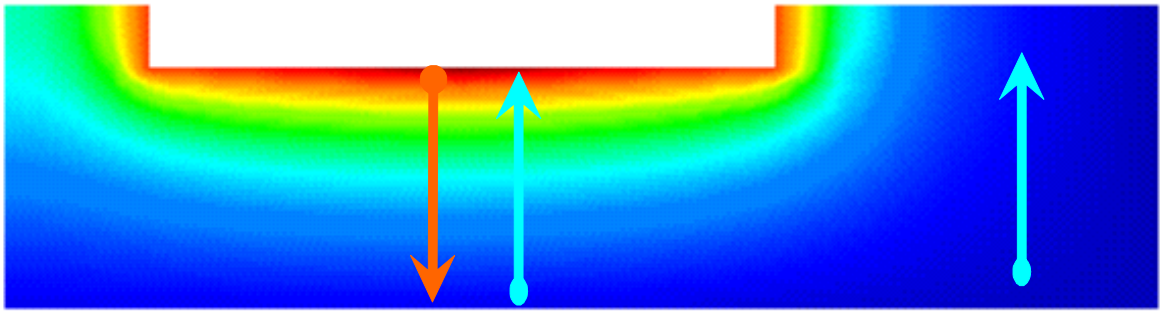

$$\mathbf{q}_l = -\mathbf{K}_{HH}(\nabla P_l - \rho_l \mathbf{g}) - \mathbf{K}_{HT}\nabla T$$

Figure 5.27. Schematic representation of the conditions related to the advective flow and thermo-osmotic flow in the *mock-up* test.

To check the possibility that this coupled process may help to explain the *mock-up* test observations, a series of analyses including the thermo-osmosis effect were carried out. It is necessary to mention the lack of experimental data concerning the phenomenological coefficient associated to the thermo-osmotic flow. For the FEBEX bentonite there are no experimental data. The thermo-osmotic constant adopted is 2.73×10^{-13} $m^2/K/s$ and falls in the range of possible values found in the literature (Soler, 1999; Djeran, 1993).

Figures (5.28) and (5.29) show, with solid lines, the results obtained considering the Thermo-osmotic Effects (ToE) for the two reference sections; the dash lines correspond to the 'OBC' case. In the hot section a somewhat better agreement with the observations can be noted in zones close to the heater, but the tendency of the ToE model can not be considered good. In zones near the hydration front the measured trend is not so well captured. The responses of sections A10 and B10 do not change under this hypothesis.

Figures (5.30) and (5.31) present the long term predictions. It can be observed that, in the hot sections, it is possible that the clay never reaches full saturation. This fact will of course depend on the real relevance of this phenomenon for the FEBEX bentonite and on test conditions. As for the case of the threshold gradient, the results presented should be considered only as an exercise performed with the aim of investigating the hypothetical response of the barrier under these assumptions, until more experimental evidence on the phenomenon becomes available.

5.3.2.3 MICRO-FABRIC EVOLUTION

In this Section a preliminary exploration of the influence of the changes in the intrinsic permeability due to changes in the clay fabric during hydration is considered. As commented in the Chapter IV, the microstructure of the compacted clay consists of dense aggregates of clay particles with intra-aggregate pores (micropores) between them. The arrangement of these clay aggregates conforms a granular skeleton of the material with interaggregate spaces (macropores) between aggregates. Figure (4.3) contains results of porosimetries carried out on FEBEX bentonite where the two dominant pore levels can be clearly identified.

Once hydration starts, the clay aggregates tend to adsorb water and swell. Due to the confinement conditions of the test (constant volume conditions practically prevail), the expansion of the microstructure is made possible by reductions of the macropores. This has a significant influence on the permeability value and hence on the hydration of the barrier. These phenomena imply a dynamic character of the clay fabric during wetting, resulting in a strong coupling between the mechanical and the hydraulic problem.

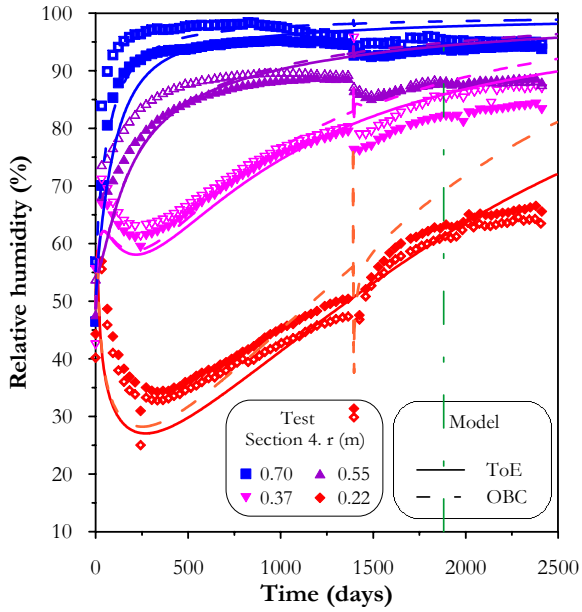

Figure 5.28. Relative humidity. Sections A4-B4. Observed versus computed values of 'ToE' (Thermo-osmotic Effect) and 'OBC' models.

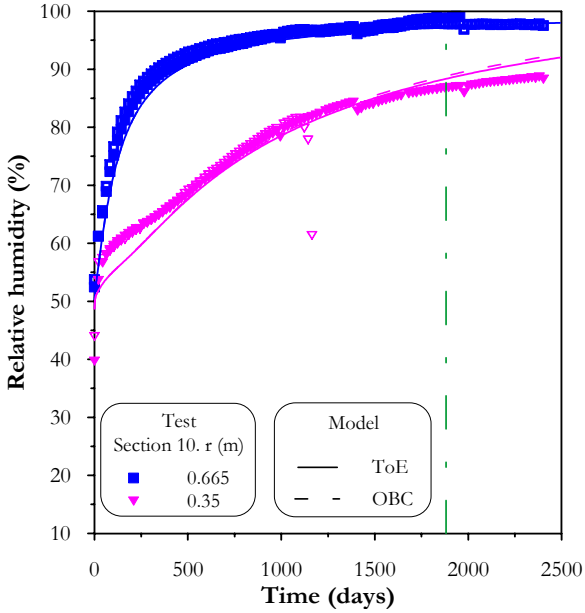

Figure 5.29. Relative humidity. Sections A10-B10. Observed versus computed values of 'ToE' and 'OBC' models.

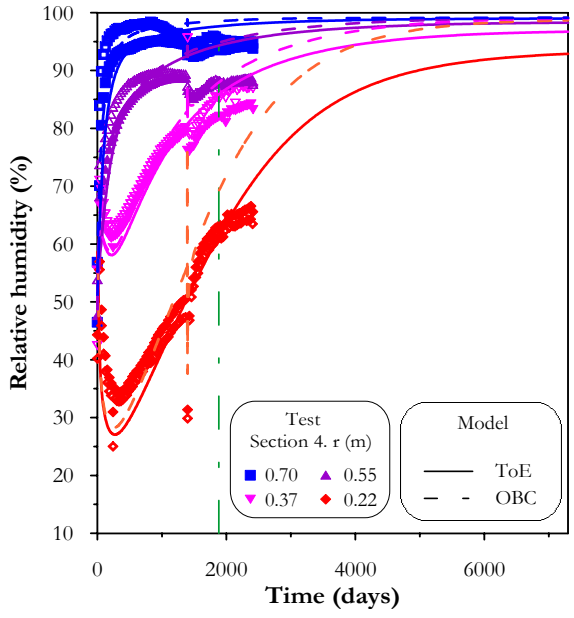

Figure 5.30. Relative humidity. Sections A4-B4. Long-term predictions 'ToE' and 'OBC'

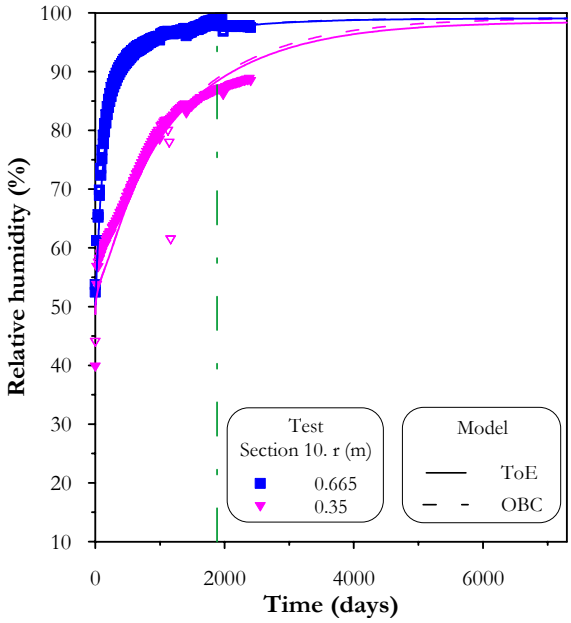

Figure 5.31. Relative humidity. Sections A10-B10. Long-term predictions 'ToE' and 'OBC'

Experimental evidences of this strong hydro-mechanical behaviour can be found in Cui *et al.* (2001), in which measured values of macroporosity and permeability at different suctions are reported. The clay used is a sodium bentonite (Kunigel clay) mixed with sand in the proportion of 7/3 in mass. Figure (5.32) presents the measured values of the void ratio of the macropores (black circles) at different suctions. Assuming that the water flow takes place predominately through the macropores, it is possible to suggest that changes in macroporosity could explain the reduction in the permeability at advanced stages of hydration.

The effect of the clay-fabric changes on the permeability of the FEBEX bentonite has been considered, initially, in a rough way. The intrinsic permeability has been reduced in the external zone (more saturated) of the barrier (until a maximum of 15 % for suctions lower than 2 MPa). Figures (5.33) and (5.34) show the results obtained considering the Micro-fabric evolution effects (MiE) for the two reference sections studied. It can be observed that this model can reproduce the behaviour observed in the barrier better than the OBC model. But, the model predictions are not so good (after the dash vertical line) because the model is incapable of reproducing the more marked decay in hydration rate. Figures (5.35) and (5.36) present the long term predictions. One difference of this case in relation to the previous phenomena analysed is that in the long term predictions a total saturation of the barrier is obtained.

As already mentioned, this is a very simplified model and, for this reason, the results presented here are only qualitative. This phenomenon is treated in a more proper framework in Section 5.4.

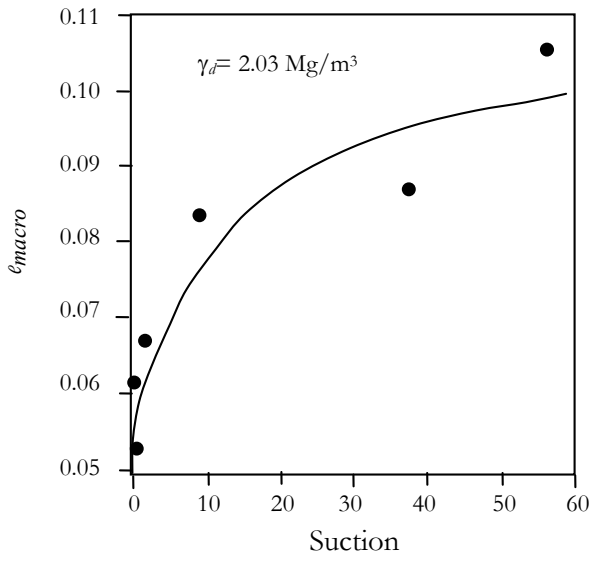

Figure 5.32. Variation of the macropore void ratio with suction (Cui *et al.*, 2001).

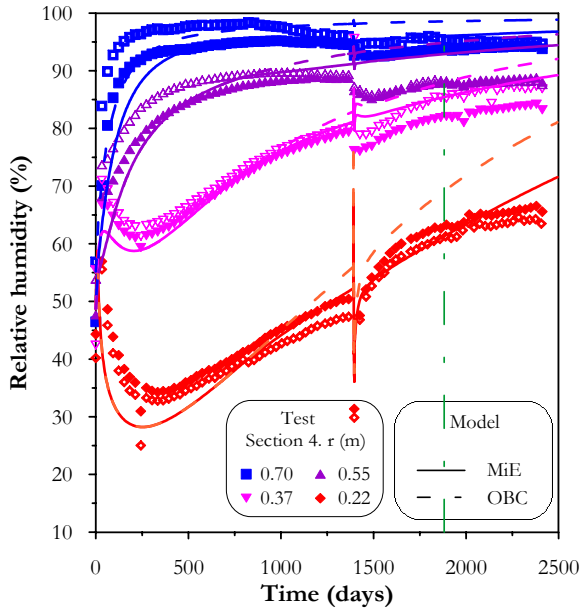

Figure 5.33. Relative humidity. Sections A4-B4. Observed versus computed values of 'MiE' (Microstructure Evolution) and 'OBC' models.

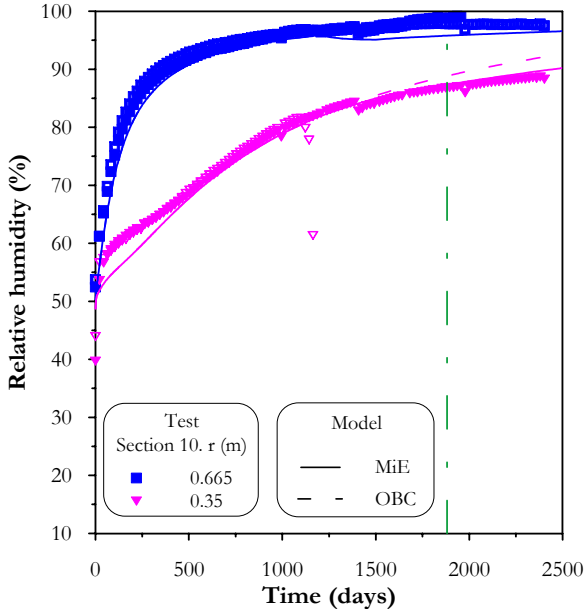

Figure 5.34. Relative humidity.. Sections A10-B10. Observed versus computed values of 'MiE' and 'OBC' models.

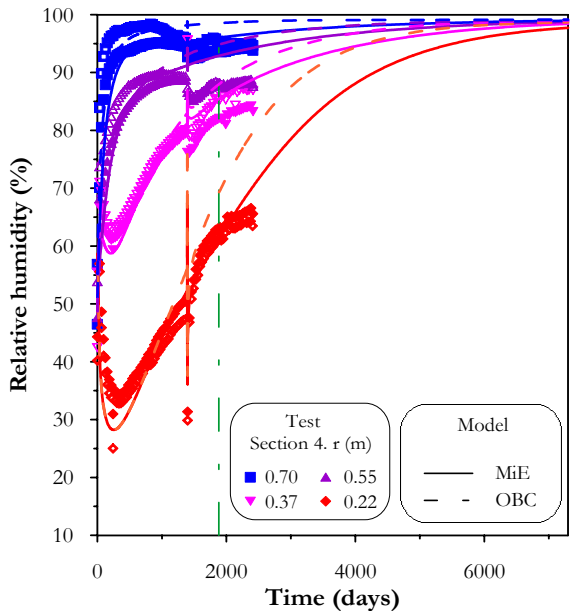

Figure 5.35. Relative humidity. Sections A4-B4. Long-term predictions 'MiE' and 'OBC' models.

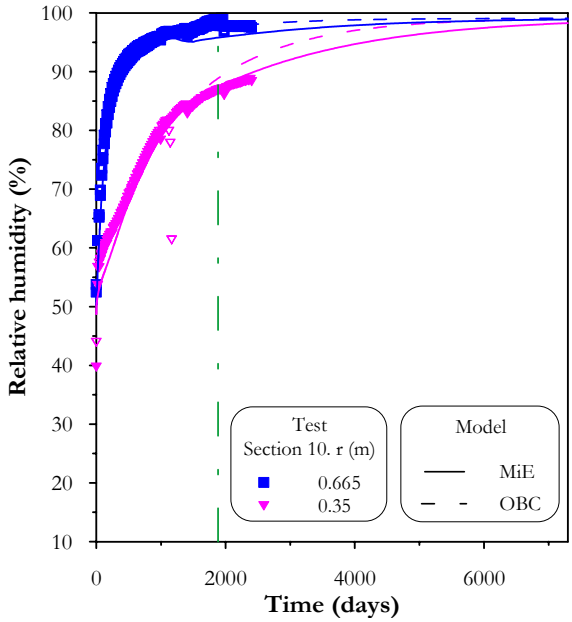

Figure 5.36. Relative humidity. Sections A10-B10. Long-term predictions 'MiE' and 'OBC' models.

5.3.3 DISCUSSION

The apparent problems observed in the hydration of the *mock-up* test have been approached by steps. The aim is not to exclude in advance some of the plausible phenomena that could explain the unexpected trends observed in the experiment. An intermediate stage of the research is the formulation of the models presented previously. Although they are very simplified, the results obtained are interesting. In this context, this study allows comparing the measurements of an actual test with the computed barrier response under the hypothetical case in which some of these effects would be present. However, due to the scarcity of experimental data available to formulate these models and due to the preliminary objective of this study, the results presented here have only a qualitative value. After all, each of these phenomena does not exclude the others and it is possible that an explanation for the whole behaviour of the barrier would require the combinations of some of them.

These analyses show the need of improving the 'classical *THM* formulation' when a complex experiment, such as the *mock-up* test, is studied. This is even clearer when the interest is focused on performance assessment involving long-term predictions. In contrast, it must be pointed out that one problem associated with these developments is the scarcity of experimental data available to formulate and to calibrate these types of models. In that sense, new laboratory tests oriented to this end (some of them currently carried out in the framework of the FEBEX project) will help the development of new models that could incorporate the more relevant observed phenomena. Finally, the *mock-up* test itself can give, in the medium term, relevant information about the phenomena in process, once the consequences of the overheating event are completely overcome and hydration has progressed still further.

Note that some of the phenomena presented as different can be closely related. For instance, in the work of Cui *et al.* (2001) it is suggested that the phenomena identified here as 'evolution of micro-fabric' and 'threshold gradient' are closely connected. On the other hand, in the work of Dixon *et al.* (1999) the results of a series of permeability tests on clays, carried out in confined conditions and under low hydraulic gradients, are analysed. The observed behaviour did not respond to the typical Darcian expectations. Two separate regions of Darcian flow were distinguished, and the 'transitional gradient' corresponds to the gradient for which the flow changed for one Darcian relationship to another. The 'transitional gradient' suggests a change in the porosity available for the flow. This fact was explained assuming that the majority of the flow at low hydraulic gradients occurs through macropores, the water at micropores is practically immobile due to its physico-chemical properties. When the hydraulic gradient exceeds the transitional gradient, the occluded or nonconductive porosity becomes available for the flow (Dixon *et al.*, 1999). These tests reflect the influence of the clay-fabric in their response and the potential relevance to integrate the clay-fabric effects in the analyses, in order to explain and reproduce more properly the clay behaviour during hydration.

Chemical effects affect some of the phenomena studied and, therefore, the explicit inclusion of geochemical variables in the analyses would help the understanding and explanation of the observed barrier behaviour. This corresponds to another line of research which involves the incorporation of chemical effects and geochemical variables in the analyses. The modelling of the chemical behaviour of expansive clays is outside the scope of this Thesis.

The incorporation of the chemical phenomena in the analysis of the *mock-up* test evolution corresponds to future work. However, a brief presentation of some aspects related to the geochemical behaviour of the FEBEX bentonite is introduced in the following paragraphs. The aim is to comment some aspects that could be interesting to foresee its potential influence on the unexpected behaviour of the *mock-up* test.

The illitization of smectites is a matter of central interest in the design of engineered barrier for radioactive waste disposal (see *i.e.* Hueckel, 2002; Hueckel & Pellegrini, 2002). The lost of some important properties of the bentonite (such as: swelling capacity, very low permeability, etc.) induced by this transformation underlies this attention. In the context of the FEBEX project a wide experimental program was carried out oriented to explore the possible transformation from the FEBEX smectite into illite. The reaction for the transformation from smectite into illite was carried out in presence of potassium solution and at temperatures between 60-200ºC. In this study, it was concluded that under disposal conditions, the FEBEX bentonite will behave as a safe barrier material with respect to illitization (Linares *et al.*, 1996; Cuadros & Linares, 1996, Huertas *et al.*, 2003). The time necessary for such transformation is so long that it can be considered not to have an effect on the barrier lifetime.

An extensive experimental study related to the effect of the osmotic suction and cation exchange over the behaviour of FEBEX bentonite was also carried out (see *i.e.* Huertas *et al.*, 2002; Musso *et al.*, 2003; Fernández, 2003). As commented in Chapter III, the extension of the double structure mechanical model to include these variables (osmotic suction and cation exchange) in the modelling were performed in the work of Guimarães *et al.* (2001) and Guimarães (2002). In that context, most of the concepts expressed in the following Sections for the double structure model, can be applied when the simulation will extend to consider these chemical phenomena.

Other chemical effect which could affect the evolution of the barrier is the precipitation/dissolution of minerals. Post-mortem analysis of the partial dismantling of the *in-situ* test will give valuable information related to the influence of the chemical effects commented above over the behaviour of FEBEX bentonite. Although, according to some *THMG* tests in cells (Cuevas *et al* 1996, FEBEX Report, 1997) it appears that the effect of these chemical phenomena is not strong for the period of times analysed here.

The preliminary analyses presented in the preceding Sections (5.3.2.1 to 5.3.2.4) correspond to an intermediate stage of the research. The next step corresponds to a more detailed analysis of theses phenomena or, at least, of those deemed more relevant. In this context, the following Sections are focused on the analysis of the phenomenon identified here as 'evolution of the micro-fabric'. This is considered the more promising phenomenon to explain the barrier behaviour because there are some experimental evidences that support its existence.

5.4 ANALYSIS OF THE *MOCK-UP* TEST USING A DOUBLE STRUCTURE FRAMEWORK

5.4.1 INTRODUCTION

This Section is oriented to analyse the *mock-up* test including the effects of clay-fabric in the modelling. As commented above, the double structure approach (presented in Chapters II, III and IV) has been used to develop a double structure model of the *mock-up* test. It is considered a more proper approach to incorporate in the analyses the effects of the clay fabric changes. Additionally, the aim is to provide a wide platform that allows including in a unified and consist framework other phenomena mentioned here, such as the chemical effects or threshold gradient

A drawback generally associated to the use of a more complex model is the difficulty to find experimental data to identify the main model parameters. The expansion of the *THM* formulation made in this Thesis is conceptually very simple and it allows extending most of the well-known laws and models to the case of double structure media. A phenomenological model has been used in this analysis.

An important point of the problem is the proper adoption of the conceptual model. The understating of the key process that controls the problem under analysis is crucial in order to formulate models that can reproduce the main trend of the material behaviour. So, in the next section, attention is focused on the presentation of some aspects related to the hydration process of expansive clays that are deemed relevant. The main mechanisms and phenomena that control the adsorption of water are discussed based mainly on the experimental work carried out on FEBEX bentonite, and also on some concepts found in the literature.

5.4.2 HYDRATION AND SWELLING OF EXPANSIVE CLAYS

5.4.2.1 EXPANSIVE CLAY BEHAVIOUR

In this Section, attention is placed on the hydration processes of expansive clays, the microstructure organization and the pores spaces. In the literature several works related to those subjects can be found (*i.e.* Push & Karland, 1996; Yong 1999; Saiyouri *et al.*, 2000; Hueckel *et al.* 2001). Different conceptual models of the clay structure and different names of its components can be found in those references. Here, the information is presented following mainly the concepts and nomenclature used in the works related to the FEBEX bentonite (Fernández, 2003; Villar 2000; Huertas *et al.* 2002).

If the clay structure is viewed in more detail, it can be seen that the primary clay particles consist of organized stacks of clay platelets, named quasicrystals. Often, these quasicrystals assemble as clay aggregates. Finally, the cluster of these clay aggregates generates a fabric with large pores between the clay aggregates. This structure corresponds to the macrostructural level in the context of the expansive model presented in this Thesis. Figure (5.38) presents a simple scheme of these concepts.

As a result, at least, three kind of pores can be distinguished:

- interlamellar space (interplatelets pores, within the primary particles);
- intra-aggregate pores (between the primary particles, within the aggregates) and;
- inter-aggregate pores (between the aggregates).

In the case of FEBEX bentonite it is assumed that the pores greater than 0.13 μm correspond to the macroporosity (Figure 4.2 Chapter IV). Pores with a size lower than this value correspond to the microporosity, with a dominant pore diameter of 0.01 μm. The interplatelets size depends on the number of water molecules present in the interlayer.

Most of the physico-chemical properties of the expansive clay are due to their small size and their sheet-like shape, which cause a very high specific surface area. Other important aspect is the negative electric charge of the smectite clay surface, mainly due to ionic substitution (iso morphal substitution) in the lattice (Mitchell, 1993; Fenández, 2003).

Three modes of clay hydration can be distinguished (Güven *et al.*, 1993; Fernández, 2003):

- Interlamellar hydration, which involves the adsorption of water molecules on the internal surface of clay particles. This water is named 'interlayer water' and occurs in the interlamellar space.
- Continuous osmotic hydration, which is related to adsorption of water on the internal an external surfaces of clay particles. This water is named 'intraparticle water' and occurs mainly in the intra-aggregate pores.
- Capillary condensation of free water, which is in the pores of the clay fabric. This water is named 'interparticle water' or 'free water'.

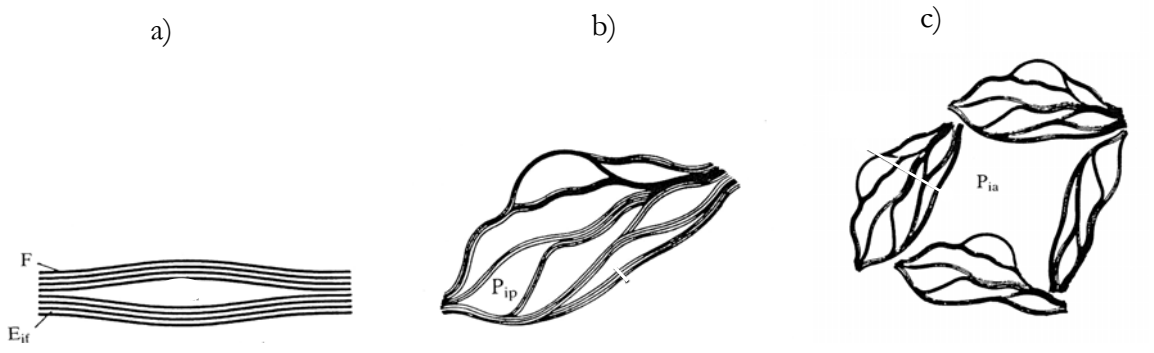

F: plate; E_{if} interplate space; P_{ip}: intraaggregate pore; P_{ia}: interaggregate pore.

Figure 5.38. Schematic representation of different types of pores (in Fernández, 2003; after Touret *et al.*, 1990): a) detail of a particle (quasicrystal), b) detail of an aggregate made up of an association of particles and c) schematic representation of a set of aggregates.

The swelling behaviour of expansive clays is due to the first two mechanisms mentioned. The first one is also known as 'inner-crystalline swelling' (Madsen & Müller-Vonmoos, 1989). This swelling is related mainly to the hydration of the exchangeable cations. The cations hydrate upon contact with water and then the water molecules are progressively ordered, layer after layer, on a plane halfway between the clay particles. This leads to a widening of the spacing between the layers, which take place in steps (Saiyouri *et al.*, 2000; Huertas *et al.*, 2002; Fernández & Rivas 2003). The type of the adsorbed interlamellar cation determines the number of water layers and hence the maximum size of the lamella stacks (Push, 1999). Generally, up to a maximum of four layers have been detected (*i.e.* Saiyouri *et al.*, 2000; Marcial, 2003). The polarity of the water plays a central role in this swelling and the water adsorbed in this step is more ordered and has less mobility than the water in the pore space (Madsen & Müller-Vonmoos, 1989). The second mechanism, also known as 'osmotic swelling', results from the large differences between the ion concentrations (mainly the cation concentration) electro-statically attracted to the surface of the clays layers and the ion concentration in the pore water.

In Fernández (2003) and Fernández *et al.* (2003), the three commented mechanisms of water adsorption have been analysed for the case of FEBEX bentonite powder. The study combines the results of the water vapour adsorption, in isotherm test, with the data obtained in X-ray analysis. These techniques gives useful information related to the location of the water and also to the changes in the basal distance of the clay layers during the hydration process. According to this study, most of the water taken up goes instantly to the microstructure and reside in the interlayer space (interlayer water). Fernández (2003) obtained that the amount of the free water varies between 0.2 to 11 % (of the total water), depending on the relative humidity. It is important to have in mind that in this test the wetting is performed controlling the water vapour concentration. According to Fernández (2003, 2004), the observed distribution of the water during hydration does not change substantially when the wetting is performed with liquid water. More experimental results related to the influence of the wetting technique on the behaviour of expansive clays during hydration can be found in Marcial (2003). In Fernández (2003), a detailed analysis of the water distribution in compacted FEBEX bentonite shows a reduction of the macroporosity when the bentonite is saturated under confined conditions. Finally, other contributions related to the behaviour of expansive clays also state that the largest amount of water is in the microstructure (for instance, Push *et al.*, 1998).

Another important aspect related to the behaviour of expansive clay is linked to the water-clay properties. Except for the free water, the rest of the water clay is more or less affected by the psycho-chemical phenomena occurring at clay particle level. The interlamellar water is strongly affected by these phenomena and it has been considered as practically immobile water under normal environmental loads by some authors (*i.e.* Hueckel, 1992). On the other hand, the properties of the intraparticle water (or 'osmotic water') will depend on its proximity to the clay particle face (Mitchell *et al.*, 1993).

The experimental determination of the water properties at the microstructural level is not a simple task. For these cases, the molecular simulations (Monte Carlo and molecular dynamics techniques) provide a detailed microscopic understanding of the clay-fluid system and help to solve some questions in these fields. Using these techniques it is possible to reproduce the stages of the clay hydration (Skipper *et al.*, 1991; Karaboni *et al.*, 1996; Hensen & Smit, 2002; Ichikawa *et al.*, 2002). For example, Figure (5.38) shows the step-wise characteristic of the interlamellar hydration reproduced by Monte Carlo simulations (Hensen & Smit, 2002).

Depending on the kind of smectite studied, an average density of the absorbed water between 1.12 and 1.38 Mg/m^3 has been obtained through Monte Carlo simulations (Skipper *et al.*, 1991). On the other hand, in Villar (2000) (and Lloret, 2004) a maximum value of water density at the micropores close to 1.20 Mg/m^3 has been experimentally estimated for the FEBEX bentonite (Figure A4.33, Appendix A4). This value has been obtained post-processing the laboratory data in order to obtain a maximum saturation degree of 1.0. However, density of microstructural-water lower than free-water density has also been reported in some experimental works (Anderson & Low, 1958; Dixon *et al.*, 1993). Regarding the water viscosity, a strong variation (up to a factor of seven) is estimated by molecular dynamic simulations, as it can be seen in Figure (5.39) (Ichikawa *et al.*, 2002).

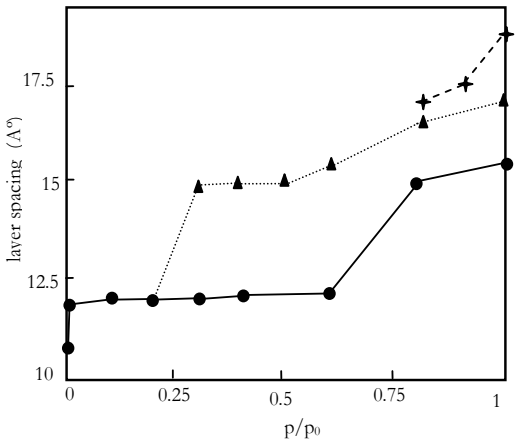

Figure 5.38. Computed layer spacing for a sodium bentonite as a function of the water vapour pressure (Hensen & Smit, 2002).

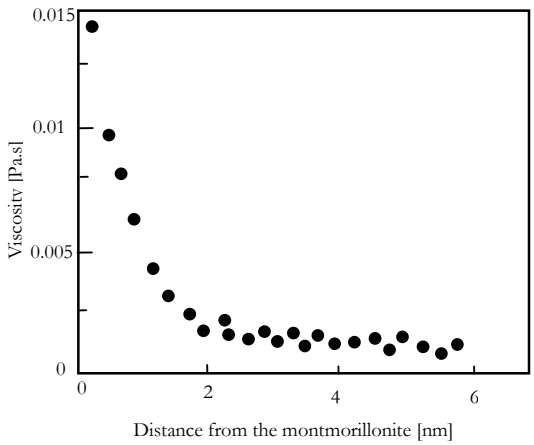

Figure 5.39. Computed viscosity using molecular dynamic simulations (Ichikawa *et al.*, 2002).

In the double structure framework is possible to adopt different water properties according with the pores level consider. Therefore, it can be adopted different properties for the microstructural water (water at the microstructural level) in relation to the ones assumed for the free water (water at the macropores). In Appendix A4 (Section A4.3) the water properties adopted in the *mock-up* model are discussed.

Some comments are now introduced related to the microstructural changes observed in MX80 bentonite at constant water content (Marcial, 2003). In that work, a detailed investigation of the clay-fabric evolution has been carried out using pore size distribution measurements by mercury intrusion and scanning electron microscope. Various clay samples, at different densities and water contents, were compacted into special cells in which they were kept to allow ageing, at constant volume and water content conditions (Marcial 2003). Figure (5.40) presents the result of the mercury intrusion pore size distribution at the initial state and for two ageing periods (30 and 90 days) of one sample with a void ratio of 0.646 and a water content equal to 8.2%.

In Figure (5.40) it can be observed a significant decrease in the inter-aggregate porosity (r >0.8 μm) and a considerable increase of the very small porosity. This is an experimental evidence that microstructural expansion implies a decrease of the inter-aggregate porosity in confined conditions. Another important aspect of this work is related to the observed time dependent changes in the microstructure. Arguments based on the redistribution of the clay water in the different pore levels help to explain this phenomenon. Also, the creation of inter-platelets porosity (inside the saturated aggregates) due to the division of the clay platelets (into packet with fewer layers) detected by Saiyouri *et al.* (2000) has been considered to support this ageing behaviour (Marcial, 2003).

Finally, an experimental study related to the changes in the fabric of the FEBEX bentonite during wetting and drying is briefly presented (Villar *et al.,* 2004). A systematic study was performed in a ESEM (Environmental Scanning Electron Microscope) controlling independently the vapour pressure and temperature around the sample. In addition, some samples have been observed using the scanning electron microscope (SEM) after a process of freeze-drying. Figures (5.41 to 5.43) present some of the results obtained in this study, more details can be found in Villar *et al.* (2004). Although the observations mainly provide qualitative information, the use of this technique is of interest to enhance the knowledge of the structure changes due heating and hydration.

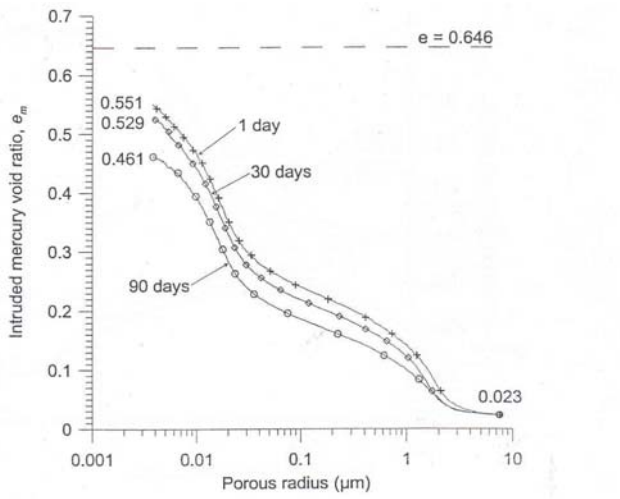

Figure 5.40. Changes in mercury porosimetry intrusion curves with time, e=0.646 w = 8.2% (Marcial, 2003).

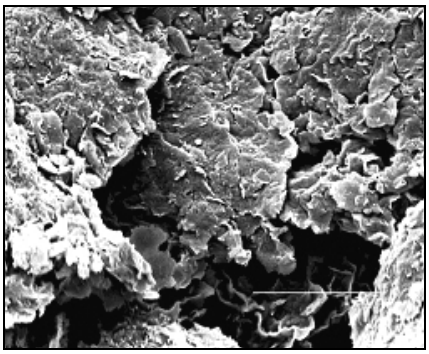

Figure 5.41. Compacted FEBEX bentonite with hygroscopic water content to ρ_d=1.40 Mg/m^3 (Villar *et al.*, 2004).

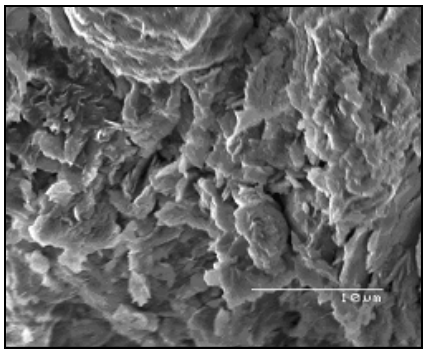

Figure 5.42. Sample after application of a suction of 10 MPa in isochoric conditions ($\rho_{d\ final}$=1.46 Mg/m^3) on bentonite initially compacted in hygroscopic conditions to ρ_d=1.65 Mg/m^3 (Villar *et al.*, 2004).

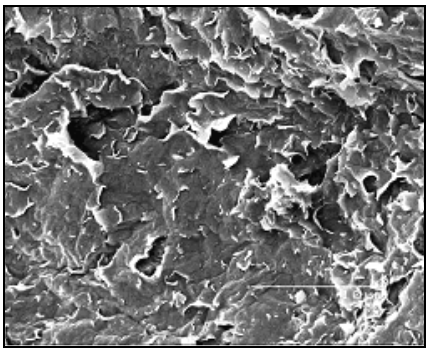

Figure 5.43. Sample after saturation in isochoric conditions (ρ_d final=1.43 Mg/m^3) on bentonite initially compacted with hygroscopic water content to ρ_d=1.65 Mg/m^3 (Villar *et al.*, 2004).

The changes in the clay structure originated by the progressive wetting of compacted bentonite with an initial dry density of 1.40 Mg/m^3 can be observed in Figures (5.41 to 5.43). Suction changes in isochoric conditions were applied to samples before the observations. The differences in final dry density are due to the rebound experienced by the bentonite after unloading. The progressive occlusion of the inter-aggregate pores due to particle swelling is apparent.

5.4.2.2 CONCEPTUAL MODELS

The aim of this Section is to analyse some of the more common conceptual models used in the modelling of expansive clay. In the case of single porosity models, generally the porous matrix is assumed as an inert solid. The mechanical law considers the deformation of the material skeleton as a function of changes in the effective stress level, suction, temperature and time (in the case of viscous materials). In expansive soils, suction reduction is related to clay swelling. The swelling implies changes in the porosity distribution and, obviously, in the permeability field due to the hydro-mechanical coupling. As an example of the changes induced in an expansive clay due to *THM* processes, some results of the thermo-hydraulic large cell tests carried out at the CIEMAT laboratory (Villar & Rivas, 2001) are presented below. These tests are involved in the laboratory tasks of the FEBEX project, and are aimed to the *THMG* characterization of the FEBEX bentonite. The cell design intents to reproduce, with the best fidelity possible, the *THMG* conditions of the ***mock-up*** test. That is, the barrier thicknesses (0.60 m), the clay density, the block discontinuities, the hydraulic and thermal gradients are the same as in the ***mock-up*** test. The cells were submitted simultaneously to heating and hydration during six, twelve and twenty-four months. In Figure (5.44) the symbols correspond to the measured values of dry density at the end of the second year of the test. It can be observed a clear density reduction in zones close to the hydration front (due to the clay swelling) and higher densities as the distance to the heater diminishes.

Figure (5.44) presents also the modelling results using a single porosity model (Villar ***et al.,*** 2004). As commented above, the dependence of intrinsic permeability on porosity implies changes in the permeability field (for instance through Equation A4.2.) According to Figure (5.44) (and Equation A4.2) the higher intrinsic permeability is computed in zones close to the hydration front of the cell, this is due to the porosity increment in these zones. This model response is not in agreement with some of the concepts found in the literature and expressed in the previous section. The greater permeability computed in zones close to the hydration front can not reproduce the tendency to a progressive reduction in the clay permeability during wetting. So, it seems that this kind of model is not the best one to simulate the hydration process of expansive clays. These shortcomings in the conceptual model are very common in most formulations and codes developed to deal with this kind of problems. See for instance the benchmark exercises presented in Alonso & Alcoverro (1999), in this work several *THM* codes are introduced and their performances are compared.

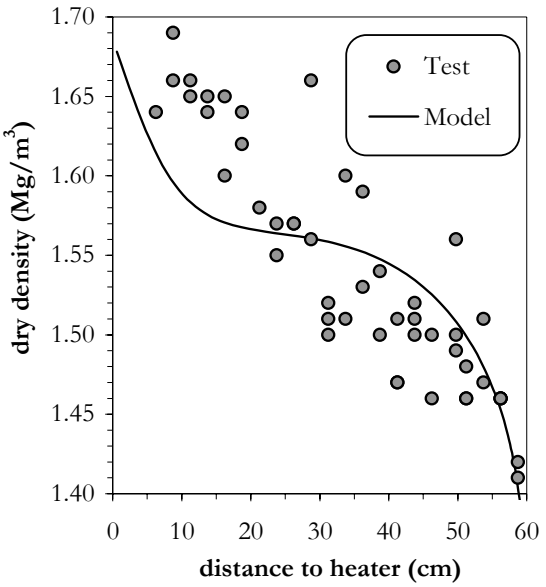

Figure 5.44. Distribution of dry density along the cell at end of the of 2 years test. Experimental and computed values (Villar *et al.,* 2004).

Some attempts to solve these drawbacks have been proposed considering the updating of intrinsic permeability only when the accessible porosity changes. Many of these models use concepts of double porosity media, with a macro porosity dependence on the degree of saturation (Olivella & Gens 2000; Thomas *et al.*, 2003). This simple idea allows catching some of the trends observed in this kind of material, but it has some important limitations. Perhaps the most relevant weakness of these models is that there is not connection between the law that controls the changes in the porosity field (consequently the medium permeability) and the mechanical problem. However, there is a strong relationship between them.

In the light of these facts, the hydration of expansive clay appears as a complex problem and, in consequence, it is not easy to describe its behaviour with simple models. At this point, it is interesting to introduce two different conceptual models of the resaturation process in bentonite. Both conceptual models are very well-known. Here, for the presentation of the models, the work of Kröhn (2002) is followed. Two main processes are distinguished during clay hydration: the flow of water through the pores space and the flow of water into the interlayer space, named 'hydration flow'. Analysing two extreme situations these mechanisms become clearer:

- resaturation with a 'very low hydration-to-flow ratio',
- resaturation with a 'very high hydration-to-flow ratio'.

Figures (5.45 and 5.46) present the schemes corresponding to both cases. These schemes illustrate a typical resaturation problem in a repository, with a clay barrier placed between the host rock and the waste canister; in this case the hydration water comes form the surrounding rocks. When the conditions for the 'very low hydration-to-flow ratio' prevail, the pore space is filled with water before a significant transfer of water to the clay microstructure occurs. In contrast, in the case of 'high hydration-to-flow ratio', the pore water can proceed into the clay barrier after the hydration at the macropore water front is more or less completed, meaning that the pore space has been reduced to a minimum behind the front.

These two models correspond to hypothetical extreme conditions, but it is interesting to analyse each case in more detail, because they are associated to two different models of clay hydration. These two conceptual models are briefly analysed in the framework of the double structure approach presented in the previous Chapters. In this context, it is considered that the main water flow takes place through the macropore spaces. This assumption is made for both conceptual models analysed below.

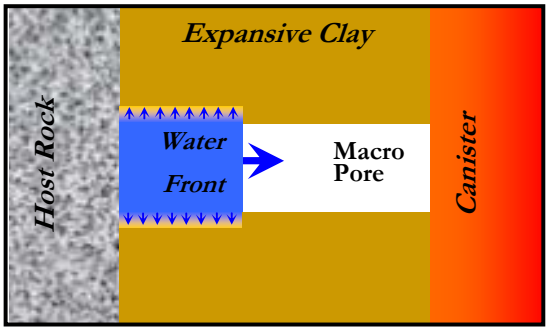

Figure 5.45. Scheme of a resaturation with a 'very low hydration-to-flow ratio' (Kröhn 2002).

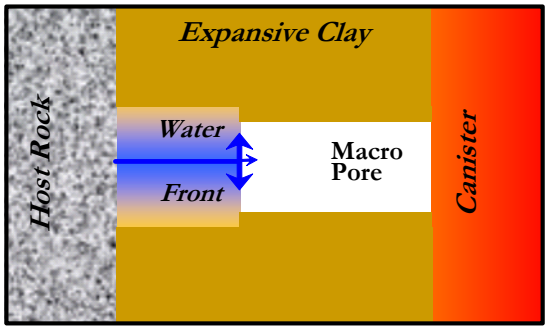

Figure 5.46. Scheme of a resaturation with a 'very high hydration-to-flow ratio' (Kröhn 2002).

The conditions required for the case of 'very low hydration-to-flow ratio' can be modelled selecting a very low value for the leakage parameter (γ^l), when a quasi-steady model of water mass transfer is considered (Section 2.2.5 Equation 2.35). This parameter can be adopted sufficiently low to allow that the liquid flow takes place firstly through the macropores, with the gradient of the macropore liquid pressure as a main driving force. After that, the difference between the water potential associated to each level tends to equilibrate progressively through the leakage term. This is a process delayed in relation to the liquid flow. The hydration and swelling of the microstructure occur due to the microstructural suction reduction. In this case the expansive clay behaves almost as an inert porous material until the macropore is nearly water saturated. This is a feasible scenario to analyse the clay hydration but, this conceptual model is in disagreement to some experimental observations. One of them is that the water uptake can not be significantly increased by applying hydraulic pressure (Push & Kasbohm, 2001; Kröhn, 2002). Laboratory tests also show that the hydration and swelling of the clay take place from the beginning of the wetting process (Fernández, 2003; Villar *et al.,* 2004).

The other extreme case, the 'very high hydration-to-flow ratio', can be modelled adopting a value close to one for the leakage parameter. This implies that during the simulation of a wetting process, the model tends to equilibrate the water potential between the macro and the microstructure instantly. After that, the Darcy's flow takes place through the macropores. In this case the hydration front acts as a sink of water from the pore space to the microstructure, instantly. Due to the microstructural suction reduction the clay particles swell, changing the porosity distribution and affecting in a strong way the permeability field and the kinetic of hydration. This conceptual model avoids the shortcomings of the previous one, but, as a drawback it does not contemplate some microstructural processes of hydration delayed in time, for example the phenomenon of ageing in expansive clay observed by Marcial (2003), explained in the previous section.

Both conceptual models presented can be used for the simulation of the hydration process in expansive clays. The proposed double structure framework can deal, in a natural way, with these two extreme conceptual models and, obviously, with in-between conditions.

Finally it is important to note that the water vapour also plays an important role in the clay hydration, especially under non-isothermal conditions. The formulation presented in Chapter II is able to handle this water transfer.

5.4.3 *MOCK-UP* DOUBLE STRUCTURE MODEL

5.4.3.1 INTRODUCTION

In the following sections double structure concepts have been used to perform a modelling exercise of the *mock-up* test. In these studies, 1-D axi-symmetrical models have been used to analyse the two characteristic sections of the test. In the 'hot cross-section' a temperature of 100º is prescribed in the contact between heater and bentonite, while in the 'cold cross-section' a temperature of 27 ºC is fixed in the internal part of the barrier. A mesh of one hundred (100) elements has been adopted. A sensitivity analysis has also been carried out to verify that the model results do not depend on the mesh adopted.

Regarding the mechanical and thermal initial conditions, the assumptions of the OBC model have been maintained (Appendix A.4). Concerning the hydraulic initial conditions inside the barrier, an initial suction has been adopted taking into account the records of the relative humidity sensors of the *mock-up* test. Finally, the same hydration and heating conditions adopted for the 'OBC' model have been prescribed (Appendix A.4).

The numerical analyses carried out do not consider the overheating event. The work is focused on the behaviour of the FEBEX clay during a normal hydration and heating test, and also on how these processes can be interpreted in a double structure context. Two sets of comparisons are shown: model output versus experimental data and comparisons between the long term predictions of the 'OBC' and the double structure model (both without overheating).

The first sets of comparisons are introduced in order to show the capacity of the model to reproduce the experimental observations and tendencies. It is important to remind that, the unexpected slow hydration of the barrier is clearly observed at dates before the overheating event. Regarding the second type of comparisons it is interesting to analyse the long term predictions of these two different conceptual models under the same test conditions.

5.4.3.2 MODEL LAWS AND PARAMETERS

In Chapter IV the mechanical expansive model has been validated using the laboratory tests available for the FEBEX bentonite. The sample dry density of these tests was 1.70 Mg/m^3, whereas the global dry density of the *mock-up* test is 1.65 Mg/m^3. In order to take into account this difference in the dry density, the pre-consolidation stress has been changed (Gens & Alonso, 1990). A value of 7.5 MPa has been adopted for p_o, which implies (according to the adopted *LC* curve) a value of 5.4 MPa for the saturated pre-consolidation stress. More details are given in Appendix A4 (Section A.4.3).

In Appendix A.4 (Section A.4.3) the selection of the models adopted for the hydraulic and thermal problem are described and discussed in detail. Here, some aspects of these models are briefly introduced. In relation to the hydraulic problem, it is assumed that the flow of liquid water takes place mainly through the macropores. The test has been simulated considering the clay behaviour during hydration according to the concept of 'very high hydration-to-flow ratio' presented previously. This decision has been adopted taking into account the observed response of the FEBEX bentonite in different laboratory tests. In this context, it has been observed that the hydration and swelling of the microstructure take place from the beginning of the wetting process (Fernández, 2003, 2004; Villar *et al.,* 2004). So, the water transfer from the macrostructure to the microstructure is considered instantaneous. That implies a low value of the leakage parameter (*i.e.* $\gamma^{/} = 1$ kg s^{-1} m^{-3} MPa^{-1}). Finally, based on experimental observations, a microstructural water density of 1.15 Mg/m^3 has been adopted (Figure A4.33, Appendix A4).

5.4.3.3 MODEL RESULTS

Figures (5.47) to (5.58) present the results obtained for a hot cross-section. Figures (5.47) to (5.50) show the comparisons between model results and tests data, whereas, Figures (5.51) to (5.54) present the long-term predictions of the 'OBC' and of the Double structure models ('Dou').

Regarding the hydraulic problem, it can be observed that the model can capture qualitatively well the evolution of the relative humidity, especially in internal zones (r = 0.22m and r = 0.37m). In general terms, it can be said that the tendency of both models are clearly different ('Dou' and 'OBC' models). This is even clearer in the comparisons between the long term predictions of both models. The double structure model predicts a locking of the hydration which implies that important zones of the barrier remain in a non-saturated condition. This is qualitatively in agreement with the tendency observed in the barrier.

In relation to the water intake (a global variable) the response of the model is also good if it is compared with the measurements. In the long term analysis, the 'Dou' model predicts a lower amount of water in relation to the one estimated with the 'OBC' model.

In this Chapter, expressions such as 'zones of the barrier will remain non-saturated' or 'no full saturation is reached' refer to the fact that the rate of water intake is so low that the saturation of the bentonite is delayed for a long time. That is to say, that virtually no full saturation of the barrier can be assumed (as it can be seen in Figures 5.51 and 5.52). Perhaps, the following information about the water intake could help as an explanation. The experimental value of the water intake rate at the day 1400 is close to 0.15 Kg/day (weekly average), while the 'Dou' model computes a rate of 0.17 Kg/day (and the one corresponding to the 'OBC' model is 0.22 Kg/day). This rate decreases largely for the last test data available (close to day 2417), with a value near 0.04 Kg/day (weekly average), whereas the rate computed by the 'Dou' model is 0.035 Kg/day (and the estimated by 'OBC' model is 0.10 Kg/day). Finally, at the last day of the analysis (7300) the rate of water intake computed by the 'Dou' model is 7.0×10^{-6} Kg/day. This is a very low value for the water intake rate and implies a very long time to reach the barrier saturation.

The temperature field is also well captured by the model. Looking at the comparisons between long terms predictions, it can be mentioned that no increment in the 'Dou' model predictions is observed (in contrast to the OBC model). The 'Dou' model results show that practically constant temperatures are maintained, at different radii and along the time. This is also a direct consequence of the hydration locking, which implies that the degree of saturation is practically constant after the day 2000 and, consequently, the thermal conductivity as well.

Finally, it can be observed that the model captures the strong hydro-mechanical coupling of this problem, reproducing the clear tendency to maintain a practically constant value of the stress level (close to 7 MPa in the test). Some delay in the model output, in relation to the experiment, can be observed. In the test this tendency is detected close to the day 1000, whereas in the model it is near the day 1400. In any case, the trend of the 'Dou' model is closer to the observed behaviour in the *mock-up* test.

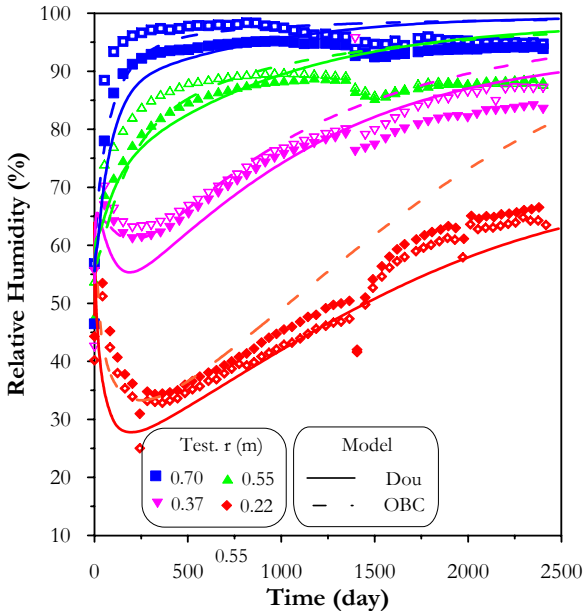

Figure 5.47. Relative humidity. Sections A4-B4. Observed versus computed values of 'Dou' (Double Structure) and 'OBC' models.

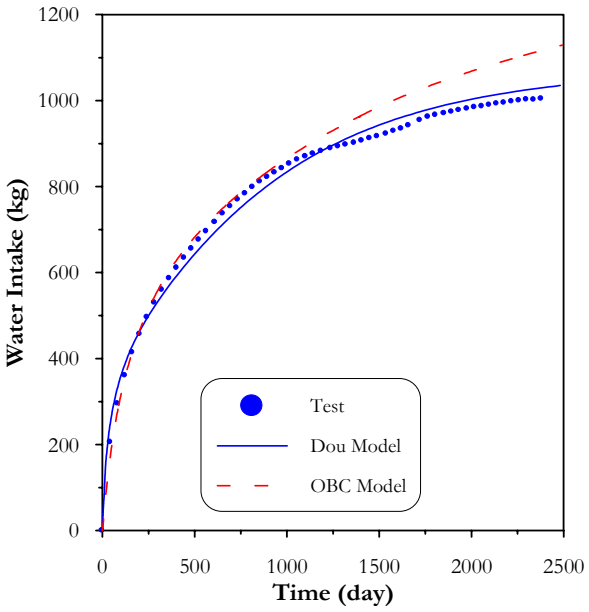

Figure 5.48. Water intake. Observed versus computed values of 'Dou' and 'OBC' models.

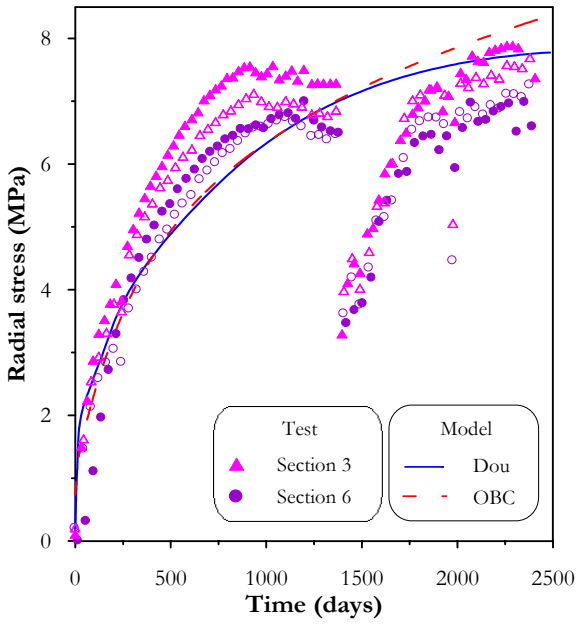

Figure 5.49. Radial stress. Sections A3-B3 and A6-B6. Observed versus computed values of 'Dou' and 'OBC' models.

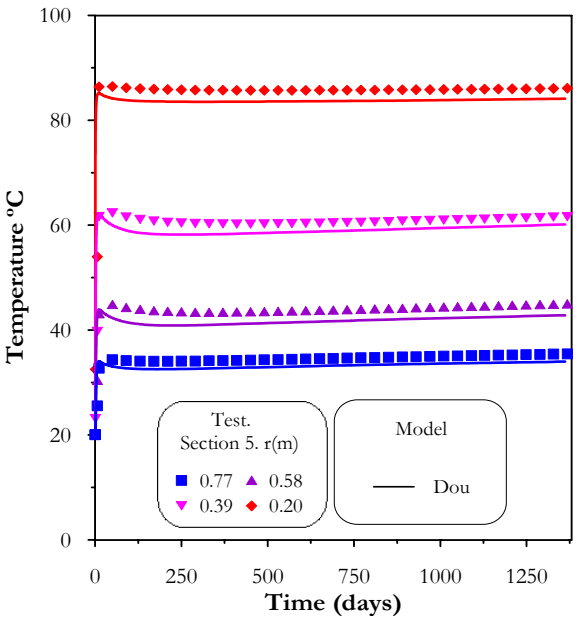

Figure 5.50. Temperature. Section A5. Observed versus computed values of 'Dou' and 'OBC' models.

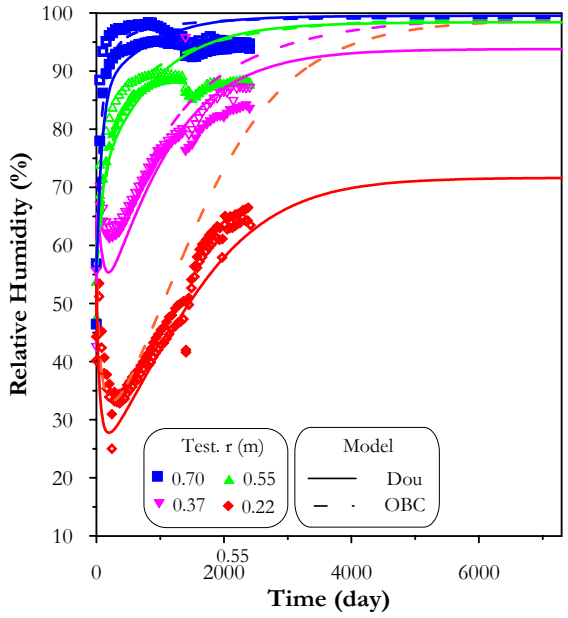

Figure 5.51. Relative humidity. Sections A4-B4. Long-terms predictions of 'Dou' (Double Structure) and 'OBC' models.

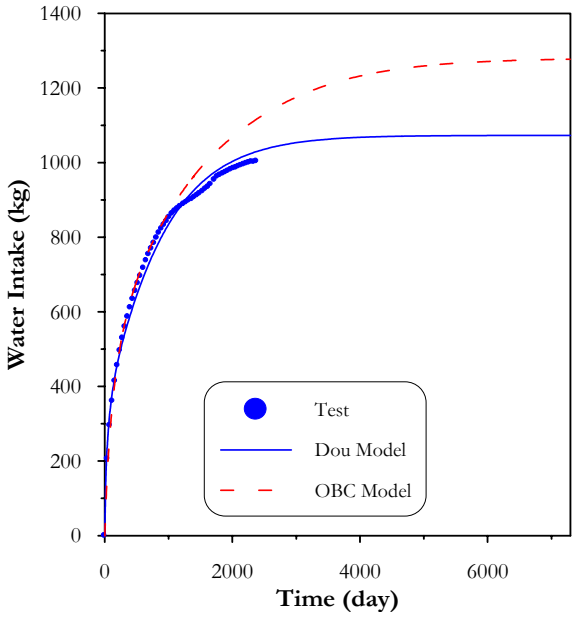

Figure 5.52. Water intake. Long-terms predictions of 'Dou' and 'OBC' models

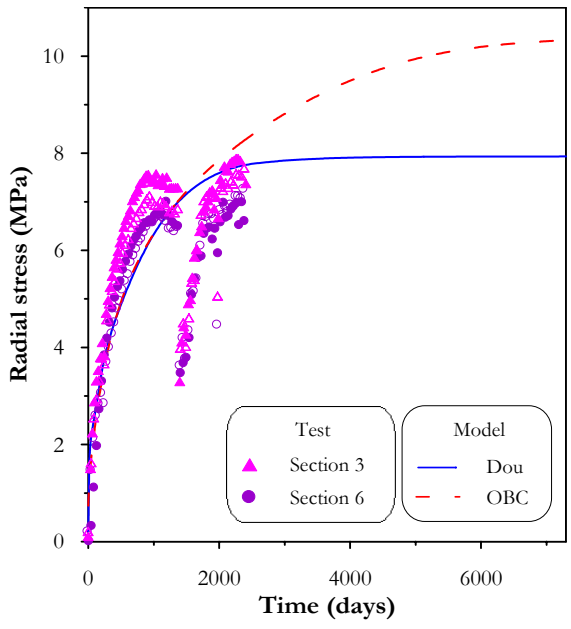

Figure 5.53. Radial stress. Sections A3-B3 and A6-B6. Long-terms predictions of 'Dou' and 'OBC' models

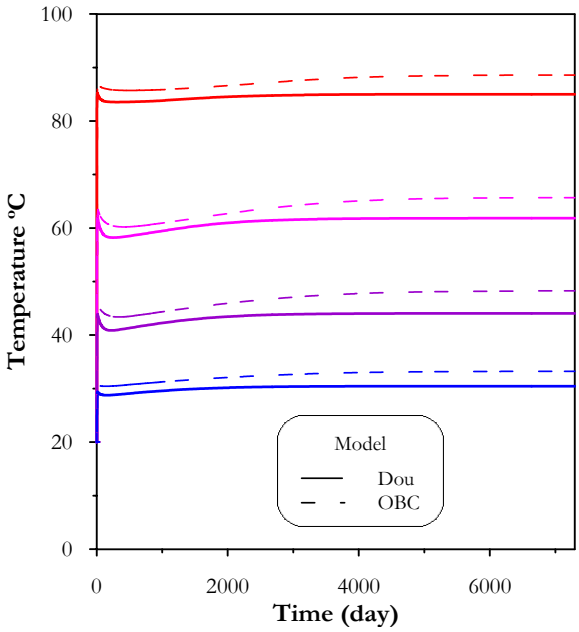

Figure 5.54. Temperature. Section A5. Long-terms predictions of 'Dou' and 'OBC' models.

Figures (5.55) and (5.56) show the evolution of porosity and intrinsic permeability for two extreme radii computed using the 'OBC' model. As expected, a similar behaviour to the one explained for the case of the thermo-hydraulic cell (Section 5.4.2.2) is observed. That is, higher permeability values (associated to lower densities) in zones close to the hydration front, and lower permeability values (related to higher densities) in more internal zones.

Figures (5.57) and (5.58) present, for the same radii, the evolution of the macro porosity and the intrinsic permeability associated to it, but now using the 'Dou' model. As it can be observed, in this model the response is very different, with a tendency to reduce the macro porosity in both locations and, consequently, to reduce also the associated intrinsic permeability. A more external radius (r=0.75m) is also included in the Figure, it can seen that this effect is more significant in zones near the hydration front. The break observed in Figures (5.57) and (5.58) for a radius of 0.70m close to the day 1400 of the test is due to a macrostructural collapse. This is explained later on.

According to this simulation, as the barrier is hydrated the pores available to the liquid flow suffer a progressive reduction. This is due mainly to the microstructure swelling under confined conditions. As a consequence, the full saturation of the barrier is delayed. This kind of hydration-locking is evident in zones close to the heater, because the reduction of the permeability in the zones close to the hydration front reduces the liquid flow supply in the internal zones which are subjected to the heater-induced drying. The final outcome is that the hydration is virtually stopped, with an important zone of the barrier in unsaturated conditions.

The analysis of the distribution of some relevant variables along the barrier computed for different times could help to a wider view of the problem. Figures (5.59) to (5.62) present the isolines of macro, micro and global void ratio; and also of degree of saturation at different times for a section which includes a heater ('cross-hot section'). The microstructure expands in the external zones due to hydration and it contracts in zones close to heater due to strong drying. The front of swelled microstructure advances progressively inside the barrier as time goes on. As for the macropores, a swelling behaviour can be seen but only at the beginning of the test and for a very thin zone close to the hydration front. This is due to a macrostructural suction reduction and also due to the interaction mechanism between structures (in this case microstructural swelling, *ms*, at low load implies a macrostructural expansion). For other times and positions the values of macro void ratio are lower than the initial ones. This is mainly due to the already commented fact of microstructural expansions under conditions of practically constant volume. The final condition corresponds to significant reductions of the macro pores along the sample, which is more marked in the external zones of the barrier. Finally, two aspects are briefly commented: one of them is that macrostructural collapses can be observed along the barrier which progressively move to more internal zones as the hydration goes on; and the other aspect is that zones close to a radius of 0.35 m are strongly affected by the condensation of water vapour coming from the inner region of the barrier (Section 5.2.2.3). This local wetting also induces a marked macro void reduction in this region. Regarding the degree of saturation, it can be mentioned that the shape of the hydration front is very similar to the micro void ratio one. This result is in agreement with the adopted conceptual model, which considers that a great amount of water is stored at the microstructure.

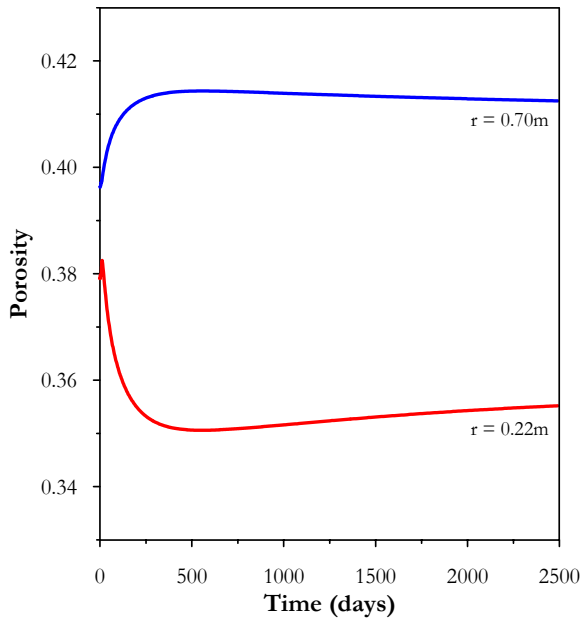

Figure 5.55. Computed evolution of porosity for two extreme radii using the 'OBC' model. Sections A4-B4.

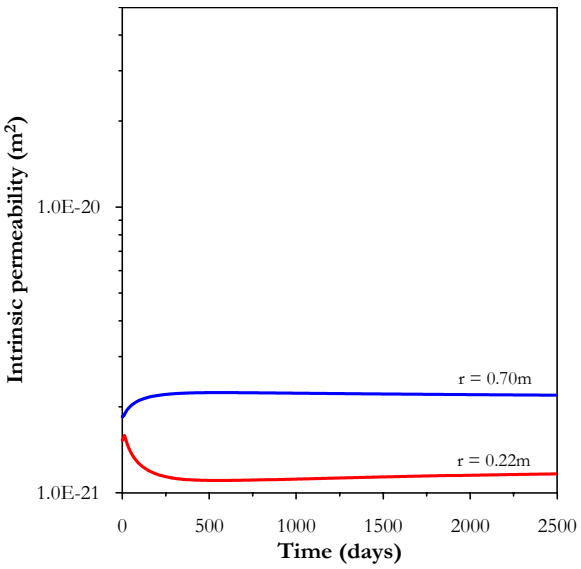

Figure 5.56. Computed evolution of intrinsic permeability for two extreme radii using the 'OBC' model. Sections A4-B4.

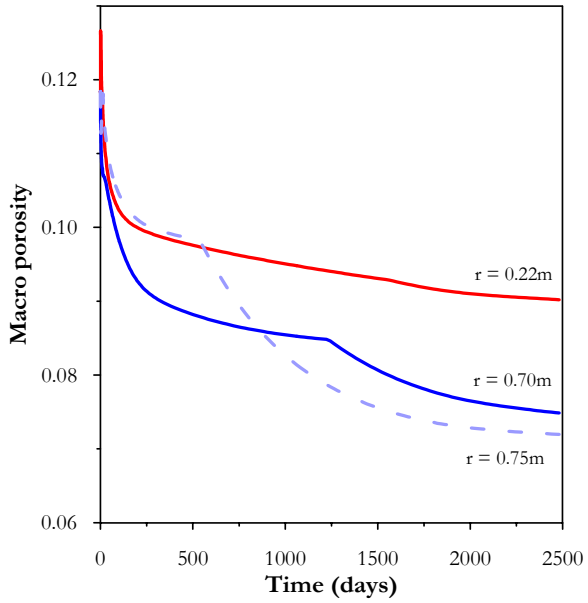

Figure 5.57. Computed evolution of macro porosity for three extreme radii using the 'Dou' model. Sections A4-B4.

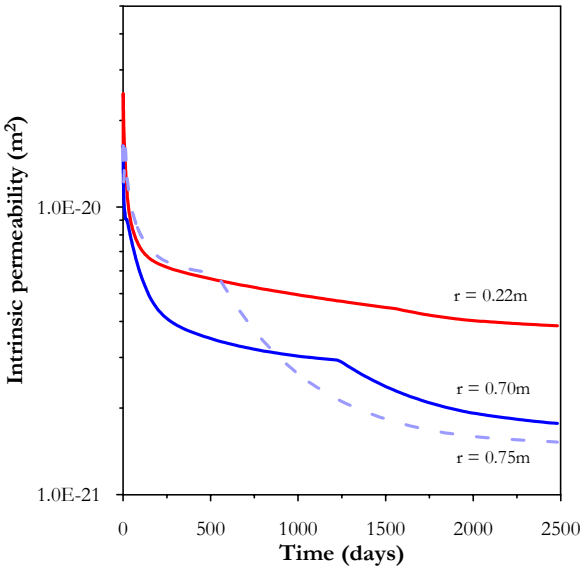

Figure 5.58. Computed evolution of intrinsic permeability for three extreme radii using the 'Dou' model. Sections A4-B4.

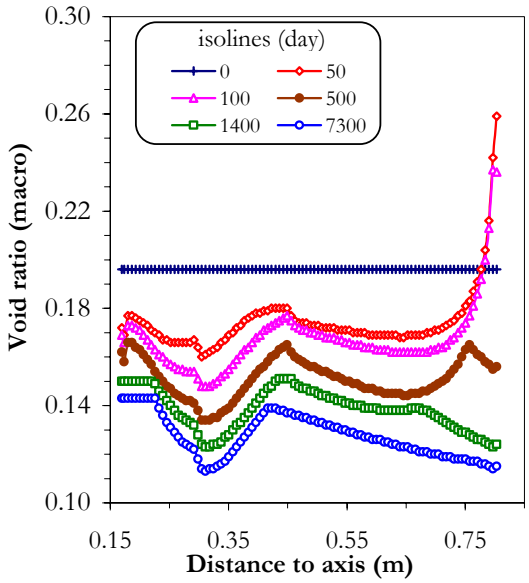

Figure 5.59. Isolines of macro void ratio along a 'hot-cross section'

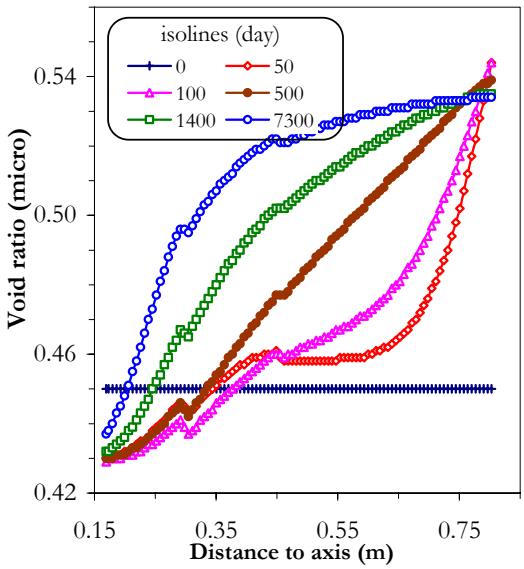

Figure 5.60. Isolines of micro void ratio along a 'hot-cross section'.

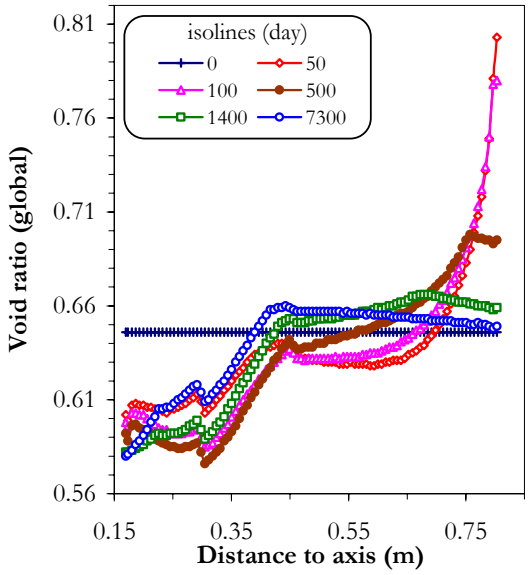

Figure 5.61. Isolines of global void ratio along a 'hot-cross section'.

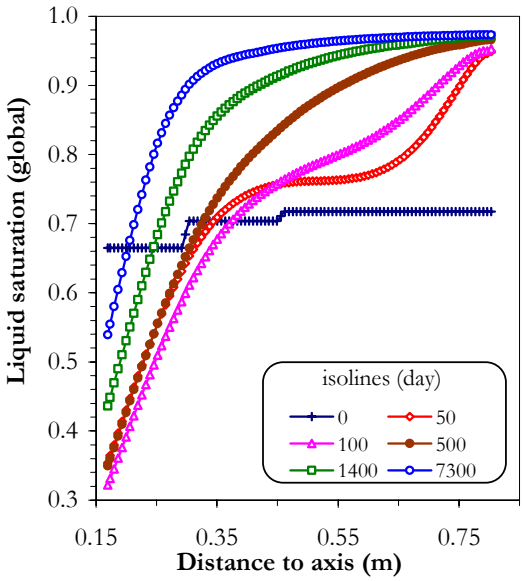

Figure 5.62. Isolines of global liquid saturation along a 'hot-cross section'.

The global void ratio is greater in the outer zones and lower in the inner regions. In that sense, the model reproduces a reduction in clay densities in zones close to the hydration front, as saturation progresses. The key point is that in this approach, under constant volume conditions, the reduction in clay density implies a reduction of the main pores available for the water flow (the macropores).

Figure (5.63) presents the results obtained in a section away from the heater. It can be observed that the evolution of the relative humidity is not so well reproduced by the model. In the long-term simulations a full saturation of the barrier is predicted in this zone (Figure 5.64).

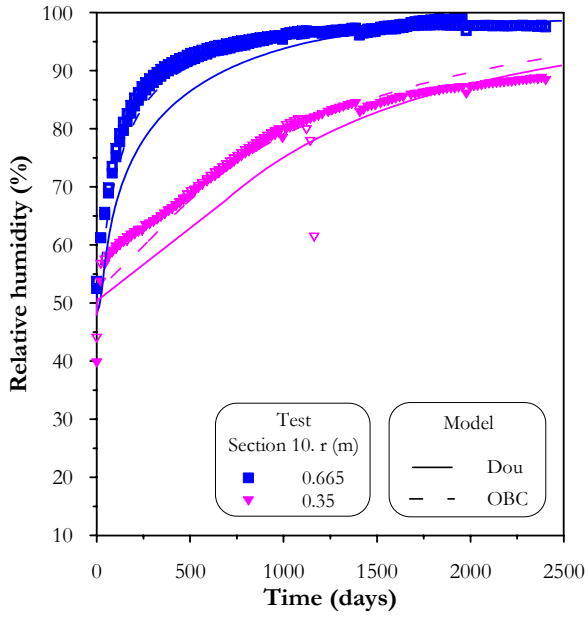

Figure 5.63. Relative humidity. Sections A10-B10. Observed versus computed values of 'Dou' and 'OBC' models.

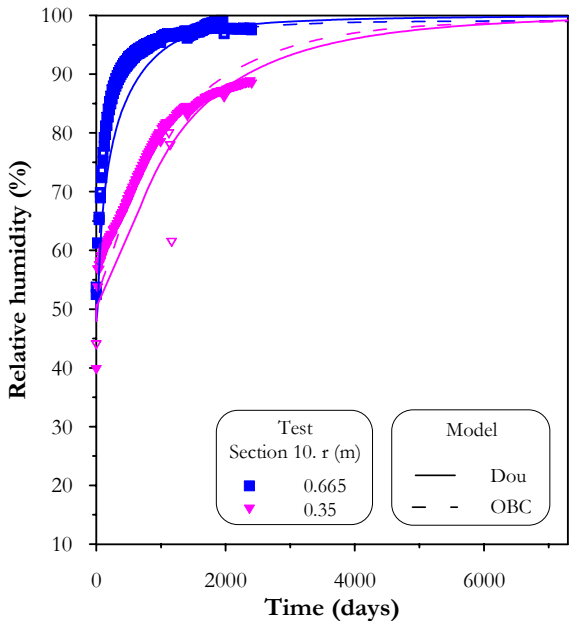

Figure 5.64. Relative humidity. Sections A10-B10. Long term-predictions of 'Dou' and 'OBC' models.

The inclusion in the modelling of the changes in the clay fabric (through the double structure approach) has allowed a more detailed analysis of the barrier behaviour, including the simulation of the main tendencies observed in the two different sections studied ('hot and cold cross sections'). The numerical results can also be considered good in quantitative terms (especially in 'hot cross sections'). It is important to have in mind that the model parameters have been obtained from the available experimental data. As commented before, the conditions in which some laboratory experiments were carried out are different respect to the actual *THM* conditions in the ***mock-up*** test, especially in the case of the permeability tests. It is highlighted that there are not experimental data related to the permeability of FEBEX bentonite under conditions of low hydraulic gradient. The long term behaviour of FEBEX bentonite has not been explored in detail either. In respect to this point, in expansive clays it has been detected that there are some microstructural phenomena which are delayed, for instance the ageing effects in the microstructure observed by Marcial (2003) (Figure 5.40). This phenomenon implies a progressive reduction of the macroporosity as the time goes on.

The existence of these two phenomena (threshold gradient and ageing effects in the microstructure) could imply additional restrictions for the hydration of the barrier. If the presence of these phenomena in the FEBEX bentonite is confirmed experimentally, the proposed framework is able to include them in the simulations. For instance, the effect of a threshold gradient can be added, as it has been presented in Section 5.3.2.1 (Figures 5.22 and 5.23) and, through the leakage term, the formulation is also able to handle the delayed effect of the microstructural expansion due to ageing.

Now the attention is focused on the performance of the double structure mechanical model. The aim is to explore the behaviour of the basic mechanisms and variables that control the mechanical response of the bentonite during the test. As it was already mentioned, the conceptual model adopted assumes equilibrium between the two structural levels considered, which implies that the macro and micro suctions have the same values. Due to that, and for the sake of simplicity, no distinction between them is made in the following graphs. But it is important to have in mind which suction plays the role in each case, according with the structural level and mechanism considered.

During the simultaneous heating and hydration of the test it is expected that different points of the barrier will follow different generalized stress paths. Figures (5.65 to 5.69) collect the main results of four characteristic positions in a 'hot-cross section'. Figures (5.65) present plots of p_o^* versus s. Figures (5.66) present the generalized-stress path on the p-s plane together with the evolution of p_o in terms of suction. Figure (5.67) present the changes in void ratios (macro, micro and total) with mean net stress, while Figure (5.68) present the changes in the same void ratios but in terms of suction. Finally, Figures (5.69) depict the movement of the stress path on the interaction functions. In all the Figures the plots are presented for four selected points, identified as: A, B, C, and D, which correspond to radii 0.22m, 0.37m, 0.55m and 0.70m, respectively. The evolution and the main features of the behaviour of each zone are commented below.

First, a point close to the heater is analysed. Figure (5.66.a) presents the stress path followed on the p-s plane by a point at a radius of 0.22m, identified as 'A' in the barrier scheme. Four main paths ('1' to '4') can be identified.

Initially this zone is submitted to an increment of p under practically constant suction (path '1'). This initial load increment is an effect coming from the more external part of the barrier. From the beginning of the test those zones suffer a wetting, which implies a microstructural expansion and due to the constant volume conditions of the test, a global increment of the net stress is computed. In Figure (5.66.a), the path '1' is presented in more detail (inside a circle), with both axes in the same lineal scale. According with the neutral lineal adopted (note that it is at 45º on this plane), this path implies a microstructural contraction (*MC* path). At this high suction the microstructure is very rigid (Equation A2.23) and this low load increment can not compress the microstructure, that is, the microstructure does not virtually change during this path (Figure 5.67 and 5.68). Consequently, the macrostructural plastic strain induced by the *mc* interaction mechanism between structures is practically null. Therefore, the hardening parameter of the macrostructure p_o^* remains practically constant during this path. Path '1' only affects the macrostructure, compressing lightly the macro pores.

Path '2' (Figure 5.66.a) is characterized by a suction reduction (due to the condensation of the water vapour) at a very low p. Now, a path corresponding to a microstructural expansion (*MS* path) is followed and the active interaction mechanism is the *ms*. This path implies a swelling at both levels, accompanied by an increment of stresses. The microstructure swells due to a reduction of the generalized microstructural stress, mainly due to the reduction of the microstructural suction. And the macrostructure expands by the combined effects of a macrostructural suction reduction and also due to the positive values of the interaction function f_s. This mechanism implies a softening of the macrostructure with a reduction of p_o^*.

Path '3' (Figure 5.66.a) is characterized by a suction increment due to the strong drying present in the zones close to the heater. During this stage hydration progresses in the external zones of the barrier and induces a progressive increment of the stress level. These two facts imply an increment of the generalized microstructural stress and consequently a tendency to a microstructural contraction is predicted (*MC* path), with the plastic mechanism *mc* now active. The macrostructure also contracts due to the combined effect of p and matric suction increments and also due to the positive values of the interaction function f_s. So, this path implies a macrostructural hardening. The break observed on the evolution of p_o^* is due to the interaction function f_s, which passes form the quasi-horizontal branch to the ascendant one during this path (Figure 5.69.a).

Path '4' (Figure 5.66.a) is related to the final hydration stage of this zone, controlled by a gradual decrease of suctions and a significant increment of p. Regarding the microstructural level, the effect of suction reduction prevails and the microstructure tends to swell. Instead, the macrostructure maintains the tendency of path '3', contracting its pores mainly due to the effect of the p increment. The *ms* is the interaction plastic mechanism active during this path (*MS* microstructural path), with negative values of the interaction function f_s. This implies a hardening of the macrostructure, associated to a wetting process under high pressure (Alonso *et al.*, 1999). At a suction close to 110 MPa, the stress path reaches the *LC* curve and drags it until the end of the analysis. At the end of this stage, small macrostructural collapses can be observed after the contact between the *LC* curve and the stress path.

The other extreme situation corresponds to a point close to the hydration front. Figure (5.66.d) presents the stress path followed on the p-s plane by a point at a radius of 0.70m, identified as 'D' in the barrier scheme. In this case the generalized stress path has also been divided in four main stages. Path '1' is controlled by an increment of p under practically constant suction. As for the point 'A', the stress increment is due to the wetting of the more external zones of the barrier. The same analysis done for the point 'A' is applicable for this other location.

Path '2' (Figure 5.66.d) is characterized by a progressive suction reduction and stress increment. This implies a change in the microstructural behaviour going from contraction to expansion, as it can be seen in the detailed graph of Figure (5.66.d). The interaction plastic mechanism active in this stage is the *ms*. The positive values of the interaction function f_s imply a macrostructural softening (reduction of p_o^*). During this stage the main compression corresponds to the macropores, due to the dominant effect of the stress increment. In this stage, the increment in stresses is also given by the progressive hydration of the external zones of the barrier. Note that this increment of p happens under relatively small changes of the macrostructural suction, in spite of the fact that the analysed radius is quite near the hydration

front. This is a direct consequence of the conceptual model adopted, in which the water transfer to the microstructure (responsible for the expansive behaviour) is faster than the flow of liquid through the macropores.

Path '3' (Figure 5.66.d) maintains this tendency to suction reduction and stress increment, but now the suction reduction is more noticeable. This implies a large microstructural swelling due to the strong reduction of the generalized microstructural stress. This microstructural expansion, under confined conditions, tends to increase the stress level and compresses even more the macropores. The plastic interaction mechanism active (*ms* mechanism) induces a macrostructural hardening due to the negative values of the interaction function during this path.

Path '4' (Figure 5.66.b) starts when the stress path reaches the *LC* curve. After that, the stress path drags the *LC* curve and both move together. The shape of the stress path in this last stage is mainly controlled by the *LC* curve. The active plastic mechanism is now the *ms*, with a constant value of one for the ratio p/p_0 along this path. During this stage the macropores reduction takes place under small changes of stresses (Figure 5.67.d), that is, a kind of macrostructural collapse occurs in this zone of the barrier at advanced phases of hydration.

Moving inwards the barrier, the next point found is one identified as 'C', with a radius of 0.55m (Figure 5.66.c). The behaviour of this point in each stage is very similar to the one described for the case of point 'D' and it is not necessary to comment it again.

Finally, the evolution of a point located at a radius of 0.37m (identified as 'B' in the barrier scheme) is briefly commented. Over these zones the water vapour has a strong influence, as it can be seen in Figures (5.66.b). If the cycle of wetting and drying followed by this point is compared with that of point 'A', two main differences can be noted: one of them is that now the wetting takes place at a higher stress level and the other is the lower amplitude of the cycles. Taking into account these facts, a similar description to that performed for the point 'A' can be made for this case. A difference in relation to the behaviour observed in point 'A' is that now the entire path is inside the *LC* curve. In both cases ('A' and 'B') the microstructure remains elastic after the cycles of the generalized microstructural stress loading and unloading (Figures 5.68.a and 5.68.b). This is due to the assumed hypothesis of reversible behaviour of the microstructure; all the plastic behaviour observed in the bentonite is ascribed to the macrostructural level.

As summary, it can be said that these Figures (5.65 to 5.69) have allowed the analysis of the main *THM* variables and couplings, in a unified framework at different points of the ***mock-up*** test as the hydration and heating of the barrier take place. It can be observed how, through the mechanical model, the *THM* variables interact affecting the clay fabric and, in consequence, the permeability field.

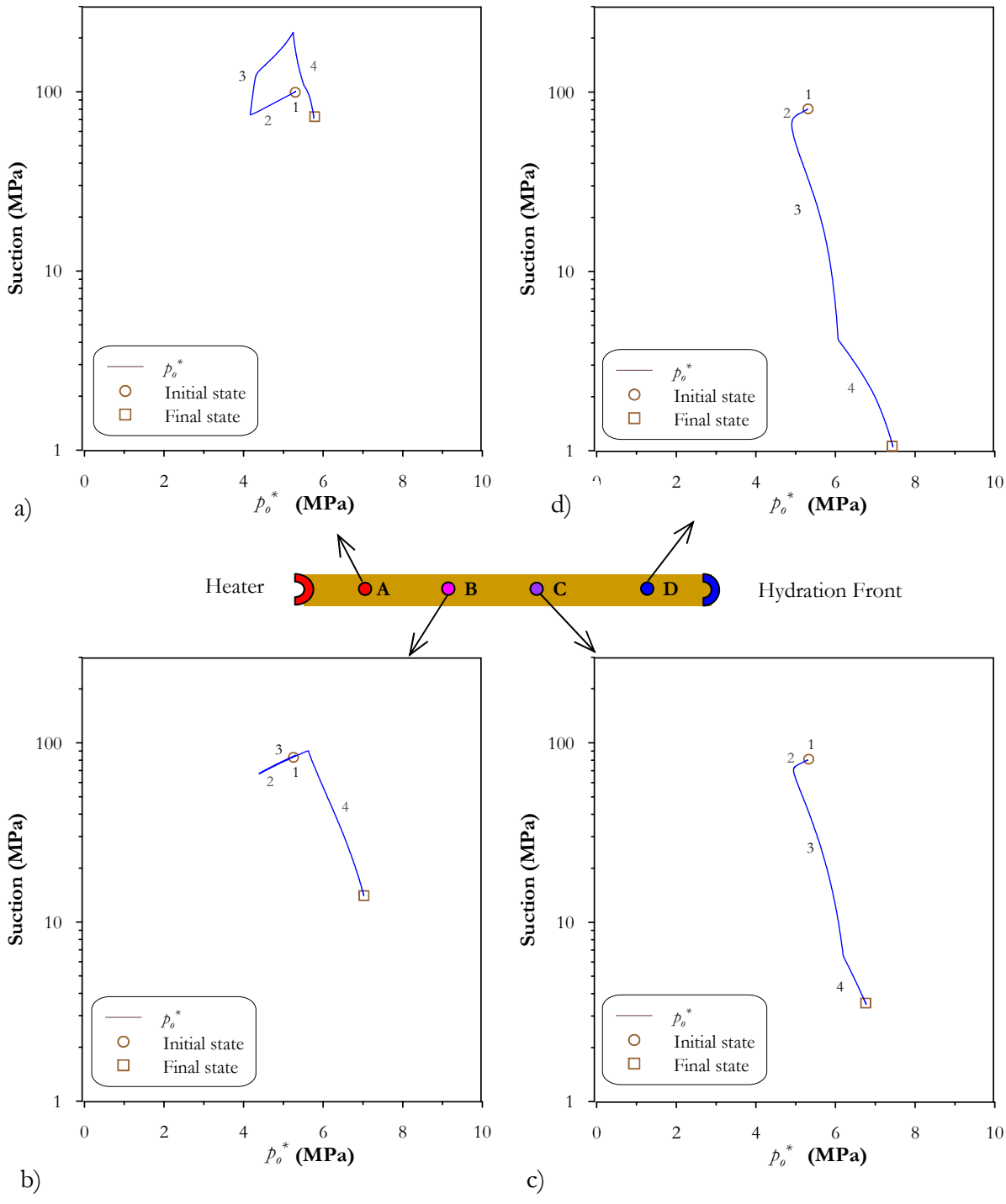

Figure 5.65. Plots of p_o^*-s path, for 4 characteristics point of the barrier, in a 'hot-cross section': A=0.22m, B=0.37m, C=0.55m and D=0.70m.

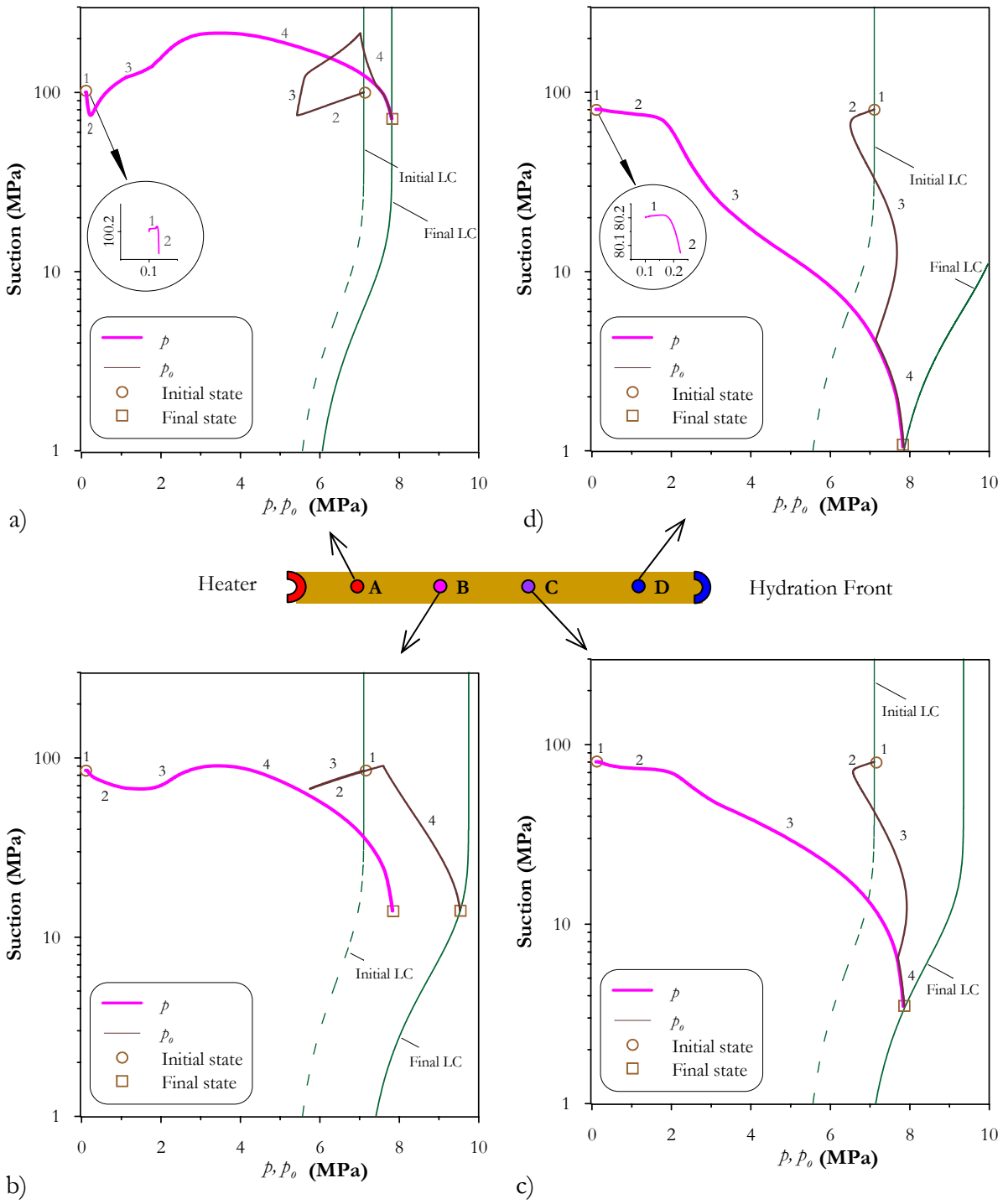

Figure 5.66. Generalized-stress path on the p-s and p_o-s plane for 4 characteristics points of the barrier in a 'hot-cross section': A=0.22m, B=0.37m, C=0.55m and D=0.70m.

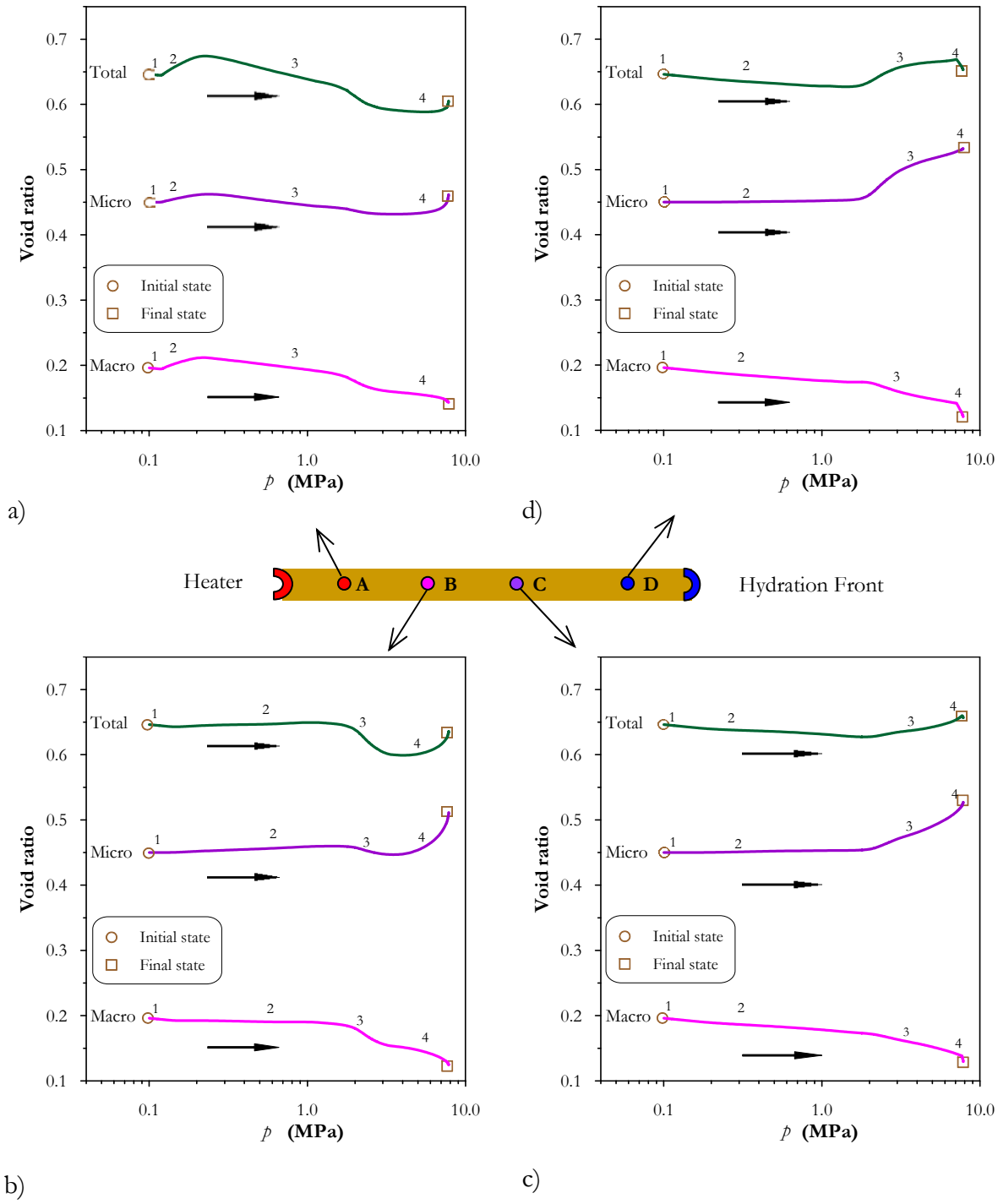

Figure 5.67. Changes of void ratios with net stress, for 4 characteristics point of the barrier, in a 'hot-cross section': A=0.22m, B=0.37m, C=0.55m and D=0.70m.

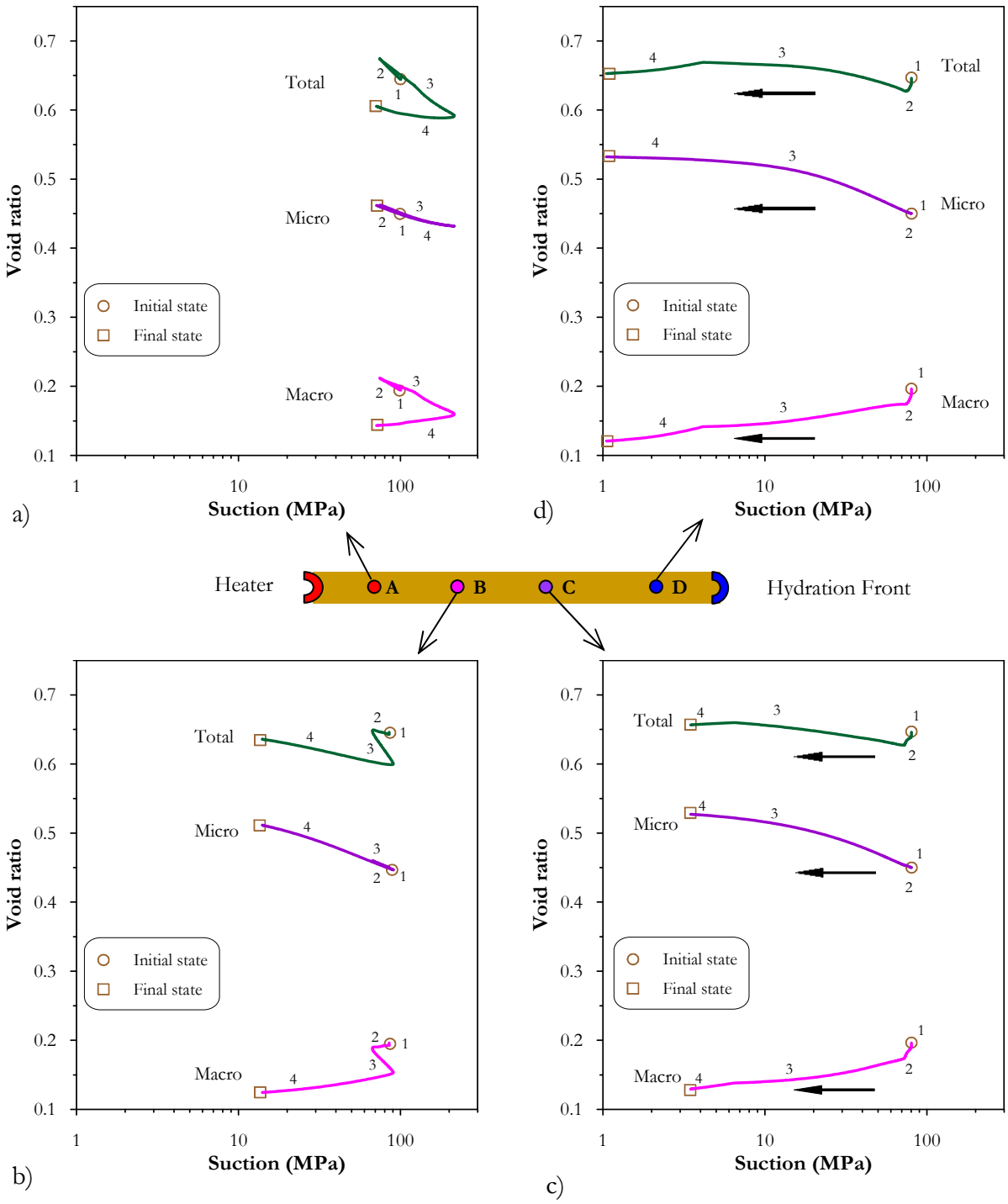

Figure 5.68. Changes of void ratios with suction, for 4 characteristics points of the barrier, in a 'hot-cross section': A=0.22m, B=0.37m, C=0.55m and D=0.70m.

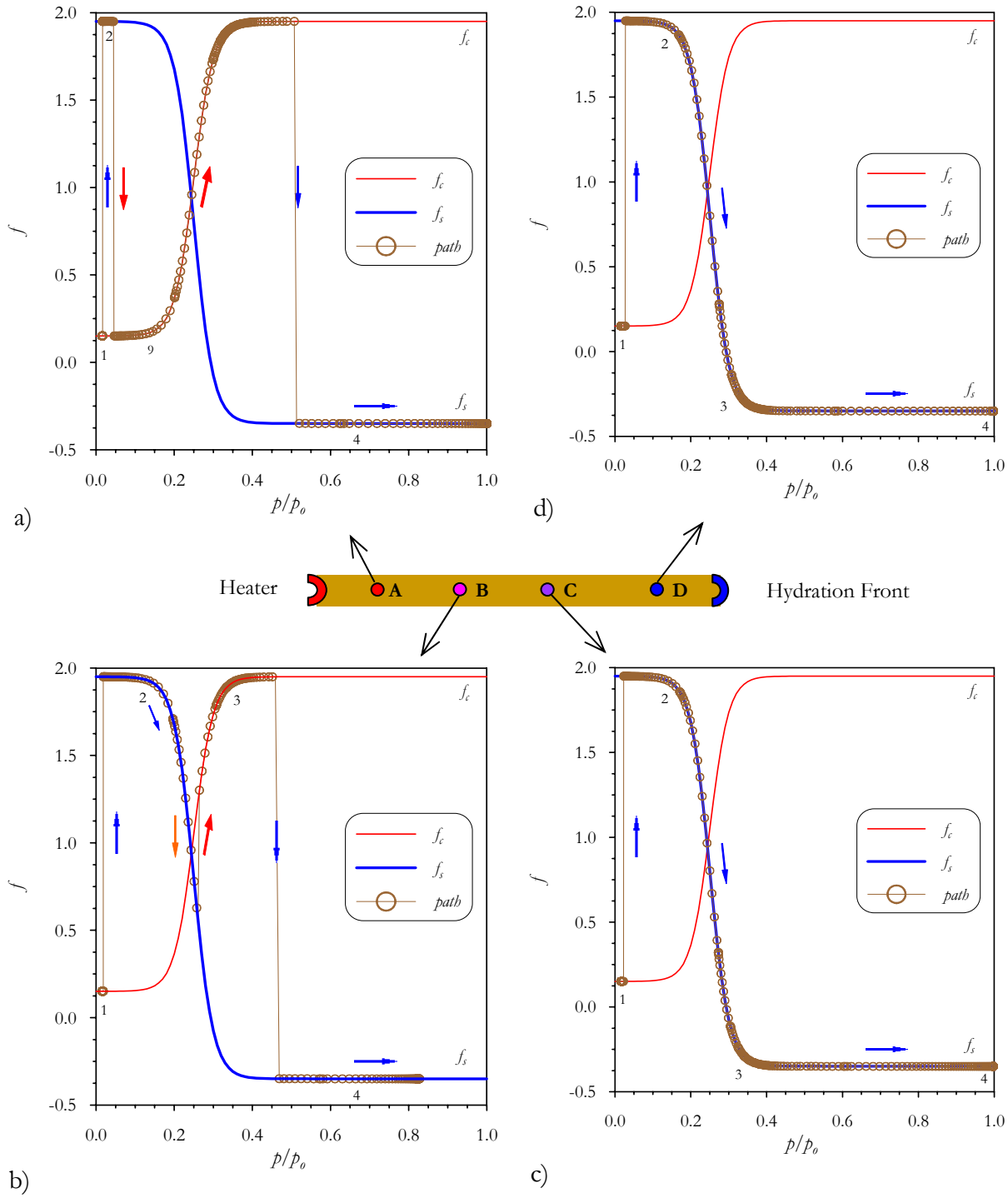

Figure 5.69. Stress paths on the interactions functions, for 4 characteristics point of the barrier, in 'cold-cross section': A=0.22m, B=0.37m, C=0.55m and D=0.70m.

5.5 CONCLUSIONS

The 'OBC' model presented in the first part of this Chapter and Anexo A.4, was formulated using a full *THM* approach for a single porosity medium, in which all of the processes and couplings deemed relevant were considered. The comprehensive laboratory works carried out in the context of the FEBEX project have allowed the identification of the main models parameters required for a 'standard *THM* model'. Therefore, it can be said that all the steps and requirements recommended to develop a 'standard *THM* model' have been fulfilled for the case of the 'OBC' model. However, the results obtained are not totally satisfactory, because the simulation over-predicts the hydration rate of the barrier. Comparing experimental data versus model results, a slowing down in the hydration kinetics of the test can be appreciated. A tendency to maintain a constant and very low rate of water intake and nearly constant values of the main variables (relative humidity and stresses) at different radii of the barrier can be observed in all the sections of the test, with a more marked trend in the cross-sections that involve heater. Changes in the constitutive law or its parameters could not reproduce accurately the test evolution. Similar problems were identified by 'numerical teams', using other numerical codes, to simulate the barrier evolution. Moreover, an unexpected behaviour similar to the one observed here has been reported in another experiment.

It seems that a 'standard *THM* model' has some shortcomings when reproducing behaviour as the one explained above. Generally, this problem is handled considering a progressive increment of the water permeability as saturation goes on, especially due to the increment of the relative permeability. However, experimental evidence reflects that the behaviour of expansive clays under hydration is more complex. The main problems in the simulation of the *mock-up* test could be ascribed to other processes or phenomena, which were not contemplated in the 'OBC' model. A series of developments were made in order to include in the analyses some additional phenomena that could explain, with physical bases, the barrier behaviour. The main conclusions of this study are presented in Section 5.3.3. As a summary, it can be said that each analysis could explain, to some extent, the unforeseen response of the experiment.

A double structure framework has also been used to simulate the *THM* behaviour of the *mock-up* test. The explicit consideration of the two structural levels gives the opportunity to define its own properties and constitutive laws, to consider the main processes that take place in each pore level, and to take into account the coupling between both pores structures. In the case of the FEBEX bentonite these two levels of pores actually exist. The modelling results can be considered good enough since the main tendencies of the observed behaviour have been correctly reproduced. It is stressed that this study can be considered as a first step in this kind of analysis and the obtained results have mainly qualitative significance.

The simulations offer also valuable information related to the mechanisms that control the main variables of the problem. In this framework, the mechanical constitutive law can be viewed as the nucleus of the model, because stresses and void ratios (macro and micro) are updated by this law when changes in the state variables of the problem (suctions, temperature and deformations) occur. In addition, the permeability field depends on the pore structure. The analysis shows, in an integrated way, how changes in the state variables of the problem affect the evolution of the main variables and helps to understand better some trends of the observed barrier evolution.

According to the model results, as the barrier hydration goes on, the pores available to the liquid flow suffer a progressive reduction. This is due mainly to the microstructure swelling under confined conditions. As a consequence, the full saturation of the barrier is delayed and in some cases could be virtually stopped. This kind of hydration-locking is evident in zones close to the heater, because of the reduction of the permeability in the zones close to the hydration front reduces the liquid flow supply in the internal zones which are subjected to the heater-induced drying. On the other hand, it is important to keep in mind that the temperature has been maintained constant in the contact between heater and bentonite (equal to 100 ºC) during all the time analysis, but, under real repository conditions the waste temperature will reduce progressively as the time goes on.

Along this Chapter, terms such as 'non-expected behaviour' or 'unforeseen response' have been used to indicate that the initial model predictions ('OBC' model) can not reproduce the experiment response. But, perhaps, the point is: Why was it assumed that this model could reproduce the barrier evolution? The long-term behaviour of expansive clays under low hydraulic gradient is not a well-known matter and it is an active subject of research and interest nowadays, moreover, when the hydration takes place under non-isothermal and confined conditions. Information related to laboratory tests under these conditions is scarce in the literature. Due to that, it was difficult to know in advance the 'expected' response of the FEBEX bentonite, at least under the conditions prevailing in a repository. For example, the permeability tests were carried out under high hydraulic gradient (between 10000 and 20000) while the hydraulic gradient prevailing in the hydration front is lower than 2000. In that sense, it would not be a surprise that the standard 'OBC' model could not reproduce the behaviour of the *mock-up* test. The availability of laboratory tests conducted under similar conditions to the ones expected in a repository is a crucial requirement in order to develop models nearer to the material behaviour under the actual *THMG* conditions.

CHAPTER VI

CLOSURE

6.1 REMARKS AND GENERAL CONCLUSIONS

In this Thesis an effort to advance in the understanding of the Thermo-Hydro-Mechanical modelling of real problems involving low permeability materials has been made. This is a relatively complex problem in which several factors make significant contributions. In this work, the major effort has been focused on the inclusion of the effects of the material-fabric on the *THM* behaviour. This document has been organized in such a way that the main conclusions are presented in detail at the end of each Chapter. Because of that, in this section only some remarks and the main general conclusions are included.

An open and general *THM* mathematical approach for porous media with two distinctive types of voids has been proposed. In spite of the relatively simple way in which concepts of double structure have been included, it has been shown that the *THM* framework is able to consider typical behaviours of such type of media. The approach has been implemented in the CODE_BRIGTH program allowing the incorporation of these concepts in numerical analyses. In general terms, it can be concluded that the double structure *THM* approach has revealed a good performance in all of the problems analysed, at least in qualitative terms. The more relevant phenomena responsible for the material behaviour, as well as their main interactions have been included in the analyses. Considering that the fields in which the formulation can be potentially applied are so wide and the processes involved are generally highly coupled and complex, it appears pretentious to affirm that the formulation is fully defined. In that sense, the aim has been to present the approach as an open framework for double structure media in which specific constitutive models for the mechanical, hydraulic and thermal problem, as well as new advances, can be integrated if the characteristics of the problem require it.

The modelling has been mainly focused on the study of the coupled *THM* process in engineered clay barriers and seals. So, special attention has been placed on the formulation of a *THM* model for expansive soils, which are generally used as a buffer material. A double structure model, based on the general framework for expansive materials proposed by Gens & Alonso (1990) has been presented. In order to be closer to the typical fabric of expansive materials, the existence of two pore structures has been explicitly included in the formulation. The distinction between the macrostructure and microstructure provides the opportunity to take into account the dominant phenomena that affect the behaviour of each structure in a consistent and adequate way. The mechanical constitutive model has been formulated using concepts of elasto-plasticity for strain hardening materials. A well-known elasto-plastic model for unsaturated soils, which describes the macrostructural behaviour, has been combined with a generalized plasticity model to reproduce the irreversible effects related to the interaction between the two structural levels.

The comprehensive mathematical framework used to formulate the model has been presented in detail. Special attention has been placed on the concepts of the generalized plasticity theory. The difficulty to clearly identify the yield surface of the plastic mechanisms associated to the coupling between the pore structures underlies the adoption of this theory. Additionally, the inclusion of generalized plasticity concepts has provided a major flexibility that makes it very suitable for practical applications and for the incorporation of new phenomena in the formulation. Also, the particular case of classical plasticity (when the yield surface can be identified) can be reproduced within this theory without problems.

In order to implement the model in the numerical code, the selection of algorithm has been based on the need of an accurate solution and also on consideration of robustness and efficiency. The numerical integration of the model has been developed using a refined Euler scheme with automatic sub-stepping and error control. The algorithm is an adaptation of Sloan's scheme (Sloan, 1987; Sloan *et al.* 2001) to the specific characteristics of this model. The algorithm has been extended to update stresses and internal variables (hardening and history variables) in terms of the increment of the generalized strains, which are: strains, macrostructural suction, microstructural suction and temperature. Another extension of the scheme is related to the handling of more than one irreversible mechanism (specifically a model based on classical plasticity plus another one based on generalized plasticity). Sloan's algorithm has two main characteristics. One of them is that the size of each sub-increment may vary through the integration process depending on the non-linearity of the constitutive relations; this allows finding efficiently the updated stresses. The other main feature of the model is that it offers the possibility to control the errors in the stresses and hardening variables up to a desired level. This permits integrating accurately the constitutive law. The performance of the algorithm in the application cases presented in this Thesis was excellent. The robustness exhibited by the scheme is especially remarkable.

A good performance of the double structure approach has been observed in the different application cases analysed in this work. Particularly interesting has been the experimental validation of the mechanical model, which considered a wide experimental program carried out on the FEBEX bentonite. It is important to highlight that despite the relative complexity of the model, only standard tests of unsaturated soil mechanics have been used to identify the great part of parameters. A good response of the model has also been observed in other application cases, involving cyclic and thermal load. It can be concluded that a deeper insight of the behaviour of the compacted bentonite, and of the basic mechanisms controlling it, has been achieved using the double structure framework. Most of the main features of behaviour are correctly reproduced by the model, allowing a more detailed examination of the role that the different variables play on the explanation of the overall behaviour of the soil.

The formulation has also been applied to other types of materials and problems; two of them have been presented in this Thesis. For instance, the problem of consolidation in fissured clays has been analysed, showing a good performance of the model when the computed outputs are compared with the results of the analytical solution available for this problem. The other case corresponds to the study of the water-flooding process in a petroleum exploitation with a preferential flow path in the formation. The results obtained in this multiphase flow case are also interesting showing the potential of the formulation to simulate these kinds of problems.

The large scale heating test known as *mock-up* test (FEBEX Project, 2001) has been studied in detail. This experiment has been analysed with models of different degree of complexity and including some phenomena generally ignored in standard *THM* simulations. Initially a model formulated in the context of a fully coupled *THM* approach for single porosity media has been used. It can be said that all the steps and requirements recommended to develop a standard *THM* model have been fulfilled. But the obtained results are not completely satisfactory, since the simulation over-predicts the hydration rate of the barrier.

Comparing experimental data versus model results, a slowing down in the hydration kinetics of the test can be observed. A tendency to maintain a constant and very low rate of water intake and nearly constant values of the main variables (relative humidity and stresses) in different radii of the barrier can be observed in all the sections of the test. It seems that a 'standard *THM* model' has some problems to reproduce accurately this type of behaviour because, generally, this problem is handled considering a progressive increment of the water permeability as saturation progresses. But experimental evidence reflects that the behaviour under hydration of expansive clays is more complex. In that sense, the problems in the simulation of the *mock-up* test could be ascribed to other processes or phenomena, which were not contemplated in this first model. So, a series of developments were made in order to include in the analyses additional phenomena that could explain, with physical basis, the barrier behaviour. The effect of a threshold gradient in the permeability law, the presence of thermo-osmotic flows and also the effects of the clay fabric evolution have been included in a set of preliminary analyses carried out using very simple models. According with the obtained results it can be said that each phenomenon could explain, to some extent, the unforeseen response of the experiment.

A more detailed analysis of the effects of the clay fabric changes on the *mock-up* test evolution has been approached using the double structure framework. The use of such kind of model seems suitable for the case of the FEBEX bentonite in which the two pore levels actually exist. The modelling results can be considered as satisfactory since the main tendencies of the observed behaviour have been correctly reproduced, including the evolutions in the characteristic sections of the barrier. It is stressed that this study can be considered as a first step in this kind of analysis and the obtained results have mainly a qualitative significance. According to the model results, as the barrier hydration goes on, the pores available to the liquid flow suffer a progressive reduction. This is due mainly to the microstructure swelling under confined conditions. As a consequence, the full saturation of the barrier is delayed and in some cases could be virtually stopped. This kind of hydration-locking is even more marked in zones close to the heater. The combination of high differences in the hydraulic gradient (in a cross section) with a significant reduction of the permeability in the zones close to the hydration front reduces the liquid flow supply to the internal zones, which are submitted to heater-induced drying.

The final comment is addressed to the usual discussion about the suitability to increment the degree of the model complexity. As a drawback of the double structure framework presented in this work, it can be mentioned that there is an increment in the number of model parameters and also a higher computational cost, associated to the increment in the number of variables. On the other hand, the fact that the conceptual model can be closer to the observed material behaviour largely compensates the commented shortcomings. The double structure model allows the consideration of processes and phenomena while simple models can not, and it becomes also a useful tool to a better understanding of the material behaviour. Several cases analysed in this Thesis are examples of the benefit that this kind of model can yield to explain complex responses observed under real conditions.

6.2 FUTURE WORK

The framework presented in this Thesis is quite general and the problems to which it can be potentially applied are significantly complex, so a significant number of lines for future work and developments are open. Some of them are proposed in the following paragraphs.

It is recommended to apply the formulation to other cases related to the *THM* behaviour of low permeability material. In relation to the design of radioactive waste disposals, there are several projects addressed towards the study of the *THM* behaviour of clay barriers. For instance, different experiments at field conditions have been carried out in the following laboratories: Grimsel (Switzerland), Aspö (Sweden), Mont Terri (France), HADES (Mol, Belgium), AECL (Canada) and Yucca Mountain (USA). The analysis of these experiments would allow extending the validation of the framework to other materials and conditions. Additionally, these experiments are generally supported by a series of laboratory tests which could help in the determination of the main models parameters.

Particularly interesting could be the application of this framework to model the *in situ* experiment, the other large-scale test of the FEBEX project. In some sections of the experiment, a similar tendency to a low hydration, as the one observed in the *mock-up* test (Chapter V), can be noted. This trend is less marked compared with the *mock-up* test observations, at least according to the measurements obtained previous to the partial-dismantling of the test, which took place on the day 1827 of the test. Note that the global density of the bentonite in this test is lower than the one of the *mock-up* test. This fact could imply either that these kind of phenomena are less noticeable or that they appear at a more advanced stages of hydration.

As commented previously, the behaviour of the materials involved in these problems is highly complex. This implies that generally a full characterization of them via laboratory tests, in which different *THM* conditions and paths are contemplated, is not easy to achieve. So, a detailed formulation of the constitutive models or the experimental determination of all the model parameters is also a difficult task. For this reason, many results presented in this Thesis can be considered mainly of qualitative significance. It is necessary to advance more in the experimental characterization of these materials and also in the formulation of constitutive models closer to the observed material behaviour in order to achieve a closer quantitative agreement. In the following paragraphs some aspects of the constitutive model are discussed in more detail.

Concerning the mechanical law for expansive materials, possibly the aspect of the model that requires a more detailed treatment is related to the temperature effects. As commented in Chapter III, a global (macroscopic) thermal response of the material is considered at the macrostructural level of the model. The scarcity of experimental data is a limitation, for the moment, to improve this model feature. Closely linked to this aspect, it could be mentioned the inclusion of the temperature as a driving force for the mass transfer of water (Ma & Hueckel, 1986). According with experimental evidences, this mass transfer process between macro and microstructure could play a significant role to explain certain features of expansive clays under non-isothermal conditions (Villar *et al.,* 2003). On the other hand, the validation of the mechanical model for other loading paths including also deviatoric loads is pending until the availability of the laboratory tests.

As expressed in Chapter III, the constitutive law adopted for the microstructural level is very simple and some improvements can be made in this line. Note that the model assumes an elastic behaviour of the microstructure, and all the irreversible behaviour is ascribed to the interaction mechanisms between pore structures (and also to the *BBM*). It is possible that some microstructural phenomena are not purely elastic, so the inclusion of a plastic behaviour of the microstructure could be necessary. Additionally the consideration of the actively clay fraction present in the material could be another interesting aspect to take into account. In this context, the work of Komine & Ogata (1994) can be considered as a reference.

Additional developments can be suggested also for the hydraulic constitutive models. Although the permeability models used in the simulations can be considered better compared with the single porosity model, the law adopted for its definition is simple and improvements can be made. The inclusion in the permeability law of more information related to the clay fabric would allow the definition of enhanced models. For instance in the works of Garcia-Bengochea *et al* (1979), Acar *et al.* (1985), Juang & Holtz (1986), Acar & Olivieri (1990), Lapierre *et al.* (1990) and Hueckel *et al.* (1997), among others, pore size distribution (PSD) data, has been used to propose permeability models based on probabilistic concepts. The development of such kind of model appears to be not simple for the case of expansive clays. Note that due to the dynamic character of the clay fabric during hydration a lot (and detailed) experimental data (PSD) is needed. Moreover, a particularly complex behaviour is observed in some tests performed over the FEBEX bentonite, in which emerging pore modes (between the macro and micro pores) appear (Romero *et al,* 2003). Similar points can be considered related to the development of models for the retention curve.

From a numerical point of view, the algorithm developed to integrate the mechanical model has exhibited a good performance in all the cases analysed in this Thesis. However, the implicit methods have some advantages that encourage their utilization in future developments. Perhaps the more relevant one is related to the fact that it provides all the information required to evaluate the consistent tangent matrix, which gives a quadratic rate of convergence for the global Newton-Raphson scheme. Additionally, the development and implementation of the model using an implicit scheme would allow the comparisons between the performances of both schemes when complex *THM* or geotechnical problems are considered.

Regarding the double structure formulation presented in Chapter II, some additional developments can be suggested. It has been assumed that thermal equilibrium between the two domains exists and, consequently, the two media have the same temperature. This hypothesis can be considered suitable for the non-isothermal problems in clayey media solved in this Thesis, in which the very low permeability allows admitting this assumption. But, when the medium is characterized by the presence of preferential flow paths this hypothesis can no longer be maintained. Different temperatures in the two media are required for a proper handling of these problems. This situation can be found in geothermal problems related to low permeability media. Also, in some petroleum productions cases this situation can be found when non-isothermal techniques are used. The extension of the double porosity formulation to this case can be made in a quite straightforward way. In this context the approach presented by Khalili *et al.* (1999) can be used as a reference work.

The mass transfer process between media has been modelled using quasi-steady models, so, a constant value for leakage parameter has been adopted. (Barenblatt *et al.*, 1960; Warren & Root, 1963; Huayakorn *et al.*, 1983; Callari & Federico, 2000). It has been considered that this type of model is suitable for many of the analyses performed in this Thesis. As commented, another treatment of the mass transfer term can be made through the unsteady models (Huayakorn *et al.,* 1983). In these models the transfer of mass between media is obtained solving the 1-D diffusion equation for an idealized geometry (parallel fracture and prismatic or spherical blocks) of the matrix pores (Streltsova-Adams, 1978; Huyakorn *et al.*, 1983, Kazemi *et al.*, 1976). The drawback of these models is related to the computational cost, because a 1D system must be locally solved at every mesh node. But, on the other hand, a more general representation of the problem is obtained. The *THM* formulation presented in this Thesis is general and both kinds of models can be used. So, a possible next step is the inclusion of unsteady models in the analysis of some problems. For instance, its extension to the case of non-expansive materials (for example: fractured rocks media) is quite direct. Other problem in which the adoption of unsteady models could be more suitable is the one related to the analysis of pellet mixtures. Perhaps a weakness of unsteady models to analyse these expansive materials, is related to the adoption of fixed geometric shape to model the pellets. This is a basic hypothesis of the model, and it is difficult that this shape will be maintained in the case of swelling materials during wetting, especially when confined conditions prevail.

Finally, it is obvious that the natural evolution of the formulation is the inclusion of geochemical variables in the double structure framework. It can be mentioned that some advances have been made in this direction. For instance, the original *THM* formulation (Olivella *et al.*, 1994) has been extended to handle the reactive transport problem (Guimarães, 2002). Some analyses related to the behaviour of engineered clays barrier including geochemical variables in the simulations have also been made (Guimarães, 2002; Guimarães *et al.*, 2003). The mechanical constitutive model has been extended to include the effects of osmotic suction and exchangeable cations on the mechanical behaviour of expansive clays (Guimarães *et al.*, 2001, Guimarães, 2002). However, there are several open research lines related to the formulation and modelling of the *THMC* behaviour of low permeability media considering the material fabric. For instance, it could be mentioned the identification and modelling of the main *THMC* phenomena and couplings that take place at each structural level; their influence on the main properties of the material and their effect on the final behaviour of low permeability media.

.

REFERENCES

Abbo, A. (1997). "Finite element algorithms for elastoplasticity and consolidation". *PhD Thesis, University of Newcastle, Australia*, 271 pp.

Accar, Y., Hamidon, A., Field, S. & Scott, L. (1985). "The effect of the organic fluids on the hydraulic conductivity of compacted kaolinite". *Hydraulic barriers in soils and rock*, ASTM STP 874, pp. 171-187.

Accar, Y. & Oliveri (1989). "Pore fluid effects on the fabric and hydraulic conductivity of laboratory-compacted clay". *Transportation Research Record*, 1219, pp. 144-159.

Aifantis, E. (1980). "On the problem of diffusion in solids". *Actha Mechanica*, Vol 37, Nº 3-4, pp. 265-296.

Al-Homoud, S., Basma, A., Malkawi, H., & Bashabsheh, A. (1995). "Cyclic swelling behavior of clays". *Journal of Geotechnical Engineering, ASCE*. Vol.121, Nº7, pp. 562-565.

Al-Mukhtar, M., Qi, Y., Alcover, J.F. & Bergaya, F. (1999). "Oedometric and water-retention behavior of highly compacted unsaturated smectites". *Can. Geotech.* J., 36, pp. 675-684.

Alonso, E. (1998). "Modelling expansive soil behaviour". *Second International Conference on Unsatured Soils*. Beijing, China. Vol.1, pp. 37-70

Alonso, E., Lloret, A., Delahaye, C., Vaunat, J., Gens, A., &. Volckaert, G. (1998). "Coupled analysis of a backfill hydration test". *Int. Jnl. Numer. Anal. Meth. Geomech*, Vol. 22(1), pp. 1-27.

Alonso, E. & Alcoverro, J. (1999). "CATSIUS CLAY Project. Calculation and testing of behaviour of unsaturated clay as barrier in radioactive waste repositories. Stage 2 : validation exercises at laboratory scale". *Technical publication* Nº 11/99 ENRESA, Spain.

Alonso, E.E., Gens, A. & Gehling, W. (1994). "Elastoplastic model for unsaturated expansive soils". *3rd Conf. Num. Meth. Geotech. Engng*, pp. 11-18.

Alonso, E.E., Gens, A. and Hight, D.W. (1987). "Special problem soils. General report. Proc". *9th Eur. Conf. SMFE*, 3, pp. 1987-1146.

Alonso, E., Gens, A. & Josa, A. (1990). "A constitutive model for partially saturated soils". *Géotechnique*, 40, 3, pp. 405-430.

Alonso, E., Gens, A. & Lloret, A. (1991). "Double structure model for the prediction of long-term movements in expansive materials". In *Computer Methods and Advances in Geomechanics Beer, Booker, Carter, (ed.) Balkema, Rotterdam*. 1; pp. 541-548.

Alonso, E.E, Lloret, A., Gens, A. & Yang D.Q. (1995). "Experimental behaviour of highly expansive double-structure clay". *Proc. 1rd Int. Conference on Unsaturated Soils, Paris*. Balkema. Vol. 1, pp. 11-16.

Alonso, E.E, Romero, E., Hoffmann, C, & Garcia-Escudero, E, (2001). "Expansive bentonite/sand mixtures in cyclic controlled-suction". *6th International Workshop on Key Issues in Waste Isolation Research*. Paris.

Alonso, E., Vaunat, J. & Gens, A. (1999). "Modelling the mechanical behaviour of expansive clays". *Engineering Geology*, 54, pp. 173-183.

Al-Rawas, A.A. & McGown, A. (1999). "Microstructure of Omani expansive soils". *Can. Geotech.* J., 36, pp. 272-299.

Anderson, D.M. & Low, P.F. (1958). "The density of water adsorbed by lithium-, sodium-, and potassium-bentonite". *Soil Science Society Am. Proceedings*, 22, pp. 99-103.

Appelo, C. & Postma, D. (1993). "Geochemistry Groundwater and Pollution". *Balkema, Rotterdam*, 536 pp.

Atabek, R. B., Felix, B., Robinet, J.C., and Lahlou, R. (1991). "Rheological behaviour of saturated expansive clay materials". *Workshop on Stress Partitioning in Engineered Clay Barriers*. Duke University, Durham, N.C.

Bai, M., Ma, Q. & Roegiers, J. (1994). "Dual-porosity behaviour of naturally fractured reservoirs". Int. Jnl. Numer. Anal. Meth. Geomech.,Vol. 18, pp. 359- 376.

Bailey, B., Crabtree, M., Tyrie, J., Elphick, J., Kuchuk, F., Romano, C. & Roodhart, L (2000). "Water Control". Oilfield Review, Spring, pp. 30-51.

Baldi, G., Hueckel, T. & Pellegrini, R. (1988). "Thermal volume changes of the mineral-water system in low-porosity clays soils". *Can. Geotech. Jnl.*, 25, pp. 807-825.

Barrenbaltt, G., Zeltov, I. & Kochina, N. (1960). " Basic concepts in the theory of seepage of homogeneous liquids in fissured rocks". *Pirkl. Mat. Mekh.* 24, pp. 852-864.

Basma, A., Al-Homoud, S., Malkawi, H. & Bashabsheh, A. (1996). "Cyclic swelling behavior of clays". *Applied Clay Science* 11, pp. 211-227.

Batchelor, G:K: (1983). "Fluid Dynamics". *Cambridge University Press.*

Bear, J. (1972). "Dynamics of fluids in porous media". *Dover Edit.*, 164 pp.

Bernier, F., Volckaert, G., Alonso, E. & Villar, M. (1997). "Suction-controlled experiments on Boom clay". *Engineering Geology*, 47, pp. 325-338.

Borja, R. (1991). "Cam-clay plasticity, Part II: Implicit integration of constitutive equations based on a nonlinear elastic stress predictor". *Computer methods in Applied Mechanics and Engineering* 88 pp 225-240.

Borja, R. & Lee, S. (1990). "Cam-clay plasticity, Part I: Implicit integration of elasto-plastic constitutive relations". *Computer methods in Applied Mechanics and Engineering* 78 pp 49-72.

Brackley, I.J., (1973). "Swell pressure and free swell in compacted clay". *Proc. III Int. Conference on Expansive Soils, Academic Press, Haifa,* 1, pp. 169-176.

Birkholzer, J. & Tsang, W. (2000). "Modelling the thermal-hydrologic processes in a large-scale underground heater test in partially saturated fractured tuff". *Water Resources Research*, Vol. 36 Nº 6, pp. 1431-1447.

Callaghan, I.C. & Ottewill, R.H. (1974). "Interparticle forces in montmorillonite gels". *Faraday Discussions of the Chemical Society,* 57, pp. 110-118.

Callari, C. & Federico, F. (2000). "FEM validation of a double-porosity elastic model for consolidation of structurally complex clayey soils". *Int. Jnl. Numer. Anal. Meth. Geomech.*,Vol. 24, pp. 367- 402

Car, E. (2000). "Modelo constitutivo para el estudio del comportamiento mecánico de las materuakles compuestos". *Phd Thesis*, Departament of materials and structures Technical University of Catalunya, Spain.

Carol, I. & Prat, P. (1999). "A multicrack model based on the theory of multisurface plasticity and two fractures energies". *Proceedings IV Conference on Computational Plasticity, Barcelona* pp. 1583-1594.

Carrera, J. (1991). "Hidrogeología de medios pocos permeables". *Memoría XXV Aniversario CIHS,* pp. 47-67.

Carrera, J., Sánchez-Vila, X., Benet, I., Medina, A., Galarza, G. & Guimerà, J. (1997). "On matrix diffusions: formulations, solution methods and qualitative effects. *Hydrogeology Journal*, 6, pp. 178-190.

Cekerevac, C. & Laloui, L. (2004). "Experimental study of thermal effects on the mechanical behaviour of a clay". *Int. Jnl. Numer. Anal. Meth. Geomech.*, Vol 28, pp. 209-228

CIEMAT Report, (2002). "19th Data Report Mock-Up test". *Informe 70-IMA-L-9-96. CIEMAT*. Madrid.

CODE_BRIGHT User's Manual (2004). *UPC Geomechanical Group.*

Crisfield, M. (1991). "Non-linear finite element analysis of solids and structures Vol 1". *John Wiles & Sons Edit.*, 345 pp.

Cuadros, J. Linares, J. (1996). "Experimental kinetic study of the smectite-to-illite transformation". *Geochim.Cosmochim.Acta,* 60, pp. 439-453.

Cuevas, J., Villar, M.V., Fernández, A. M., Gómez, P. & Martín, P.L. (1996). "Pore waters extracted from compacted bentonite subjected to simultaneous heating and hydration". *Applied Geochemistry*, 12, pp. 473-481.

Cui, Y., Loiseau, C. & Delage, P. (2001). "Water transfer through a confined heavily compacted swelling soil". *Proc. 6th International Workshop on Key Issues in Waste Isolation Research, Paris,* pp. 43-60

Cui, Y., Loiseau, C. & Delage, P. (2002a). "Microstructure changes of a confined swelling soil due to suction controlled hydration". *Proceedings 3rd Int. Conference on Unsaturated Soils, Recife*, 2, pp. 593-598

Cui, Y., Sultan, N. & Delage, P. (2000). "A thermomechanical model for clays". *Can. Geotech. Jnl.*, 37, pp. 607-620.

Cui, Y.J., Yahia-Aissa, M., Dalage, P. (2002b). "A model for the volume change behavior of heavily compacted selling clays". *Engineering Geology*, 64, pp. 233-250.

Cuisinier, O. & Masrouri, F. (2001). "Study of the hydromechanical behaviour of a swelling soil from low to very high suctions". *6th International Workshop on Key Issues in Waste Isolation Research, Paris*, pp. 61-70.

Chen, F.H., & Ma, G, H. (1987). "Swelling and Shrinkage Behaviour of Expansive Clays". *Proc. 6th Int. Conference on Expansive Soils,* New Delhi. Vol. 1, pp. 127-129.

Day, R.W. (1994). "Swell-Shrink Behaviour of Compacted Clay". *Journal of Geotechnical Engineering, ASCE*. Vol 120 Nº3, 618-623.

de Borst, R. & Heeres, O. (2002). "A unified approach to the implicit integration of standard, non-standard and viscous plasticity models". *International Journal for Numerical and Analytical Methods in Geomechanics* Vol. 26, 1059-1070.

de Marsily, G. (1986). "Quantitative Hydrogeology". *Academic Press, Inc.* ISBN 0-12-208916-2. 440 pp.

Demars, K & Charles, R. (1982). "Soil volume changes induced by temperature cycling". *Can. Geotech. Jnl.*, 19, pp. 188-194.

Delage, P, Howat, M. & Cui, Y. (1998). "The relationship between suction and swelling properties in a heavily compacted unsaturated clay". *Engineering Geology* 50. 1-2 pp. 31-48.

Delage, P, Sultan, N. & Cui, Y. (2000). "On the thermal consolidation of Boom clay". . *Can. Geotech. Jnl.*, 37, pp. 343-354.

Djeran, I. (1993). "Étude des duffusions thermique et hydraulique dans una argile soumise á un champ de température". *Sciences et techniques nucléaires rapport.* Commission des Communautés européennes, ISBN 1018-5593.

Dif, A. & Bluemel, F. (1991). "Expansive soil under cyclic drying and wetting". *Technical note, Geotech. Testing J. GTJODJ*, Vol 14. Nº1 Vol. 1, 96-102.

Dixon, D., Gray, M. & Hnatiw. (1992). "Critical gradients and pressures in dense swelling clays". *Can. Geotech. Jnl.*, 29, pp. 1113-1119.

Dixon, D., Gray, M., Lingnau, B., Graham, J. & Campbell, S. (1993). "Thermal expansion testing to determine the influence of pore water structure on water flow through dense clays". *Proceedings of 46 th Annual Canadian Geotechnical Conference,* pp. 177-184

Dixon, D., Graham, J. & Gray, M. (1999). "Hydraulic conductivity of clays in confined tests under low hydraulic gradients". *Can. Geotech. Jnl.*, 36, pp. 815-825.

Dixon, D., Chandler, N., Graham, J. & Gray, M. (2002). "Two large-scale sealing tests conducted at Atomic Energy of Canada's underground research laboratory: the buffer-container experiment and the isothermal test". *Can. Geotech. Jnl.*, 39, pp. 503-518.

Dueck, A. & Börgesson, L. (2001). "Constant volume tests with suction control performed on a swelling clay". *6th International Workshop on Key Issues in Waste Isolation Research, Paris*, 83-101

ENRESA (1997). "Reunión de urgencia para analizar incidencias durante la hidratación de la maqueta y decidir eventuales actuaciones". *Acta de Reunión 70-ST-C-9-27.* Madrid.

FEBEX Project, (2000). "Full-scale engineered barriers experiment for a deep geological repository for high level radioactive waste in crystalline host rock". *Final project report.* EUR 19612 EN, European Commission, Brussels.

FEBEX Report, (1997). "Caracterización geoquímica de bentonita compactada: efectos producidos por flujo termohidráulico". *Informe 70-IMA-M-0-2. CIEMAT*. Madrid.

FEBEX Report, (1998). "Preoperational Thermo-Hydro-Mechanical (THM) modelling of the 'mock-up' test". *Publicación Técnica Nº 10/98. ENRESA*. Madrid.

Fernández, A. Mª. (2003). "Caracterización y modelización del agua intersticial de materiales arcillosos: Estudio de la bentonita de Cortijo de Archidona". *Phd Thesis*. Madrid. pp 559.

Fernández, A. Mª. (2004). Personal communication.

Fernández, A. Mª., Baeyens, B., Bradbury, M. & Rivas, P. (2003). "Analysis of the pore water chemical composition of a Spanish compacted bentonite used in an engineered barrier". *Applied Clay Science*. in press.

Fernández, A. Mª. & Rivas, P. (2003). "Analysis of types and distribution of waters in the FEBEX bentonite used as an engineered barrier". *EUROCLAY 2003 Congress, Modena (Italy)*. pp. 96-97.

Fredlund, D., & Xing, A. (1994). "Equations for the soil-water characteristic curve". *Can. Geotech. Jnl.*, 31, pp. 521-532.

Fuente-Cantillana, J., Garcia-Siñeriz, J. & Tuñon, S. (2001). "Monte-Terri Heating Experiment (HE) 'As-built' report". *AITEMIN Report*.

Garcia Escudero, E. (2001). "Comportamiento de los suelos expansivos bajo ciclos de succión". *Tesina de Especialidad* Geotechnical Engineering Department, Technical University of Catalunya, Spain.

Garcia-Bengochea, I., & Lowel, C. (1981). "Correlative measurements of pore size distributiuon and permeability in soils". *In Peremability and ground water contaminant transport; Zimmiie, T., & Riggs, C. American Society for testing and materials,* Philadelphia, Nº 746, pp. 137-150.

Garcia Molina, A., Gens, A. & Olivella, S. (1996). "Un modelo constitutivo para suelos no saturados sometidos a variaciones térmicas: formulación, implementación y aplicaciones". *III Congreso de Métodos Numéricos en Ingeniería. Spain,* pp. 503-512.

Gatmiri, B. & Delage, P. (1997). "A formulation if fully coupled thermal-hydraulic-mechanical behaviour of saturated porous media-numerical approach". *Int. Jnl. Numer. Anal. Meth. Geomech*, Vol. 21, pp. 199- 225.

Gawin, D., Baggio, P. & Schhrefler, B.A. (1995). "Coupled heat, water and gas flow in deformable porous media". *Int. J. Num. Meth. Fluids*, 20: pp. 967-987.

Gens, A. 1995. "Constitutive Laws". In *Modern issues in non-saturated soils, A. Gens P. Jouanna & B. Schrefler (ed.)*: Wien New York: Springer-Verlag. pp. 129-158.

Gens, A. (2003). "The role of geotechnical engineering for nuclear energy utilisation". *Proceeding of XIII European Conference of Soils Mechanics and Geotechnical Engineering, Prague.*

Gens, A. & Alonso, E.E. (1992). "A framework for the behaviour of unsaturated expansive clays". *Can. Geotech. Jnl.*, 29, pp. 1013-1032.

Gens, A., Guimarães, L., Olivella, S., & Sánchez, M. (2003). "Analysis of the THMC behaviour of compacted swelling clay in radioactive waste isolation". *International Conference on Coupled T-H-M-C Processes in Geosystem. Fundamentals, Modelling, Experiment and Applications. GeoProc 2003. Stockholm.*

Gens, A., Garcia Molina, A, Olivella, S., Alonso, E.E. & Huertas, F. (1998). "Analysis of a full scale in-situ test simulating repository conditions". *Int. Jnl. Numer. Anal. Meth. Geomech*, Vol. 22, pp. 515- 548.

Gens, A. & Olivella, S. (2001). "THM phenomena in saturated and unsaturated porous media. Fundamentals and formulation". *Revue.française de génie civil*, Vol 5, Nº 6, pp. 693-717.

Ghafouri, H. & Lewis, R. (1996). "A finite element double porosity model for heterogeneous deformable porous media". *Int. Jnl. Numer. Anal. Meth. Geomech*, Vol. 20, pp. 831- 844.

Graham, J., Tanaka, N., Crilly, T. & Alfaro, M. (2001). "Modified cam-clay modelling of temperature effects in clays". *Can. Geotech. Jnl.*, 38, pp. 608-621.

Guimarães, L. N. (2002). "Análisis multi-componente no isotermo en medio poroso deformable no saturado". *Phd Thesis*, Geotechnical Engineering Department, Technical University of Catalunya, Spain.

Guimarães L. do N., Gens, A., Olivella, S. 1999. "THM and reactive transport coupling in unsaturated porous media". *In 7th Int. Symp. on Numerical Models in Geomech., NUMOG VII.* Rotterdam: Balkema, pp. 303-308.

Guimaraes L., Gens A. & Olivella S. (2003). "Coupled analysis of damage formation around wellbores. *International Conference on Coupled T-H-M-C Processes in Geosystem. Fundamentals, Modelling, Experiment and Applications. GeoProc 2003. Stockholm.*

Guimaraes L., Gens A., Sánchez M., Olivella S. (2001). "Chemo-mechanical modelling of expansive materials". *6th International Workshop on Key Issues in Waste Isolation Research.* Paris.

Güven, N., Low, P., Mitchell. J., Sposito, G. & van Olphen, H. (1993). "Clay-water interface and its rheological implciations". *CMS Workshop Lectures*. Vol. 4. R.E.Ferrel Editor. The clay mineral Society, Colorado, USA.

Güven, N., (1990). "Longevity of bentonite as buffer material in a nuclear-waste repository" *Engineering Geology,* 28. pp 233-247.

Hansbo, S. (1960). "Consolidation of clay with special reference to influence of vertical sand drains". *Swedish Geotech. Inst. Proc.* Nº 18 Stockholm.

Hensen, E. & Smit, B. (2002). "Why clays swell". *J. Phys. Chem. B.* 106, pp. 12664-1667.

Heeres, O. 2001. "Modern Strategies for the Numerical Modelling of the Cyclic and Transient Behaviour of Soils". *PhD Thesis, Delft University Press.*

Hoffmann, C. (2004). "Caracterización hidromecánica de mezclas formadas por pellets de bentonita. Estudio Experimental y Constitutivo". *Phd Thesis*, Geotechnical Engineering Department, Technical University of Catalunya, Spain.

Hueckel, T. (1992). "Water-mineral interaction in hygromechanics of clay exposed to environmental loads: a mixture-theory approach". *Can. Geotech. Jnl.*, 29, pp. 1071-1086.

Hueckel, T. (2002). "Reactive plasticity for clays during dehydration and rehydration. Part 1: concepts and options". *International Journal of Plasticity*, 18, pp. 281-312.

Hueckel, T., & Baldi, G. (1990). "Thermoplasticity of saturated clays: experimental constitutive study". *Journal of Geotechnical Engineering, ASCE*, Vol 116 Nº 12, pp. 1778-1795.

Hueckel, T., & Borsetto, M. (1990). "Thermoplasticity of saturated soils and shales: constitutive equations". *Journal of Geotechnical Engineering, ASCE*, Vol 116 Nº 12, pp. 1765-1777.

Hueckel, T., Kaczmarek, M. & Caramuscio, P. (1997). "Theoretical assessment of fabric and permeability changes in clays affected by organic contaminants". *Can. Geotech. Jnl.*, 34, pp. 588-603.

Hueckel, T., Loret, B. & Gajo, A. (2001). "Swelling materials as reactive, deformable, two-phase continua: basic modelling concepts and options". *Clay Behaviour: Chemo-mechanical coupling, Workshop*. Maratea, Italy.

Hueckel, T. & Pellegrini, R. (2002). "Reactive plasticity for clays: application to a natural analog of long-term geomechanical effects of nuclear waste disposal". *Engineering Geology*, 64, pp. 195-215.

Huertas, F., Caballero, E., Jimenez de Cisneros, C., & Linares, J. (2002). "Propiedades fisico-químicas de la bentonita. Efectos de los cationes de cambio". Estación Experimental del Zaidín. *ENRESA Report: 70-ZAI-L-5-09*.

Huertas, F.J., Huertas, F., Caballero, E., Jimenez de Cisneros, C., & Linares, J. (2003). "Evolución de las propiedades fisico-químicas de la bentonita en los condicionantes de un almacenamiento (proyecto FEBEX II)". *Ponencia V Jornadas de I+D y desarrollo tecnológico de Residuos Radiactivos, ENRESA, Publicación Técnica 08/2003*, Tarragona, Spain.

Hughes, T.J. (1980). "Generalization of selective integration procedures to anisotropic and nonlinear media". *International Journal of Num. Meth. in Eng.* Vol. 15, pp. 1413-1418.

Huyakorn, B., Lester & Faust. C. (1983). "Finite element techniques for modelling groundwater flow in fractured aquifers". *Water Resources Research*, Vol. 19, Nº 4, pp.1019-1035

Ichikawa, Y., Kawamura, K., Fujii, N. & Theramast Nattavut. (2002). "Molecular dynamics and multiscale homogenization analysis of seepage/diffusion problem in bentonite clay". *Int. J. Num. Meth. Engng*, 54 pp. 1717-1749.

Justo, J.L. Delgado, A., Ruiz, J. (1984). The influence of stress-path in the collapse-swelling of soils at the laboratory. *Proc. V Int. Conference on Expansive Soils*, Inst. of Civil Eng of Australia, Adelaide, pp. 67-71.

Juang, C. & Holtz, R. (1986). "A probabilistic permeability model and the pore size density function". *International Journal for Numerical and Analytical Methods in Geomechanics* Vol. 10, pp. 543-553.

Kaczmarek, M., Hueckel, T., Charla, T., & Imperiali, T. (1997). "Transport through a clay barrier with the contaminant concentration dependent permeability". *Transport in porous media*, 29(2), pp. 159-178.

Karaboni, S., Smit, B., Heidug, W., Urai, J. & van Oort, E. (1996). "The swelling of clays: molecular simulations of the hydration of montmorillonite". *Science*, Vol 271. pp. 1102-1105.

Kazemi, H., Merril, L., Porterfield, K. & Zeman, P. (1976). "Numerical simulation of water-oil flow in naturally fracturated reservoirs". *Soc. Pet. Eng. Jnl.* 16, pp. 317-326.

Komine, A. & Ogata, N. (1994). "Experimental study on swelling characteristics of compacted bentonite". *Can Geotech Jnl,* 31, pp. 478-490.

Komine, A. & Ogata, N. (1998). "Thermal influence on compacted bentonite for nuclear waste disposal". In *Environmental Geotechnics. Sêco e Pinto (ed.).* Balkema Rotterdam.

Khalili, N. & Valliappan, S. (1991). "Flow through fissured porous media with deformable matrix: implicit formulation". *Water Resources Research*, Vol.27, Nº 7, pp. 1703-1709.

Khalili, N., Valliappan, S. & Wan, C. (1999). "Consolidation of fissured clays". *Géotechnique*, 49, Nº 1, pp. 75-89.

Khalili, N., Valliappan, S. & Geiser, F. (2000). "A fully coupled thermo-hydro-mechanical model for double porous media". *ECOMAS* 2000, 49, Barcelona.

Kraehenbuehl, F.,Stoeckli, M.F., Brunner, F., Kahr, G., and Müller-Vonmoos, M. (1987). "Study of the water-bentonite system by vapour adsorption, immersion calorimetry and X-ray technique: I Micropore volumes and internal surface areas, following Dubinin's theory". *Clay Minerals*, 22, pp. 1-9.

Kröhn, K. (2002). "New conceptual models for the resaturation of bentonite". *Proc. of Workshop on clay microstructure and its importance to soil behaviour.* Lund, Sweden. Editor Roland Push. pp.32-40.

Laloui, L. & Cekerevac, C. (2003). "Thermo-plasticity of clays: an isotropic yield mechanism". *Computed and Geotechnics*, 30, pp. 649-660.

Lapierre, C., Leroueil, S. & Locat, J. (1990). "Mercury intrusion and permeability of Louiseville clay". *Can. Geotech. Jnl.*, 27, pp. 761-773.

Leonards, G. (1962). "Engineering properties of soils". In *Foundation Engineering, G.A. Leonards (ed.).* McGraw-Hill, New York pp. 102-124.

Lewis, R. & Ghafouri, H. (1997). "A novel finite element double porosity model for multiphase flow through deformable fractured porous media". *Int. Jnl. Numer. Anal. Meth. Geomech*, Vol. 21, pp. 789-816.

Lignau, B., Graham, J., Yarechewski, D., Tanaka, N., & Gray, M. (1996). "Effects of temperature on strength and compressibility of sand-bentonite buffer". *Engineering Geology* 41, pp. 103-115.

Linares, J., Barahona, R., Huertas, F., Caballero, E., Cuadros, J., Huertas, F.J., Jiménez de Cisneros, C., Linares, C., Rodríguez, J. & Martín-Vivaldi, M. (1996). "Alteración hidrotermal de las bentonitas de Almería". Monografía ENRESA, 8/96.

Loret, B., Hueckel, T. & Gajo, A. (2002). "Chemo-mechanical coupling in saturated porous media: elastic-plastic behaviour of homoinic expansive clays". *Int. J. solids and Structures*, 39, pp. 2773-2806.

Low, P. (1961). "Physical chemistry of clay-water interaction". *Adv. Agron.* 13, pp. 269-327.

Lloret, A. (2004). Personal communciation.

Lloret, A., Daucousse D. & Alonso E. (2003). "Results of in-situ measurements of water content and dry density". ENRESA, FEBEX Report, 70-UPC-L-5-012.

Lloret, A. & Villar, M (2001). "Variation of the intrinsic permeability of expansive clays upon saturation". In *Clay Science for Engineering, Adachi & Fukue (ed.)*. Balkema Rotterdam; pp. 259-266.

Lloret, A., Villar, M. & Pintado, X. (2001). "Ensayos THM: Informe de Síntesis". FEBEX Report, 70-UPC-M-0-04.

Lloret, A., Villar, M.V., Sánchez, M., Gens, A., Pintado, X., & Alonso, E. (2003). "Mechanical behaviour of heavily compacted bentonite under high suction changes". *Géotechnique,* 53(1): 27-40

Lubliner, J. 1991. "A simple model of generalized plasticity". *Int. J Solids Structures*, Vol. 28, Nº6, pp. 769-778.

Lubliner, J. & Auricchio, F. 1996. "Generalized plasticity and shape-memory alloys". *Int. J Solids Structures*, Vol. 33, Nº7, pp. 991-1003.

Ma, F. & Hueckel, T. (1992). "Stress and pore pressure in saturated clay subjected to heat frm radioactive waste: a numerical simulation". *Can Geotech Jnl,* 29, pp. 1087-1094.

Madsen, F. & Müller-VonMoos, M. (1989). "The swelling behaviour of clays". *Applied Clay Science*, 4, pp. 143-156.

Martin, P., & Villar, M., (1997). "Propiedades hidráulicas del geotextile utilizado en el ensayo de maqueta del proyecto FEBEX". Informe Técnico *ENRESA: 70-IMA-L-3-32.*

Martin, P., & Villar, M., (2004). "Mock-Up hydration problems". (in preparation). CIEMAT. *ENRESA: 70-CIE-X-N-NN.*

Marcial, D. (2003). "Comportement hydromecanique et microstructural des materiaux de barriere ouvragee". *Phd Thesis* CERMES L' Ecole Nationales des ponts et chausses France.

Marcial, D., Delage, P. & Cui, Y.J. (2002). "On the high stress compression of bentonites". *Can Geotech Jnl*, 39, pp. 812-820.

Master , I., Pao, W. & Lewis, R. (2000). "Coupling temperature to a double-porosity model of deformable porous media". *Int. J. Numer. Meth. Engng*, 49, pp. 421-438.

Miller, R. & Low, P. (1963). "Threshold gradient for water flow in clay systems". *Sols Sci. Soc. Amer. Proc.* 33, pp. 605-609.

Mitchell, J. (1991). "Conduction phenomena: from theory to geotechnical practice". *Géotechnique*, 41, 3, pp. 299-340

Mitchell, J. (1993). "Fundamentals of soil behaviour". *2nd ed. John Wiley & Sons*, 437 pp.

Modaressi, H. & Laloui, L. (1997). "A thermo-viscoplastic constitutive model for clays". *International Journal for Numerical and Analytical Methods in Geomechanics* Vol. 21, pp. 313-335.

Murad, M. & Cushman, J. (1997). "A multiscale theory of swelling porous media: II. Dual porosity models fro consolidation of clays incorporating physicochemical effects". *Transport in porous media*, 28, pp. 69-108.

Murad, M. & Cushman, J. (2000). "Thermomechanical theories for swelling porous media with microstructure". *International Journal of Engineering Science* 38, pp 517-564.

Musso, A. & Federico, F. (1993). "Consolidation of highly fissured clays". *Rivista Italiana di Geotecnia*; 3, 247-273 (in Italian).

Musso, G, Romero, E., Gens, A. & Catellanos, E. (2003). "The role of the structure in the chemically induced deformations of FEBEX bentonite". *Applied Clay Science,* 23, pp.229-237.

Navarro, V. (1997). "Modelo del comportamiento mecánico e hidráulico de suelos no saturados en condiciones no isotermas". *Phd Thesis*, Geotechnical Engineering Department, Technical University of Catalunya, Spain.

Navarro, V. & Alonso, E. (2000). "Modelling swelling soils for disposal barriers". *Computed and Geothecnics*, 27, pp. 19-43.

Navarro, V & Alonso, E. (2001). "Secondary compression of clays as a local dehydration process". *Géotechnique*, 51, Nº 10, pp. 859-869.

Neuzil, C. (1986). "Groundwater flow in low-permeability environments". *Water resources research*, Vol 22, Nº 8, pp. 1163-1195.

Olivella, S., (1995). "Non-isothermal multiphase flow of brine and gas through saline media". *Phd Thesis*, Geotechnical Engineering Department, Technical University of Catalunya, Spain.

Olivella, S., Carrera J., Gens, A. & Alonso, E.E. (1994). "Non-isothermal multiphase flow of brine and gas through saline media". *Transport in porous media*, 15, pp. 271-293.

Olivella, S., Gens, A., Carrera, J. & Alonso, E.E. (1996). "Numerical formulation for a simulator (CODE-BRIGHT) for the coupled analysis of saline media". *Engineering Computations*, 13, 7, pp. 87-112.

Olivella, S. & Gens, A. (2000). "Vapour transport in low permeability unsaturated soils with capillary effects". *Transport in porous media*, 40, pp. 219-241.

Ormerod, E.C. & Newman, A.C.D. (1983). "Water sorption of Ca-saturated clays:II. Internal and external surfaces of montmorillonite". *Clay minerals*, 18, pp. 289-299.

Ortiz, M & Simo, J. (1986). "An analysis of a new class of integration algorithms for elasto-plastic constitutive relations". *International Journal for Numerical Methods in Engineering* Vol. 23, pp. 353-366.

Pasquiou, A. (2001). "Pellets d'argile gonflante elaboration et caracterisation hydromecanique". *Phd Thesis* L' Université des Sciences et Technologie de Lille, France.

Pastor, M., Zienkiewics, O., & Chan, A. (1990). "Generalized plasticity and the modelling of soil behaviour". *International Journal for Numerical and Analytical Methods in Geomechanics* Vol. 14, pp. 151-190.

Pintado, X., (2002). "Caracterización del comportamiento termo-hidro-mecánico de arcillas expansivas". *Phd Thesis*, Geotechnical Engineering Department, Technical University of Catalunya, Spain.

Pollock, D.W. (1986). "Simulation of fluid flow and energy transport processes associated with high-level radioactive waste disposal in unsaturated alluvium". *Water resource research* Vol. 22 (5), pp. 765-775.

Potts, D. & Ganendra, D. (1992). "A comparison of solution strategies for non-linear finite element analysis of geotechnical problems". *Proceedings of the Third International Conference on Computational Plasticity,* Barcelona, pp. 803-814

Potts, D. & Ganendra, D. (1994). "An evaluation of substepping and implicit stress point algorithm". *Computer Methods in Applied Mechanics and Engineering,* 119 pp. 341-354

Potts, D. & Gens, A. (1985). "A critical assessment of methods of correcting for drift from the yield surface in elastoplastic finite element analysis". *International Journal for Numerical and Analytical Methods in Geomechanics*, Vol. 9, pp. 149-159.

Potts, D. & Zdravković, L. (1999). "Finite Element analysis in geotechnical engineering. Theory". *Thomas Telford Edit,* 440 pp.

Pousada, E. (1984). "Deformabilidad de arcillas expansivas bajo succión controlada". *PhD Thesis, Technical University of Madrid*, Spain.

Push, R. (1982). "Mineral water-interaction and their influence on the physical behaviour of highly compacted Na bentonite". *Can. Geotech. Jnl.*, 19, pp. 381-387

Push, R. (1998). "Microstructural evolution of buffer clay". *Proc. Of workshop on microstructural modelling of natural and artificially prepared clay soils with special emphasis on the use of clays for waste isolation.* Lund pp. 31-38.

Push, R & Güven, N., (1990). "Electron microscopic examination of hydrothermally treated bentonite clay" *Engineering Geology,* 28. pp 303-314.

Push, R & Karnland, O., (1996). "Physico/chemical stability of smectite clays" *Engineering Geology,* 41. pp 73-85.

Push, R & Kasbohm, J. (2001). "Can the water content of highly compacted bentonite be increased by applying a high water pressure?". *Technical Report TR-01-33.* SKB. pp. 30.

Pusch, R. & Moreno L. (2001). "Saturation and permeation of buffer clay". *6th International Workshop on Key Issues in Waste Isolation Research*, Paris, pp. 71-81.

Rizzi, E., Giulio, M. & Willam, K., (1996). "On failure indicators in multi-dissipative materials". *Int. J. Solids Structures*, Vol 33, Nº 20-22, pp. 3187-3124.

Romero, E. (1999). "Characterisation and thermal-hydro-mechanical behaviour of unsaturated Boom clay: an experimental study". *PhD Thesis, Technical University of Catalonia, Spain.*

Romero, E., Gens, A. & Lloret, A. (1999). "Water permeability, water retention and microstructure of unsaturated Boom clay". *Engineering Geology,* 54, pp. 117-127.

Romero, E., Gens, A. & Lloret, A. (2003). "Suction effects on a compacted clay under non-isothermal conditions". *Géotechnique,* 53, Nº 1, pp. 65-81.

Romero, E., Hoffmann, C., Castellanos, E. Suriol, J. & Lloret, A. (2003). "Microstrcutural changes of compacted bentonite induced by hydro-mechanicals actions". *Large scale field tests in granite – Field emplacement and instrumentation techniques, Workshop.* Sitges, Spain. (CD format)

Roscoe, K.H. & Burland, J.B. (1968). "On the generalized stress-strain behaviour of the 'wet' clay". In: Heyman, J., Leckie, F.A. (Eds), *Engineering Plasticity. Cambridge University Press, Cambridge*, pp. 535-609.

Russell, A., & Swartzendruber, D. (1971). "Flux-gradient relationship for saturated flow of water through mixtures of sand, silt and clay". *Sols Sci. Soc. Amer. Proc.* 35, pp. 21-26.

Saix, C. (2001). "Consolidation thermique par chaleur d'un sol non saturé". *Canadian Geotech. Jnl.* 28, pp. 42-50.

Saiyouri, N., Hicher, P. & Tessier, D. (2000). "Microstructural approach and transfer water modelling in highly compacted unsaturated swelling clays". *Mech. of Cohes.-Frict Mater.* 5 pp. 41-60.

Samper, J., Montenegro, L., & Zheng, L. (2002). "ULC contribution to the FEBEX II project meeting of Septembre 26th, 2002". E.T.S. Ingenieros de caminos Universidad de La Coruña. *ENRESA Report: 70-ULC-D-6-03.*

Sánchez-Palencia E. (1980). "Non-homogeneous media and vibration theory". In *Lecture Notes in Physics, J. Ehlers (ed.)*, Springer, Berlin, Vol.127.

Sánchez, M. & Gens, A. (2001). "Report on *THM* modelling results. FEBEX II". *UPC Geomechanical Group. ENRESA Report: 70-UPC-L-5-010.*

Sánchez, M. & Gens, A. (2002). "Second report on *THM* modelling results. FEBEX II". *UPC Geomechanical Group. ENRESA Report: 70-UPC-L-5-011.*

Sánchez, M. & Guimarães, L. (2002)."A sub-stepping strategy for the double structure expansive model". *UPC Geomechanical Group, Internal Report.*

Sears, F. & Zemansky, S. (1966). "Física". Aguilar.

Sheng, D., Swith, D. & Sloan, S. (2002). "An explicit integration scheme for unsaturated soil models". *Proc. 3rd Int. Conference on Unsaturated Soils, Recife*, I, pp. 125-131

Simo, J, & Hughes, T. (1998). "Computational Inelasticity". *Springer-Verlag*, 392 pp.

Simo, J, & Taylor, R. (1985). "Consistent tangent operators for rate-independent elastoplasticity". *Computer Methods in Applied Mechanics and Engineering,* 48, pp. 101-118

Simoni, L., & Schrefler, A. (2001). "Parameter identification for suction-dependent plasticity model". *International Journal for Numerical and Analytical Methods in Geomechanics* Vol. 25, pp. 273-288.

Skipper, N., Refson, K. & Mc Connell, J. (1991). "Computer simulation of interlayer water in 2:1 clays". *J. Chem. Phys.* 94 11, pp. 7434-7445.

Sloan, S., (1987). "Sub-stepping schemes for the numerical integration of elasto-plastic stress-strain relations". *Int. Jnl for Numerical Methods in Engineering.* Vol 24, pp. 893-911.

Sloan, S. Abbo, A. & Sheng, D. (2001). "Refined explicit integration of elastoplastic models with automatic error control". *Engineering Computation,* Vol 18 Nº 1/2, pp. 121-154.

Sloan, S. & Booker, J. (1992). "Integration of Tresca and Mohr-Coulumb constitutive relations in plane strain elastoplasticity". *Int. Jnl for Numerical Methods in Engineering.* Vol 33, pp. 163-196.

Soler, J. (1999). "Coupled transport phenomena in the opalinus clay: implications for radionuclide transport". Paul Scherrer Institut Nº 99-07- ISSN 1019-0643.

Sorbie, K.S. & Mackay, E.J. (2000). "Mixing of injected, connate and aquifer brines in waterflooding and its relevance to oilfield scaling". *Journal of Petroleum Science & Engineering*, 27, pp. 85-106.

Streslotva-Adams, T. (1978). "Well hydraulics in heterogeneous aquifer formations". *Adv. Hydrosci.* 11, pp. 357-423

Subba Rao, K.S. & Styadas, G. (1987). "Swelling Potential with Cycles of Swelling and Partial Shrinkage". *Proc. 6th Int. Conference on Expansive Soils*, New Delhi. Vol. 1, pp. 137-142.

Sultan, N., Delage, P, & Cui, Y. (2002). "Temperature effects on the volume change behaviour of Boom clay". *Engineering Geology,* 64, pp. 135-145.

Svemar, C. & Push, R. (2002). "Äspö Hard Rock Laboratory". *International Progress Report IPR-00-30*. SKB.

Tamagnini, C., Castellanza, R. & Nova, R. (2002). "Implicit integration of constitutive equations in computational plasticity". *Revue française de génie civil*, Vol 6, N°5, pp 1051-1067.

Tanaka, N., Graham, J. & Crilly, T. (1997). "Stress-strain behaviour of reconstituted illitic clay at different temperatures". *Engineering Geology* 47, pp. 339-350.

Thomas, H., & Cleall, P. (1999). "Inclusion of expansive clay behaviour in coupled thermo hydraulic mechanical models". *Engineering Geology,* 54 (1-2), pp. 93-108.

Thomas, H.R. & He, Y. (1995). "An analysis of coupled heat, moisture and air transfer in a deformable unsaturated soil". *Géotechnique*, 45: pp. 667-689.

Thomas, H., Cleall, P. & Hashm, A. (2001). "Thermal/hydraulic/chemical/mechanical (THCM) behaviour of partly saturated soil". In *Desai et al. (ed.) Computer Methods and Advances on Geomechanics, Rotterdam: Balkema*, 1: pp. 743-748.

Thomas, H., Cleall, P., Chandler, N., Dixon, D., & Mitchell, H. (2003). "Water infiltration into a large-scale in-situ experiment in an underground research laboratory". *Géotechnique*, 53, Nº 2, pp 207-224.

Tripathy, S., Subba, K. & Fredlund, D. (2002). "Water content-void ratio swell-shrink paths of compacted expansive soils". *Canadian Geotech. Jnl.* 39, pp. 938-959.

Tuli, A., Kosugi, K. & Hopmans, J. (2001). "Simultaneous scaling of soil water retention and unsaturated hydraulic conductivity functions assuming lognormal pore-size distribution". *Adv. Water Resources,* 24, pp. 677-689.

Vallejan, B. (2004). "Numerical modelling of the hydromechancial behaviour of FoCa clay powder and pellets mixtures (in preparation)". *PhD Thesis, Technical University of Catalonia, Spain.*

van Genuchten, R. (1978). "Calculating the unsaturated hydraulic permeability conductivity with a new closed-form analytical model". *Water Resource Research*. 37(11), pp. 21-28.

Vaunat, J., Cante, J., Ledesma, A., & Gens, A. (2000). "A stress point algorithm for an elastoplastic model in unsaturated soils". *International Journal of Plasticity*, 16, pp.121-141.

Villar, M.V. (1999). "Investigation of the behaviour of bentonite by means of suction-controlled oedometer tests". *Engineering Geology*, 54, pp. 67-73.

Villar, M.V. (2000). "Thermo-hydro-mechanical characterization of Cabo de Gata Bentonite (in Spanish)". *Ph. D. Thesis,* Complutense University, Madrid.

Villar, M.V. & Cuevas, J. (1996). "Caracterización geoquímica de bentonite compactada. Efectos producidos por flujo termo-hidráulico". *Informe Técnico 70 IMA-M-0-02.*

Villar, M.V., & Lloret, A. (2003). "Temperature influence on the hydro-mechanical behaviour of a compacted bentonite". *Large scale field tests in granite – Field emplacement and instrumentation techniques, Workshop.* Sitges, Spain.

Villar, M.V., Martin, P., Lloret, A. & Romero, E. (2004). "Final Report on Thermo-Hydro-Mechanical Laboratory Test". FEBEX II. *ENRESA Report: 70-IMA-L-0-97.*

Villar, M.V., Romero, E. & Lloret, A. (2003). "Thermo-mechanical and geochemical effects on the permeability of high-density clays". *Large scale field tests in granite – Field emplacement and instrumentation techniques, Workshop.* Sitges, Spain.

Villar, M. & Rivas, P. (2001). "Ensayos termo-hidráulicos en celdas grandes: propiedades hidro-mecánicas". CIEMAT. *ENRESA Report: 70-IMA-L-0-76.*

Volckaert, G., Dereeper, B., Put, M., Ortiz, L., Gens, A., Vaunat, J., Villar, M.V., Martin, P.L.,Imbert, C., Lassabatère, T., Mouche, E., Cany, F. (2000). "A large-scale in situ demonstration test for repository sealing in an argillaceous host rock". *Reseal project - Phase I.* EUR 19612 EN, European Commission, Brussels.

Warkentin, B.P., Bolt, G.M. & Miller, R.D. (1957). "Swelling pressure of montmorillonite". *Soil Science Society of America Proceedings*, 21, pp. 495-497.

Warren, J. & Root, P. (1963). "The behaviour of naturally fracturated reservoirs". *Trans AIME* 22. Nº 8, pp. 245-255.

Wiebe, B., Graham, J., Tang, G.X. & Dixon, D. (1998). "Influence of pressure, saturation, and temperature on the behaviour of unsaturated sand-bentonite". *Canadian Geotech. Jnl.* 35, pp. 194-205.

Wilson, R. & Aifantis, E. (1982). "On the theory of consolidation with double porosity. *Int. J. Engng Sci.* Vol. 20, Nº 9, pp. 1019-1035.

Wissmann, J. & Hauck, C. (1983). "Efficient elastic-plastic finite element analysis with higher order stress point algorithms". *Computers and Structures.* Vol. 17, pp. 89-95.

Yong, R.N. (1999). "Overview of modelling of clay microstructure and interactions for prediction of waste isolation barrier performance". *Engineering Geology*, 54, pp. 83-91.

Yamaguchi, E. (1993). "A comparative study of numerical methods for computing stress increments in elastic-plastic materials". *Proceeding of the Asia-Pacific Symposium on Advances in Plasticity and its applications, Hon Kong,* pp 625-6230.

Zienkiewics, O, Leung, A. & Pastor, M. (1985). "Simple model for transient soil loading in earthquake analysis. I. Basic model and its application". *International Journal for Numerical and Analytical Methods in Geomechanics* Vol. 9, pp. 453-476.

APPENDIX A.1

A.1.1 CONSOLIDATION OF FISSURED CLAYS. CLOSED FORM SOLUTION.

In this appendix the analytical solution obtained by Musso & Federico (1993) is briefly presented. The solution can be expressed in terms of the non-dimensional excess pore pressures:

$$u_1 = \frac{p_1}{q} \tag{A1.1}$$

$$u_2 = \frac{p_2}{q} \tag{A1.2}$$

where q is the uniform pressure increment. The non-dimensional parameters are:

$$\mu = \frac{k_1}{k_2} \tag{A1.3}$$

$$\rho = \frac{m_v}{\gamma} \tag{A1.4}$$

Considering the expression proposed by Musso & Federico (1993) for the leakage term:

$$\gamma' = 10\frac{k_2}{\gamma_w s_b^2} \tag{A1.5}$$

together with the two continuity Equations (2.43) and (2.44), the system of differential equations may be written as (Musso & Federico, 1993):

$$\frac{\partial^2 u_1}{\partial Z^2} = \frac{1}{\omega_{11}}\frac{\partial u_1}{\partial T_v} + \frac{1}{\omega_{12}}\frac{\partial u_2}{\partial T_v} + \Psi_1\left(u_1 - u_2\right) \tag{A1.6}$$

$$\frac{\partial^2 u_2}{\partial Z^2} = \frac{1}{\omega_{21}}\frac{\partial u_1}{\partial T_v} + \frac{1}{\omega_{22}}\frac{\partial u_2}{\partial T_v} - \Psi_2\left(u_1 - u_2\right) \tag{A1.7}$$

the non-dimensional coefficients are expressed as:

$$\omega_{\xi\tau} = \frac{\rho\mu^{(2-\xi)}}{(-1)^{(2-\xi)} + \rho\delta_\xi\delta_\tau}; \qquad (\xi, \tau = 1,2) \tag{A1.8}$$

$$\Psi_\xi = 10\mu^{(-2+\xi)}\lambda^2; \qquad (\xi = 1,2) \tag{A1.9}$$

Initial and boundary conditions are given by (Musso & Federico, 1993):

$$u_{\xi}\left(Z,0\right)=1;\qquad \left(\xi=1,2\right) \tag{A1.10}$$

$$u_{\xi}\left(0,T_{v}\right)=0;\qquad \left(\xi=1,2\right) \tag{A1.11}$$

$$\frac{\partial u_{\xi}\left(1,T_{v}\right)}{\partial Z}=0;\qquad \left(\xi=1,2\right) \tag{A1.12}$$

The solution for u_1 and u_2 can be expressed in a closed form as follows (Musso & Federico, 1993):

$$u_{1}\left(Z,T_{v}\right)=2\sum_{n}^{\infty}\left(A_{m}e^{\lambda_{1}T_{v}}+B_{m}e^{\lambda_{2}T_{v}}\right)\sin\left(mZ\right) \tag{A1.13}$$

$$u_{2}\left(Z,T_{v}\right)=2\sum_{n}^{\infty}\left(C_{m}e^{\lambda_{1}T_{v}}+D_{m}e^{\lambda_{2}T_{v}}\right)\sin\left(mZ\right) \tag{A1.14}$$

where:

$$m=\frac{(2n+1)\pi}{2} \tag{A1.15}$$

$$\Delta=\varpi_{12}\varpi_{21}-\varpi_{11}\varpi_{22} \tag{A1.16}$$

$$C_{11}^{*}=\frac{\varpi_{11}\varpi_{12}\varpi_{21}}{\Delta} \tag{A1.17}$$

$$C_{12}^{*}=\frac{\varpi_{11}\varpi_{21}\varpi_{22}}{\Delta} \tag{A1.18}$$

$$C_{21}^{*}=\frac{\omega_{11}\omega_{12}\omega_{22}}{\Delta} \tag{A1.19}$$

$$C_{22}^{*}=\frac{\varpi_{12}\varpi_{21}\varpi_{22}}{\Delta} \tag{A1.20}$$

$$G_{11}=-m^{2}C_{11}^{*}-\psi_{1}\left(C_{11}^{*}+C_{21}^{*}\right) \tag{A1.21}$$

$$G_{12}=+m^{2}C_{11}^{*}+\psi_{1}\left(C_{11}^{*}+C_{21}^{*}\right) \tag{A1.22}$$

$$G_{21}=m^{2}C_{21}^{*}+\psi_{2}\left(C_{12}^{*}+C_{22}^{*}\right) \tag{A1.23}$$

$$G_{22} = -m^2 C_{22}^* - \psi_2 \left(C_{12}^* + C_{22}^* \right) \tag{A1.24}$$

$$\Delta^* = \left(G_{11} + G_{22} \right)^2 - 4 \left(G_{11} + G_{22} - G_{12} + G_{21} \right) \tag{A1.25}$$

$$\lambda_1 = \frac{G_{11} + G_{22}}{2} + \frac{\sqrt{\Delta^*}}{2} \tag{A1.26}$$

$$\lambda_2 = \frac{G_{11} + G_{22}}{2} - \frac{\sqrt{\Delta^*}}{2} \tag{A1.27}$$

$$A_m = \left[-u_{1,0} \left(\lambda_2 - G_{11} \right) + u_{2,0} G_{12} \right] \left(m \sqrt{\Delta^*} \right)^{-1} \tag{A1.28}$$

$$B_m = \left[+u_{1,0} \left(\lambda_1 - G_{11} \right) - u_{2,0} G_{12} \right] \left(m \sqrt{\Delta^*} \right)^{-1} \tag{A1.29}$$

$$C_m = A_m \frac{\lambda_1 - G_{11}}{G_{12}} \tag{A1.30}$$

$$D_m = B_m \frac{\lambda_2 - G_{11}}{G_{12}} \tag{A1.31}$$

A.1.2 MASS TRANSFER MODELS

As explained in Section 2.2.5, there are two main sets of approaches for modelling the mass transfer between media: the quasi-steady one and the unsteady one. The first quasi-steady model was proposed by Barenblatt *et al.* (1960), for the case of a fractured rock mass. They suggested that the mass of the liquid which flow from one porous medium to the other, per unit of time and per unit of volume, can be expressed as:

$$\Gamma = \frac{\Pi \mathbf{k}_2 \sigma^2}{\mu} \rho_l \left(P_{l1} - P_{l2} \right) \tag{A1.5}$$

where Π is a no dimensional parameter (considered constant), σ is the specific surface of the fracture (surface per unit volume of medium), μ is the liquid viscosity, ρ_l is the liquid density and k_2 is the porous matrix permeability.

Another known model is the proposed by Warren & Root (1963). They consider 'a permeable medium which contains regions which contribute significantly to the pore volume of the system but contribute negligibly to the flow capacity'. This kind of heterogonous material is idealized as a double porosity medium composed of a system of regular fractures and blocks of rock matrix. The following expression is suggested for the mass transfer term:

$$\Gamma = \rho_l \frac{\beta \, \mathbf{k}_2}{\mu} \left(P_{l1} - P_{l2} \right) \tag{A1.5}$$

where:

$$\beta = \frac{4n(n+2)}{l^2}; \qquad l = \begin{cases} d_1 & n = 1 \\ \dfrac{2d_1 d_2}{d_1 + d_2} & n = 2 \\ \dfrac{3d_1 d_2 d_3}{d_1 d_2 + d_1 d_3 + d_3 d_2} & n = 3 \end{cases} \qquad \text{(A1.5)}$$

n= 1, 2 and 3 numbers of orthogonal families of discontinuities.

d_1, d_2, d_3 are the fracture intervals between fractures for each direction

Different quasi-steady models for the mass transfer equation have been proposed in terms of geometric characteristics of the media, as the one introduced in Chapter II (and in this Appendix) for the case of fissured clays (Equation A1.5). In Wilson & Aifantis (1982) a procedure to find the unknown parameter of the model is suggested, for the case of fissured media.

In Alonso *et al.* (1991), a double structure model is proposed to analyze the expansive behaviour of a claystone, characterized by the development of two main swelling stages (primary and secondary swelling). A local transfer of water is considered between the macro level (interconnected macroporosity) and the expansive clay minerals (micro level). A sensitivity analysis is performed to identify the dimensionless parameters which control the rate of swelling.

Another way to handle the mass transfer between the two media corresponds to the unsteady models. As commented in Chapter II, in the unsteady models the fluid interaction at the interface between both media is considered solving a 1-D diffusion equation for an idealized geometry of the matrix pores (Streltsova-Adams, 1978; Huyakorn *et al.,* 1983, Kazemi *et al.,* 1976). For instance, Figure (A1.1) shows a scheme of the finite difference discretization of the radial flow region, in an idealized spherical matrix block. The leakage term can be obtained solving a transient problem for a given initial state and considering that the liquid pressures are the same at the interface between the two media. So, in the local problem (medium 1), the boundary condition at the interface between both media (for r = radius of the sphere) is given by the liquid pressure in medium 2. More details related to this technique can be found, for instance, in Huyakorn *et al.* (1983). In the formulation presented in this Thesis, the balance equation corresponding to one media is solved (for instance, Equation 2.23 for j=2) and the interchange term is obtained solving an unsteady problem (generally 1D model) for each node of the mesh. All the cases presented in this Thesis have been solved using quasi-steady models.

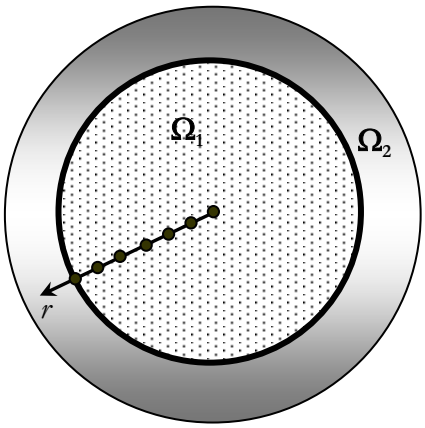

Figure A1.1. Finite difference discretization of the radial flow region in an idealized spherical matrix blocks (Huyakorn *et al.* 1983).

APPENDIX A.2

A.2.1 GENERALIZED PLASTICITY MODEL. PARTICULAR CASE

In this section the simulation of a problem with more than one yield surface is presented. The objective is to explore the capabilities of the generalized plasticity model and of the implemented algorithm to handle this particular case of classical plasticity.

A.2.1.1 MODEL FORMULATION

In the contributions of Alonso *et al.* (1994) and Alonso *et al.* (1999), a mathematical formulation of the model is proposed. Based on classic plasticity an elasto-plastic model with kinematic hardening was suggested. In those work it is assumed the existence of an elastic domain for this plastic mechanism, bounded by two yield surface (both are parallel to the neutral line). Each yield surface is associated to each one of the two types of microstructural paths. That is, one for the *MC* path and the other for the *MS* path. Figure (A2.1) shows a schematic representation of the elastic domain and the associated yield surfaces. An additional hypothesis of the model is related to the assumption that a constant distance between yield surfaces is maintained during the analysis (*i.e.*, the two surfaces move always together).

As commented in Section 3.2.4 a generalized plasticity model is able to consider the existence of yield surfaces that bound an elastic domain. The irreversible strains occur only when the stress path reaches the yield surface. In this section, an elasto-plastic model with a similar conceptual as the suggested in Figure (A2.1) is presented.

In this case two hardening variables are considered:

- p_0^C: is an internal variable which stores the maximum value of the effective microstructure stress experimented by the material under microstructural contraction path.

- p_0^S: is an internal variable which stores the minimum value of the effective microstructure stress experimented by the material under microstructural swelling path.

Although the two variables are required, it is necessary to store only one of them due to the hypothesis of constant distance between the two yield surfaces. These two variables allow following the evolution on the *p-s* plane of the two surfaces which bound the elastic domain:

$$F_C = \hat{p} + p_0^C = 0 \tag{A2.1}$$

$$F_S = \hat{p} + p_0^S = 0 \tag{A2.2}$$

The treatment of this irreversible mechanism has been made in similar way as in classical plasticity. In the case of stress state inside the elastic domain, only reversible strains are induced and this plastic mechanism is not active. When one of the yield surfaces is reached this mechanism is active and plastic strains are induced.

The procedure followed to detect the plastic mechanisms active (*lc*, *ms* or *mc*) is similar to the one proposed by Carol & Prat (1999). Now the system (3.52) can be expressed as:

$$\begin{bmatrix} -\dot{F}_{LC} \\ -\dot{F}_{\beta} \end{bmatrix} = \begin{bmatrix} \overline{H}_{LC} & \overline{h}_{\beta} \\ \overline{h}_{LC} & \overline{H}_{\beta} \end{bmatrix} \begin{bmatrix} \dot{\lambda}_{LC} \\ \dot{\lambda}_{\beta} \end{bmatrix} + \begin{bmatrix} \dot{e}_{LC} \\ \dot{e}_{\beta} \end{bmatrix} + \begin{bmatrix} \dot{s}^{M}_{LC} \\ \dot{s}^{M}_{\beta} \end{bmatrix} + \begin{bmatrix} \dot{s}^{m}_{LC} \\ \dot{s}^{m}_{\beta} \end{bmatrix} + \begin{bmatrix} \dot{t}_{LC} \\ \dot{t}_{\beta} \end{bmatrix} \tag{A2.3}$$

According to Carol & Prat (1999), each $\dot{\lambda}_i$ can be either positive in combination with $\dot{F}_i = 0$ (plastic loading), or zero in combination with $\dot{F}_i < 0$ (elastic unloading). The matrix and the right-hand side vectors are known in advance, the remaining two vectors contain the unknowns of the system.

The detection of the active surfaces is an iterative procedure that starts generally assuming that all the surfaces are active. In this case the whole left-hand vector is null, and the system can be solved to obtain the plastic multipliers. If one of the plastic multipliers obtained is negative this surface is dropped and the system is solved for the other mechanism as a single plasticity model.

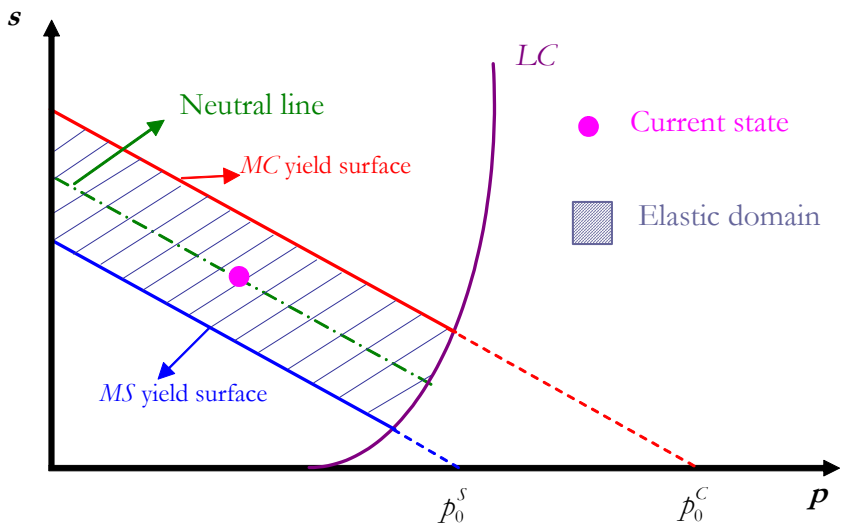

Figure A2.1. Graphical summary of the double structure elasto-plastic model with the yield surfaces associated to the interaction mechanisms

A.2.1.2 APPLICATION CASE

As an application case a hypothetical swelling pressure test is analyzed. As commented, the main objective of this modelling is to verify the capabilities of the model to deal with the presence of an elastic domain, and consequently, to activate (or not) the different plastic mechanisms considered (*lc*, *mc* and *ms*) during the simulation. The main parameters of the model are presented in Table A.2.1.

Figure A.2.2 presents the stress path on the *p-s* plane followed after the hydration under confined conditions of an expansive material. As it can be observed, the stress path is similar to the one recorded in the experiments (Figure 3.15). Figure A.2.3 presents the evolution of the hardening parameters (associated to each plastic mechanism) in relation to the suction changes. Figure A.2.4 presents the changes of the macro and void index versus the suction reduction. And Figure A.2.5 shows the stress path over interactions functions.

The initial state is assumed in the elastic domain, that is, inside the *LC* yield curve and between the yield surfaces associated to the *MC* and *MS* mechanisms. This initial state is indicated by '0' in the Figures (A.2.2 to A.2.5), and corresponds to an initial suction of 10 MPa and a very low stress. During the first stage of wetting the response is elastic until the stress path reaches the *MS* yield surface, point '1'. During the step '0-1' there are not changes in the history variables (elastic zone) and the tendency to swelling of the microstructure is compensated by the contraction of the macrostructure, in order to keep the constant volume condition of the test.

When the contact point '1' is reached the *MS* plastic mechanism is active. From this point on, the stress path pushes forward the *MS* yield surface and both move together. The f_s interaction function has positive values over this path and that implies a macrostructural softening (decreasing values of p_o^*), with the movement of the *LC* yield surface to the left. The slope of this step is controlled by the ratio of stiffen (Gens & Alonso 1992). From the point '2' on, the tendency to an increment of *p* dominates over the decrease in suction, and the stress path returns to the elastic domain (between yield surfaces *SD2* and *SI2*; and inside de *LC2* yield surface). Now the microstructure change the behaviour and tends to contract (*MC* path), and, consequently, the macrostructure expands (this change in behaviour can be observed in Figure A2.4, point '2').

The wetting progresses with the stress path inside the elastic domain, until the *LC* curve is reached; point '3'. It can be observed that during the step '2-3' there are no changes in the hardening variables and the *LC* is fixed, it maintains the position corresponding to the last updating, point '2'. The contact point '3' also corresponds to the macrostructural collapse, with a strong reduction of the macropores and, as a consequence microporosity increases. The *LC* curve is dragged by the stress path which, in turn, is controlled by shape of the *LC* yield curve. Until point '4', in which the yield surface related to the *ms* mechanism is reached, the stress path is inside the elastic domain of the interaction mechanism. It can be observed that the hardening variable associated to the coupling mechanism is not modified between the points indicated as '2' and '4'. During the last part of the path ('4-5') two plastic mechanisms are active, those associated to the *LC* and *MS* yield surfaces.

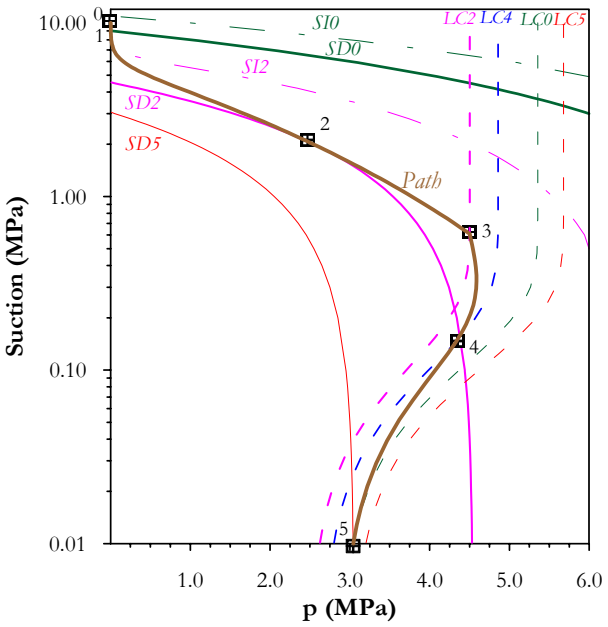

Figure A2.2. Stress path of the net mean stress and positions of yield surfaces on the *p*-*s* plane.

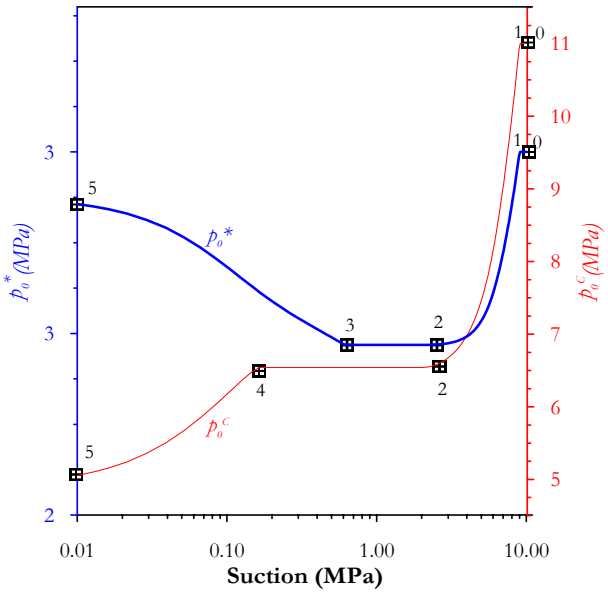

Figure A2.3. Evolution of the hardening parameters (p_0^*, p^C_0) during the test.

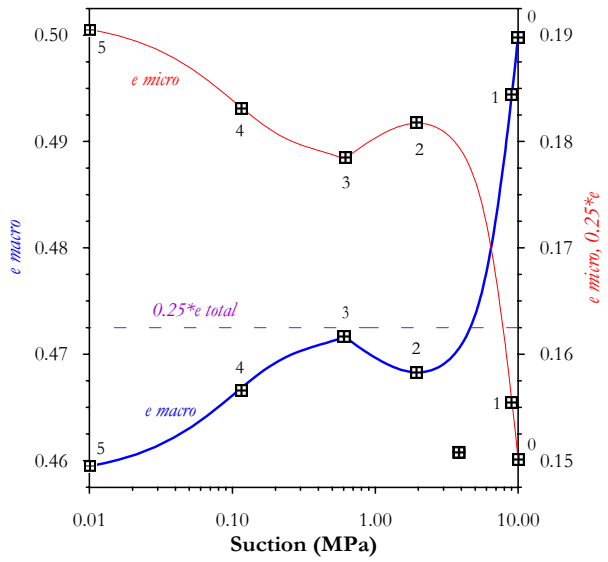

Figure A2.4. Evolution of the history variables (macro, micro and total void index) during the test.

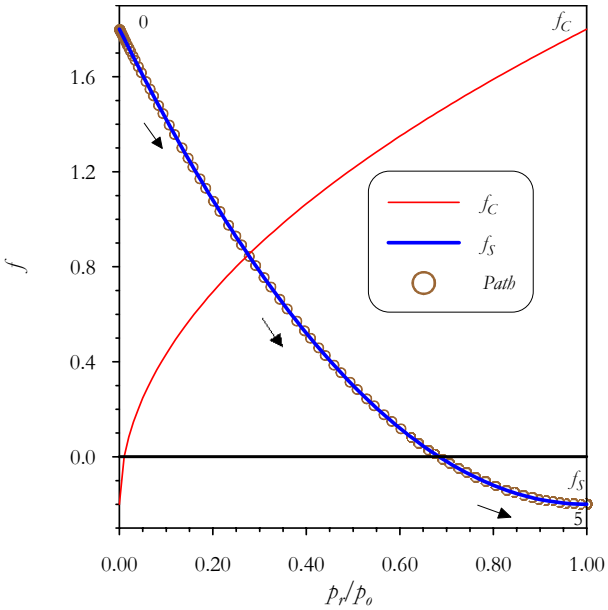

Figure A2.5. Movement of the stress sate on the f_C and f_S interaction functions.

As a conclusion of this modelling exercise it can be mentioned that the proposed framework to integrate the double structure model is general enough and it can reproduce without problems the materials responses controlled by the presence of more than one yield surfaces. It is noted also, that the implemented model can handle complex paths involving different dissipative mechanisms, which are activated or deactivated at some stages of the simulation.

Table A2.1

Parameters used to define the elasto-plastic constitutive law used in Section A.2.1.2

Parameters defining the Barcelona Basic Model for macrostructural behaviour						
κ	κ_s	$\lambda_{(0)}$	p_c (MPa)	r	β (MPa^{-1})	p_o^* (MPa)
0.010	0.008	0. 20	0.10	0.85	12.00	3

Parameters defining the law for microstructural behaviour	
α_m (MPa^{-1})	β_m (MPa^{-1})
5.0x10^{-05}	5.0x10^{-03}

Interaction mechanisms	
p_0^C (MPa)	p_0^S (MPa)
11.0	9.0
Interaction function for *ms* path	Interaction function for *mc* path
$f_C = -0.20 + 2.00\left(p / p_o\right)^{0.5}$	$f_S = -0.20 + 2.0\left(1 - p / p_o\right)^2$

A.2.2 *BBM* MODEL. COMPLEMENTARY EQUATIONS

A detailed description of the *BBM* model can be found in Alonso *et al.,* (1990) and Gens (1995), here the more relevant equations used in this Thesis are presented. The model is formulated in terms of stresses invariants, suction, temperature and internal variables. Generically can be written as:

$$F_{LC} = f(p, J, \theta, s_M, T, \varepsilon_v^p) \tag{A2.4}$$

where the three stresses invariants are:

$$p = \frac{1}{3}\left(\sigma_x + \sigma_y + \sigma_z\right) \tag{A2.5}$$

$$J^2 = 0.5 \ \ \text{trace}\left(\mathbf{s}^2\right) \tag{A2.6}$$

$$\theta = -\frac{1}{3}\sin^{-1}\left(1.5\sqrt{3}\ \det \mathbf{s}/J^3\right) \tag{A2.7}$$

$$\mathbf{s} = \boldsymbol{\sigma} - p\mathbf{I} \tag{A2.8}$$

$$\boldsymbol{\sigma} = \boldsymbol{\sigma}_t - \mathbf{I}p_f \tag{A2.9}$$

where:

$$p_f = p_g \quad if \quad p_g > p_l\ ; \qquad \text{otherwise} \qquad p_f = p_l \tag{A2.10}$$

$\boldsymbol{\sigma}_t$ is the total stress vector and $\mathbf{I}$ is the identity tensor.

The *BBM* yield surface is the one adopted in Equation (3.1). Some of the variables of this Equation are presented here.

p_s considers the dependence of shear strength on suction and temperature, which is expressed as:

$$p_s = -ks e^{-\rho\Delta T} \tag{A2.11}$$

where k and ρ are model parameters and ΔT is the temperature increment, respect to the reference temperature T_o.

The equation that defines the set of yield p_0 values for each associated suction (***i.e.*** the family of *LC* curves on a *p-s* plane) is given by:

$$p_0 = p_c\left(\frac{p_{0T}^*}{p_c}\right)^{\frac{\lambda_{(0)}-\kappa}{\lambda_{(s_M)}-\kappa}} \tag{A2.12}$$

where p_c is a reference stress, κ is the elastic stiffness parameter for changes in net mean stress, p_{0T}^* is the pre-consolidation net mean stress for saturated conditions and current temperature. $\lambda_{(sM)}$ is the compressibility parameter for changes in net mean stress for virgin states of the soil, which depends on suction according to:

$$\lambda_{(s_M)} = \lambda_{(0)}\left[r + (1-r)e^{-\zeta s_M}\right] \tag{A2.13}$$

where *r* is a parameter which defines the minimum soil compressibility (at infinite suction) and ζ is a parameter which controls the rate of decrease of soil compressibility with macrostructural suction.

In order to isolate a single yield curve from Equation (A2.12), it is necessary to specify the pre-consolidation net stress for saturated conditions p_{0T}^{*}, which may be viewed as the hardening parameter of the *BBM* model. According to Gens (1995), the thermal effect has been included considering a dependence of the hardening parameter on temperature, as follows:

$$p_{0T}^{*} = p_{0}^{*} + 2\left(\alpha_1 \Delta T + \alpha_3 \Delta T \left|\Delta T\right|\right) \tag{A2.14}$$

where α_1 and α_3 are material parameters.

The hardening law adopted is presented in Chapter III (Equation 3.2). The plastic potential is given Equation (3.3). Finally, the normal vector to yield surface is defined as:

$$\mathbf{n}_{LC} = \frac{\partial F_{LC}}{\partial \boldsymbol{\sigma}} \tag{A2.15}$$

A.2.3 DOUBLE STRUCTURE CONSIDERATIONS

In this section some details are presented related to some variables of the double structure model. Figure (A2.6) shows the phase diagram adopted and Equations (A2.16) to (A2.20) contain some of the variables used in this work.

$$V = V_s + V_{v_a m} + V_{v_a M} = V_m + V_{v_a M} \tag{A2.16}$$

$$V_{va} = V_{v_a m} + V_{v_a M} \tag{A2.17}$$

$$e = \frac{V_{v_a}}{V_s} = e_M + e_m = \frac{V_{v_a M}}{V_s} + \frac{V_{v_a m}}{V_s} \tag{A2.18}$$

$$\bar{e}_m = e_m = \frac{V_{v_a m}}{V_s} \tag{A2.19}$$

$$\phi = \frac{V_{v_a}}{V} = \phi_M + \phi_m = \frac{V_{v_a M}}{V} + \frac{V_{v_a m}}{V} \tag{A2.20}$$

the subscript *M* identifies the macrostructure level, *m* the microstructure level, *s* the solid phase and v_a the void space. *V* is the volume and ϕ is porosity.

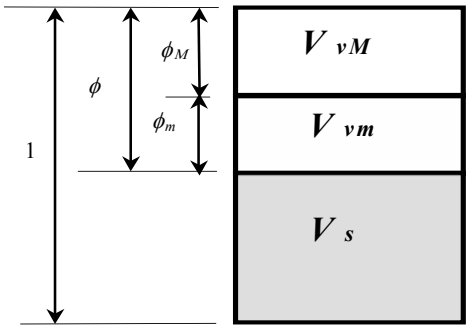

Figure A2.6. Phase diagram adopted.

It should be pointed out that the variables that appear in the balance equations for the porous medium, as a whole, should be global ones, *i.e.* they should refer to the total volume. Instead, in local balance equations, or in microstructural constitutive equations, local variables (identified with an upper bar) should be used. In other words, in the first case the global representative elementary volume should be referred as (*REVG*) whereas in the second case the local representative elementary volume should be referred as (*REVL*) Figure (A2.7) shows a schematic representation of them.

The microstructural strains defined in Equation (3.9) (Chapter III) are related to a *REVG,* because a model assumption is that deformations of the microstructure and macrostructure can be added (Equation 3.11). But in fact, the microstructural law is related to a *REVL,* therefore*:*

$$\dot{\bar{\varepsilon}}^{e}_{vm} = \dot{\bar{\varepsilon}}_{vm} = \frac{\dot{\hat{p}}}{\bar{K}_m} = \frac{\dot{p}}{\bar{K}_m} + \chi \frac{\dot{s}_t}{\bar{K}_m} \tag{A2.21}$$

where $\bar{K}_m$ is the microstructural bulk modulus, the expression of which depends on the elastic law adopted for the microstructural behaviour. Here two models have been considered (Alonso 1998), which can be selected depending on the kind of problem analysed. The exponential law, based on the *DDL* theory (Equation A2.22); and one based on a logarithmic law for void ratio and mean stress relationship (Equation A2.23).

$$\bar{K}_m = \frac{e^{-\alpha_m \hat{p}}}{\beta_m} \tag{A2.22}$$

$$\bar{K}_m = \frac{\left(1+\bar{e}_m\right)}{\kappa_m}\hat{p} \tag{A2.23}$$

where $\bar{e}_m$ is the microstructural void index, and α_m, β_m and κ_m are model parameters. In notation the upper bar identifies local variables; that is, those which are referred to a *REVL*. So, before adding strains of different structural levels (for example, Equation 3.11), it is necessary to refer them to the same *REV*. There are several alternatives to do so, here, a simple procedure has been followed. First the solid mass balance of the microstructure is applied, which can be expressed as:

$$\frac{\partial}{\partial t}\left(\rho_s\left(1-\bar{\phi}_m\right)\right)+\nabla.\left(\rho_s\left(1-\bar{\phi}_m\right)\dot{\mathbf{u}}_m\right)=0 \tag{A2.24}$$

Operating in a similar way as in Olivella *et al.* (1994), it is obtained:

$$\dot{\bar{\phi}}_m=-\left(1-\bar{\phi}_m\right)\dot{\bar{\varepsilon}}_{vm} \tag{A2.25}$$

$$\dot{\bar{e}}_m=\dot{e}_m=-\left(1+e_m\right)\dot{\bar{\varepsilon}}_{vm} \tag{A2.26}$$

From Equations (A2.21) and (A2.26), the volumetric strain increment can be decomposed as:

$$\dot{\varepsilon}_v=-\frac{\dot{e}_m+\dot{e}_M}{\left(1+e\right)}=-\frac{\left(1+e_m\right)\dot{\bar{\varepsilon}}_{vm}}{\left(1+e\right)}-\frac{\dot{e}_M}{\left(1+e\right)}=\dot{\varepsilon}_{vm}+\dot{\varepsilon}_{vM} \tag{A2.27}$$

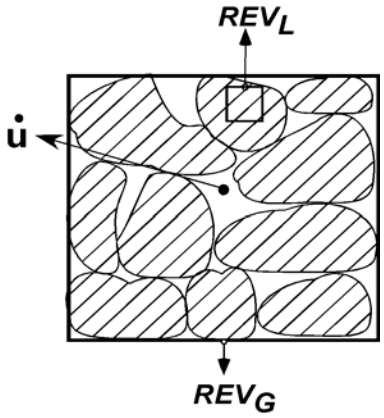

Figure A.2.7. Representation of global and local representative elementary volumes

Finally, the microstructural volumetric strain referred to the *REVG* is:

$$\dot{\varepsilon}_{vm} = -\frac{(1+e_m)\dot{\bar{\varepsilon}}_{vm}}{(1+e)} = \frac{\dot{\hat{p}}}{K_m} \qquad (A2.28)$$

where:

$$K_m = \frac{(1+e)}{(1+e_m)}\bar{K}_m \qquad (A2.29)$$

The microstructural bulk modulus obtained given by (A2.29) is the one applied in Equation (3.9).

A.2.4 GENERALIZED PLASTICITY MODEL. PLASTIC FLOW DIRECTION

At the image point projection it is assumed that η, θ, s and T are maintained constant during projection. The following equations define the projection:

$$p^* = \frac{\left[\frac{g(\theta)}{g(-30^o)}\right]^2 M^2 p_o - \eta^2 p_s}{\left[\frac{g(\theta)}{g(-30^o)}\right]^2 M^2 + \eta^2} \quad ; \quad J^* = \frac{1}{\sqrt{3}}\eta\left(p^* + p_s\right) \qquad (A2.30)$$

where:

$$\eta = \frac{\sqrt{3}J}{p + p_s} = \frac{\sqrt{3}J^*}{p^* + p_s} \qquad (A2.31)$$

with $s^* = s$; $\theta^* = \theta$ and $T^* = T$.

Regarding the direction of the plastic strain increment (related to this plastic mechanism) a non-associated flow rule in the plane s=constant and T=constant is suggested. This is a similar assumption as that made for the *BBM* by Alonso ***et al.*** (1990) and Gens (1995).

The components of the normal to the plastic potential at the image point Equation (3.21) are defined as:

$$\frac{\partial G}{\partial p^*} = \left[\frac{g(\theta)}{g(-30^o)}\right]^2 M^2\left(2p^* + p_s - p_0\right) \tag{A2.32}$$

$$\frac{\partial G}{\partial J^*} = 6\alpha J^* \tag{A2.33}$$

$$\frac{\partial G}{\partial \theta^*} = -\frac{2g(\theta)g'(\theta)}{\left[g(-30^o)\right]^2} M^2\left(p^* + p_s\right)\left(p_0 - p^*\right) \tag{A2.34}$$

A.2.5 ELASTIC MODEL

In this section the elastic tensors for the general case are presented. More details can be found in CODE_BRIGHT User's Manual (2004).

The elastic matrix is evaluated as follows:

$$\mathbf{D}_e = \begin{bmatrix} K+\frac{4}{3}G_t & K-\frac{2}{3}G_t & K-\frac{2}{3}G_t & 0 & 0 & 0 \\ & K+\frac{4}{3}G_t & K-\frac{2}{3}G_t & 0 & 0 & 0 \\ & & K+\frac{4}{3}G_t & 0 & 0 & 0 \\ & & & G_t & 0 & 0 \\ symm & & & & G_t & 0 \\ & & & & & G_t \end{bmatrix} \tag{A2.35}$$

where K is the global bulk modulus and G_t is the shear modulus. They may be computed considering the elastic contribution of the two pore structures. The suggested expressions based on bulk and shear modulus for each medium defined appropriately with respect to the total volume of the mixture can be defined as (i.e. Car, 2000):

$$K = \left(\frac{1}{K_M} + \frac{1}{K_m}\right)^{-1}; \qquad G_t = \left(\frac{1}{G_{tM}} + \frac{1}{G_{tm}}\right)^{-1} \tag{A2.36}$$

where K_M is the macrostructural bulk modulus for changes in mean stress, computed as:

$$K_M = \frac{\left(1+e_M\right)}{\kappa_i} p \tag{A2.37}$$

The microstructural bulk modulus (K_m) is defined by Equation (A2.29).

The shear modulus G_t can be obtained from a linear elastic model with constant Poisson's coefficient:

$$G_{tj} = \frac{3(1-2\mu)K_j}{2(1+\mu)}; \qquad j = M, m \tag{A2.38}$$

The macrostructural bulk modulus for changes in suction has been computed considering the following law:

$$K_s = \frac{(1+e_M)(s_M + p_{at.})}{\kappa_s} \tag{A2.38}$$

Finally the macrostructural bulk modulus for changes in temperature is evaluated through the expression (Gens, 1995):

$$K_T = \frac{1}{(\alpha_0 + 2\alpha_2 \Delta T)} \tag{A2.38}$$

A.2.6 HYDRAULIC EQUILIBRIUM BETWEEN PORES STRUCTURES

In this Section some complementary aspects of the procedure followed to derive the rate equations introduced in Section 3.3.1 (Chapter III) are presented.

A.2.6.1 AUXILIARY EXPRESSIONS FOR THE MACROSTRUCTURAL MODEL

Once yield occurs, that is $F_{LC} = 0$, the stresses must remain on the yield surface during plastic deformations. This constraint is enforced by the consistency condition, which can be expressed as:

$$\dot{F}_{LC} = 0 = \mathbf{n}_{LC} \cdot \dot{\boldsymbol{\sigma}} + l_{LC}\, \dot{s} + d\, \dot{T} + H \left(\dot{\varepsilon}^{p}_{vLC} + \dot{\varepsilon}^{p}_{v\beta} \right) \dot{F}_{LC} \tag{A2.39}$$

where:

$$l_{LC} = \frac{\partial F_{LC}}{\partial s} \tag{A2.40}$$

$$d = \frac{\partial F_{LC}}{\partial T} \tag{A2.41}$$

$$H = \frac{\partial F_{LC}}{\partial p_0} \frac{\partial p_0}{\partial p_0^*} \frac{\partial p_0^*}{\partial \varepsilon_v^p} \tag{A2.42}$$

$$\dot{\varepsilon}_{vLC}^p = \dot{\lambda}_{LC} \, \mathbf{m}^T \cdot \mathbf{m}_{LC} \tag{A2.43}$$

$$\dot{\varepsilon}_{v\beta}^p = \dot{\lambda}_{\beta} \, \mathbf{m}^T \cdot \mathbf{m}_{\beta} \tag{A2.44}$$

This mechanism is active if:

$$\dot{F}_{LC} = 0 \qquad \text{and} \qquad \dot{\lambda}_{LC} > 0 \tag{A2.45}$$

In Equation (A2.39) $\dot{\varepsilon}_{v\beta}^p$ considers the movements of the *LC* yield curve when the interaction mechanism between structures is active.

The net stress increment can be expressed as:

$$\dot{\boldsymbol{\sigma}} = \mathbf{D}_e \cdot \left(\dot{\boldsymbol{\varepsilon}} - \dot{\boldsymbol{\varepsilon}}_s^e - \dot{\boldsymbol{\varepsilon}}_T^e - \dot{\boldsymbol{\varepsilon}}_{LC}^p - \dot{\boldsymbol{\varepsilon}}_{\beta}^p \right) = \mathbf{D}_e \cdot \left(\dot{\boldsymbol{\varepsilon}} - b \, \mathbf{m} \dot{s} - c \, \mathbf{m} \dot{T} - \dot{\lambda}_{LC} \, \mathbf{m}_{LC} - \dot{\lambda}_{\beta} \, \mathbf{m}_{\beta} \right) \tag{A2.46}$$

After some algebra on (A2.39) and (A2.45), Equation (3.37) is obtained:

$$\dot{\lambda}_{LC} \, \overline{H}_{LC} + \dot{\lambda}_{\beta} \, \overline{h}_{\beta} = \dot{e}_{LC} + \dot{s}_{LC} + \dot{t}_{LC} \tag{A2.47}$$

where:

$$\overline{H}_{LC} = H_{LC} + H_{LC}^e = H_{LC} + \mathbf{n}_{LC}^T \cdot \mathbf{D}_e \cdot \mathbf{m}_{LC} \tag{A2.48}$$

$$\overline{h}_{\beta} = h_{\beta} + h_{\beta}^e = h_{\beta} + \mathbf{n}_{LC}^T \cdot \mathbf{D}_e \cdot \mathbf{m}_{\beta} \tag{A2.49}$$

$$\dot{e}_{LC} = \mathbf{n}_{LC}^{T} \cdot \mathbf{D}_e \cdot \dot{\boldsymbol{\varepsilon}} \tag{A2.50}$$

$$\dot{s}_{LC} = \left[l_{LC} + l_\beta + \mathbf{n}_{LC}^{T} \cdot \left(\boldsymbol{\alpha}_s + \boldsymbol{\beta}_s \right) \right] \dot{s} \tag{A2.51}$$

$$\dot{t}_{LC} = \left(d + \mathbf{n}_{LC}^{T} \cdot \boldsymbol{\alpha}_T \right) \dot{T} \tag{A2.52}$$

$$\boldsymbol{\alpha}_s = -b\, \mathbf{D}_e \cdot \mathbf{m} = \left(\frac{1}{K_s} + \frac{\chi}{K_m} \right) \mathbf{D}_e \cdot \mathbf{m} \tag{A2.53}$$

$$\boldsymbol{\beta}_s = -\frac{1}{H_\beta} \omega_\beta \chi \mathbf{D}_e \cdot \mathbf{m}_\beta \tag{A2.54}$$

$$\boldsymbol{\alpha}_T = c\, \mathbf{D}_e \cdot \mathbf{m} = \frac{1}{K_T} \mathbf{D}_e \cdot \mathbf{m} \tag{A2.55}$$

$$H_{LC} = -H \mathbf{m}^{T} \cdot \mathbf{m}_{LC} \tag{A2.56}$$

$$h_\beta = -H \mathbf{m}^{T} \cdot \mathbf{m}_\beta \tag{A2.57}$$

$$l_\beta = -\frac{1}{H_\beta} h_\beta \omega_\beta \chi \tag{A2.58}$$

A.2.6.2 AUXILIARY EXPRESSIONS FOR THE GENERALIZED PLASTICITY MODEL

For the generalized plasticity model, a procedure similar to the one suggested by Pastor *et al.* (1990) has been followed. Firstly, a decomposition of strain increment it is assumed:

$$\dot{\boldsymbol{\varepsilon}} = \dot{\boldsymbol{\varepsilon}}^{e} + \dot{\boldsymbol{\varepsilon}}_{LC}^{p} + \dot{\boldsymbol{\varepsilon}}_{\beta}^{p} \tag{A2.59}$$

Then, pre-multiplying by $\mathbf{n}^{T}{}_{\beta} \mathbf{D}_e$ and operating, it gives:

$$\begin{aligned} \mathbf{n}_\beta^{T} \cdot \mathbf{D}_e \cdot \dot{\boldsymbol{\varepsilon}} = \mathbf{n}_\beta^{T} \cdot \dot{\boldsymbol{\sigma}} + b\, \mathbf{n}_\beta^{T} \cdot \mathbf{D}_e \cdot \mathbf{m} \dot{s} + c\, \mathbf{n}_\beta^{T} \cdot \mathbf{D}_e \cdot \mathbf{m} \dot{T} + \frac{\chi}{H_\beta} \omega_\beta \mathbf{n}_\beta^{T} \cdot \mathbf{D}_e \cdot \mathbf{m}_\beta \dot{s} + \\ \dot{\lambda}_\beta\, \mathbf{n}_\beta^{T} \cdot \mathbf{D}_e \cdot \mathbf{m}_\beta + \dot{\lambda}_{LC}\, \mathbf{n}_\beta^{T} \cdot \mathbf{D}_e \cdot \mathbf{m}_{LC} \end{aligned} \tag{A2.60}$$

After some algebra on (A2.46) and (A2.60), Equation (3.38) is obtained:

$$\dot{\lambda}_{LC}\,\bar{h}_{LC} + \dot{\lambda}_{\beta}\,\overline{H}_{\beta} = \dot{e}_{\beta} + \dot{s}_{\beta} + \dot{t}_{\beta} \tag{A2.61}$$

where:

$$\bar{h}_{LC} = h^{e}_{LC} = \mathbf{n}^{T}_{\beta} \cdot \mathbf{D}_{e} \cdot \mathbf{m}_{LC} \tag{A2.62}$$

$$\overline{H}_{\beta} = H_{\beta} + H^{e}_{\beta} = H_{\beta} + \mathbf{n}^{T}_{\beta} \cdot \mathbf{D}_{e} \cdot \mathbf{m}_{\beta} \tag{A2.63}$$

$$\dot{e}_{\beta} = \mathbf{n}^{T}_{\beta} \cdot \mathbf{D}_{e} \cdot \dot{\boldsymbol{\varepsilon}} \tag{A2.64}$$

$$\dot{s}_{\beta} = \mathbf{n}^{T}_{\beta} \cdot \left(\boldsymbol{\alpha}_{s} + \boldsymbol{\beta}_{s}\right)\dot{s} \tag{A2.65}$$

$$\dot{t}_{\beta} = \mathbf{n}^{T}_{\beta} \cdot \boldsymbol{\alpha}_{T}\,\dot{T} \tag{A2.66}$$

A.2.7 HYDRAULIC NON-EQUILIBRIUM BETWEEN PORES STRUCTURES

Here only the new expressions (or those that are modified) are presented, the rest correspond to the case of hydraulic equilibrium (Section A.2.6 and 3.3.1).

A.2.7.1 AUXILIARY EXPRESSIONS FOR THE MACROSTRUCTURAL MODEL

The consistency condition for this case is expressed as:

$$\dot{F}_{LC} = 0 = \mathbf{n}_{LC} \cdot \dot{\boldsymbol{\sigma}} + l_{LC}\,\dot{s}_{M} + d\,\dot{T} + H\left(\dot{\varepsilon}^{p}_{vLC} + \dot{\varepsilon}^{p}_{v\beta}\right) \tag{A2.67}$$

where now:

$$l_{LC} = \frac{\partial F_{LC}}{\partial s_{M}} \tag{A2.68}$$

The net stress increment can be expressed as:

$$\dot{\boldsymbol{\sigma}} = \mathbf{D}_e \cdot \left(\dot{\boldsymbol{\varepsilon}} - \dot{\boldsymbol{\varepsilon}}^e_{sM} - \dot{\boldsymbol{\varepsilon}}^e_{sm} - \dot{\boldsymbol{\varepsilon}}^e_T - \dot{\boldsymbol{\varepsilon}}^p_{LC} - \dot{\boldsymbol{\varepsilon}}^p_\beta \right) \quad or$$
$$\dot{\boldsymbol{\sigma}} = \mathbf{D}_e \cdot \left(\dot{\boldsymbol{\varepsilon}} - b_M \mathbf{m} \dot{s}_M - b_m \mathbf{m} \dot{s}_m - c\ \mathbf{m} \dot{T} - \dot{\lambda}_{LC}\ \mathbf{m}_{LC} - \dot{\lambda}_\beta\ \mathbf{m}_\beta \right) \tag{A2.69}$$

Operating in a similar way as Section A.2.6.1, the following expression is obtained:

$$\dot{\lambda}_{LC} \overline{H}_{LC} + \dot{\lambda}_\beta \bar{b}_\beta = \dot{e}_{LC} + \dot{s}^M_{LC} + \dot{s}^m_{LC} + \dot{t}_{LC} \tag{A2.70}$$

where:

$$\dot{s}^M_{LC} = \left[l_{LC} + \mathbf{n}^T_{LC} \cdot \boldsymbol{\alpha}_{sM} \right] \dot{s}_M \tag{A2.71}$$

$$\dot{s}^m_{LC} = \left[l_\beta + \mathbf{n}^T_{LC} \cdot \left(\boldsymbol{\alpha}_{sm} + \boldsymbol{\beta}_{sm} \right) \right] \dot{s}_m \tag{A2.72}$$

$$\boldsymbol{\alpha}_{sM} = -b_M \mathbf{D}_e \cdot \mathbf{m} = \frac{1}{K_s} \mathbf{D}_e \cdot \mathbf{m} \tag{A2.73}$$

$$\boldsymbol{\alpha}_{sm} = -b_m \mathbf{D}_e \cdot \mathbf{m} = \frac{\chi}{K_m} \mathbf{D}_e \cdot \mathbf{m} \tag{A2.74}$$

$$\boldsymbol{\beta}_{sm} = -\frac{1}{H_\beta} \omega_\beta \chi \mathbf{D}_e \cdot \mathbf{m}_\beta \tag{A2.75}$$

A.2.7.2 AUXILIARY EXPRESSIONS FOR THE GENERALIZED PLASTICITY MODEL

Operating in a similar form as indicated in Section A.2.6.2:

$$\dot{\lambda}_{LC} \bar{h}_{LC} + \dot{\lambda}_\beta \overline{H}_\beta = \dot{e}_\beta + \dot{s}^M_\beta + \dot{s}^m_\beta + \dot{t}_\beta \tag{A2.76}$$

where:

$$\dot{s}_{\beta}^{M} = \mathbf{n}_{\beta}^{T} \cdot \boldsymbol{\alpha}_{sM} \dot{s}_{M} \tag{A2.77}$$

$$\dot{s}_{\beta}^{m} = \mathbf{n}_{\beta}^{T} \cdot \left(\boldsymbol{\alpha}_{sm} + \boldsymbol{\beta}_{sm} \right) \dot{s}_{m} \tag{A2.78}$$

A.2.8 P-MATRIX

In this appendix, with the objective of the completeness, some definitions given by Rizzi *et al.* (1996) have been transcribed.

A.2.8.1 DEFINITIONS

- The "principal submatrix" $\mathbf{A}_\alpha$ of matrix $\mathbf{A} \in \mathcal{R}_{nxn}$, is the matrix whose entries lie in rows and columns of **A** indexed by sets $\alpha \subseteq \{1,2,..,n\}$ (*i.e.* . $\mathbf{A}_\alpha$ is a submatrix of **A** whose diagonal is part of the diagonal of **A**). The determinant of $\mathbf{A}_\alpha$ is called a "principal minor" of **A**.

- The matrix $\mathbf{A} \in \mathcal{R}_{nxn}$, is said to be a *P-matrix* when all its principal minors are positive.

A.2.8.2 "P-MATRIX" PROPERTIES.

- All real eigenvalues of **A** and its principal sub-matrices are positive.

- **A** does not reverse the sign of any vector, except the zero vector, *i.e.*

  $x_i(\mathbf{A} \bullet \mathbf{X})_i \leq 0. \quad \forall i=1,2,...n \qquad$ implies $\mathbf{X} = 0$

A.2.9 ONE PLASTIC MECHANISM ACTIVE

When only the *lc* plastic mechanism is active a procedure similar as the one presented in Gens (1995) has been followed. That is, considering the procedure follow in Section A.2.6.1, the expressions of elasto-palstic tensors which define the stress-strain relation (3.47) are the following:

$$\mathbf{D}_{ep} = \mathbf{D}_{e} \cdot \left[\mathbf{I} - \frac{1}{\overline{\overline{H}}_{LC}} \mathbf{m}_{LC} \cdot \mathbf{n}_{LC}^{T} \cdot \mathbf{D}_{e} \right] \tag{A2.79}$$

$$\boldsymbol{\gamma}_{s} = \boldsymbol{\alpha}_{s} - \frac{1}{\overline{\overline{H}}_{LC}} \mathbf{D}_{e} \cdot \mathbf{m}_{LC} \left(l + \mathbf{n}_{LC}^{T} \cdot \boldsymbol{\alpha}_{s} \right) \tag{A2.80}$$

$$\boldsymbol{\gamma}_{T} = \boldsymbol{\alpha}_{T} - \frac{1}{\overline{\overline{H}}_{LC}} \mathbf{D}_{e} \cdot \mathbf{m}_{LC} \left(d + \mathbf{n}_{LC}^{T} \cdot \boldsymbol{\alpha}_{T} \right) \tag{A2.81}$$

When only the β plastic mechanism is active a procedure similar as the one presented in Pastor *et al.* (1990) has been followed. That is, considering the procedure follow in Section A.2.6.2, the expressions of elasto-palstic tensors which define the stress-strain relation (3.47) are the following:

$$\mathbf{D}_{ep} = \mathbf{D}_e \cdot \left[\mathbf{I} - \frac{1}{\overline{\overline{H}}_\beta} \mathbf{m}_\beta \cdot \mathbf{n}_\beta^T \cdot \mathbf{D}_e \right] \tag{A2.82}$$

$$\boldsymbol{\gamma}_s = \left(\boldsymbol{\alpha}_s + \boldsymbol{\beta}_s\right) - \frac{1}{\overline{\overline{H}}_\beta} \mathbf{D}_e \cdot \mathbf{m}_\beta \mathbf{n}_\beta^T . \left(\boldsymbol{\alpha}_s + \boldsymbol{\beta}_s\right) \tag{A2.83}$$

$$\boldsymbol{\gamma}_T = \boldsymbol{\alpha}_T - \frac{1}{\overline{\overline{H}}_\beta} \mathbf{D}_e \cdot \mathbf{m}_\beta \mathbf{n}_\beta^T \cdot \boldsymbol{\alpha}_T \tag{A2.84}$$

APPENDIX A.3

A.3.1 MIXTURES OF CLAY PELLETS AND CLAY POWDER

A.3.1.1 BASIC RELATIONS

The basic relationships used for the material analysed in Chapter IV (Section 4.4) are presented in this Appendix. Figure (A3.1) shows a scheme of this material.

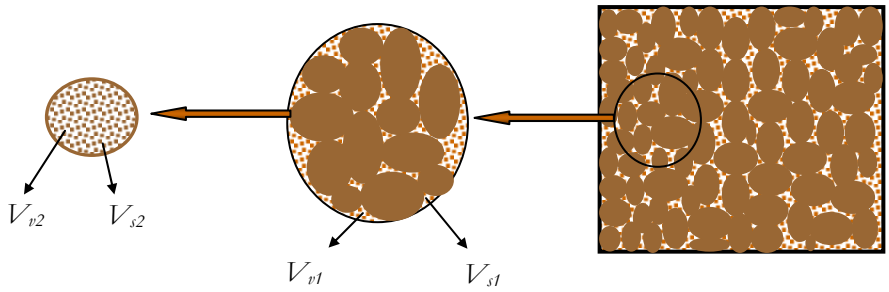

Figure A3.1. Scheme of the mixture of clay powder and highly compacted clay pellets.

Figure (A3.2) shows the associated phase diagram adopted. Subscripts refer to the particular medium considered, 1 or 2. According to this diagram, the total volume (V) is decomposed into:

$$V = \underbrace{V_{s1} + V_{v1}}_{V_1} + \underbrace{V_{s2} + V_{v2}}_{V_2} \tag{A3.1}$$

where the subscripts s identifies the solid phase, v_a the void space, *1* the medium 1 (clay powder) 2 the medium 2 (clay pellets).

The bulk specific weight and the solid specific weight are expressed as:

$$\gamma_d = \frac{P_s}{V}; \qquad \gamma_s = \frac{P_s}{V_s} \tag{A3.2}$$

where P_s is the solid weight. In the case analyzed herein both media have the same γ_s. It is possible to express the bulk specific weights of each porous medium as:

$$\gamma_{d1} = \frac{P_{s1}}{V_1}; \qquad \gamma_{d2} = \frac{P_{s2}}{V_2} \tag{A3.3}$$

where P_{s1} is the solid weight of medium 1, and P_{s2} is the solid weight of medium 2.

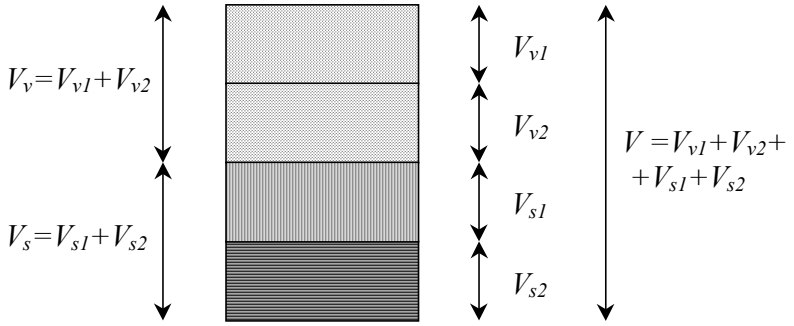

Figure A3.2. Phase diagram adopted

The clay pellets-powder mixture is defined through the ratio:

$$\xi = \frac{P_{s2}}{P_{s1} + P_{s2}} \tag{A3.4}$$

Total bulk porosity is expressed as:

$$\phi = \frac{V_v}{V} = \phi_1 + \phi_2 \tag{A3.5}$$

The initial global porosities for each medium can be computed as:

$$\phi_1 = \frac{V_{v1}}{V} = \left[1 - \xi\frac{\gamma_d}{\gamma_{d2}} - (1-\xi)\frac{\gamma_d}{\gamma_s}\right]; \qquad \phi_2 = \frac{V_{v2}}{V} = \xi\,\gamma_d\left[\frac{1}{\gamma_{d2}} - \frac{1}{\gamma_s}\right] \tag{A3.6}$$

The global void ratios are given by the following expressions:

$$e_1 = \frac{V_{v1}}{V_s} = \frac{\phi_1}{(1-\phi)}; \qquad e_2 = \frac{V_{v2}}{V_s} = \frac{\phi_2}{(1-\phi)}; \qquad e = \frac{V_v}{V_s} = e_1 + e_2 \tag{A3.7}$$

As commented in Section A.2.3 (Appendix A.2), global variables are used in the global balance equations (for instance ϕ_1 and ϕ_2 in Equations 2.12, Chapter II). Whereas, constitutive laws are expressed, generally, in terms of local variables (*i.e.* referred to the own medium). The initial local void ratios are given by:

$$\overline{e}_1 = \frac{V_{v1}}{V_{s1}} = \frac{\gamma_s}{(1-\xi)}\left[\frac{1}{\gamma_d} - \frac{\xi}{\gamma_{d2}}\right] - 1 = \frac{e_1}{(1-\xi)}; \qquad \overline{e}_2 = \frac{V_{v2}}{V_{s2}} = \frac{\gamma_s}{\gamma_{d2}} - 1 = \frac{e_2}{\xi} \tag{A3.8}$$

And the local porosities are expressed as:

$$\overline{\phi}_1 = \frac{V_{v1}}{V_1} = \frac{\overline{e}_1}{(1+\overline{e}_1)} = \frac{e_1}{e_1 + (1-\xi)}; \qquad \overline{\phi}_2 = \frac{V_{v2}}{V_2} = \frac{\overline{e}_2}{(1+\overline{e}_2)} = \frac{e_2}{e_2 + \xi} \tag{A3.9}$$

A.3.1.2 ELASTIC MODEL

The volumetric strain increment of the medium 1, due to p and s_1 increment is computed according to:

$$\dot{\overline{\varepsilon}}^{e}_{v_1} = \frac{\dot{p}}{K} + \frac{\dot{s}_1}{K_s} \tag{A3.13}$$

where K is the bulk modulus related with p, a similar expression to (A2.37) is used, but now κ_i depend on the s_1, through the following law (Volckaert *et al.,* 2000):

$$\kappa_i = \kappa_{i0}\left(1 + \alpha_{sj}\ln\left(\left(s_j + p_{atm}\right)/p_{atm}\right)\right); \qquad j = 1,2 \tag{A3.14}$$

where α_{sj} is a parameter that relates stiffness with suction.

For the medium 2, the generalized stress is given in terms of p and s_2, according to (Alonso 1998):

$$\hat{p} = p + s_{l2}\, s_2 \tag{A3.15}$$

where s_{l2} is the degree of saturation of pellets. In this case, to evaluate the microstructural net stress it is taken into account that the pellets are unsaturated, and the Equation suggested by Alonso (1998) is adopted.

The volumetric strain increment due to $\hat{p}$ increment is given by:

$$\dot{\varepsilon}^{e}_{v2} = \frac{\dot{\hat{p}}}{K_2} \tag{A3.15}$$

where K_2 is computed with Equation (A2.23), but for this case the parameter which control the stiffness of medium 2 depends on the s_2 through Equation (A3.14). Thus, the expansive behaviour of clay powder and clay pellets has been taken into account.

APPENDIX A.4

A.4.1 OBC MODEL OF *MOCK-UP* TEST

A.4.1.1 INTRODUCTION

The aim of this Appendix is to present some complementary information related to the coupled *THM* analyses of the *mock-up* test introduced in Section 5.2 (Chapter V). The OBC model was developed at the beginning of the operational stage of the test and attempt to incorporate all available information obtained from laboratory test of FEBEX bentonite. Another objective of this Appendix is to present with more details some aspects of the *THM* formulation briefly introduced in the Chapters of the Thesis.

The theoretical framework adopted in the analysis is the fully coupled *THM* formulation for single porosity media proposed by Olivella *et al.* (1994). The balance equations are similar to the ones introduced in Section 2.2.2, expressed now for the case of single porosity medium. In the following sections the main constitutive equations adopted for the OBC model together with the equilibrium restrictions and also some phase physical properties are briefly introduced.

A.4.1.2 CONSTITUTIVE EQUATIONS

A.4.1.2.1 THERMAL

Conductive heat flow is assumed to be governed by Fourier's law:

$$\mathbf{i}_c = -\lambda \nabla T \tag{A4.1}$$

where λ is the global thermal conductivity of the porous medium and S_l is the volumetric liquid fraction. Based on experimental results of FEBEX bentonite (FEBEX Project, 2000) the following law has been adopted:

$$\lambda = \lambda_{sat}^{\,S_l} \lambda_{dry}^{\,(1-S_l)} \tag{A4.2}$$

where the values of λ_{sat} = 1.15 and λ_{dry} = 0.47 W/mºC have been obtained based on the experimental measurements presented in Figure (A4.1).

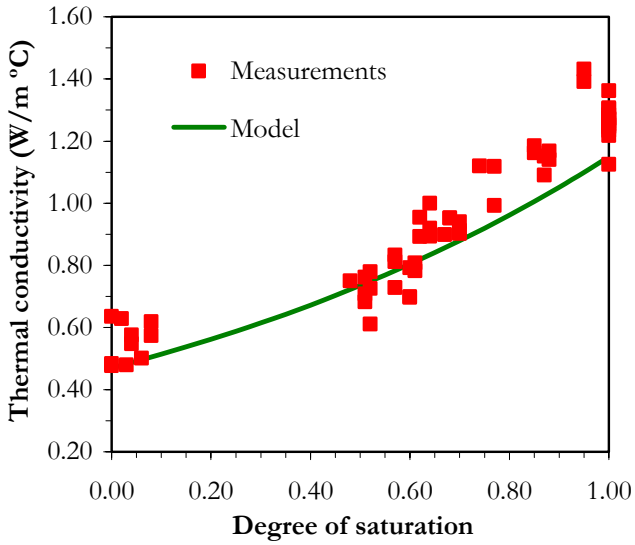

Figure A4.1. Experimental results and adopted thermal conductivity law for the FEBEX bentonite.

The internal energy for the medium is computed assuming that it is additive in relation to the phase (Olivella *et al.*, 1994).

$$E = E_s \rho_s (1-\phi) + E_l \rho_l S_l \phi + E_g \rho_g S_g \phi \tag{A4.3}$$

where E_s, E_l and E_g are the specific internal energies corresponding to each phase, i.e., the internal energy per unit mass of phase. ρ_s, ρ_l, ρ_g, are the densities of the three phases, ϕ is the porosity and S_g is the gas fraction with respect to the pore volume.

The gas phase energy is usually expressed as (Olivella *et al.*, 1994):

$$E_g \rho_g = \left(E_g^w \omega_g^w + E_g^a \omega_g^a \right) \rho_g = E_g^w \theta_g^w + E_g^a \theta_g^a \tag{A4.4}$$

where E^w_g and E^a_g are the specific internal energies of species (respectively water and air), that is, internal energy per unit of mass of species. ω^w_g and ω^a_g are the mass fraction of water and air species in gas phase, respectively. This additive decomposition is admissible for the gaseous phase in the assumption of mixture of gasses.

It is not so direct that the same decomposition is also valid for the liquid phase, however the same assumption will be made since the significance of the internal energy of dissolved air is small (Olivella *et al.*, 1994; Gens & Olivella, 2001):

$$E_l \rho_l = \left(E_l^w \omega_l^w + E_g^a \omega_l^a \right) \rho_l = E_l^w \theta_l^w + E_g^a \theta_l^a \tag{A4.5}$$

The values of the specific internal energies for the individual species are (Batchelor, 1983; Pollock, 1983, and Gens & Olivella, 2001):

E^w_l =4180.0 $(T\text{-}T_0)$ J/kg; E^w_g =2.5e^6+1900.0 $(T\text{-}T_0)$ J/kg; E^a_g =1006.0 $(T\text{-}T_0)$ J/kg, and E^a_g =1006.0 $(T\text{-}T_0)$ J/kg.

It can be noted that the specific internal energy of the vapour (water in gas phase) contains an additional term that represents the latent heat in vapour. The thermal consequences of evaporation/condensation are therefore taken into account in a straightforward way (Gens & Olivella, 2001).

Finally, the law obtained from the experimental data of FEBEX bentotine (reported in Villar & Cuevas, 1996) and suggested in the FEBEX Report (1998) has been assumed for the internal energy per unit mass of solid phase. This expression is given by:

$$E_s = E_s^o T + c_p T^2 \tag{A4.6}$$

where the two models parameters are: E^0_s = 732.52 and c_p =1.38 (FEBEX Report, 1998). For the steel the values adopted for these parameters are E^0_s = 480 and c_p =0 (Sears & Zemansky, 1966).

A.4.1.2.2 HYDRAULIC

Advective fluxes are computed using generalized Darcy's law, expressed as (Gens & Olivella, 2001):

$$\mathbf{q}_\alpha = -\mathbf{K}_\alpha \left(\nabla P_\alpha - \rho_\alpha \mathbf{g} \right); \qquad \alpha = l, g \tag{A4.7}$$

where P_α is the phase pressure. $\mathbf{K}_\alpha$ is the permeability tensor of α phase and $\mathbf{g}$ is the gravity vector. The permeability tensor is not constant but, in turn it, depends on other variables:

$$\mathbf{K}_\alpha = \mathbf{k}\frac{k_{r\alpha}}{\mu_\alpha}; \qquad \alpha = l, g \tag{A4.8}$$

where $\mathbf{k}$ is the intrinsic permeability tensor, μ_α is the dynamic viscosity of the α phase. Finally, $k_{r\alpha}$ is the α phase relative permeability.

The dependence of intrinsic permeability on pore structure is considered in terms of porosity. Two different laws were used in the analysis. In the first one the intrinsic permeability of the bentonite depends on porosity according to:

$$\mathbf{k} = k_0 \frac{\phi^3}{(1-\phi)^2}\frac{(1-\phi_0)^2}{\phi_0^3}\mathbf{I} \tag{A4.9}$$

where k_0 is the reference permeability at the reference porosity ϕ_0. The other model used in the sensitivity analysis (Section A.4.2) corresponds to an exponential law, presented as follows:

$$\mathbf{k} = k_0 \exp[b(\phi-\phi_0)]\mathbf{I} \tag{A4.10}$$

where k_0 is the intrinsic permeability at the reference porosity ϕ_0, and b is a model parameter. Figure (A4.2) presents experimental measurements of saturated permeability at different densities for FEBEX bentonite. This figure also presents the results for the two models presented before. The reference permeability adopted is $k_0 = 1.9\text{x}10^{-21}$ m^2 for a reference porosity of $\phi_0 = 0.4$. For the exponential model the parameter is $b = 30$.

The relative permeabilities of liquid and gaseous phases are made dependent on the degree of saturation according to:

$$a)\ k_{rl} = S_{el}^{\ n}; \qquad b)\ k_{rg} = (1-k_{rl}) \tag{A4.11}$$

where:

$$S_{el} = \frac{S_l - S_{lr}}{S_{ls} - S_{lr}} \tag{A4.12}$$

where S_{lr} , S_{ls} and n are model parameters. Equation (A4.11.a) considers the reduction of hydraulic permeability as the degree of saturation decreases. This variation is very difficult to determine directly and it is necessary to resort to indirect means of estimation. During the pre-operational study, the parameters of the relative permeability law for the bentonite were

determined from back-calculating the results of the hydration test carried out in small cell (FEBEX Report, 1998). The law determined in that study has been adopted in the OBC model. The law parameters are: S_{lr} = 0.01; S_{ls} = 1.0 and n = 3. A series of sensitivity analyses have been performed in order to evaluate the influence of this law in the final results. Some of these studies are introduced in Section A.4.1.5.4.

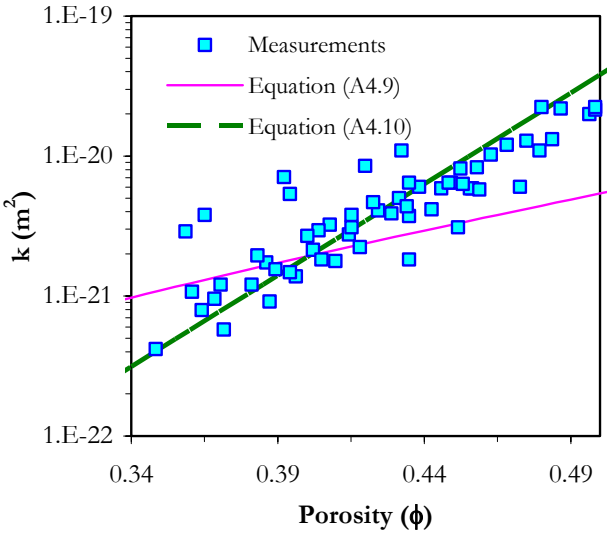

Figure A4.2. Variation of saturated permeability with porosity. Experimental data and adopted models for the intrinsic permeability law

Very low values of intrinsic permeability were measured in FEBEX bentonite under saturated conditions (Figure A4.2). On the other hand, much higher values are observed when the permeability to gas was measured in unsaturated conditions. Differences close to seven orders of magnitude were measured between water and gas permeablility for dry densities ranged form 1.65 and 1.70 Mg/m^3 (for instance, a gas permeability close to 2.2x10^{-15} m^2 were measured for a $S_l \approx 0.61$ and for a dry density of 1.70 Mg/m^3; Lloret & Villar, 2001). According to that, it is difficult to assume a single value of intrinsic permeability for FEBEX bentonite. As commented in Olivella & Gens (2000), if the value of intrinsic permeability for water was used, the gas permeability that one would obtain is several orders of magnitude smaller that the actual values. In fact, in that case the gas permeability is computed as the product of the intrinsic permeability (evaluated for the corresponding porosity) by the relative permeability to gas obtained applying Equation (A4.11.b), divided in the gas viscosity (Equation A4.8). The correct inclusion in the modelling of this high contrast between gas and liquid permeabilities is an open matter of discussion and it seems that more experimental results and theoretical developments are needed for a proper understanding and simulation of this problem. In the OBC model, a very simple correction has been adopted to consider a gas permeability closer to the values measured in the laboratory. In order to maintain the concept of intrinsic permeability, until more information is available, a correction has been applied to the relative permeability law, pre-multiplying Equation (A4.11.b) by a factor greater enough

(close to 1.0×10^7) to ensure a gas mobility in the FEBEX bentonite close the values of gas permeability measured in the laboratory tests.

The retention curve relates the degree of saturation of the material with suction. The law adopted is the following:

$$S_{el} = \left[1 + \left(\frac{s}{P_o} \right)^{\frac{1}{1-\lambda_o}} \right]^{-\lambda_o} f_d \tag{A4.13}$$

where:

$$f_d = \left(1 - \frac{s}{P_d} \right)^{\lambda_d} \tag{A4.14}$$

where P_o and λ_o are model parameters. The function f_d is included in order to model properly the high suction range. Similar functions were proposed previously by other authors (*i.e.* Fredlund & Xing, 1994; Romero, 1999). Here P_d is related with the suction at 0 degree of saturation and λ_d is a model parameter. When $\lambda_d = 0$ the original model (*i.e.* Gens *et al.,* 1998) is recovered.

Figure (A4.3) presents the results of tests carried out at conditions of constant volume over FEBEX bentonite (Villar *et al.*, 2004). In the same Figure, the adopted model is presented. The model parameters are: $P_0 = 20$ MPa; $\lambda_0 = 0.18$, $P_d = 1100$ MPa, and $\lambda_d = 1.10$.

The relation between P_0 and surface tension (σ) suggested by Olivella *et al.* (2001), has been extended to this model, that is:

$$P_o = P_{T_0} \frac{\sigma_T}{\sigma_{T_0}} \tag{A4.15}$$

where the surface tension N/m has been obtained fitting values of surface tension with the following expression (Olivella, 1995):

$$\sigma_T = 0.03059 \exp\left(\frac{252.93}{273.15 + T} \right) \tag{A4.16}$$

By varying P_0 in accordance with this expression, a dependence of the retention curve with temperature is introduced. Therefore, suction will decrease with temperature for a given degree of saturation (Olivella *et al.,* 2001). Note that the thermal effect involved is limited.

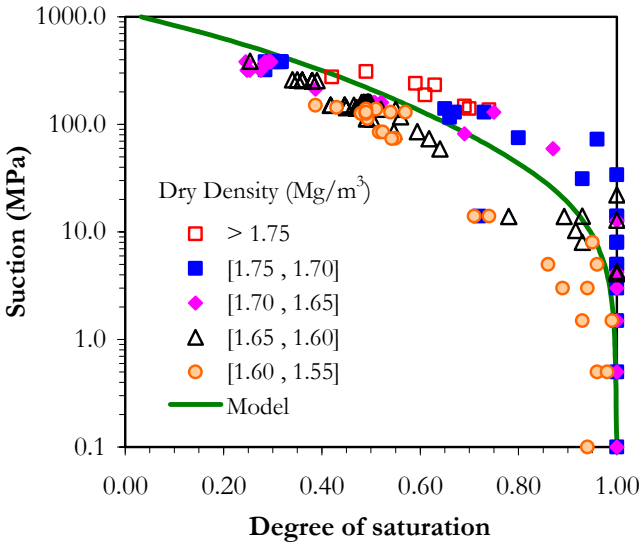

Figure A4.3. Retention curve adopted in the analyses, together with the experimental data of FEBEX bentonite (symbols).

Experimental results have shown that, in most cases, the influence of temperature on retention curve is indeed small (Villar *et al.*, 2004). Some experimental results of FEBEX bentonite at different temperatures are discussed in Section A4.2.

Non-advective fluxes of species inside the fluid phases are computed through Fick's law, which expresses them in terms of gradients of mass fraction of species through a hydrodynamic dispersion tensor that includes both molecular diffusion and mechanical dispersion (*i.e.* Olivella *et al.*, 1994; Gens & Olivella 2001):

$$\mathbf{i}_\alpha^i = -\mathbf{D}_\alpha^i \nabla \omega_\alpha^i ; \qquad i = w, a; \qquad \alpha = l, g \tag{A4.17}$$

where $\mathbf{D}^i_\alpha$ is the dispersion tensor of the medium.

For vapour diffusion, the following expression for the hydrodynamic dispersion tensor is adopted (*i.e.* Olivella, 1995):

$$\mathbf{i}_g^w = -\mathbf{D}_g^w \nabla \omega_g^w = -\left(\phi \rho_g S_g \tau D_m^w \mathbf{I} + \rho_g \mathbf{D}_g'\right) \nabla \omega_g^w \tag{A4.18}$$

where $\mathbf{D}_g^w$ is the dispersion tensor, τ is the tortuosity, D_m^w is the dispersion coefficient corresponding to molecular diffusion of vapour in air and D'_g is the mechanical dispersion tensor. The tortuosity takes into account the fact that the vapour diffusion takes place inside the voids of a porous media. A value of $\tau = 0.8$ has been adopted (Lloret *et al.,* 2001). The molecular diffusion coefficient is given by (*i.e.* Olivella, 1995 and Gens & Olivella, 2001):

$$D_m^w = 5.9x10^{-12}\frac{\left(273.15+T\right)^{2.3}}{P_g} \tag{A4.19}$$

where D_m^w is in m^2/s, P_g is in MPa and T in ºC. It can be noted that in vapour diffusion, the *THM* couplings are evident: effect of temperature through the variation of molecular diffusion with temperature; hydraulic effect through the influence of degree of saturation; and mechanical effects due to porosity changes (Gens & Olivella, 2001).

A usual expression for the mechanical dispersion is (*i.e.* Olivella, 1995 and Gens & Olivella, 2001):

$$\mathbf{D}'_g = -\mathbf{q}_g\mathbf{I} + \left(d_l - d_t\right)\frac{\mathbf{q}_g\mathbf{q}_g^t}{\left|\mathbf{q}_g\right|} \tag{A4.20}$$

Where d_t and d_l are transversal and longitudinal dispersivities respectively. In this case it has been assumed that the molecular diffusion is dominant and the mechanical dispersion of vapour has been neglected. So, the equation (A4.20) has been presented for completeness of the formulation only.

The same consideration can be made regarding diffusion of air in the liquid phase:

$$\mathbf{i}_l^a = -\mathbf{D}_l^a\nabla\omega_l^a = -\left(\phi\rho_l S_l\tau D_m^a\mathbf{I} + \rho_l\mathbf{D}'_l\right)\nabla\omega_l^a \tag{A4.21}$$

A.4.1.2.3 MECHANICAL PROBLEM

The *THM* version of the *BBM* presented in Appendix A.2 has been adopted in this analysis. As explained in Chapter III, the *BBM* can not reproduce the swelling behaviour of FEBEX bentonite. In the FEBEX Report (1998), some modifications in the elastic part of the model are introduced in order to reproduce the expansive behaviour of FEBEX bentonite. Due to the high compaction that the bentonite blocks have been subjected to, the description of the behaviour of the material inside the yield surface is particularly important. The variation of stress-stiffness with suction and, especially, the variation of swelling potential with stress and suction have been considered (FEBEX Report, 1998). The resulting elastic model is the following:

$$\dot{\varepsilon}_v^e = \frac{\kappa_i}{(1+e)}\frac{\dot{p}}{p} + \frac{\kappa_s}{(1+e)}\frac{\dot{s}}{(s+0.1)} + (\alpha_0 + \alpha_2 \Delta T)\dot{T} \tag{A4.22}$$

$$\dot{\varepsilon}_s^e = \frac{\dot{J}}{G} \tag{A4.23}$$

where:

$$\kappa_i = \kappa_i (1 + \alpha_s s) \tag{A4.24}$$

$$\kappa_s = \kappa_{s0} (1 + \alpha_{sp} \ln p / p_{ref}) \tag{A4.25}$$

$$G = \frac{E}{2(1+\nu)} \tag{A4.26}$$

where E is the young module.

The parameters of the mechanical model were adopted during the pre-operational stage and at the beginning of the operational stage. Some of the tests presented in Chapter IV were used in that work. Figure (A4.4) presents the model prediction in a swelling pressure test. The stress path prescribed in the simulation is similar to the one followed by a point located close to the heater, that is, an initial drying (in this case close to the 200 MPa) and then a wetting. In the same Figure, the results of the swelling pressure tests coded as SP1 and SP2 are shown. Table 4.1 (Chapter IV) present the main information related to these tests. Note that the model results can be considered as model predictions, because these tests were carried out after parameter determination. As it can be observed, the model results can be considered satisfactory, because the stress path is quite well reproduced as well as the predicted value of the swelling pressure.

Figure (A4.5) shows the main experimental data available for the FEBEX bentonite (for dry densities between 1.60 and 1.70 Mg/m^3). The data identified as CIEMAT and UPC correspond to eodemetric tests carried out at constant vertical stress and in conditions of constant water content (hygroscopic conditions). The data coded as Pintado (2002) were performed under conditions of free expansion and with a liquid degree of saturation close to 92 %. In the same Figure the result corresponding to the elastic thermal model adopted are also presented. Table (A4.1) presents the adopted parameters of the *BBM* model for the FEBEX bentonite.

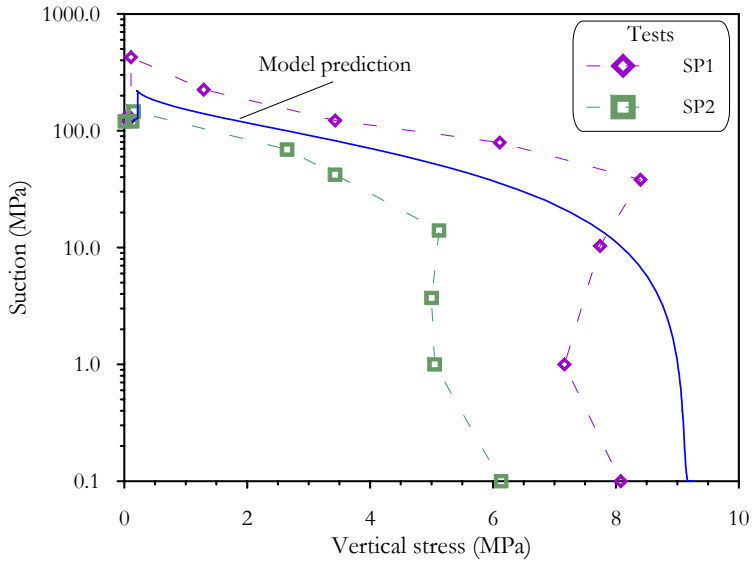

Figure A4.4. Computed stress path for swelling pressure tests using the *BBM*. SP1 and SP2 experimental results are provided for comparison.

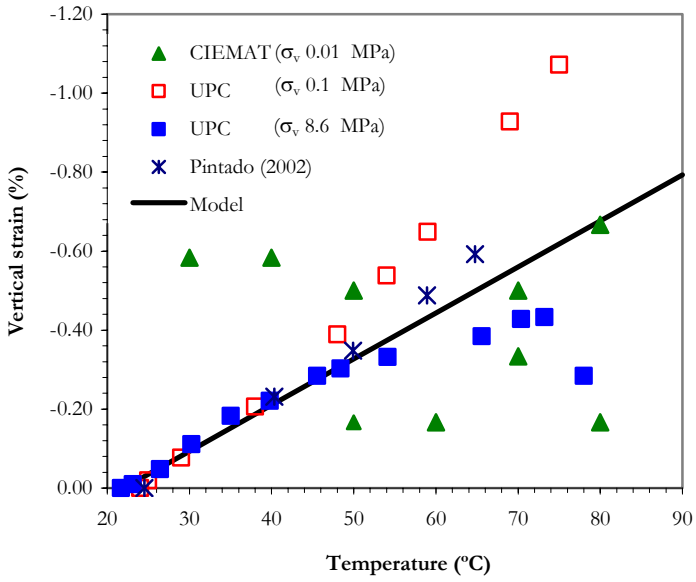

Figure A4.5. Comparisons between computed and measured thermal swelling at constant water content (Villar *et al.*, 2004; Pintado, 2002).

Table A4.1

Parameter for the *BBM* mechanical constitutive model. FEBEX bentonite

Elastic	*Parameters*	*Plastic*	*Parameters*
κ_i	0.05	$\lambda_{(0)}$	0.15
κ_s	0.30	r	0.925
μ	0.40	ζ	0.10
α_s (MPa)	-0.003	ρ ($^oC^{-1}$)	0.20
α_{sp}	-0.147	k_c	0.10
p_{ref} (MPa)	0.01	p_c (MPa)	0.50
α_0 ($^oC^{-1}$)	$1.5x10^{-4}$	M	1.00
α_2($^oC^{-2}$)	0	α	0.53
		p_o^* (MPa)	12.0
		α_1 ($^oC^{-1}$)	0
		α_3 ($^oC^{-2}$)	0

A.4.1.3 EQUILIBRIUM RESTRICTIONS

As explained in Chapter II, it is assumed that phase changes are rapid in relation to the characteristic times typical of this problem. So, they can be considered in local equilibrium, giving rise to a set of equilibrium restrictions that must be satisfied at all times (Olivella, 1995 and Gens & Olivella, 2001).

The vapour concentration in the gaseous phase is governed by the psychometric law, which can be expressed as (*i.e.*Gens & Olivella, 2001):

$$\theta_g^w = \left(\theta_g^w\right)^0 \exp\left(\frac{\Psi M_w}{R\left(273.15+T\right)\rho_l}\right) \tag{A4.27}$$

where θ_g^w is the vapour concentration in the gas phase; $(\theta_g^w)^0$ is the vapour concentration in the gas phase in equilibrium with a liquid at flat surface (at the sample temperature); Ψ is the total water potential of the water (excluding gravity terms), in this case it is related to suction ($\Psi = P_l - P_g$); M_w is the molecular mass of the water (0.018 kg/mol) and R the gas constant (8.314 J/mol/°K). The gases law relates vapour density and vapour pressure (*i.e.* Olivella, 1995):

$$\left(\theta_g^w\right)^0 = \frac{M_w P_{v(T)}}{R\left(273.15+T\right)} \tag{A4.28}$$

For pure water the vapour pressure has been approximate as (*i.e.*Olivella, 1995):

$$P_{v(T)} = 136075 \exp\left(\frac{-5239.7}{273.15+T}\right) \tag{A4.29}$$

To define the amount of air dissolved in water, Henry's law is adopted. This law expresses a linear relationship between the concentration of air in dissolution and the partial pressure of air (P_a) in the gaseous phase:

$$\theta_l^a = \omega_a^l \rho_l = \frac{P_a}{H}\frac{M_a}{M_w}\rho_l \tag{A4.30}$$

where M_a is the molecular mass of the air (0.02895 kg/mol), and H is Henry's constant (1000 MPa).

A.4.1.4 PHASE PHYSICAL PROPERTIES

The properties of the fluid phase appear in the balance equations and in the constitutive laws. In general, they depend on the composition of the phase and on the state variables (temperatures and pressures). Some of them are introduced below.

The function of density for the liquid phase can be expressed as (*i.e.* Olivella, 1995 and Gens & Olivella, 2001):

$$\rho_l = 1002.6 \exp\left(4.5x10^{-4}\left(P_l - 0.1\right) - 3.4x10^{-4}T\right) \tag{A4.31}$$

where T is expressed in ºC, P_l in MPa and in ρ_l kg/m^3. This expression must have a cut-off for large negative liquid pressures; if not, unrealistic low liquid density is obtained.

The air density is obtained from the law of ideal gases:

$$\theta_g^a = \frac{M_a P_a}{R\left(273.15+T\right)} \tag{A4.32}$$

The density of the gas phase is obtained adding the partial densities of the two species:

$$\rho_g = \theta_g^w + \theta_g^a \tag{A4.33}$$

Finally, the viscosity of the liquid and gas phase are, respectively (*i.e.* Olivella, 1995):

$$\mu_l = 2.1x10^{-12} \exp\left(\frac{1808.5}{273.15+T}\right) \tag{A4.34}$$

$$\mu_g = 1.48x10^{-12} \exp\left(\frac{(273.15+T)^{1/2}}{1+\frac{119}{(273.15+T)}}\right) \tag{A4.35}$$

where T is expressed in ºC and μ_α in MPa.s.

A.4.1.5 MODELLING

All the analyses have been carried out using the computer program CODE_BRIGHT introduced in Chapter II. One-dimensional and two-dimensional meshes have been used in the simulations. The 1-D analyses have been helpful in the first stage of the analysis to examine the basic patterns of thermal, hydraulic and mechanical behaviour of the test. A series of sensitivity analyses have also been performed, some of them are presented in Section A.4.1.5.4. The 2-D analysis has been performed with the final adopted parameters and conditions.

A 1-D radial discretization is adopted taking advantage of the symmetry of the problem and of the relative long size of the heaters compared with the bentonite thickness. Figure (A4.6) shows the various zones considered in the discretization. The main interest lies in the buffer zone that has a thickness of 63.6 cm (zone C). The heater (zone B) and the confining structure (zoned E) are also represented (steel). Between the confining structure and the buffer, three layers of geotextile have been placed to ensure a uniform distribution of the hydraulic boundary conditions. This geotextile has been incorporated in the mesh (zone D). The properties of this material have been reported in Martin & Villar (1997). The mesh has 50 linear elements, not uniformly distributed. In the zone C the mesh is denser close to the hydration boundary and close to the heater. A series of sensitivity analyses were carried out in order to ensure the no dependence of the results on the mesh.

To obtain a better estimation of the effect of real geometry of the *mock-up* test, *THM* coupled analyses have been performed using 2-D axisymetric longitudinal section. Only one half of the problem is analysed because of symmetry. The same five zones considered in the 1-D model have been contemplated in the 2-D mesh. The mesh has 580 quadrilateral bilinear elements with 4 integration points. Selective integration according to Hughes (1980) has been adopted (more details in Olivella *et al.*, 1995 and CODE_BRIGHT User's Manual, 2004). It can be found more information in relation to this modelling in: FEBEX Report (1998), FEBEX Project (2000), Sánchez & Gens (2001) and Sánchez & Gens (2002).

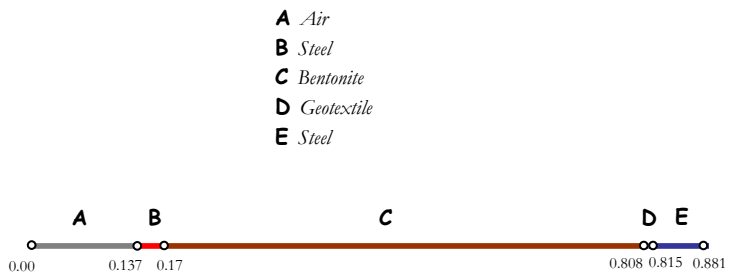

Figure A4.6. 1-D geometry used in the simulations.

A.4.1.5.1 INITIAL CONDITIONS

Hydraulic: The initial water content of the bentonite is 14 %. This corresponds to a global degree of the saturation of the barrier of 58.1 %. Before the start of the heating, the ***mock-up*** test was flooded to try to achieve the closure of the gaps between the bentonite bricks prior to the performance of the main test. The procedure used and the events observed during and after the flooding are described in ENRESA (1997). During this flooding stage a total of 634 kg of water were intaken in the barrier. This implies a global degree of saturation of the barrier close to 71.50 %. An initial suction of 105 MPa has been adopted for the whole barrier, this suction is close to the ones measured (in average terms) in the central and internal zones of the barrier just before the heater was switched on. According with the retention curve adopted, this implies an initial degree of saturation close to 65.2 %. In order to ensure that the test and the model have the same initial amount of water at the beginning of the heating, an initial (isothermal) hydration has been simulated until the global degree of saturation of the ***mock-up*** model reach the same value of the test (that is 71.50 %). Post-mortem analyses of the thermo-hydraulic cells (Villar & Rivas, 2001) and of the ***in-situ*** test have shown a complete closure of the gaps and joints between blocks, and a rather homogeneous material was observed close to these discontinuities.

Thermal: An initially uniform temperature of 20 ºC is assumed in the entire domain. This is consistent with CIEMAT Report (2002) data.

Mechanical: A hydrostatic value of 0.11 MPa has been adopted, approximately equal to the weight of the bentonite in the mid diameter of the buffer.

A.4.1.5.2 BOUNDARY CONDITIONS

Hydraulic: An applied water pressure of 0.55 MPa is applied in the geotextile (***i.e.*** at the interface between steel and bentonite) in accordance with CIEMAT Report (2002) data. Regarding the gas pressure it is not clear if the experiment is airtight or not. A series of numerical analyses have been carried out in order to evaluate the sensitivity of the results in relation to this condition. No strong dependence of the results has been detected. The analysis presented herein assumes that the test is airtight.

Thermal: The thermal boundary conditions at: r = 0.15 m, radial coordinate of the heater elements are as follows:

- 0 - 6 days constant power 250 W/heater
- 6 days - t_{100} constant power 500 W/heater
- > t_{100} T = 100 ºC

t_{100} is the time at which the temperature reaches 100 ºC at some point in the bentonite. In the performed analysis is 15.6 days. On the external boundary, the following radiation condition has been applied:

$$j_e = \gamma_e \left(T^0 - T \right) \tag{A4.36}$$

Where j_e is the heat flow, T^0 is the prescribed temperature (T^0 = 20 ºC) and γ_e is the radiation coefficient. A coefficient γ_e =5 has been adopted. This value has been adjusted in order to ensure the prescribed condition (T^0) on the outer boundary.

Mechanical: A stress free outer boundary has been prescribed.

A.4.1.5.3 MODEL RESULTS

The main trend of the *THM* behaviour of the ***mock-up*** test has been presented in detail in Chapter V. In Chapter V the analysis has been focused on two representative cross sections of the test (Sections A4-B4, and A10-B10). Special attention has also been placed in the description of the main *THM* phenomena and coupling that take place during the simultaneous heating and hydration of the experiment. Herein, complementary information related of this modelling is presented. The aim is to allow a wider view of the barrier behaviour, as well as of the model performance. In that sense, Figures (A4.7 to A4.9) present for other four sections the comparisons between the evolutions of measured and computed values of temperature, relative humidity and stresses, respectively. All the instrumented sections of the test have been presented. The distributions of variables in different sections of the barrier for different times also offer a good representation of the barrier behaviour. Figures (A4.10 and A4.11) present the distribution of temperature in longitudinal and transversal sections, respectively. Figures (A4.12 and A4.13) present for the same sections the distribution of relative humidity. In these plots the measured variables in positions close to these sections have also been represented. Figures (A4.14) present the distribution of porosity in two transversal and longitudinal sections. Finally, Figures (A4.15 to A4.18) present, for different times of the analysis, contours of temperature, saturation degree, radial stress and porosity, respectively.

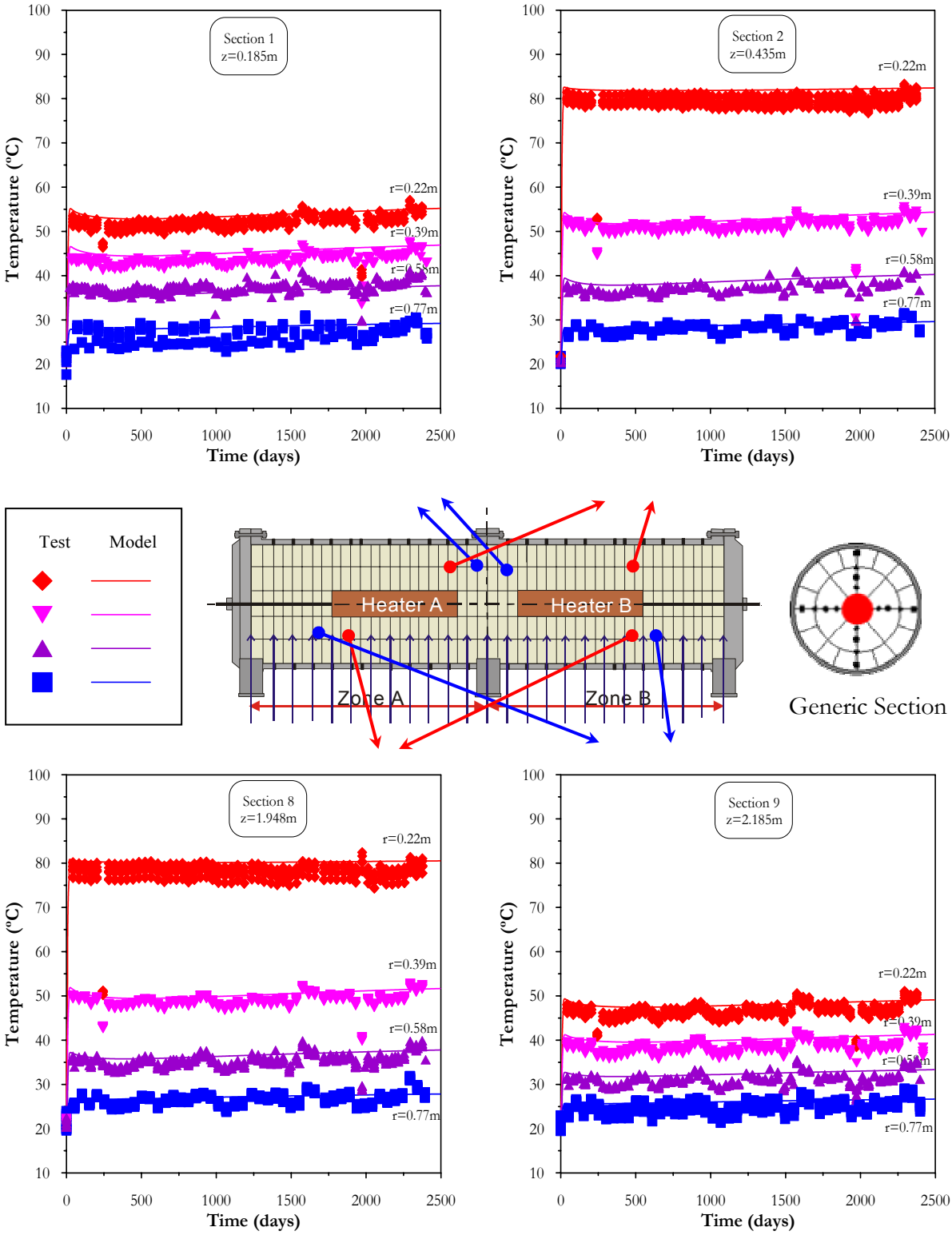

Figure A4.7. Evolution of temperature in the *mock-up* test. Sections 1, 2, 8 and 9. Observed versus computed values (OBC model).

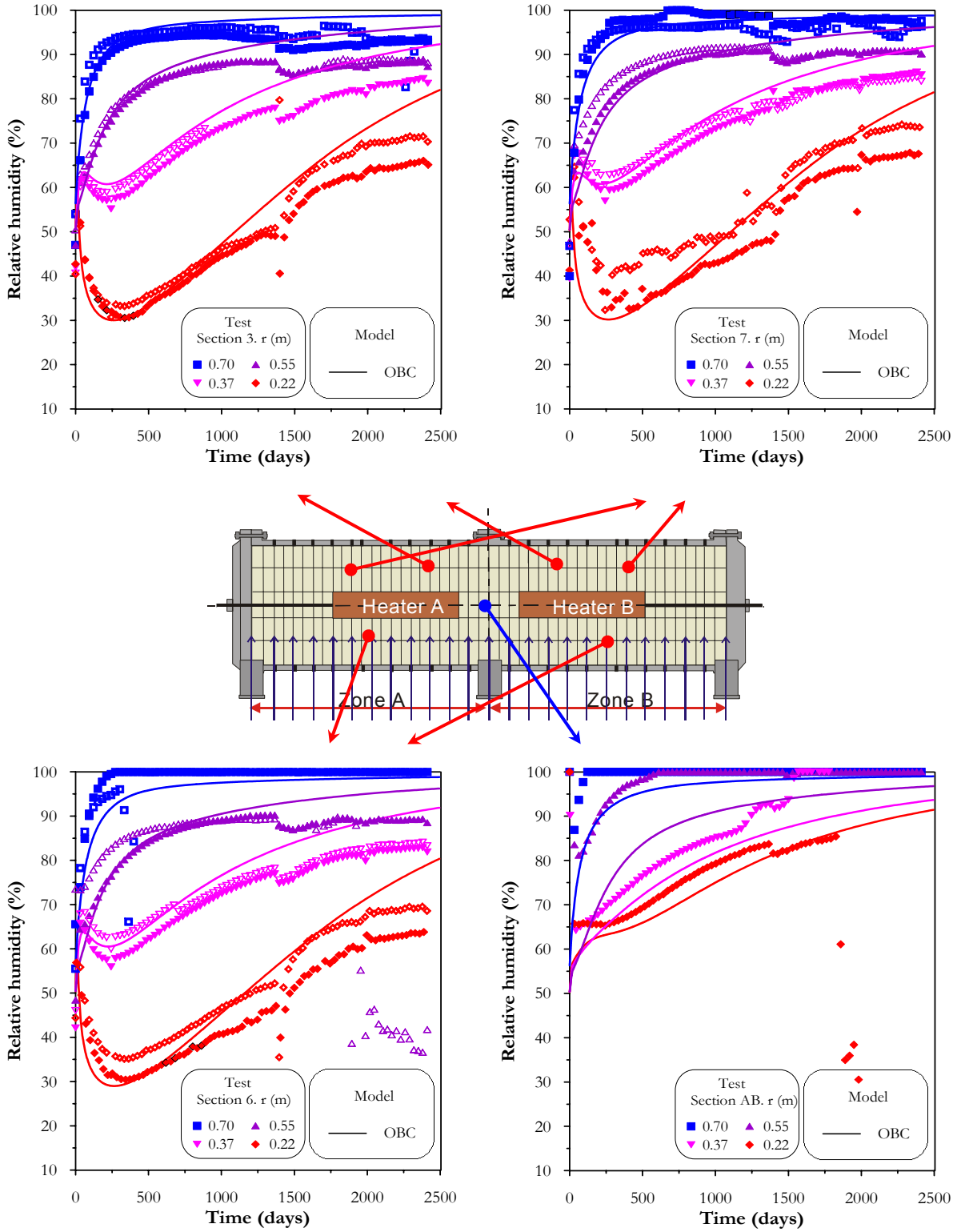

Figure A4.8. Evolution of relative humidity in the *mock-up* test. Sections 3, 6, 7 and AB. Observed versus computed values (OBC model).

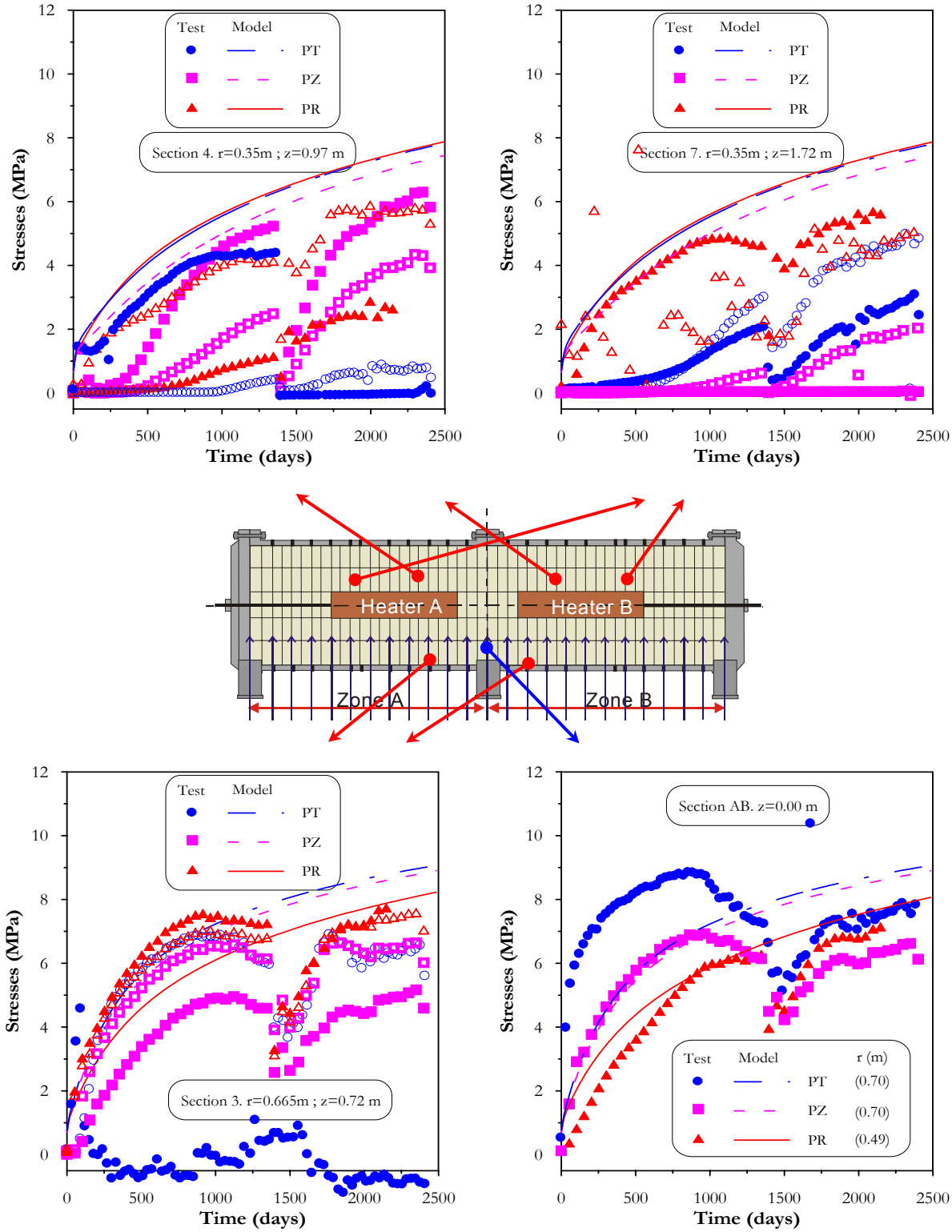

Figure A4.9. Evolution of stresses in the *mock-up* test. Sections 3, 4, 7 and AB. Observed versus computed values (OBC model).

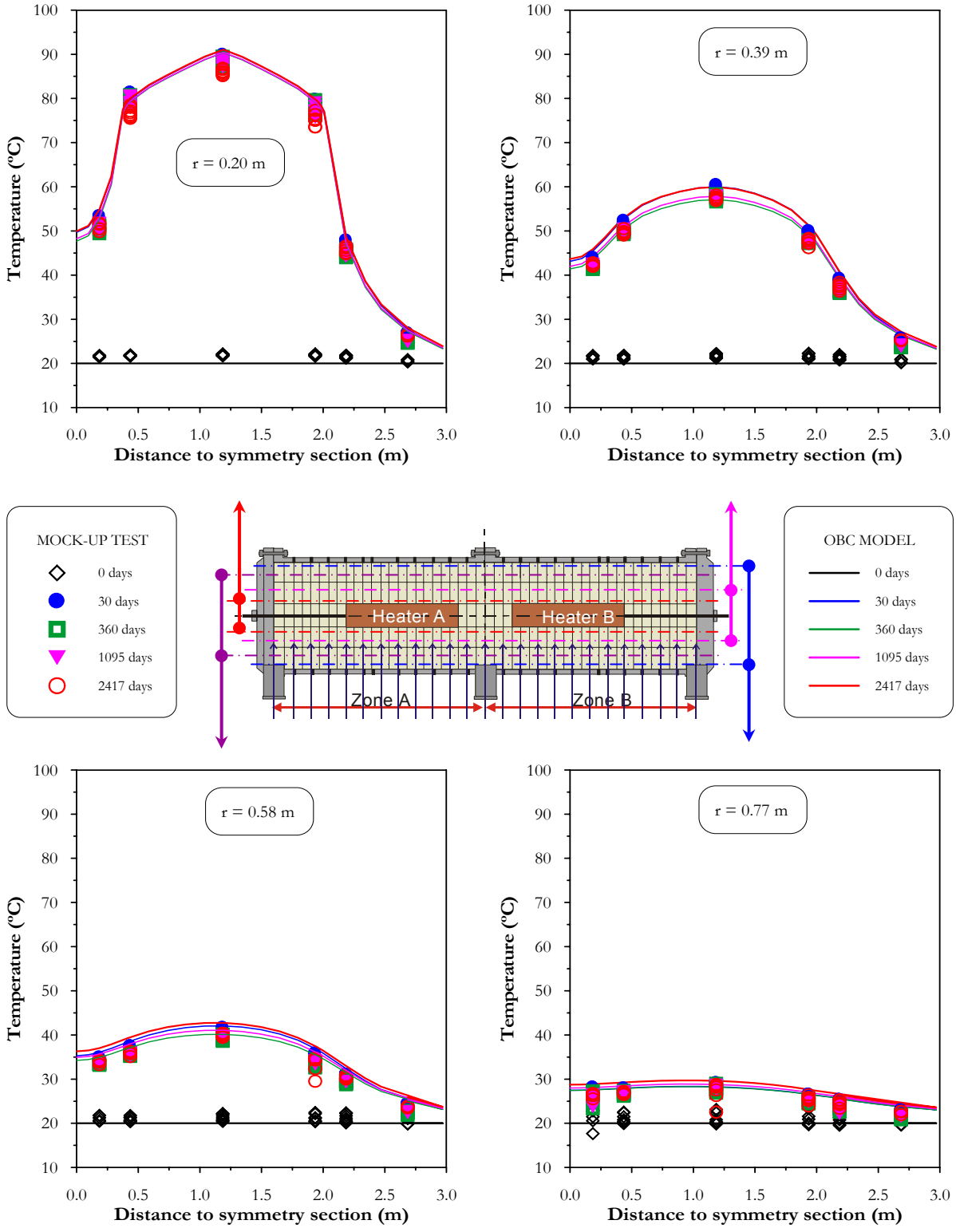

Figure A4.10. Distributions of temperatures in longitudinal sections of the *mock-up* test. Radii: 020, 0.35, 0.58 and 0.77 (m). Observed versus computed values (OBC model).

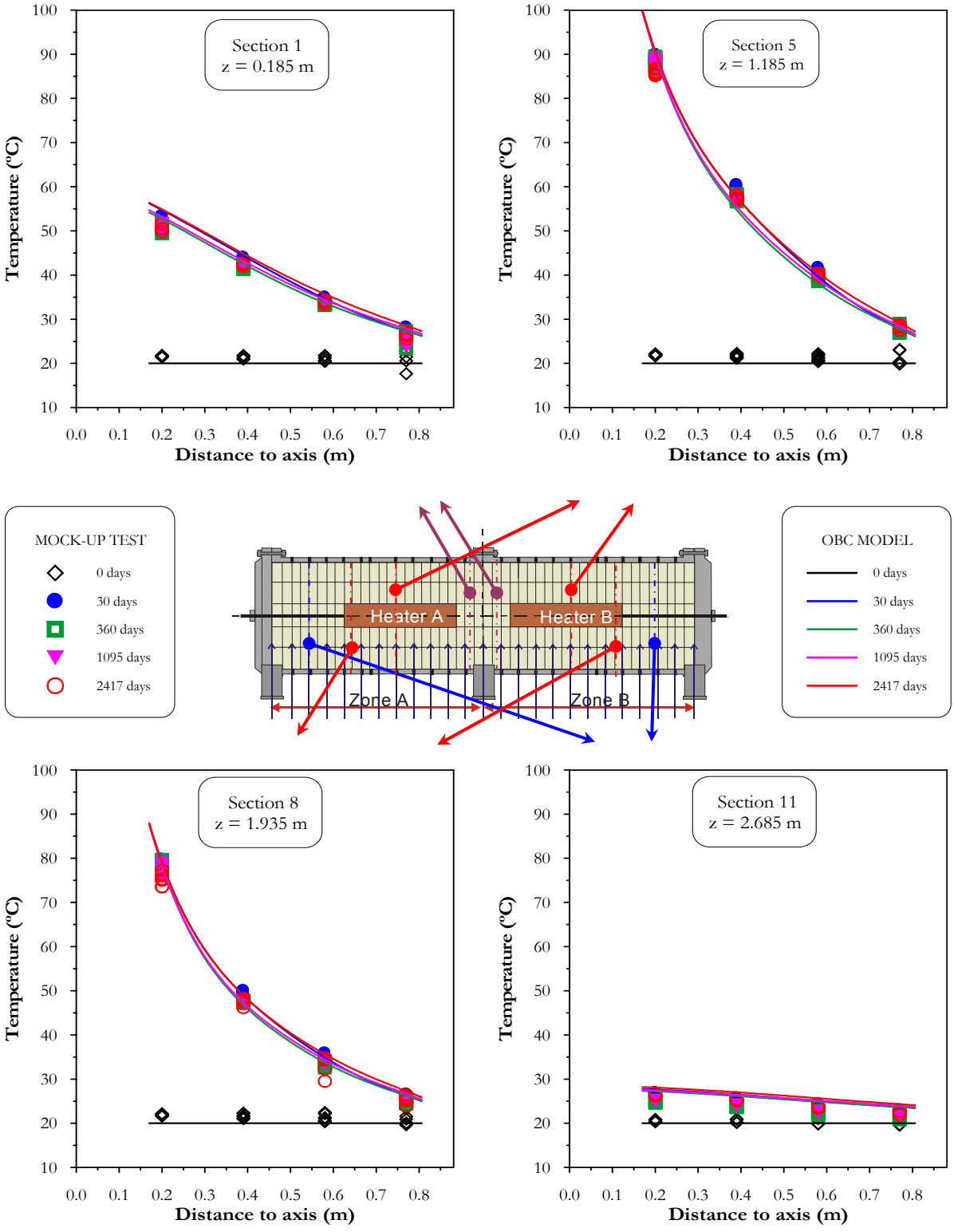

Figure A4.11. Distributions of temperatures in transversal sections of the *mock-up* test. Sections 1, 5, 8 and 11. Observed versus computed values (OBC model).

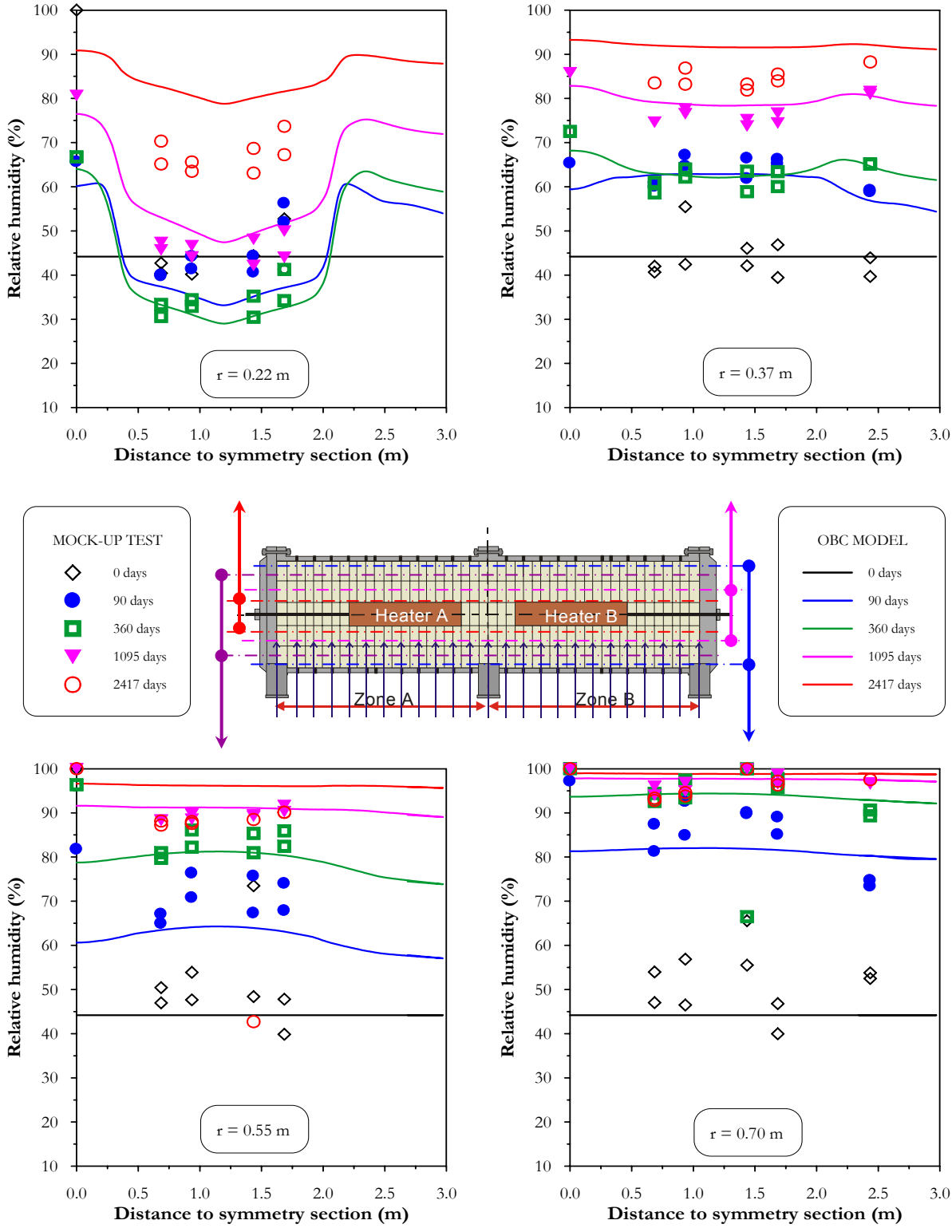

Figure A4.12. Distributions of relative humidity in longitudinal sections of the *mock-up* test. Radii: 022, 0.37, 0.55 and 0.70 (m). Observed versus computed values (OBC model).

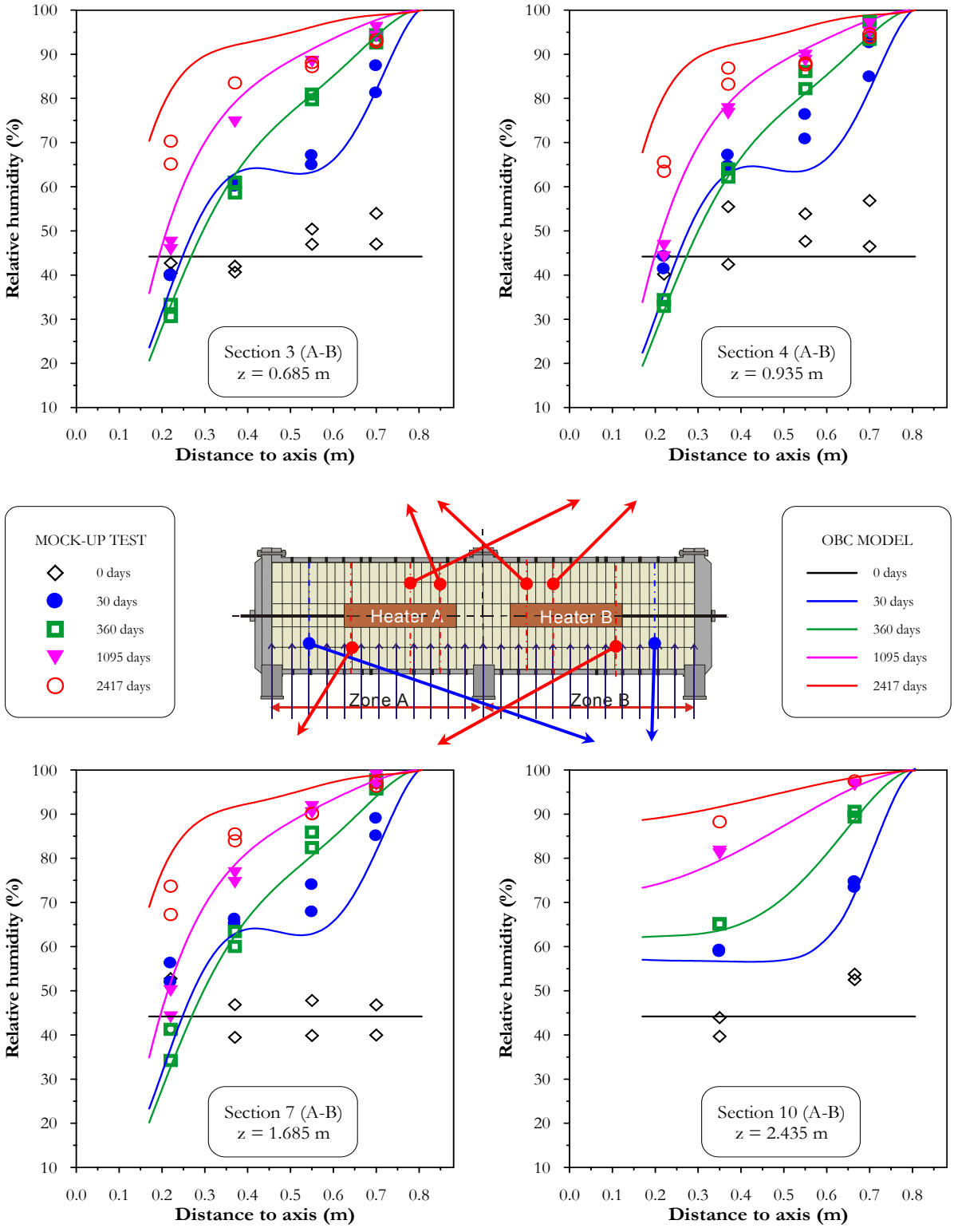

Figure A4.13. Distributions of relative humidity in transversal sections of the *mock-up* test. Sections 3, 4, 7 and 10. Observed versus computed values (OBC model).

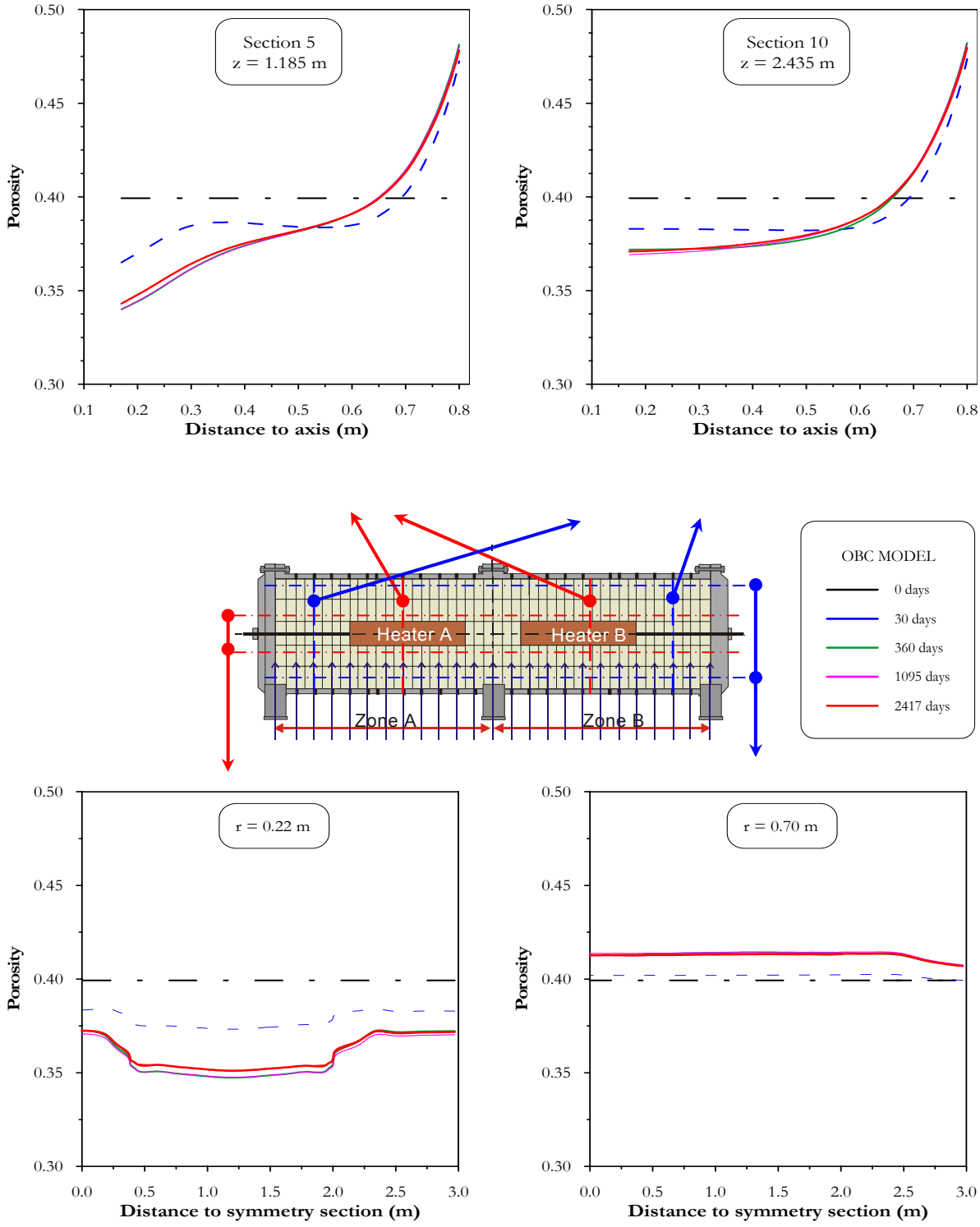

Figure A4.14. Distributions of porosity in transversal and longitudinal sections of the *mock-up* test. (OBC model).

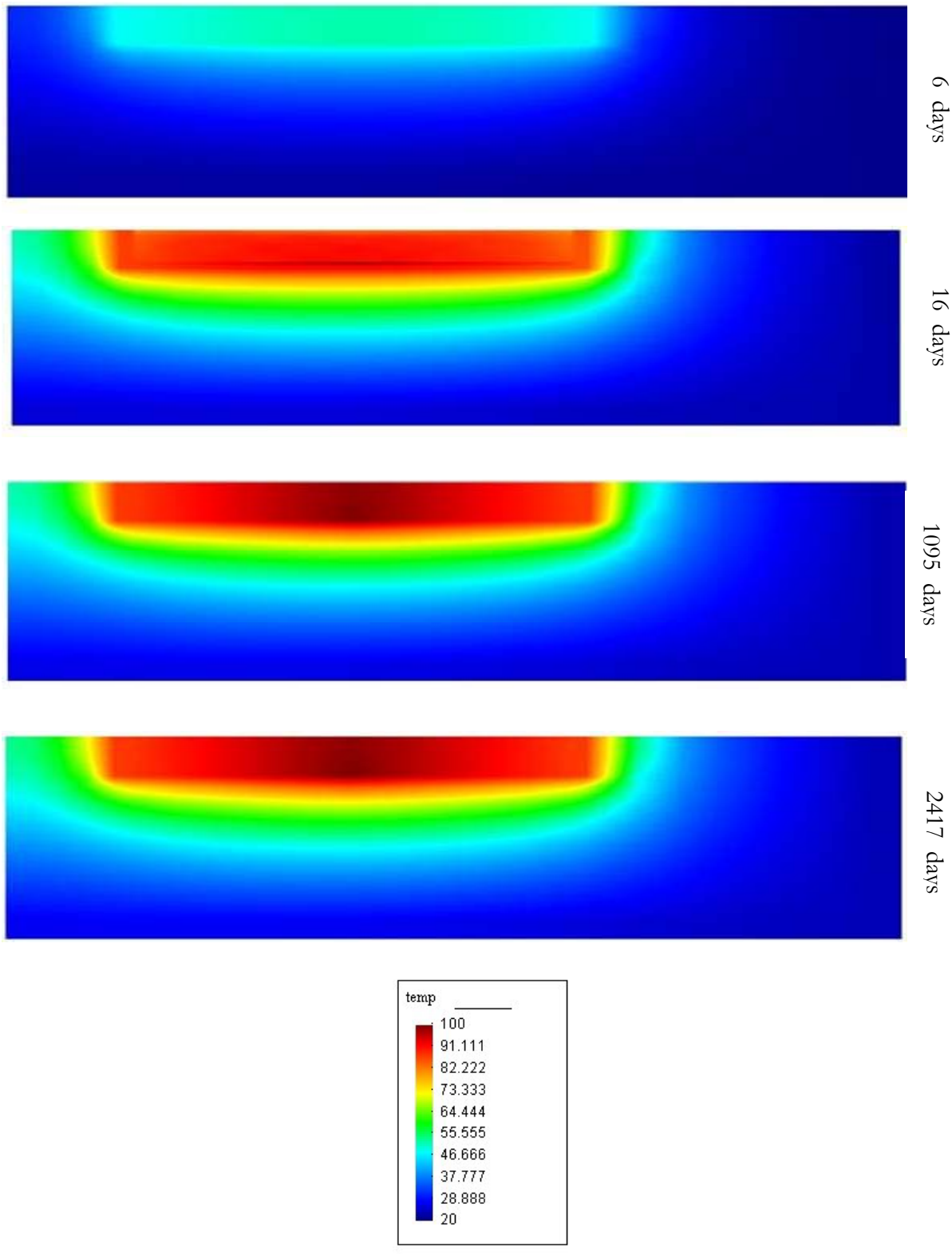

Figure A4.15. Contours of temperature for different times of analysis. OBC model, *mock-up* test.

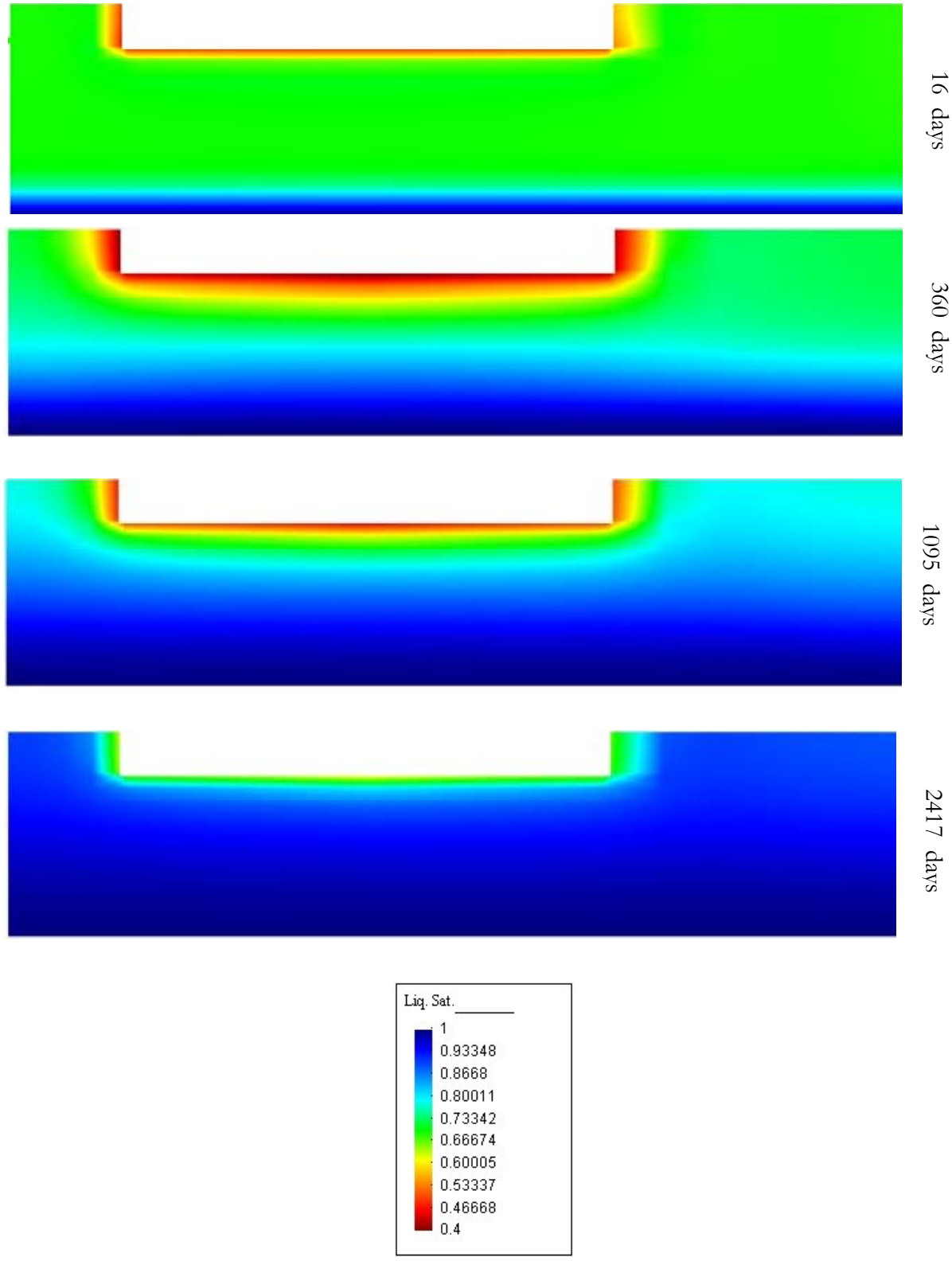

Figure A4.16. Contours of liquid saturation for different times of analysis. OBC model, *mock-up* test.

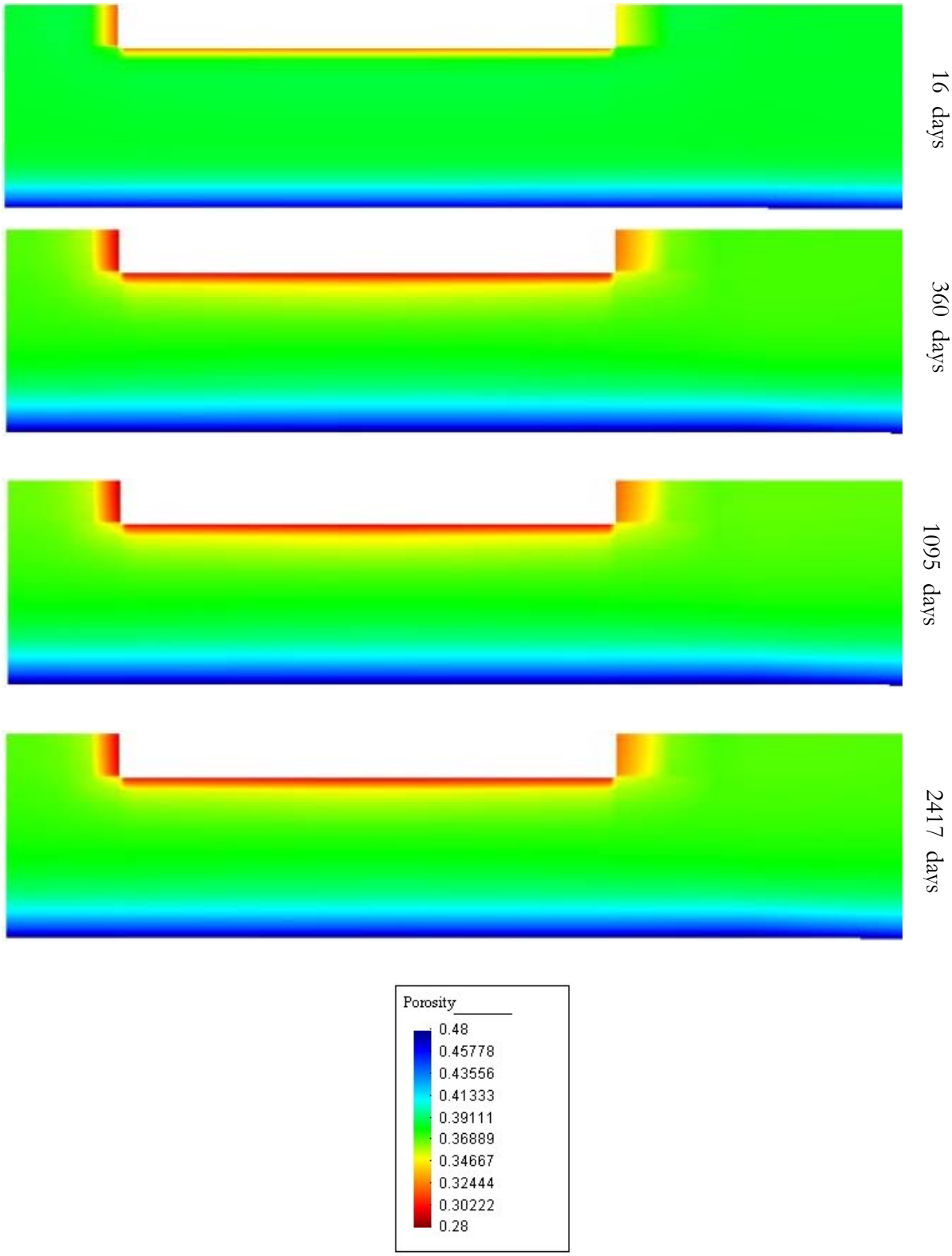

Figure A4.17. Contours of porosity for different times of analysis. OBC model, *mock-up* test.

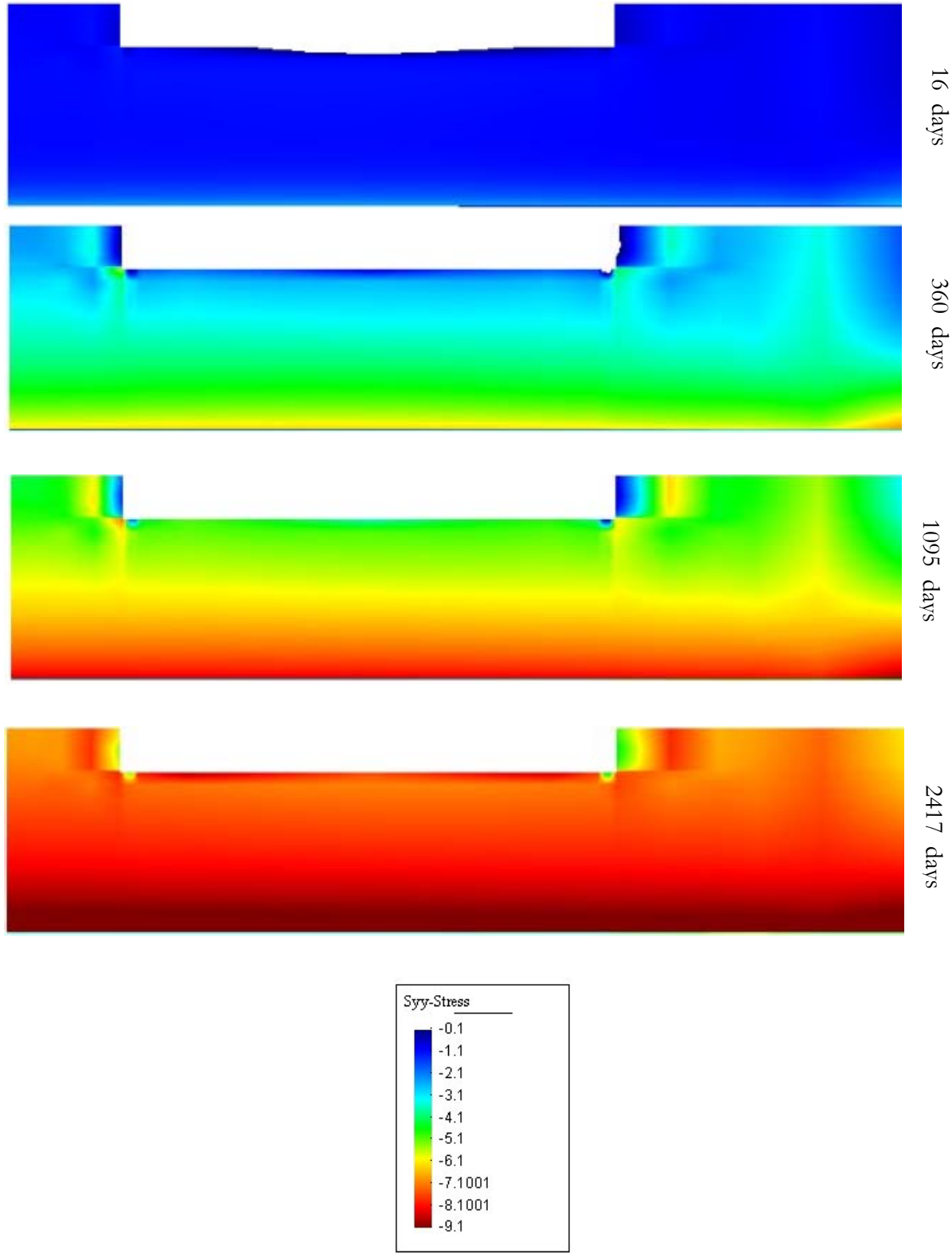

Figure A4.18. Contours of radial stress for different times of analysis. OBC model, *mock-up* test.

A.4.2 SENSITIVITY ANALYSES

Sensitivity analyses are very convenient for complex cases as the one presented here, in which the problem is controlled by a large number of parameters, often uncertain, and affected by the interaction between a variety of phenomena. The sensitivity analyses have been carried out in different stages of the FEBEX project. During the preoperational stage of the project a series of sensitivity study were performed with two main aims: i) to check the effect of variations of parameters on results, and ii) to improve the understanding of the system performance. A summary of the analyses carried out in this stage can be found in the FEBEX Report (1998).

A series of sensitivity analyses were also performed at the beginning of the operational stage. The aim of this study was to check the sensitive of the model results in relation to the changes in the constitutive law (or parameters) with physical meaning and consistent with the experimental observations of the FEBEX bentonite. Finally, when the OBC model could not explain the tendencies of the experiment (at advanced stages of hydration), a series of sensitivity analyses were performed. The aim of these analyses was to explore whether, with minor modifications of the constitutive laws or parameters, it was possible to explain and to reproduce in a more adjusted way the global evolution of the tests.

In these last studies the 1D axisymetric model has been used. The results obtained with this model can be considered significantly approximated. For instance, Figures (A4.19) present the comparisons between the outputs of the two models, *i.e.* 1D and 2D axisymetric, for a 'hot cross-section'.

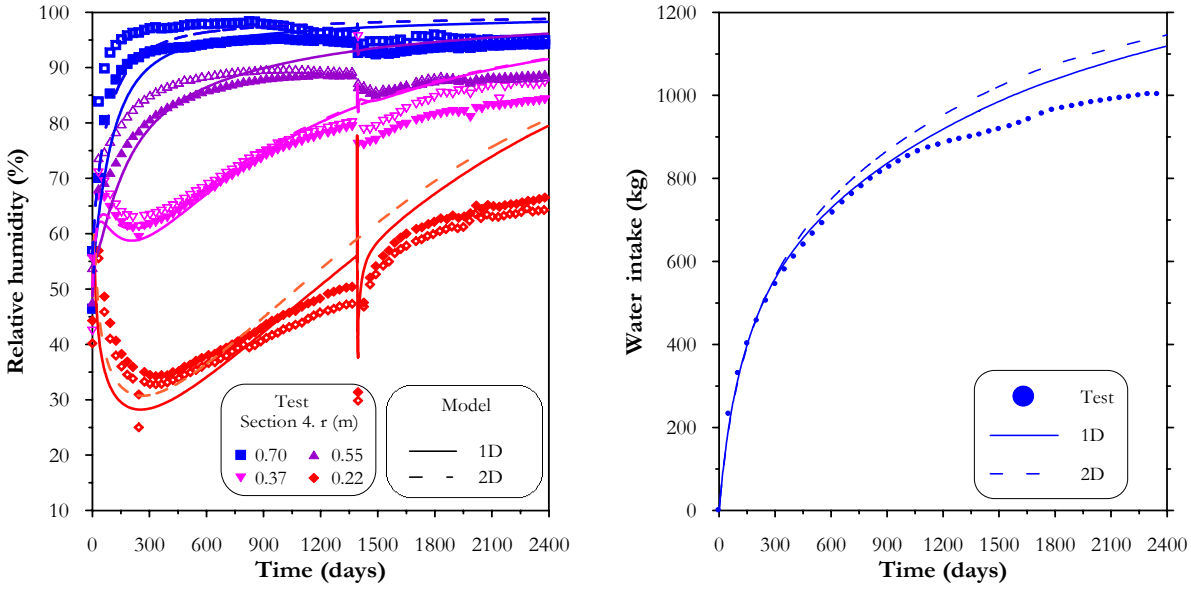

Figure A4.19. Comparisons between the model results of 1D and 2D axisymetric. A 'hot cross-section' has been analyzed. Observed versus computed values (OBC model).

In the following paragraphs some of the sensitivity analyses performed are introduced. In each simulation only one constitutive law has been changed, and the other laws correspond to the ones adopted in OBC model. The different cases analysed are presented separately according with the constitutive law considered.

Intrinsic permeability: This constitutive law plays an important role in the evolution of the water entry and also in the water distribution inside the barrier. In the OBC analysis, the model defined by Equation (A4.9) is the one adopted to account for the variation of intrinsic permeability with porosity (Figure A4.2). However, according to this Figure, the exponential law given by Equation (A4.10) appears as more adequate to fit the experimental data. The analysis coded as 'kint' considers this intrinsic permeability law. Figures (A4.20 to 22) present the results obtained with this model. Figure (A4.22) shows that the initial water entry is higher than for the OBC case. This is because the law selected implies larger variations of intrinsic permeability as porosity increases. So, the outer zones hydrate more quickly because they are now attributed to higher permeability (see Figure A4.14). The opposite behaviour can be noted in the inner zones of the barrier, because now, permeabilities will be lower and, therefore, the advective flow coming from the wetter zones will also be smaller and the hydration will slow down.

The model results obtained with this model can not be considered satisfactory. As explained in Chapter V, single porosity models can not handle properly the influence of the pore structure on the behaviour of expansive clays. It seems that, the explicit consideration of the clay fabric, their main pores levels, and their interaction are crucial points for a proper modelling of this kind of problems.

Relative permeability: As commented in Section (A4.1.2.2) the relative permeability law was obtained indirectly. This constitutive law could also play a relevant role in the kinetics of the barrier hydration. In the analysis presented here as 'krel' a power coefficient λ=5 has been adopted. As it can be observed in Figures (A4.23 to A4.26) the model response is not good.

Retention curve: Another relevant law in the modelling of non-saturated expansive clays is the retention curve. In the literature many laws to model the water retention capacity of the soils can be found (van Genuchten, 1982; Ferdlund & Xie, 1998; Romero, 1999, among others). As it can be observed in Figure (A4.3), the water retention capacity of the FEBEX bentonite depends on dry density. On the other hand, Figure (A4.14) shows that the clay porosity varies according with position and time. The retention curve adopted in the OBC model is very simple and is not able to account the changes in the retention curve due to changes in the dry density. A first modification of the proposed retention curve (Equation A4.13) is related to the inclusion, in a simplified way, of the dependence on dry density. Figures (A4.26 and A4.27) present the results obtained using a modified retention curve that expresses the relation between degree of saturation and suction as:

$$S_e = \left[1 + \left(\frac{s}{P_o f_\phi} \right)^{\frac{1}{1-\lambda_o}} \right]^{-\lambda_o} f_d \qquad \text{(A4.37)}$$

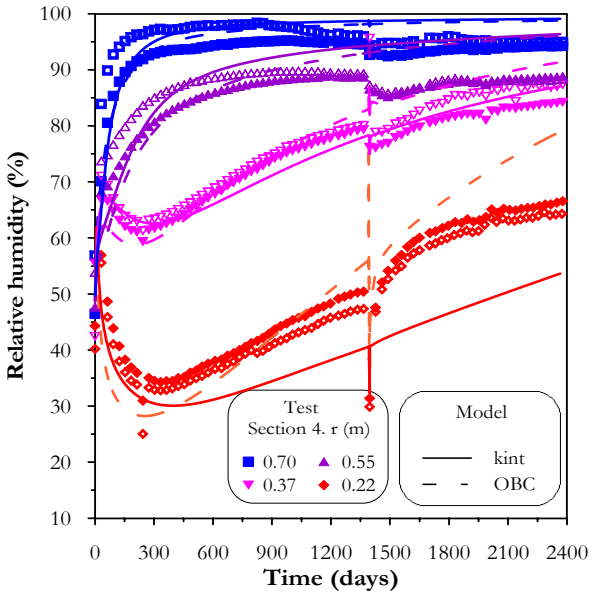

Figure A4.20. Relative humidity evolution. Sections A4-B4. Observed versus computed values of 'kint' and 'OBC' models.

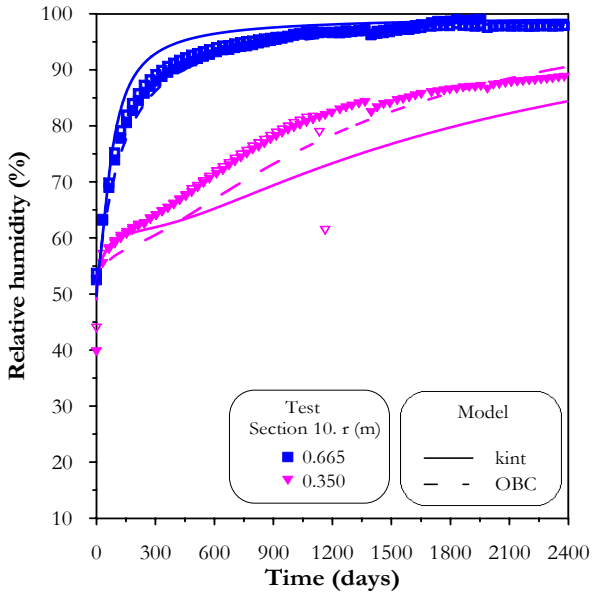

Figure A4.21. Relative humidity evolution. Sections A10-B10. Observed versus computed values of 'kint' and 'OBC' models.

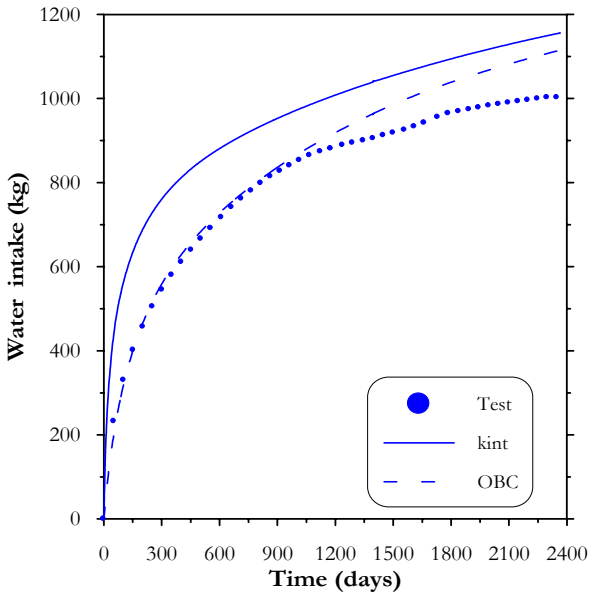

Figure A4.22. Water intake. Observed versus computed values of 'kint' and 'OBC' models.

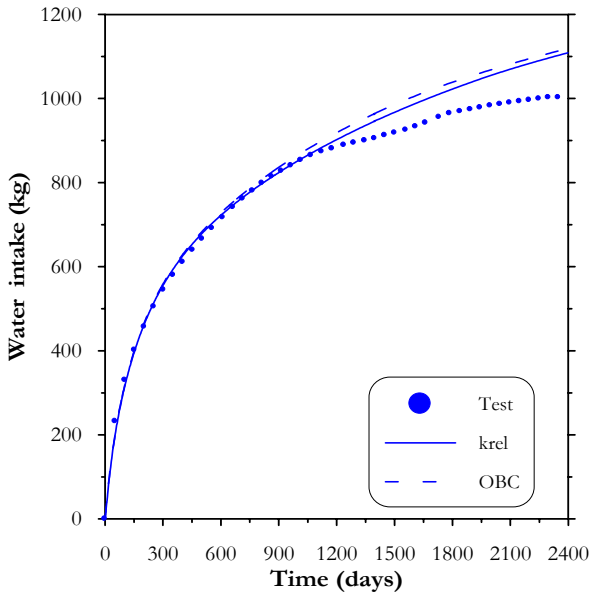

Figure A4.23. Water intake. Observed versus computed values of 'krel' and 'OBC' models.

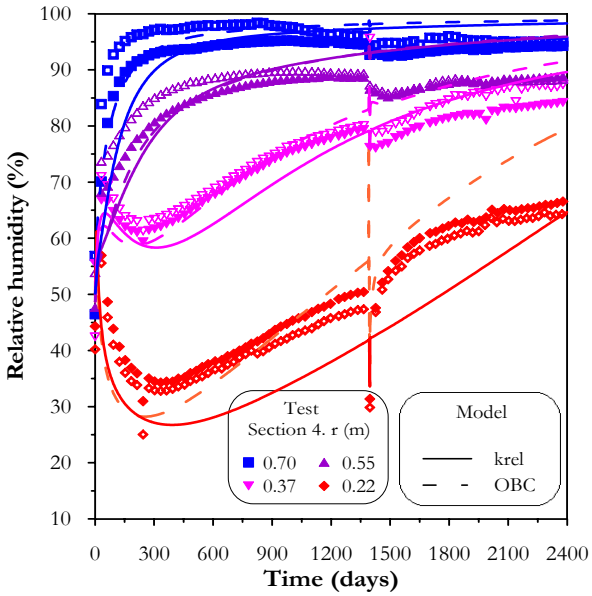

Figure A4.24. Relative humidity evolution. Sections A4-B4. Observed versus computed values of 'krel and 'OBC' models.

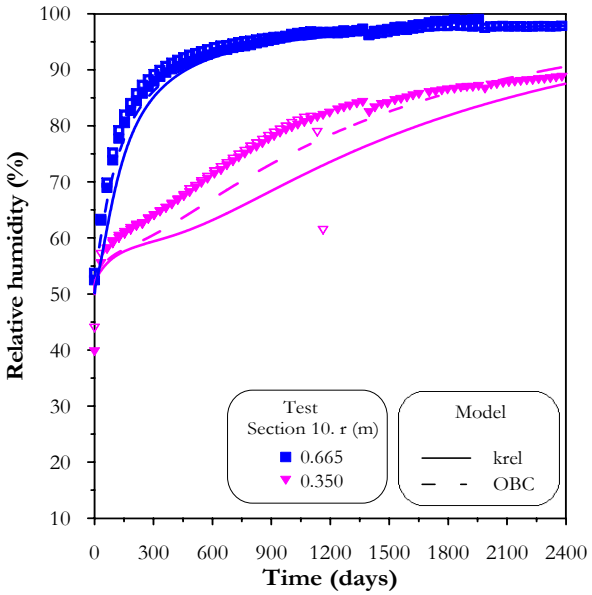

Figure A4.25. Relative humidity evolution. Sections A10-B10. Observed versus computed values of 'krel and 'OBC' models.

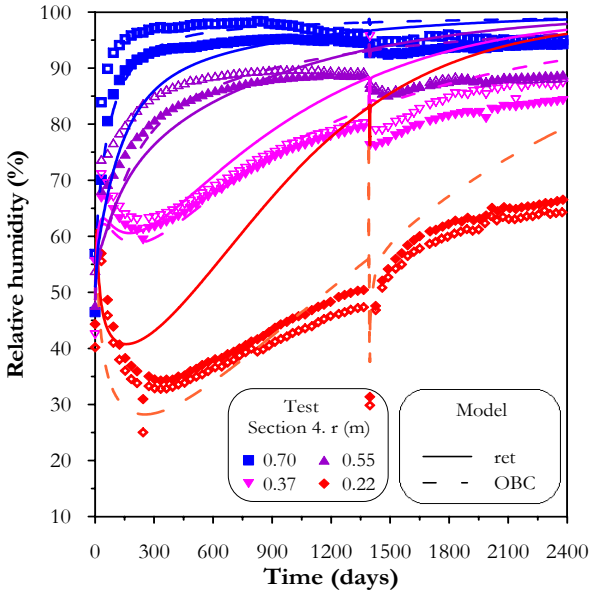

Figure A4.26. Relative humidity evolution. Sections A4-B4. Observed versus computed values of 'ret' and 'OBC' models.

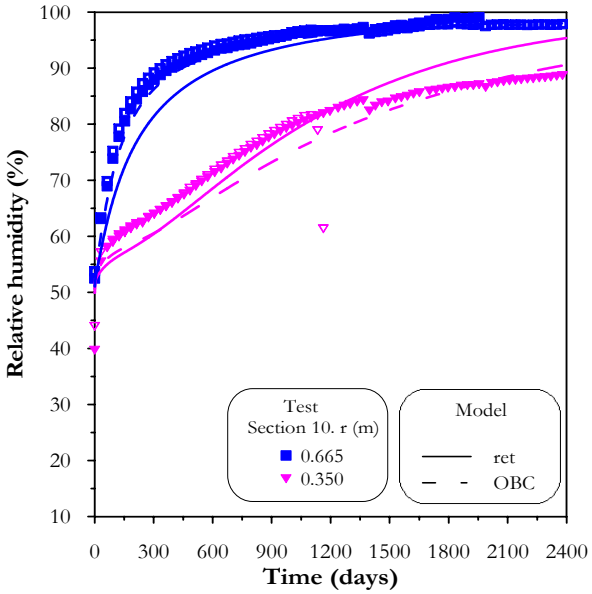

Figure A4.27. Relative humidity evolution. Sections A10-B10. Observed versus computed values of 'ret' and 'OBC' models.

where f_d is given by (A4.14) and f_ϕ considers the dependence of the retention curve on porosity according to:

$$f_\phi = exp\left[-\eta\left(\phi - \phi_o\right)\right] \tag{A4.38}$$

where the parameter η controls the variations of P_o due to porosity changes. When $\eta = 0$ the original model is recovered (Equation A4.13). Figure (A4.28) presents the retention curves for different values of dry density together with the experimental data.

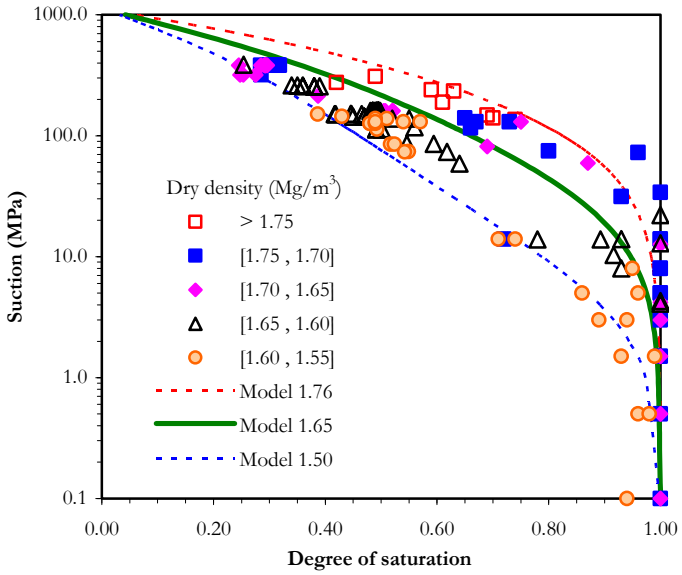

Figure A4.28. Retention curve adopted in the analyses coded as 'ret'. Models and experimental data for different FEBEX bentonite dry densities.

The model results obtained with this modified retention curve are again unsatisfactory, and they certainly can not explain the slowing down of the *mock-up* hydration.

Another aspect analysed in the context of FEBEX project is the influence of the temperature in the water retention capacity. Many tests, at different temperature and under different conditions (confined and unconfined) were carried out. Figure (A4.29) shows the experimental results for a dry density of 1.75 Mg/m^3, carried at three different temperatures and under constant volume conditions. It can be observed that the influence of temperature on the water retention capacity is not strong.

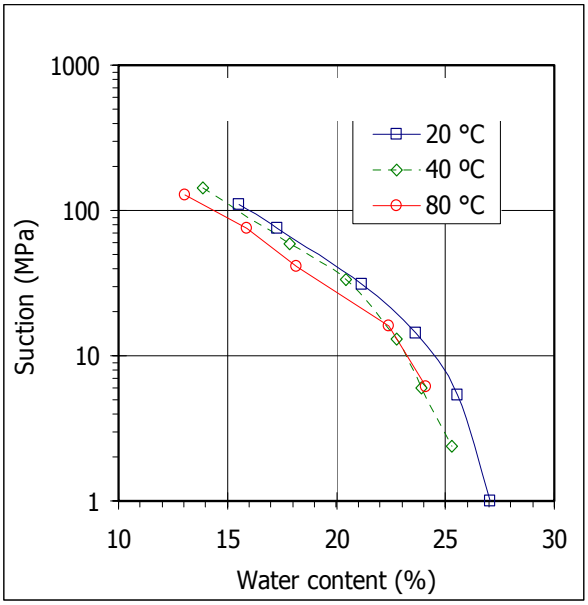

Figure A4.29. Retention curves of FEBEX bentonite at constant volume for different temperatures and at a dry density of 1.70 Mg/m^3 (Villar *et al.*, 2004).

Figure (A4.30) presents the results of tests performed under unconfined conditions. It can be observed that also in this case the effect of temperature is not very important.

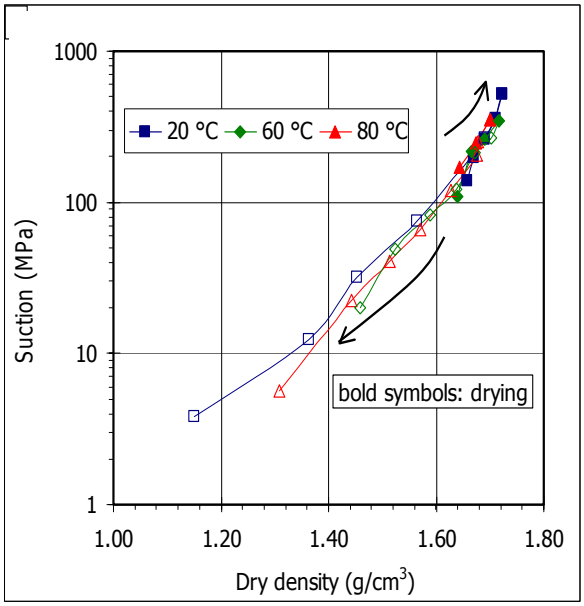

Figure A4.30. Evolution of dry density in the retention curves in unconfined specimens of FEBEX bentonite compacted in drying/wetting paths at initial dry density 1.65 Mg/m^3(Villar *et al.*, 2004).

As commented in Section A.4.1.2.2, the model proposed for the retention curve take roughly into account the effect of temperature. In Figure (A4.31), it can be checked that the implemented model considers the influence of temperature in a way consistent with the experimental results. Due to the minor effect that temperature appears to have on retention curves and due to the limited information available, no modifications are introduced in this law.

Other aspect also explored in the experimental program of the FEBEX project was the study of the hysteretic behaviour of FEBEX bentonite (Lloret *et al.*, 2001). This is a complex problem and it is not so easy to establish strong conclusions, but, it can be said that, for relatively high dry density (higher than 1.60 Mg/m^3) and for drying/wetting paths, the effect of hysteresis is not significant (Lloret *et al.*, 2001). Anyway, during the preoperational stage of the project, a retention curve model that includes the effect of hysteresis was introduced and no satisfactory results were obtained.

A number of similar sensitivity analyses were performed regarding other constitutive laws, other models parameters and also combining some of them, reaching at similar conclusions. They are not presented in this Thesis. According to this wide sensitivity study, it can be said that it was not possible to obtain one set of constitutive laws with physical meaning and consistent with the experimental observations. Finally, it is possible to conclude that, although changes in parameters can lead to better agreements locally, it does not appear that such strategy would lead to a global explanation of the behaviour that includes all the observations made.

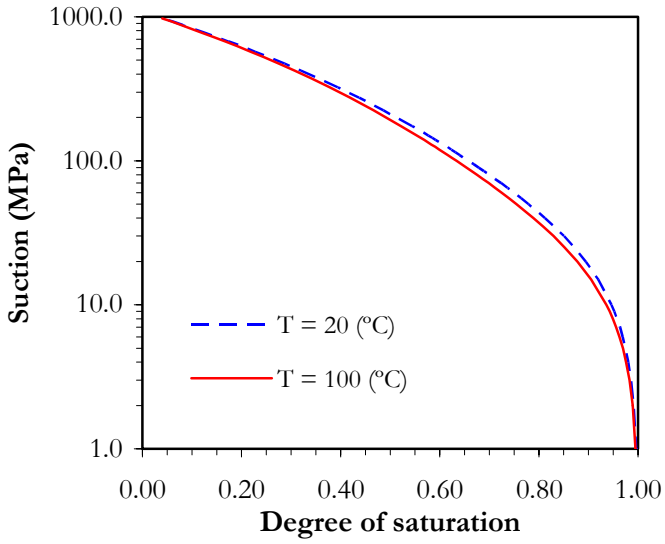

Figure A4.31. Effect of the temperature on the adopted retention curve model.

A.4.3 *MOCK-UP* DOUBLE STRUCTURE MODEL

A.4.3.1 MODEL LAWS AND PARAMETERS

In relation to the hydraulic problem, it is assumed that the water flow obeys the Darcy's law. The driving force of this flux is the gradient of liquid pressure (in this conceptual model the macro and micro liquid pressures are the same). It is necessary to define three main hydraulic constitutive laws, which are: the intrinsic permeability law, the relative permeability law and the retention curve model.

Several models have been proposed to evaluate the soil permeability. A comprehensive analysis of the classical permeability models can be found in Leonards (1962) and Bear (1972), among others. Conventional models try to predict the soil permeability based on the grain size distribution parameters or on volumetric relationship including the medium porosity or the void ratio. Theoretical models based on equivalent capillary flow model (known as capillary models) and on the concept of hydraulic radius (which is a characteristic length parameter; Leonards, 1962) have been widely used in soils mechanics. This kind of models has shown a good performance in uniformly graded sands, but they were not suitable to predict the permeability of compacted clays. Perhaps the most used permeability law is the one known as Kozeny-Carman equation, which is a hydraulic radius models (*i.e.* Leonards, 1962; Bear, 1972). Inspired in this equation, some authors have proposed permeability laws which include parameters that intent to fit experimental data, this kind of models are generally used in clayey soils (Gens *et al.*, 1998).

More recently, probabilistic concepts have been used to include the effect of the clay fabric on the permeability models. For instance, in the works of Garcia-Bengochea *et al.* (1979), Juang & Holtz (1986), Lapierre *et al* (1990) and Tuli *et al.* (2001), the Pore Size Distribution (PSD) has been used to predict the soil permeability using probabilistically based flow models. These models generally consider laminar flow through a cylindrical capillary of diameter 'x'. As commented by Romero (1999), in these models the main difference arises in the way of how two cross-sections (separated by a distance 'L') are considered to be connected. One extreme case corresponds to the assumption of a completely random connection (each section is independent of the other), and on the other extreme situation the pores considered in two cross-sections (nearby) are correlated. Juang & Holtz (1986) assume that the connection between pores are partially correlated, that is the pores of the same size, on two cross-section, have a greater probability of being connected than of pores of other diameter. Based in this assumption, a good correlation between PSD and measured permeability were obtained (Juang & Holtz, 1986; Romero, 1999). Romero (1999) concludes that: "the permeability is very sensitive to the magnitude and frequency of the large pore mode".

PSD have also been used to study the effects of organic fluids on the clays fabric and also on permeability (Acar *et al.,* 1985; Acar & Olivieri, 1990; Hueckel *et al.,* 1997). In the work of Hueckel *et al.* (1997) a theoretical permeability model has been proposed idealizing the clay fabric as an organized two-dimensional periodic structure of solid particles. In this conceptual model a series system is considered, in which the smaller channels (associated to the smaller pores in a bimodal PSD) connect the larger channels (which could be associated to the larger pores).

Good results have been obtained using such kind of model when the problem of contaminant transport through a clay barrier is simulated (Kaczmarek *et al.*, 1997). Finally, Hueckel *et al.* (1997) conclude that: "for water permeability in a bimodal series pores system, the smaller pore mode is critical, as a connector between the larger pores, rather than the larger pore size itself".

It can be noted the strong differences between the conclusions at which Romero (1999) arrives (based on Juang & Holtz, 1986, assumptions) and the ones obtained by Hueckel *et al.* (1997). The two kinds of models are based on PSD, but the differences arise in the interpretation of the experimental data and, consequently, in the conceptual flow model adopted. Models supported by PSD have other limitations, based mainly on the uncertainties of the experimental techniques used to obtain the PSD (generally by mercury porosimetry intrusion). In spite of these problems, models based on PSD can be considered as an improvement in relation to the one based on grain size distribution or void ratio, especially when inert materials are studied. In the case of expansive clays, the use of such permeability models is not so direct because the soil fabric changes as a consequence of the interactions between water and clays minerals. Finally, it is interesting to mention that these theoretical laws generally have some parameters used to fit experimental data. For instance, in the model presented in Juang & Holtz (1986) the unknown parameter is related to the connection ('L') between two cross sections, and, in the model proposed by Hueckel *et al.* (1997) the unknown parameter is related to the evolution of the smaller pore size (Kaczmarek *et al.,* 1997). So, direct measurements of permeability are usually necessary (as concluded by Lapierre *et al.*, 1990), and some degree of fitting is generally required.

Considering the aspects commented above, it seems that known permeability models based on PSD are not suitable for modelling non-saturated expansive clays. The development of such kind of model appears as not simple. Note that, due to the dynamic character of the clay fabric during hydration, the formulation of a permeability model based on PSD needs a lot (and detailed) experimental data, which are not available at the moment. So, in this work it is decided to use a permeability model based on basic concepts, but in which the main *HM* couplings and the interactions between the pores structures observed in the FEBEX bentonite are taken into account.

It is assumed that the flow of liquid water takes place mainly through the macropores. In the proposed double structure approach it is possible to consider that the water can flow also through the micro level (pores lower than 0.13 μm, in the case of FEBEX bentonite, Figure 4.1). However, in this simulation, a very low permeability for the microstructural level has been adopted, considering that the contribution of this level to the total water flow is small. This hypothesis could be changed if it is deemed convenient, considering the permeability of the pores available for the water flow of this medium; and considering also the water properties of this medium (water viscosity and water density).

It is also assumed that the intrinsic permeability is a function of the macro porosity through an exponential law (Equation A.4.10). The exponential law is considered as an initial approximation. It is important to keep in mind that in the double structure framework, the evolution of the clay fabric (macro and micro porosity) is controlled by the changes in the main variables of the problem (displacements, temperature, macro and micro suctions), which are considered in a fully coupled way. In this context, the main phenomena that affect the changes in both pores levels, and their mutual interactions, are taken into account. A boundary condition of this permeability model corresponds to the saturated state.

The saturated permeability of FEBEX bentonite is known for different initial densities, measured under conditions of constant volume (Villar, 1999; FEBEX Project, 2000). To determine the model parameters of the permeability law, a series of numerical simulations of the permeability tests (for different initial dry densities) have been performed solving them as a boundary value problem. The mechanical model presented in Chapter IV (Section 4.2) has been used in the modelling. Figure (A.4.32) presents the measured saturated permeability of FEBEX bentonite at different densities together with the results obtained in the simulation using the exponential model (Equation A.4.10) in terms of macroporosity.

A model in terms of the degree of saturation of the macro level (Equation A4.11.a) has been adopted for the relative permeability law. Table (A4.2) presents the parameters adopted for the permeability laws (intrinsic and relative permeability).

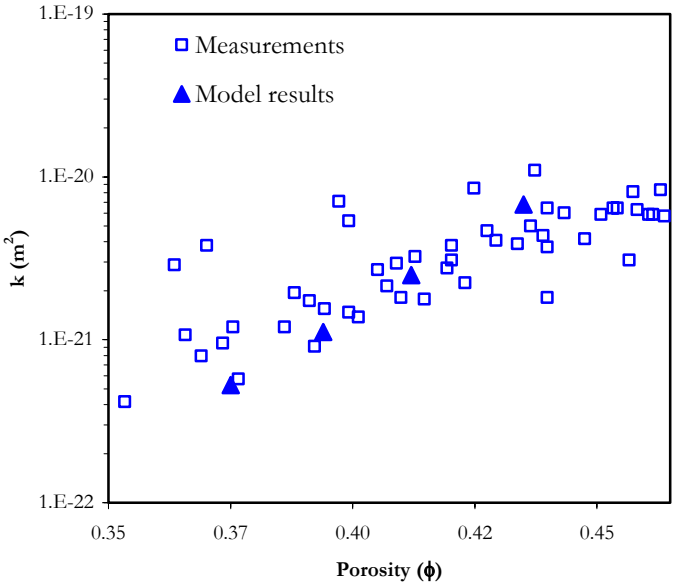

Figure A4.32. Measured saturated water permeability of FEBEX betonite (FEBEX Project, 2000), together with model results obtained after simulations of permeability tests.

As commented in Chapter V, some contributions report that the properties of the microstructural water are different than the ones of the free water (Skipper *et al.*, 1991; Villar, 2000; Ichikawa *et al.*, 2002; Lloret, 2004). Figure (A4.33) shows the values of the mean water density obtained post-processing the laboratory data in order to obtain a maximum saturation degree of 1.0 (Villar, 2000; Lloret, 2004). Considering the dry density of the FEBEX bentonite in the *mock-up* test (1.65 Mg/m^3), a microstructural water density of 1.15 Mg/m^3 has been adopted.

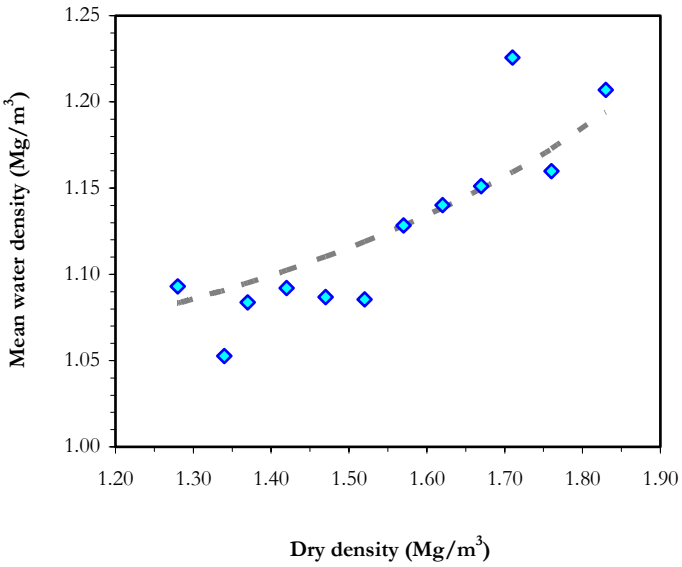

Figure A4.33. Computed variation of the water density in terms of the FEBEX bentonite dry density (Lloret, 2004).

In the double structure model the water retention capacity of the soil is obtained considering the water stored in the two pore levels. One retention curve is defined for each medium and the global degree of saturation is obtained according to Equation (2.29). In order to compute the water retained at the microstructural level, a retention curve close to the experimental data of higher density has been adopted. At high density the microstructural level prevails (the macropore practically disappear). It is noted that all the pores lower than 0.13 μm (intruded or not) are considered as micropores (Figure 4.3). But, the capability to retain water in these two different types of micropores (intra-aggregate pores or interlamellar space, Chapter V, Section 5.4.2.1) is different, due to the different phenomena that take place in each one of them. Perhaps, the inclusion of another (intermediate) pores level allows handling more properly this fact. In this Thesis only the two main levels (macro and micro) have been considered. On the other hand, the adoption of the retention curve for the macrostructural level has been made in order to obtain a global degree of saturation that fall in the range of experimental data available for the FEBEX bentonite.

Figure (A4.34) presents the retention curves adopted for each media, in terms of suction and saturation degree of the media. Additionally, this Figure shows the modelling results of a wetting path (at constant volume) in terms of the global degree of saturation and suction. Even though this model is very simple, it allows considering explicitly the amount of water stored at each structural level. This is an active point of research and the formulation is left open to the incorporation of more sophisticated models.

The law adopted for the retention curves is the one expressed in Equation (A4.13). Table (A4.2) contains the model parameters.

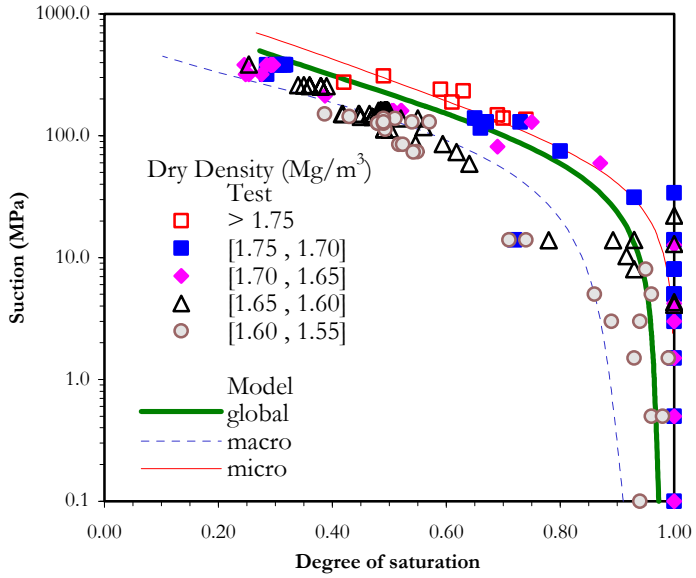

Figure A4.34. Water retention curve, experimental data and adopted models.

Table A4.2

Parameters related to the flow problem of Section 5.4.3

Parameters defining the retention curve

$P_{0\,1}$(MPa)	$P_{0\,2}$(MPa)	λ_{o1}	λ_{o2}	λ_{d1}	λ_{d2}	$P_{d1} = P_{d2}$ (MPa)
$1.0\text{x}10^{-5}$	85	0.01	0.35	4	0.5	1100

Parameters defining the permeability law

$k_{0\,1}$(m^2)	ϕ_o	b	n
$5.0\text{x}10^{-20}$	0.14	50	1

Leakage parameter (kg s^{-1} m^{-3} MPa^{-1}) = 1.0

Regarding to the thermal problem the generalized Fourier's law for double structure media presented in Chapter II is adopted. The thermal conductivity is given by Equation (2.27). The same parameters of 'OBC' model have been adopted for λ_{dry} and λ_{sat} (*i.e.* λ_{sat} = 1.15 and λ_{dry} = 0.47 W/m ºC).

Finally, in relation to the mechanical problem, the model parameters determined in Chapter IV (Section 4.2) has been adopted. The parameter β_m has been reduced in order to adjust slightly the test measurements. This implies a lesser swelling capacity of the material, that could be related to the observed tendency of FEBEX bentonite to decrease the swelling capacity (and swelling pressure) with temperature (Villar *et al.*, 2004). Additionally, as commented in Chapter V, to take into account the dry density of the clay barrier the pre-consolidation stress has been changed (Gens & Alonso, 1990). Table (A4.3) contains the model parameters.

Table A4.3

Main parameters of the elasto-plastic constitutive law used in Section 5.4.3

Parameters defining the Barcelona Basic Model for macrostructural behaviour

κ	κ_s	$\lambda_{(0)}$	p_c (MPa)	r	ζ(MPa^{-1})	p_o^* (MPa)	α_0(ºC^{-1})
0.007	0.001	0.080	0.50	0.90	0.20	5.4	1.5x10^{-05}

Parameters defining the law for microstructural behaviour

α_m (MPa^{-1})	β_m (MPa^{-1})
2.1x10^{-02}	2.0x10^{-03}

Interaction functions

$$f_C = 1 + 0.9 \tanh\left(20\left(p / p_o\right) - 0.25\right) \;;\; f_S = 0.8 - 1.1 \tanh\left(20\left(p / p_o\right) - 0.25\right)$$